Kingdom of Saudi Arabia
King Abdulaziz City For
Science and Technology
General Directorate Of
Research Grants Programs

ARP-13-46

FINAL REPORT

AN INVESTIGATION OF CRUSTAL AND UPPER MANTLE STRUCTURE BENEATH RIYADH REGION FROM SPECTRAL ANALYSIS OF LONG PERIOD P-WAVE DATA

Dr. Abdullah M. Al-Amri
Dr. Talal A. Mokhtar
Dr. Altan Necioglu

KING SAUD UNIVERSITY

1995G.

ص.ب ٦٠٨٦ – الرياض ١١٤٤٢ – هاتف ٤٨٨٣٥٥٥-٤٨٨٣٤٤٤ – فاكس ٤٨١٣٨٧٨ – بريد إلكتروني GDRGP@KACST.EDU.SA
P.O.Box. 6086 - Riyadh 11442 - Telephone. 4883555-4883444 - Fax. 4813878 - E-mail.. GDRGP@KACST.EDU.SA.

RIYADH REGION FROM SPECTRAL ANALYSIS OF LONG PERIOD P-WAVE DATA

Dr. Abdullah M. Al-Amri

الخلاصة

تم اشتقاق السرع التركيبية للقشرة الأرضية والجزء العلوي من الوشاح باستخدام نتائج التحليل الطيفي لنسب السعة العمودية للموجات الطولية. استخدمت نسب المركبات العمودية إلى الأفقية للحصول على معامل التحول القشري اعتماداً على اختلافات السمك، والسرع القشرية، والكثافة، وقيمة وزاوية السقوط عند الجزء السفلي من القشرة والجزء العلوي من الوشاح.

ولإنجاز هذا الهدف فقد تم اختيار أفضل أربعين زلزالاً سجلتها محطة الرياض ذات الفترة الدورية طويلة المدى خلال الفترة من ١٩٨٦ إلى ١٩٩٤م لغرض التحليل استناداً على المعايير التالية : يتراوح العمق البؤري ما بين ١٠ – ٣٠٠ كم، والزلازل قدرها أكبر من (٥) درجات حسب مقياس ريختر، والمسافة البؤرية تتراوح ما بين ٩ إلى ٨٩ درجة.

اعتمدت حسابات التحاليل الطيفية على مقارنة النسب الطيفية المسجلة مع النسب النظرية المحسوبة باستخدام مصفوفة ثومبسون – هاسكل للنماذج القشرية للطبقات الأفقية. ودلت نتائج النموذج القشري المشتق على تغير السمك القشري من ثلاث اتجاهات مختلفة :

١ – من ٢٠ – ١٢٠ درجة (شمال شرق – جنوب شرق).
٢ – من ١٢٥ إلى ٢٢٠ درجة (جنوب شرق – جنوب غرب).
٣ – من ٢٢٥ إلى ٣٦٠ درجة (شمال غرب إلى شمال).

واعتمد اختيار النموذج المشتق على مقارنة النماذج النظرية التي تبين أعلى معامل للمضاهاة المتقاطعة مع نسب المعاملات المسجلة. وقد اقترح النموذج المشتق أن القشرة يبلغ سمكها ٤٤ كم تقريباً وتتألف من خمس طبقات متميزة :

١ – الطبقة العلوية سمكها (٢) كم وسرعتها ٥,٦ كم/ث.
٢ – الطبقة الثانية وسمكها (١٠) كم وسرعتها ٦,٢ كم/ث.
٣ – الطبقة الثالثة وسمكها (٧) كم وسرعتها ٦,٥ كم/ث.
٤ – الطبقة الرابعة وسمكها (١٤) كم وسرعتها ٦,٨ كم/ث.
٥ – الطبقة السفلية من القشرة ويبلغ سمكها (١١) كم وذات سرعة تصل إلى ٧,٥ كم/ث.

ويتراوح عمق انقطاع موهو تحت الرصيف الغربي من (٤٤) كم في اتجاه شمال شرق – جنوب شرق إلى (٤١) كم عمق في اتجاه جنوب غرب – شمال غرب وبسرعة تصل إلى ٨,٢ كم في الجزء العلوي من الوشاح.

ABSTRACT

The crustal and upper mantle velocity structure of the central Arabian Platform has been derived using the spectral analysis of long period P-wave amplitude ratios. The ratio of the vertical to the horizontal component is utilized to obtain crustal transfer function based on thickness variations , crustal velocities , densities and the angle of incidence at the lower crust and upper mantle.

Forty well-defined earthquakes recorded at RYD long-period station during the period from 1986 to 1994 were selected for the analysis based on the following criteria : focal depths range between 10 and 300 km , body-wave magnitudes greater than 5.0 and the epicentral distances range from 9 to 89 degrees. Spectral analysis calculations were based on comparing the observed spectral ratios with those computed from theoretical P-wave motion obtained using the '' Thomson- Haskell '' matrix formulation for horizontally layered crustal models.

The derived crustal model indicates a change in crustal thickness in three different azimuthal sectors : 1) from 20 to 120 degrees (NE to SE) , 2) from 125 to 220 degrees (SE to SW) and 3) from 225 to 360 degrees (SW to N). The selection of the most suitable model was based on the identification of theoretical model which exhibits the highest cross correlation coefficient with the observed transfer function ratio. The model suggested that the crust consists of five distinct layers. The upper crustal layer has a P-wave velocity of about 5.6 km/sec and is about 2.0 km thick. The second layer has a velocity of about 6.2 km/sec and 10 km thick . The third layer shows a velocity of 6.5 km/sec and 7 km thick. The fourth layer has a velocity of about 6.8 Km/sec and 14 km thick. The lower crustal layer has a velocity of about 7.5 km/sec and 11 km thick. The Mohorovicic discontinuity beneath the Arabian Platform varies from 44 km depth in the NE and SE to 41 km depth in the NW and SW with 8.2 km/sec upper mantle velocity.

ACKNOWLEDGMENTS

This is the final progress report of the research project AR-13-46 . The authors would like to express their thanks to King Abdulaziz City for Science and Technology for funding this project. This work would not have been possible without the generous assistance of KACST and KSU .

We would like to express our deepest appreciation to Dr. Ali A. Ghareeb of the Seismological Observatory , King Saud University for his tremendous help and carrying out data processing during the entire project. His willingness to devote his time greatly facilitated the completion of the project. Some contributions made by co-investigator Dr. Talal Mokhtar are also acknowledged.

Dr. Niyazi Turkelli, the project consultant, whose expert guidance and continuing advice made this work possible. We owe him a deep debt of gratitude and a great deal of thanks. Grateful acknowledgment is also extended to the anonymous referees for their helpful suggestions and criticism.

Finally and most importantly, we would like to extend our sincerest thanks to the Seismological -Geophysical Observatory , King Saud University for providing this project with the earthquake data.

PAGE

LIST OF TABLES

LIST OF FIGURES

PAGE

CHAPTER 1.
INTRODUCTION

One of the main tasks of seismology has been to determine the crustal structure around the world. Various techniques have been used including travel-time studies, surface wave dispersion, controlled source profiling, gravity and magnetic measurements and the use of body wave spectral techniques.

The body wave spectral techniques make use of the Thomson - Haskell matrix method. The observed spectra are compared with the theoretical ones that are obtained from the horizontally layered earth models.

1.1. PURPOSE AND SCOPE OF THE STUDY

The purpose of this study is to determine the crustal and upper mantle structure beneath the Riyadh region from spectral analyses of long period P-waves. To achieve our objectives, suitable earthquakes which were recorded at the seismological-geophysical observatory of the King Saud University between 1985 and 1993 have been utilized. The analyses were based on the matrix method of Thomson-Haskell in which theoretical spectra obtained from the horizontally layered earth models have been compared with the observed spectra.

The earth model obtained from this investigation will provide the crustal and upper mantle structure beneath the Riyadh region which is the first in the Kingdom. Furthermore, earthquake location programs need precise a velocity structure. This in turn will help seismic risk and hazard studies in the Kingdom. Finally, our results will contribute to the global tectonics investigations involving the Arabian plate.

1.2. GEOLOGIC AND TECTONIC SETTING

The Arabian plate is a relatively small lithospheric plate whose boundaries are representative of the different types of plate boundary (Figure 1.1). The majority of earthquakes and tectonic activities are concentrated along three belts in the Arabian plate . The first is the Zagros fold belt that extends about 1500 km in a northwesterly direction from Oman through west Iran and northeast Iraq to Turkey. The continental part of the Arabian plate is colliding with the Persian plateau to the east and the Turkish plateau to the north along the Zagros-Taurus belt (Taken , 1972; Dewey et al., 1973 ; Stocklin , 1974).The second belt extends from the central Red Sea region south to Afar and then east through the Gulf of Aden. This belt indicates active sea-floor spreading along the axial trough (Girdler and Styles, 1974; 1978; Hall et al., 1977; Le Pichon and Francheteau, 1978). A less-defined third belt is a complex transform type boundary (Ben-Menahem et al., 1976) , namely the Dead Sea Transform that extends about 1000 km from the northern tip of the Red Sea, through Lebanon, Syria, and terminates in southern Turkey.

The surface geological and tectonic settings of the Arabian plate consist mainly of : 1) The Arabian shield in the west and 2) The Arabian platform in the east. The Arabian shield is an area of about 650,000 km comprised chiefly of stratified volcanic and plutonic rocks of late Proterozoic to early Cambrian age, bounded on the west by Cenozoic rocks of the narrow coastal plain of the Red Sea and on the north and east by gently dipping Paleozoic and Mesozoic sedimentary strata of the 'cover rock' succession. The region as a whole is separated from the Nubian shield on the west by the Red Sea rift (Greenwood et al., 1980). Tectonically, the shield is divided into five terrains or microplates separated by two types of suture zones of two types: island arc-island arc collisional sutures and island arc-continental collisional sutures. The western shield is composed of three intraoceanic island-arc terrain (Asir, Hijaz, Midyan), whereas the eastern shield includes two terrains of continental affinity (Afif , Ar Rayan).Three major tectonic trends are recognized in the shield. The oldest tectonic lineaments are the N-S trends which prevail all over the southern, central, and northern Arabian shield .The second major set of tectonic are the NE trends. The Ad Damm fault runs from the coastal plain of the

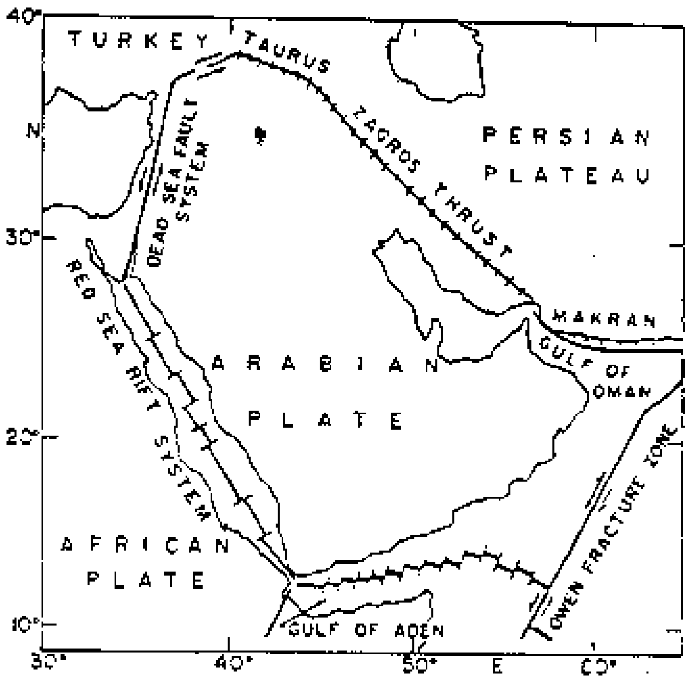

Figure 1.1. Map showing the different tectonic boundaries of the Arabian plate (after Barazangi).

Red Sea over a length of some 130 km. The third major set of tectonic lineaments are the NW trends, the Najd fault system. It is one of the most prominent Precambrian-Cambrian sinistral wrench fault systems. It is believed that this system is the result of plate collision between the African craton and the Arabian plate. To the east , the shield is bounded by the Arabian platform(the stable and the unstable shelf areas). The platform consists of the Paleozoic and Mesozoic sedimentary rocks that unconformably overlays the shield and dip very gently and uniformly to the E-NE towards the Arabian Gulf (Powers et al., 1966).Two major Tertiary tectonic trends in the Red Sea region. These are the NE and NW faults. The NE trending faults could be considered as newly formed transverse faults related to the opening of the Red Sea and sea-floor spreading. The NW faults are those responsible for rifting and opening of the Red Sea. They form structural basins or have been filled by mafic dykes.

1.3. PREVIOUS CRUSTAL STRUCTURE STUDIES IN SAUDI ARABIA.

The first seismic refraction survey of the Red Sea was carried out by the research vessels Vema and Atlantis in 1958. Fifteen refraction profiles were made parallel to the Red Sea axis. The seismic velocities of the shield rocks near the Red Sea margins lie between 5.5 and 6.4 km/sec. In 1967 R.R.S.Discovery shot three more refraction profiles in the NE corner of the Red Sea, and those showed a continental basement structure. Girdler (1969) interpreted the high-velocity basement in the axial trough of the Red Sea as oceanic crust and the lower-velocity basement in the shelves as continental material. Most, if not all, of the crustal structure studies conducted in Saudi Arabia have been based on the Saudi Arabian Deep Refraction profile. In 1978, seismic-refraction profiles were recorded by the US Geological Survey along a 1000 km line across the Arabian shield (Figure 1.2). The profile begins in Paleozoic and Mesozoic cover rocks near Riyadh, leads southwesterly across three major Precambrian tectonic provinces (The Shammar, Najd, and Hijaz-Asir), traverses Cenozoic rocks of the coastal plain near Jizan, and terminates at the outer edge of the Farasan bank in the southern Red Sea (Mooney et al., 1985; Prodehl, 1985). Mooney et al, (1985) applied the two-dimensional ray tracing technique to analyze the crustal structure beneath the Arabian shield

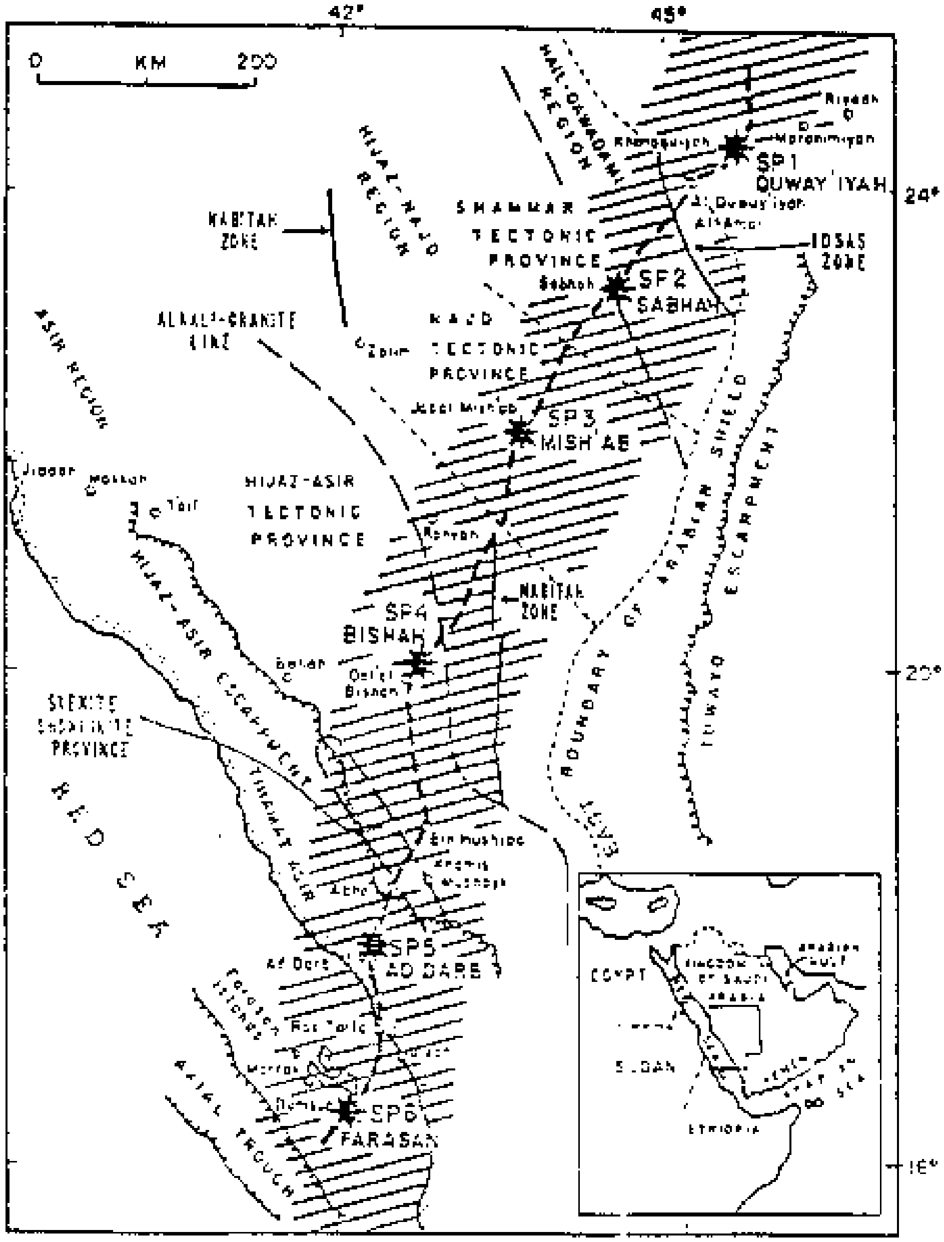

Figure 1.2. Index map showing the locations of shot points of the 1978 seismic refraction profile (after Mooney et al., 1985)

and platform. The general features of their results are as follows: The Arabian shield is composed, to first-order, of two layers, each about 20 km thick, with average velocities of about 6.3 and 7.0 km/s , respectively. The crust thins rapidly to less than 20 km total thickness at the western shield margin . The depth of the Moho discontinuity beneath the shield varies from 43 km in the NE to 38 km in the SW with a 8.2 km/s mantle compressional velocity in the NE to 8.0 km/s in the SW (Figure 1.3) .The average upper crustal velocity of Shot point 1 (in the NE of the profile) near Riyadh is approximately 6.25 km/s and shows a variation of 0.2 km/s at a given depth. The mid-crustal discontinuity occur at 21 km depth. There is a strong velocity gradient from 6.8 to 7.9 km/s in the lower crust between 31 and 43 km depth, and the velocity contrast at the Moho discontinuity is only 0.2 km/s. These variations indicate lateral variations in the near-surface structure, particularly between 30 and 60 SW of shot point 1. Prodehl (1985) applied a two-dimensional interpretation technique to the same data set. His result for central Arabia show a crustal thickness of about 40 km and an upper mantle velocity of 8.2 km/s. His model shows a crustal velocity inversion at 10-12 km depth beneath the Arabian platform. He also shows that the Moho beneath the Arabian shield is not a first order discontinuity but is rather a transition zone where the velocity increases rapidly from about 7.4 to 8.2 km/s in a few kilometers. Mokhtar et al., 1988 used the short period Rayleigh waves recorded in the seismic deep-refraction profile across the Arabian shield. The Q structure was determined from the attenuation coefficients of the decay of the amplitude spectrum of the fundamental mode. They found that shear-wave Q increased from 30 in the upper 50 m to 150 at 500 m depth and the underlying material has a Q of 400-700 for the outer cropping igneous rocks. Badri (1989) also carried out his measurements on the Saudi Arabian refraction profile using two independent computational techniques , namely the spectral amplitude ratio (SAR) and pulse broadening method (PBM). He computed the attenuation characteristics in the crust and upper mantle in central Saudi Arabia and found that the Qp values range from 40-310 for the Pg phase in the Arabian platform and from 50 to nearly 850 in the Arabian shield. An average Q value of 165 is assigned to the upper crust in the Arabian platform while in the shield the upper crustal Q nearly 1560. An average Q value of 1075 is assigned to the upper mantle beneath the Arabian shield. Badri (1991) derived the crustal velocity model for central

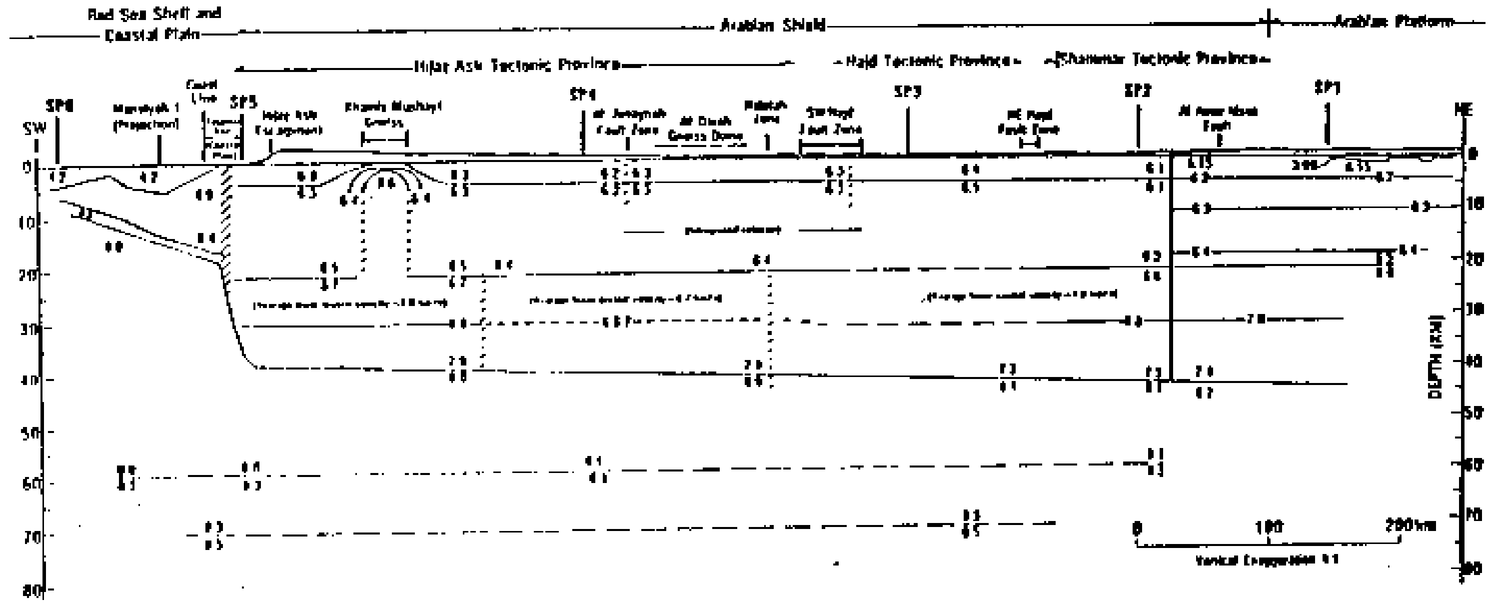

Figure 1.3. Composite cross-section of the crust and upper mantle of the Arabian shield from the Red Sea to the Arabian platform (after Mooney et al., 1985)

Saudi Arabia. His model shows that the crust consists of four distinct layers approximately 42 km thick under the Arabian platform and thins gradually in the SW direction to about 38 km under the shield. The upper crust consists of two layers : the upper layer has a P-wave velocity of about 6.08 km/s and is about 3 km thick and thins to about 1 km in the platform. The lower layer has a P-wave velocity of about 6.2 km/s and is about 14 km thick which thin to about 7 km beneath the platform. The intermediate crustal layer has a P-velocity of about 6.38 km/s. The lower crust has a P-wave velocity of about 15 km thick (1.4). The study of the seismic crustal structure of the Arabian peninsula has been attempted, using surface signal

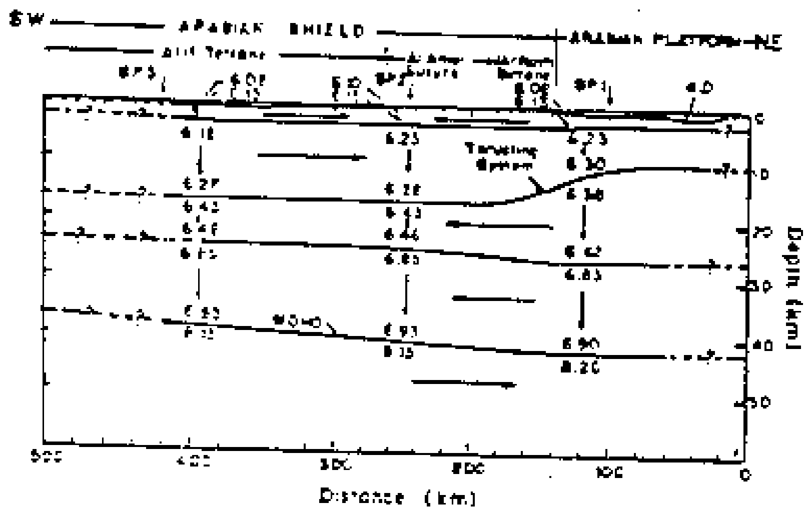

Figure 1.4. Interpretation of the crustal structure along the seismic profile between shot point 1 and shot point 3 (after Badri, 1991).

observation and teleseismic earthquakes . Studies of shear waves on the path Addis Ababa-Shiraz (which passes thorough the Afar depression) have shown that the average crustal thickness for this region is about 35 km (Niazi, 1968; Knopoff and Fouda , 1975). Shear-wave velocity models from these studies show a pronounced low-velocity zone with the top of the zone at 100 - 140 km depth. Phase velocities of the Arabian shield are lower than those of the Canadian shield; however, they are higher than those of the U.S. Gulf Coastal Plain (Knopoff and Fouda , 1975). More recently, Mokhtar et al., 1992 used the earthquake data of a single station located inside the Arabian peninsula (RYD) and three WWSSN stations (JER, SHI, and

TAB) in the surrounding areas. The seismic shear velocity structures of the different tectonic provinces of the Arabian Peninsula have been determined using surface wave dispersion from RYD to WWSSN stations. the results are summarized in Table 1 as follow :

The inversion of Rayleigh waves group and phase velocities of the data from RYD indicates that the Arabian shield can be modeled by two layers , each of which is 20 km thick with shear velocity of 3.61 km/s in the upper crust and 3.88 km/s in the lower crust. The underlying upper mantle velocity is 4.61 km/s and the crust-upper mantle boundary is at depth of about 40 km . Inversion of both Love and Rayleigh waves group and phase velocities show that the Arabian platform upper and lower crust are comparable in their thickness to those of the shield , but with shear velocities of 3.4 km/s and 4.0 km/s respectively. The upper mantle velocity beneath the platform is 4.4 km/s and the crust-upper mantle boundary is at depth of about is 45 km/s. The sedimentary sequence covering most of the Arabian platform has an average thickness of 5 km and its shear velocity is 2.31 km/s. Its thickness increases toward the east under the interior platform and basins where it amounts to 7 km on the average and consists of two layers , an upper 3 km with shear velocities of 2 km/s and a lower 4 km with shear velocity of 3.24 km/s. Generally speaking, no locally recorded earthquake data have been used to determine the crustal characteristics of the Arabian plate. Previous studies indicate that the structure in the upper crust and the nature of the crust-upper mantle boundary are not well-established. It should be emphasized that the Saudi Arabian deep refraction profile which was recorded by the U.S. Geological Survey extended only to about 100 km southwest of Riyadh and did not include it. Therefore, in order to develop an accurate crustal model beneath the Riyadh region, earthquake events recorded from distances of 10^0 to 100^0 at Riyadh station were analyzed.

1.4. DATA SOURCE AND EARTHQUAKE SELECTION

In this research, the earthquakes meeting certain requirements and recorded by the long and intermediate period seismographs of the Riyadh (RYD) station of the King Saud University's Seismological Geophysical Observatory were utilized.

Seismological Geophysical Observatory was established in 1985. It has a 30 station network covering most of the Kingdom. The central station is located in the university campus and equipped with 3 short, 3 intermediate (wide band) and 3 long period (narrow band) seismographs. In addition to the analog recording on paper, the signals are digitally recorded since 1992.

The amplitude response curves of the long period seismographs are shown in Figures 1.5.- 1.10. in Appendix I. They are periodically calibrated and response curves did not show significant difference from each other.

The monthly bulletins of the observatory and the *Monthly Listings* of the Preliminary Determination of Epicenters "PDE" of the United States Geological Surveys the USGS were used for the preliminary selection of the earthquakes. The earthquake source parameters, hypocentral coordinates, origin-times, magnitudes, and depths were taken from the *Monthly Listings*. These source parameters together with the station coordinates were used as inputs for the computer program of Herrmann (1978) to calculate the epicentral distance, azimuth, back azimuth, P-wave arrival time and angles of incidence and emergence of P-wave. According to the above procedure, we got 420 events.

Earthquake selection started by reviewing the available microfilm cassettes to check if those list of selected events are recorded by RYD station or not and what the quality was of these records. Second step was to view the seismograms. Only a 70 out of the 420 events have been clearly recorded at Riyadh station (long and intermediate) from the period of 1985 up to 1992. But due to the low signal to noise ratio of (RYD) station at times as well as clipping of the traces due to large amplitudes and a malfunctioning component, the number of the selected events reduced to only 30 well recorded events which we thought that were not sufficient data for our study.

- In order to increase the number of selected events, we enlarged the distance range to be from 5° to 100° and focal depth to be as shallower as 15 km even below 10 km as long as the P-wave onset was very clear and there was no interference by other phases. During the reviewing process, a few near events which fulfilled the requirements of such type of study were added to our list to be 57 very good events. The list of the earthquakes studies are given in Appendi.: II.

Through the selection procedures of the 57 well recorded earthquakes, the following criteria has been carefully considered:

1-Magnitude greater than 5

2-Shallow and intermediate focal depth (6 to 213 KM)

3-Distance range from 5^0 to 100^0

4-Clear and impulsive first onset recorded at the 3-components

CHAPTER 2.

INSTALLATION AND INTEGRATION OF THE SYSTEM

This study required some specific hardware and software for carrying out seismogram digitization, data processing and plotting and word processing. The entire workstation and peripherals were purchased from Kinemetrics Inc. Pasadena, California, USA The seismic workstation was received in September 1993 and installed in building 4 , College of Science , King Saud University . System integration consists of the following :

2.1 SYSTEM HARDWARE :

I -DELL PowerLine EISA 486/50 MHz Personal Computer with

- -32 Mbyte RAM , 256 Kbyte Cache
- -3.5 and 5.25 Floppy Disk Drives
- - 1.4 GByte Maxtor SCSI Hard disk
- - NEC 5FG 21 SVGA monitor
- - ATI Graphics Ultra pro EISA

II -PINNACLE MICRO PM0650 IPC , 654 Mbyte, 5.25" External Magneto-Optical Disk Drive

III -PINNACLE MICRO OMD-600 HS , 654 , 5.25" , Rewritable optical disk.

IV -NUMONICS AccuGrid Digitizing Table 36" X 48" with 16 button cursor , 0.0005" resolution

V -HP 7550 plus plotter , 1 Mb memory

VI-HP LaserJET IIID Printer , 300 dpi , 2 Mb RAM .

VII-HP ScanJET IIp scanner.

Figure 2.1 shows the block diagram of the acquired hardware.

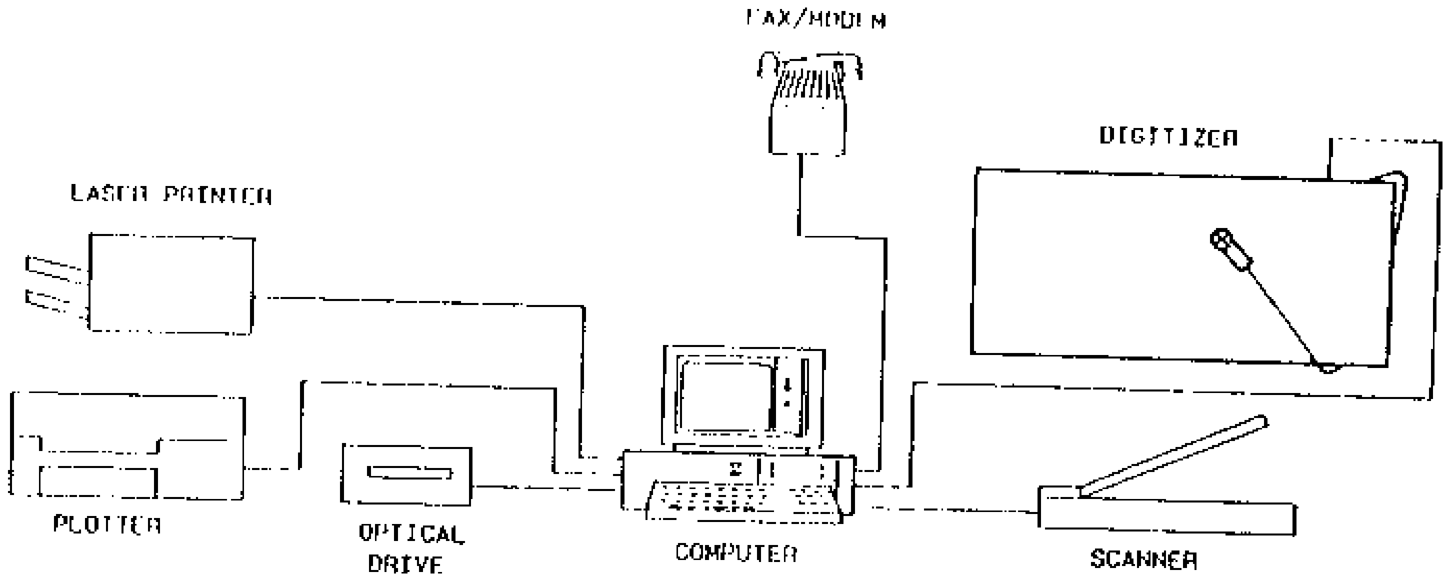

Figure 2.1. Computer system and peripherals.

2.2 SYSTEM SOFTWARE

- Microsoft DOS 5.0 , Windows 3.1
- Microsoft FORTRAN 5.1 compiler
- dBASE IV
- Kinemetrics' Development package (w/source code) SWS 1 for seismological data analysis .
- DIGIT Seis software (.DAT converter)
- PITSA 3.0 (Programmable Interactive Toolbox for Seismological Analysis)
- IASPEI (- International Association of Seismology and Physics of the Earth's Interior Seismological Library , V. 1, 2 ,and 3
- PrintAplot Program
- Scanview Software (.Data converter)
- PC PAINTBRUSH IV plus.

System block diagram is shown in Figure 2.2.

2.3. SYSTEM INSTALLATION AND TRAINING

This includes system engineering, system integration, system testing, and the running of all necessary software required to operate the different peripherals described herein. The aforementioned installation was carried out by Kinemetrics senior Engineer Dr. Amadej Trnkoczy and Engineer Ogie Kuraica. Training on how to maintain and operate the different components for 7 working days followed the system installation. Six staff members participated in the training program.

2.4. PROJECT' S MAJOR COMPUTER PROGRAMS

The main objective of this study is to determine the crustal and upper mantle structure using the spectral analysis of P wave data. In order to fulfill this objective, this study has implemented an advanced seismological package programs as seen in Figure 2.2. The most important seismological programs relevant to this study in the order of usage are as follows.:

- Sigma Scan: Used in conjunction with the digitizer to make 2D measurements

  The main features are;

  1. X Y coordinate measurements,

  2. distance measurement (straight line and curvilinear),

  3. area measurement

  4. angle measurement

  5. polar coordinate measurement

  6. user defined transforms,

  7. spread sheet editing,

  It allows one to arbitrarily orient the seismograms, calibrate for the time marks, digitize in manual or automatic mode etc.

- Seisdig (The Digitized Seismogram Program)

  Main features are;

  1. It allows one to arbitrarily orient the seismograms, calibrate for the time marks,

  accepts digitized

  data from Sigma Scan ,

  2. corrects for pen curvature and offset,

  3. corrects for negative loops (due to backward movement of the hand)

  4. allows editing of each point by enlarging the traces,

  5. resamples the traces

  6. saves the traces as ASCII files

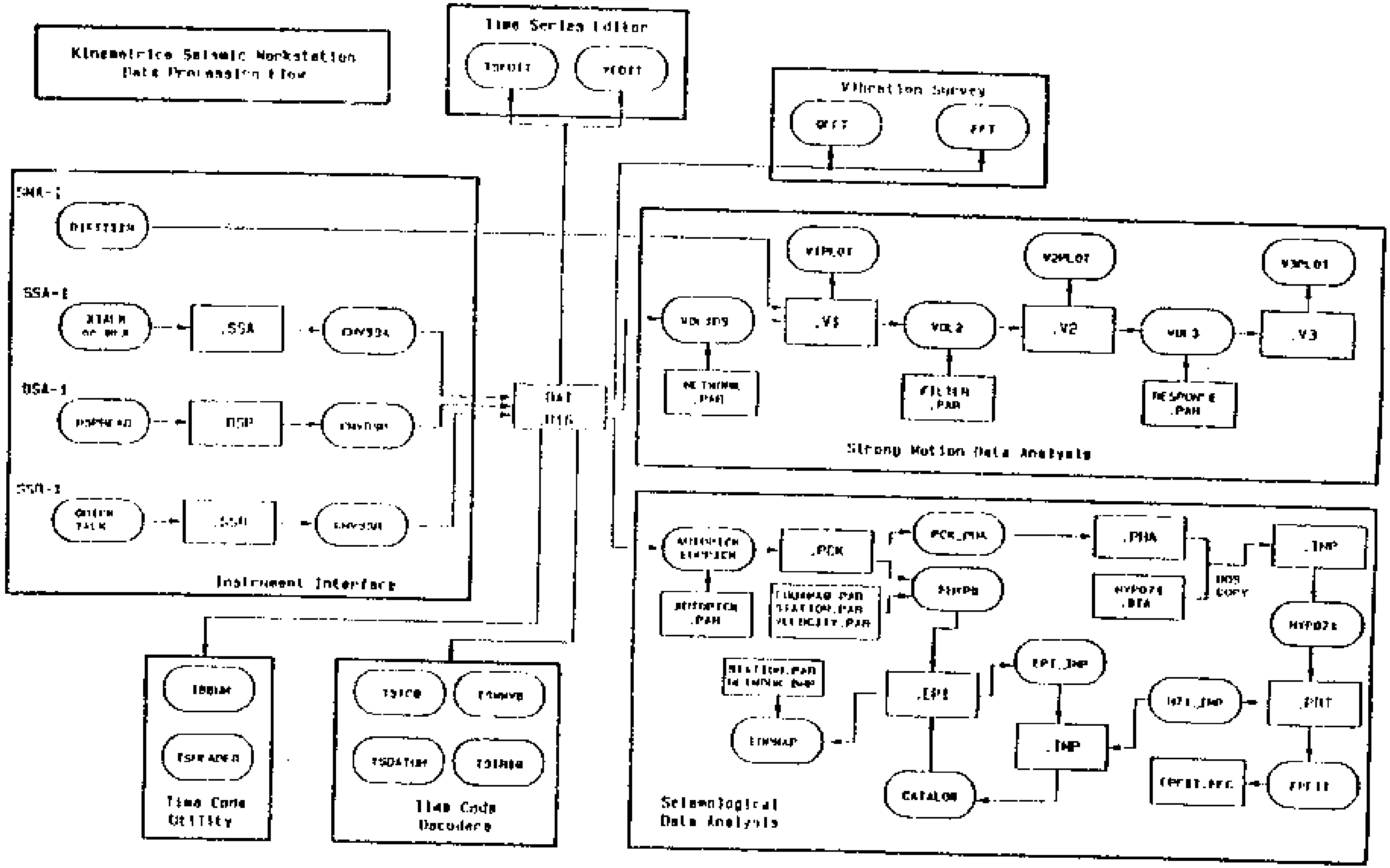

Figure 2.2. Software block diagram.

2.4.1. IASPEI'S VOLUME 5 PITSA PROGRAM

Programmable Interactive Toolbox for Seismological Analysis (PITSA).

This is the fifth volume of the IASPEI software library (Lee, 1989) which have been edited by Scherbaum and Johnson (1992). This software package designed for doing station-based digital seismological signal processing. PITSA enables one to determine onset times in various ways , estimate earthquake magnitudes, integrate or differentiate the signal ,analyze particle motions, perform convolution or deconvolution, correct for transfer function, cross correlate traces ,and perform FFT and inverse FFT.

PITSA consists of two parts , the Kernel and Front end . The PITSA kernel performs the signal processing and the front end depends on the operating system and defines the look and feel of PITSA on a particular machine . The following examples show some features of PITSA.

- Seismological oriented data format.

It uses a data format to meet the specific needs of earthquake seismology. PITSA stores plotting, station, and event information for each trace in ISAM file . It automatically adjusts its plotting to different sampling rates . Once the data are in memory , traces can be copied onto each other , deleted , added to other traces and written back to disk as combined file systems .

- Filtering. A number of filtering algorithms are implemented in PITSA, including Butterworth low pass, high pass, band pass, a notch filter and deranging filter which removes the effect of a single low-velocity layer below the recording site . After each processing step , PITSA displays the original trace together with the processed trace .

- Spectral analysis. The complex spectra of data traces can be calculated . The display of the resulting spectra can be done in either linear , logarithmic or mixed scales.

- Particle motion analysis : Particle motion plots are a powerful tools for signal analysis , useful for making an estimate for the direction of the incoming P phase or detecting shear wave splitting .

Phases can be picked from the particle motion plots .

- Trace utilities: A number of utilities in PITSA allow to perform simple mathematical operations on the traces , including adding and subtracting them , scaling them differently , and resampling at a different rate.

2.4.2. IASPEI'S VOLUME 2 TOOLBOX OF PLOTTING AND DISPLAYING SEISMIC AND OTHER DATA

This is a very useful toolbox which consists of PixPLot, PenPlot, GoPlot, RecSec, Acrospin and DoPlot modules, which were designed to plot seismic data. A brief explanation of each module is as follows.

PixPlot is a stand-alone plotting program for X-Y type plots on the computer's screen. Plotting instructions are very easy to use. A command file should be created (it is ASCII) to be inputted to the PixPLot. The data to be plotted can be either in ASCII or binary format. To prepare an ASCII command file any text editor can be utilized provided no formatting is done. To obtain a hard copy Epson or IBM Proprinter dot matrix printer can be used.

PenPlot is designed to work with PixPlot program. As for PixPlot a command file in ASCII should be prepared to include the necessary instructions and/or data to be plotted. A Hewlett Packard pen plotter connected to the PC can plot 150 data points per minute. Before plotting a final copy on HP plotter it is a good practice to plot it on the screen by PixPlot. This allows one to make necessary correction and changes.

GoPlot provides a menu driven interface to PixPlot. It is designed to plot data quickly in a menu driven environment.

The RecSec program module was designed to plot record sections from seismic refraction data. Since the reflection and refraction data are of SEGY (or similar) format, the foreign data sets should be converted to this format. Plots of this program can go either to a graphic screen or to a Houston Instruments DMPL plotter. It has no capabilities for filtering, stacking, applying statistics or making variable area plots.

The AcroSpin package allows one to rotate, translate and scale 3D wire frame objects. In seismological application the SpinSum program can convert the hypocenter data to

AcroSpin format and supports Hypo71, Hypo71PC, Hypoellipse, Hypoinverse, PDE and EDR formats.

The DoPlot program is a control program that links a text editor with PixPLot in an integrated environment so that one stays in DoPLot while editing data and commands as well as plotting data.

In our research work we mainly used PixPlot and PenPlot to generate the plots of the digitized, filtered traces as well as the spectra of all of the earthquake analyzed.

2.5. THOMSON-HASKELL MATRIX PROGRAM TO CALCULATE THEORETICAL SPECTRA

The mathematics of the program is given in Chapter 3. The set of programs calculate the theoretical spectra for a given earth model at the surface of the earth. There may be as many layers as one wishes. The layers are assumed to be horizontal, isotropic, homogeneous. The seismic velocities are taken to be constant in each layer. The input to the programs is a P wave emerging at the bottom of the crust and passing through it. The frequency band is controllable and usually matches the frequency pass band of the seismograph.

The theoretical spectrum is correlated with the observed spectrum. The layer parameters are systematically modified one at a time to obtain a maximum correlation coefficient. The model yielding this maximum is taken to be the representing model.

Information about running the programs is given within the programs as comments. Appendix VI. lists the programs.

CHAPTER 3.

METHODOLOGY

3.1 MATHEMATICAL BACKGROUND

The seismic energy radiated from a seismic source is a function of both time and space. The characteristics of a seismogram depend on the source function, properties of the propagation path, crustal structure under the receiving station and the characteristics of the recording system. The propagation of seismic wave from the source to a seismic station can be thought as a system of cascaded filters (linear systems) as illustrated in Figure 3.1.

INPUT	FILTERS	OUTPUT

$$X(\omega) \,.\, H_1(\omega) \,.\, H_2(\omega) \,.\, H_3(\omega) \,.\, H_4(\omega) \ldots\ldots H_n(\omega) = Y(\omega)$$

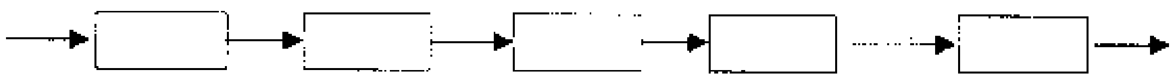

$$x(t) * h_1(t) * h_2(t) * h_3(t) * h_4(t) * \ldots\ldots * h_n(t) = y(t)$$

Figure 3.1. Illustration of a linear cascaded system

In any linear system the system characteristics can be determined if the relation between input and the output is known. The transfer function of a linear system is defined as the ratio of the Fourier, Laplace or z-transform of the output to that of the input. If input x(t) and the output y(t) have transforms $X(\omega)$ and $Y(\omega)$, respectively, and the impulse response function h(t) has $H(\omega)$ then the transfer function can be written as

$$H(\omega) = Y(\omega)/X(\omega) \tag{3.1}$$

The output in seismograph system is the record resulting from the propagation of an input wave, x(t), through a linear elastic medium which can be represented as a convolution of the input motion with the impulse response function h(t) of the medium.

$$y(t) = \int_{-\infty}^{\infty} h(t)\, x(t-\tau)\, d\varepsilon \tag{3.2}$$

or

$$y(t) = h(t) * x(t)$$

where * denotes the convolution operation.

In the frequency domain the convolution operation becomes a multiplication;

$$Y(\omega) = X(\omega) \,.\, H(\omega) \tag{3.3}$$

Here $Y(\omega)$ is the frequency response of the medium to the input motion x(t) which has transform $X(\omega)$

In the foregoing analyses the transfer functions of any horizontally layered crustal model are the basis for obtaining theoretical spectral responses of the earth systems. The spectra at the surface for incident plane wave for any angle of incidence can be computed. Then the spectra at the free surface are the product of the source spectrum, transmission characteristics of the transmitting media before the crust, the response of the crust and the recording system.

In order to eliminate the unknown functions, the spectral ratio of the vertical to the horizontal component are taken, assuming the source spectra, the transmission characteristics of the transmitting media and the instrument responses are the same for both.(vertical and horizontal components).

The vertical and horizontal spectral amplitude components of the body waves at the free surface can be written as:

$$Z(\omega) = A_0(\omega) \cdot C_z(\omega) \cdot I(\omega) \qquad (3.4)$$

$$H(\omega) = A_0(\omega) C_h(\omega) \cdot I(\omega)$$

where $C_z(\omega)$ and $C_h(\omega)$ are the vertical and horizontal crustal transfer functions computed by the matrix formulation, $A_0(\omega)$ is the body wave spectrum incident at the base of the crust, and $I(\omega)$ is the amplitude response of the recording system. Because the instrument responses of both vertical and horizontal seismograph systems are same, we can eliminate them by dividing $Z(\omega)$ by $H(\omega)$ and obtain the theoretical crustal transfer ratio $T(\omega)$ which is independent of $A_0(\omega)$ and $I(\omega)$, Hasegewa (1971).

$$T(\omega) = \frac{Z(\omega)}{H(\omega)} = \frac{C_z}{C_h} \qquad (3.5)$$

This procedure then provides more localized crustal information than the surface wave dispersion methods which give crustal models representing total earth structure averaged over the propagation path. It should be remembered that this transfer function is a function of the angle of emergence of the P waves at the bottom of the crust and the characteristics of the propagation path.

It is generally assumed that the earth's crust is made of horizontal, homogeneous, isotropic layers that has its system function that can be used to find the response of the crustal structure. In practice, for known horizontal and vertical component ground motion the left hand side of Equation (3.5) can be computed and compared with the right hand side which represent the theoretical transfer function of a particular crustal model. In equation (3.5) the nature of the input motion is generally not known. However, if the source function for the radial and vertical components are assumed to be the same, then by working with the ratios, the unknown effects of source function, properties of the medium traversed can be eliminated.

3.2. DEVELOPMENT OF THOMSON-HASKELL MATRIX FORMULATION

In large number of problems the earth is regarded as a vertically inhomogeneous half space. However, the theory of wave propagation for such a model is very difficult and has not been developed well. This earth model, in turn , can be approximated by a large number of plane, parallel and homogeneous layers. The elastodynamic equation can be solved for each layer. The wave motion should satisfy the elastodynamic equation with appropriate boundary conditions, i.e., continuity of stress and displacement at each interface.

For solving problems for such a multilayered earth system Haskell (1953) developed a matrix method following Thomson's (1950) approach. In the calculations of the dispersion of Rayleigh waves in a layered medium, the dependence of phase velocity on the wave length is expressed by the vanishing of a certain determinant, whose elements are functions of the phase velocity, wave length, and the densities and elastic moduli of the layers.

The determinant is six-by-six in the case of Rayleigh waves on a two-layer half space. For an n-layered half space the boundary conditions would yield a square determinant of the order (4n-2). Even for a rather small n, the computation of such a determinant solving for (angular frequency) as a function of c (phase velocity) would be tremendous.

To get around this (to overcome this) Thomson (1950) formulated the problem in terms of matrices and developed a method which is very useful for computations.

Let us consider a medium consisting of 2 solid half spaces separated by system of (n-1) solid layers as shown in Figure 3.2. This yields a total of (n+1) layers all of which are isotropic, homogeneous within itself and are separated from their neighbor and differ physically.

We denote the upper half space " layer 0" and the lower space "layer n". The interface "m" designates the boundary between layer m and layer (m+1). The x-axis is taken parallel to the

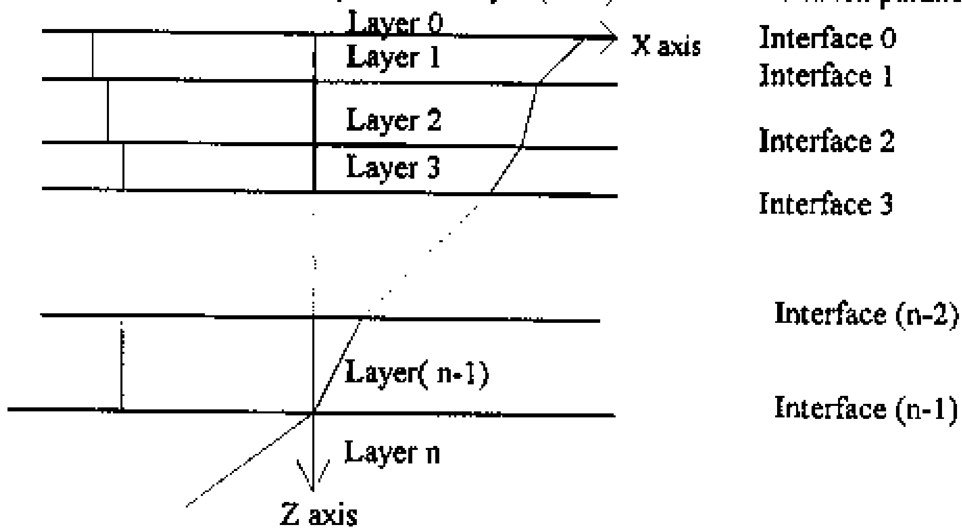

Figure 3.2. Layered earth model for the development of the matrix formulation

layer with the positive sense in the direction of propagation. The positive z-axis is taken as directed into the medium. It is assumed that all wave motion to be in the x-z plane so that all partial derivatives with respect to they-direction vanish.

We let, for the m the layer

ρ_m : density

d_m : thickness

λ_m, μ_m : Lame elastic constants

$\alpha_m = \left[(\lambda_m + 2\mu_m)/\rho_m\right]^{1/2}$

$\beta_m = \left[\mu_m/\rho_m\right]^{1/2}$

$k = \omega/c = 2\pi$ / wave length = wave number

$k_\alpha = \omega/\alpha$

$k_\beta = \omega/\beta$

Let us assume a time harmonic plane wave with displacement vector $\bar{s} = (u,0,w)$

The Helmholtz equations for the elastic potentials are;

$$(\nabla^2 + k_\alpha^2)\varphi = 0 \qquad (\nabla^2 + k_\beta^2)\psi = 0 \tag{3.6}$$

Since the boundary conditions must be satisfied everywhere, the apparent phase velocity in the x direction is constant as a consequence of Snell's law. Assuming the wave propagation in the positive x-direction, the solution to the equation of elastodynamics, in terms of potentials are;

$$\begin{aligned} \varphi &= [A' \exp(ikaz) + A'' \exp(-ikaz)] \exp ik(ct - x) \\ \psi &= [B' \exp(ikbz) + B'' \exp(-ikbz)] \exp ik(ct - x) \end{aligned} \tag{3.7}$$

where

$$a = \begin{cases} +\left[(c/\alpha)^2 - 1\right]^{1/2} & c\rangle\alpha \\ -i\left[1 - (c/\alpha)^2\right]^{1/2} & c\langle\alpha \end{cases} \qquad b = \begin{cases} +\left[(c/\beta)^2 - 1\right]^{1/2} & c\rangle\beta \\ -i\left[1 - (c/\beta)^2\right]^{1/2} & c\langle\beta \end{cases} \tag{3.8}$$

Each of which may be written in the form;

$$\varphi = \{(A'+A'') \cos kaz + i\,(A'-A'') \sin kaz\} \exp ik\,(ct-x) \tag{3.9}$$

The stress-strain relations and the displacement components which are pertinent to the boundary conditions are, in terms of the potential functions,

$$\sigma_{zz} = -\lambda\, k_\alpha^{\,2}\varphi + 2\mu\left(\frac{\partial^2\varphi}{\partial z^2} + \frac{\partial^2\psi}{\partial x\partial z}\right), \qquad \sigma_{xz} = \mu\left(2\frac{\partial^2\varphi}{\partial x\partial z} + \frac{\partial^2\psi}{\partial x^2} - \frac{\partial^2\psi}{\partial z^2}\right) \tag{3.10}$$

$$u = \frac{\partial\varphi}{\partial x} - \frac{\partial\psi}{\partial z}\,, \quad w = \frac{\partial\varphi}{\partial z} + \frac{\partial\psi}{\partial x} \tag{3.11}$$

Letting $C' = (A' + A'')$, $C'' = (A' - A'')$, $D' = (B' + B'')$, $D'' = (B' - B'')$

we can substitute the solutions into these relations and write, since exp ik (ct-x) is a common factor,

$$
\begin{aligned}
iku / k^2 &= \dot{u} / ck^2 = (C' \cos kaz + iCC'' \sin kaz) + b(D'' \cos kbz + iD' \sin kbz) \\
ikw / k^2 &= \dot{w} / ck^2 = -a(C'' \cos kaz + iC' \sin kaz) + (D' \cos kbz + iD'' \sin kbz) \\
\sigma_{zz} / k^2 &= \rho(2\beta^2 - c^2)(C' \cos kaz + iC'' \sin kaz) + 2\rho\beta^2 b(D'' \cos kbz + iD' \sin kbz) \\
\sigma_{xz} / k^2 &= 2\rho\beta^2 a(C'' \cos kaz + iC' \sin kaz) + \rho\beta^2 (b^2 - 1)(D' \cos kbz + iD'' \sin kbz)
\end{aligned}
\qquad (3.12)
$$

where $\dot{u} = i\omega u$ and $\dot{w} = i\omega w$ since the wave is time-harmonic.

We can write these four equations in vector notation as

$$(1 / k^2)\, \overline{U} = M\, \overline{C} \quad or$$

$$(1/k^2)\cdot \begin{bmatrix} iku \\ ikw \\ \sigma_{zz} \\ \sigma_{xz} \end{bmatrix} = \begin{bmatrix} C' \\ C'' \\ D'' \\ D' \end{bmatrix} \qquad (3.13)$$

where M is a four-by-four matrix.

$$
\begin{bmatrix}
\cos kaz & i \sin kaz & b \cos kbz & ib \sin kbz \\
-ia \sin kaz & -a \cos kaz & i \sin kbz & \cos kbz \\
\rho(2\beta^2 - c^2) \cos kaz & i\rho(2\beta^2 - c^2) \sin kaz & 2\rho\beta^2\, b \cos kbz & 2i\rho\beta^2\, b \sin kbz \\
2i\rho\beta^2\, a \sin kaz & 2\rho\beta^2\, a \cos kaz & i\rho\beta^2\, (b^2 - 1) \sin kbz & \rho\beta^2\, (b^2 - 1) \cos kbz
\end{bmatrix}
$$

We have not yet specified the location of the z = 0 plane so we will now set it coincident with the (m-1) interface which is the boundary between layer (m-1) and layer m. Across this interface the boundary conditions specify that $\overline{U}_{m-1} = \overline{U}_m$. The matrix relation for $\overline{U}_m$ is $(1/k^2)\overline{U}_m = M_m \overline{C}_m$ or, denoting at z = 0 as E_m,

$(1/k^2)\overline{U}_m = E_m \overline{C}_m$ where E_m is the four-by-four matrix;

$$\begin{bmatrix} 1 & 0 & b_m & 0 \\ 0 & -a_m & 0 & 1 \\ \rho_m(2\beta^2_m - c^2) & 0 & 2\rho_m\beta^2_m b_m & 0 \\ 0 & 2\rho_m\beta_m^2 a_m & 0 & \rho_m\beta^2_m(b^2_m - 1) \end{bmatrix} \qquad (3.15)$$

If the boundary conditions are to be satisfied, it must also be true that, at z = 0,

$(1/k^2)\overline{U}_{m-1} = E_m\overline{C}_m$

We have now related $\overline{U}_{m-1}$ to $\overline{C}_m$ and therefore have established a relation between one layer and the next.

Since $\overline{C}_m$ constant throughout layer m , the relation $(1/k^2)\overline{U}_m = M_m\overline{C}_m$ is valid everywhere in that layer. If the thickness of the layer is d_m, the value of z at the bottom of the layer is z = d_m, and we can write the matrix expression at the interface m as

$(1/k^2)\overline{U}_m = D_m\overline{C}_m$ where $D_m = M_m$ at z = d_m . Making use of the inverse matrix, we can solve the relation at the interface (m-1) to obtain

$$\overline{C}_m = E_m^{-1}\cdot(1/k^2)\overline{U}_{m-1} \qquad (3.16)$$

and substitute this into the expression at the interface m for the result;

$$(1/k^2)\overline{U}_m = D_m E_m^{-1}\cdot(1/k^2)\overline{U}_{m-1} \qquad (3.17)$$

where the values of the U's are those values at the bottom of their respective layers. Letting

$A_m = D_m E_m^{-1}$ we can write this in the simplified form

$$\overline{U}_m = A_m\overline{U}_{m-1} \qquad (3.18)$$

The four-by-four matrix A_m is related to the physical parameters of layer m and contains as variables the apparent phase velocity, c, and the frequency, ω . It is important to note that only the thickness of the layer d_m, and not the variable z is involved. Since this is the case , the same reasoning would hold for any layer and we can write $\overline{U}_i = A_i\overline{U}_{i-1}$.

Hence, we situate the z=0 plane at the interface and write $\overline{U}_1 = A_1\overline{U}_0$ which , by substitution, yields $\overline{U}_2 = A_2A_1\overline{U}_0$ .We see that we can propagate the vector $\overline{U}$ through any layered system by the repeated matrix product operation

$$\overline{U}_m = A_m A_{m-1}\cdots A_1\overline{U}_0 \qquad (3.19)$$

where $\overline{U}_m$ is the value at the bottom of the m th layer and $\overline{U}_0$ is the value at the bottom of the upper half space. For the layered system we originally assumed, we can write this transfer function as

$$\overline{U}_{n-1} = \prod_{k=1}^{n-1} A_k \overline{U}_0 \qquad (3.20)$$

where $\prod_{k=1}^{n-1} A_k$ is a four-by-four matrix, being a product of four-by-four matrices.

We need a function to propagate the amplitude vector $\overline{C}$, however. We obtain this by substituting the relations

$$\overline{C}_n = E_n^{-1} \cdot (1/k^2)\overline{U}_{n-1} \quad \text{and} \quad (1/k^2)\overline{U}_0 = D_0 \overline{C}_0 \qquad (3.21)$$

into the above transfer function and arriving at the expression

$$\overline{C}_n = E_n^{-1} (\prod_{k=1}^{n-1} A_k) D_0 \overline{C}_0 \qquad (3.22)$$

which allows us to propagate the amplitude from one half space to the other. This relation yields four equations which may be solved for two reflected amplitudes and the two transmitted amplitudes. As an example, for a P wave incident from below, $A''_0 = B_0'' = 0$ and the quantities solved for are A_n''/A_n', B_n''/A_n' , A_0'/A_n' and B_0'/A_n'.

If the upper half space is fluid (the earth's core, for example), only P waves will be transmitted and the theory must be adjusted slightly. The tangential stress is zero at the solid-liquid interface and the matrix for the fluid layer is in a somewhat different form than derived here.

If the upper half space is vacuum i.e., the earth's surface, both the normal and shear stresses must vanish at the free surface. In this case we have

$$\overline{U}_0 = (1/k^2)\left[iku_0, ikw_0, 0, 0\right] \qquad (3.23)$$

which simplifies matters somewhat. The transfer function is then ;

$$\overline{C}_n = E_n^{-1} (\prod_{k=1}^{n-1} A_k)\ (1/k^2)\overline{U}_0 = J(1/k^2)\overline{U}_0 \qquad (3.24)$$

where J is defined by;

$$J = E^{-1}(\prod_{k=1}^{n-1} A_k (1/k^2) \qquad (3.25)$$

The matrix equation (3.25) can be decomposed into the following four equations under the applicable boundary conditions noting that $u = i\omega u$

$$A'+A''= 1/k^2 (\frac{u_0}{c} J_{11} + \frac{w_0}{c} J_{12}) \qquad (3.26)$$

$$A'-A''= 1/k^2 (\frac{u_0}{c} J_{21} + \frac{w_0}{c} J_{22}) \qquad (3.27)$$

$$B'-B''= 1/k^2 (\frac{u_0}{c} J_{31} + \frac{w_0}{c} J_{32}) \qquad (3.28$$

$$B'+B''= 1/k^2 (\frac{u_0}{c} J_{41} + \frac{w_0}{c} J_{42}) \qquad (3.29$$

For the case of an incident P wave of unit amplitude in n'th layer A' and B' will respectively have the values of 1 and 0. Solving equations (3.26 to (3.29) simultaneously, we get,

$$\frac{u_0}{c} = 2D^{-1}(J_{32} - J_{42}) \qquad (3.30)$$

$$\frac{w_0}{c} = 2D^{-1}(J_{41} - J_{31}) \qquad (3.31)$$

$$A''=D^{-1} \ [(J_{11}+J_{21})(J_{32}-J_{42})-(J_{12}+J_{22})(J_{31}-J_{41})] \qquad (3.32)$$

$$B''=2D^{-1} \ (J_{32}J_{42}-J_{31}J_{42}) \qquad (3.33)$$

where

$$D = (J_{11}-J_{21})(J_{32}-J_{42})-(J_{12}-J_{22})(J_{31}-J_{41}) \qquad (3.34)$$

Using the E_m matrix in Equation (3.15)

$$\frac{u_{m-1}}{c} = -(\frac{\alpha_m}{c})^2 (A'+A'') - \upsilon_m b(B'-B'') \qquad (3.35)$$

$$\frac{w_{m-1}}{c} = -(\frac{\alpha_m}{c})^2 a(A'-A'') + \upsilon_m (B'-B'') \qquad (3.36)$$

where $\upsilon_m = \frac{2\beta_m{}^2}{c^2}$.

Then the surface displacement can be calculated in terms of the input amplitude for vertical and horizontal components by dividing (3.30) by the coefficient of A" in (3.35) and dividing Equation (3.31) by the coefficient of A" in Equation(3.36). These are;

$$TU(\omega) = \frac{2c^2(J_{42} - J_{32})}{\alpha_n{}^2 D} \tag{3.37}$$

$$TW(\omega) = \frac{2c^2(J_{41} - J_{31})}{\alpha_m{}^2 r_{\alpha m} D} \tag{3.38}$$

The transfer functions for the vertical and horizontal components are the functions of P and S wave velocities, layer thicknesses and the layer densities, the angle of emergence of the plane wave at the base of the layered system and the frequency of the incident wave.

These equations have been coded for computers to calculate the theoretical spectra for P and S waves for given earth models.

3.3. CRUSTAL AND UPPER MANTLE STRUCTURE STUDIES USING THOMSON- HASKELL METHOD

Phinney (1964) used Haskell's matrix method to calculate the spectral response of a layered crust to compare observed long period P wave spectra from distant earthquakes recorded at Albuquerque and Bermuda. By taking the ratio of vertical spectrum to the horizontal he obtained a function that depended on the structure beneath the station. He applied a power spectrum analysis and a lag window to minimize the effects of portion of signals right after the P phase. The crust under Albuquerque was found to be 40 km thick and the P wave velocities in lower crust ranged between 6.6 to 7.0 km/sec. For Bermuda he obtained a 12 km thick normal oceanic crust, depressed elastically by the weight of the volcanics making up the island.

In order that the method be of practical use, the theoretical curves must be neither too sensitive nor too insensitive to changes in the model parameters. Enough data must also be collected so that they can be assessed for repeatability and variability.

The theoretical properties of the transfer ratio can be summarized as follows.

1. The effects of intermediate and deep crustal structure can be isolated in the behavior of the three crustal peaks in the transfer ratio. The positions of these peaks are neither too sensitive nor insensitive to reasonable variations in structure. The upper frequency limit of 0.2 Hz. is sufficient to include all frequencies which can reasonably investigated using standard long period recordings.

2. The peak positions are insensitive to changes in phase velocity. Therefore this can be ignored and data from a large range of distances can be utilized.

3. A thin low-velocity surface layer has no effect on the crustal peaks. The thicknesses large than 3 or 4 km. have an effect.

Hannon (1964) used the Thomson-Haskell method to compute the synthetic surface motion due to the dilatational waves striking the base of a layered system. He constructed theoretical seismograms from the transmission coefficients of crustal models.

Leblanc (1967) studied the effects of truncation of the seismic signal (the effect of time window) on the crustal transfer functions. Imposing a time window on the signal to minimize the effects of later arrivals such as pP and PcP reduces the duration of the signal which in turn affects the spectra. He attempted to show that crustal transfer functions extracted from the short period data may be used to determine fine structures.

The short period teleseismic events that were recorded on the deep horizontal sediments of central Alberta were analyzed by Ellis and Basham (1968) to test the Thomson-Haskell matrix method. They concluded that in the areas with horizontally layered sediments the theory is not fulfilled due to scattering and anomalous PS conversions in the crust and upper mantle.

Using the matrix method Fernandez and Careage (1968) determined the crustal thicknesses for the central United States and La Paz, Bolivia. They averaged the several observations and obtained 42. For the crustal thickness in the central United States with P wave velocity of 6.6 km/s. For the Bolivian Andes at La Paz, they obtained a crustal thickness of 64 km. and P wave velocity of 6.7 km./s. Their results agreed with similar determinations using independent methods. They concluded that in order to use the P wave spectra in all determinations, earthquakes of magnitude 6 and above may be used at teleseismic distances of 2000 to 6000 km. The focal depths are not critical and shallow depth earthquakes may be used but deeper events are preferable

The method was successfully utilized by many investigators. Necioglu (1969) used S waves recorded at LRSM (Long Range Seismic Measurements) stations in the U.S. to infer the crustal and upper mantle structure beneath some stations. Bonjer et al. (1970) studied the crustal structure under the East African Rift system. Hasegewa (1971) studied the structure under the Yellowknife area in Canada. Kurita (1972a, b, c) obtained the crustal structure down to 220 km. in the central and western United States

Turkelli (1984) made use of the digital P wave data of Seismic Research Observatories (SRO) ANTO station to determine the crustal structure in central Anatolia using the matrix formulation. His results were consistent with those determined from the travel time data of Turkish earthquakes (Necioglu et al., 1981).

3.4. DIGITIZATION OF SEISMOGRAMS

Sigma Scan PC PROGRAM has been applied using the scan jet IIP table for hand digitization channel by channel (tens of points per wave) using the SIGMA SCAN software. While using the SIGMA-SCAN digitizer, there is no need to do any of seismogram coordinate system corrections.

The digitization includes several steps; seismogram preparation and manipulation, calibration of seismogram for time and amplitude scale, digitization of the traces and related time marks and file organization.

Seismogram preparation is carried out as follows;

- seismogram is aligned parallel to the edge of the digitizing table,
- three minute marks are marked ant their coordinates are determined
- a reference line is drawn for the seismic trace,
- the length of the selected minute marks is measured,
- a line perpendicular to the reference line is drawn from the minute mark and its length is measured,

Seismogram manipulation includes the following;

- the length of the digitization window is not less than two minutes with three time marks and it is the same for all 3 seismograms (vertical, north-south and east-west)
- several tens of points per wave were digitized to minimize the folding effect i.e., to increase the Nyquist frequency ($N_q = 1/2\Delta t$) , where Δt is the digitizing interval.
- digitization usually started at the first minute mark prior to P-onset (at least 30 seconds earlier than the first P-wave arrival time) and continued for another 40 seconds or less.

Calibration of the seismogram.

The X and Y coordinates of the signal and the time marks have to be calibrated before starting digitizing. This is done by entering the values of X and Y for the three points and defining the units and sampling rate.

The digitization starts at the first minute mark before the signal and continues until the third minute mark after the P wave portion of the signal.

Finally, the digitized 3-components data for each event stored as a raw data to be analyzed by the digital data processing program (SEISDIG).

After completing the digitization process, SEISDIG program was applied for editing individual traces and evidently misplaced data points and other corrections for each event as follow:

1.-pen curvature correction data from RYD station (long and intermediate) are recorded by a curvilinear pen. By running pen curvature program and pen axis displacement correction program curvature is corrected.

2.-run negative loop correction to delete negative time loops generated during manual digitization.

3.-re-sampling by run equidistant correction program to re-sample trace with higher frequency than the average digitizing frequency (512 points).

Figure 3.3. shows original Riyadh long period seismograms, Figure 3.4 is the replot of the digitized seismograms for the same event as an example. The rest of the plots for the digitized seismograms are shown in Figures 3.5 to 3.44. in Appendix III.

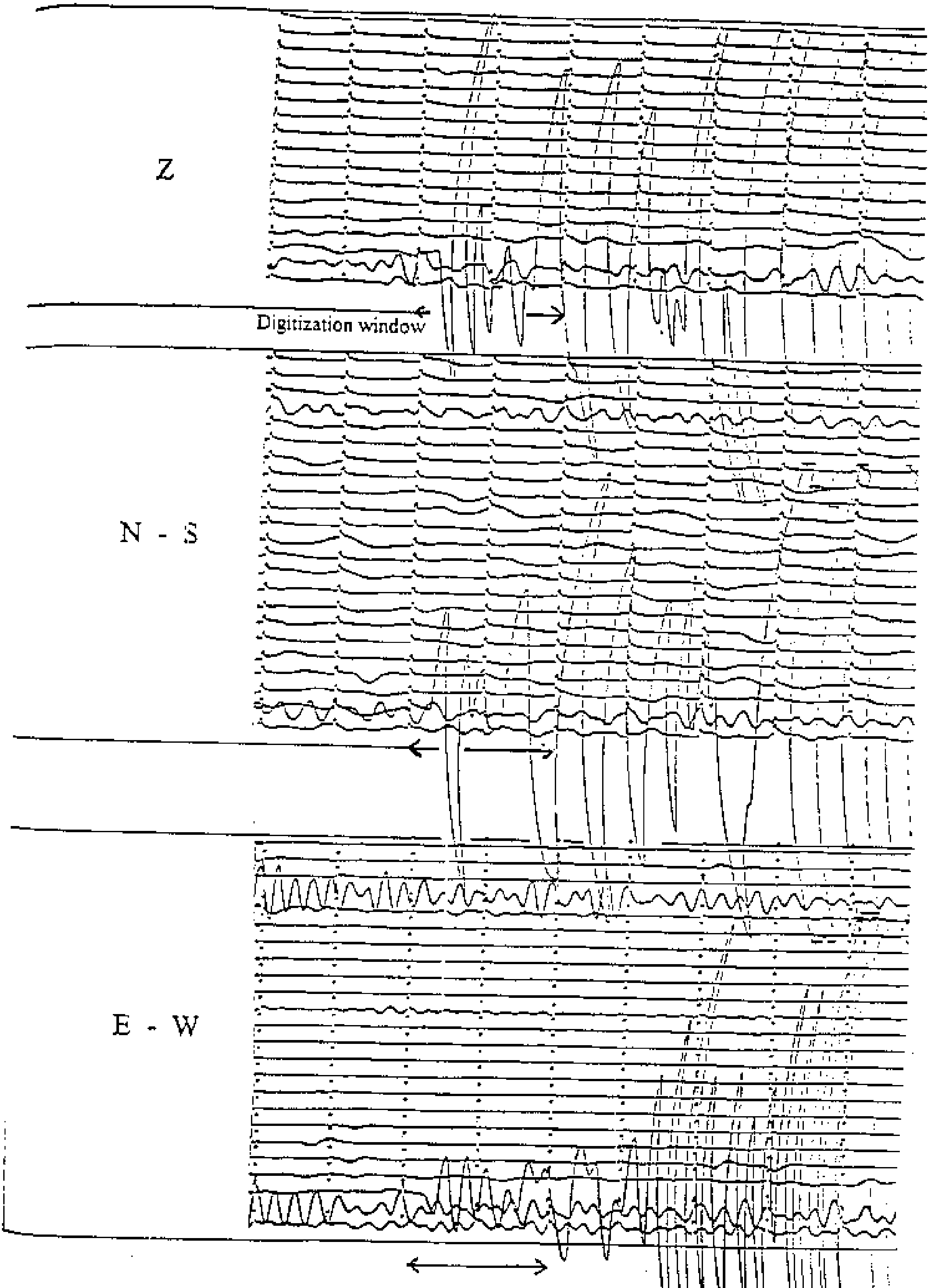

Figure 3.3. Copy of original Riyadh long period seismograms of the earthquake of December 7, 1988.

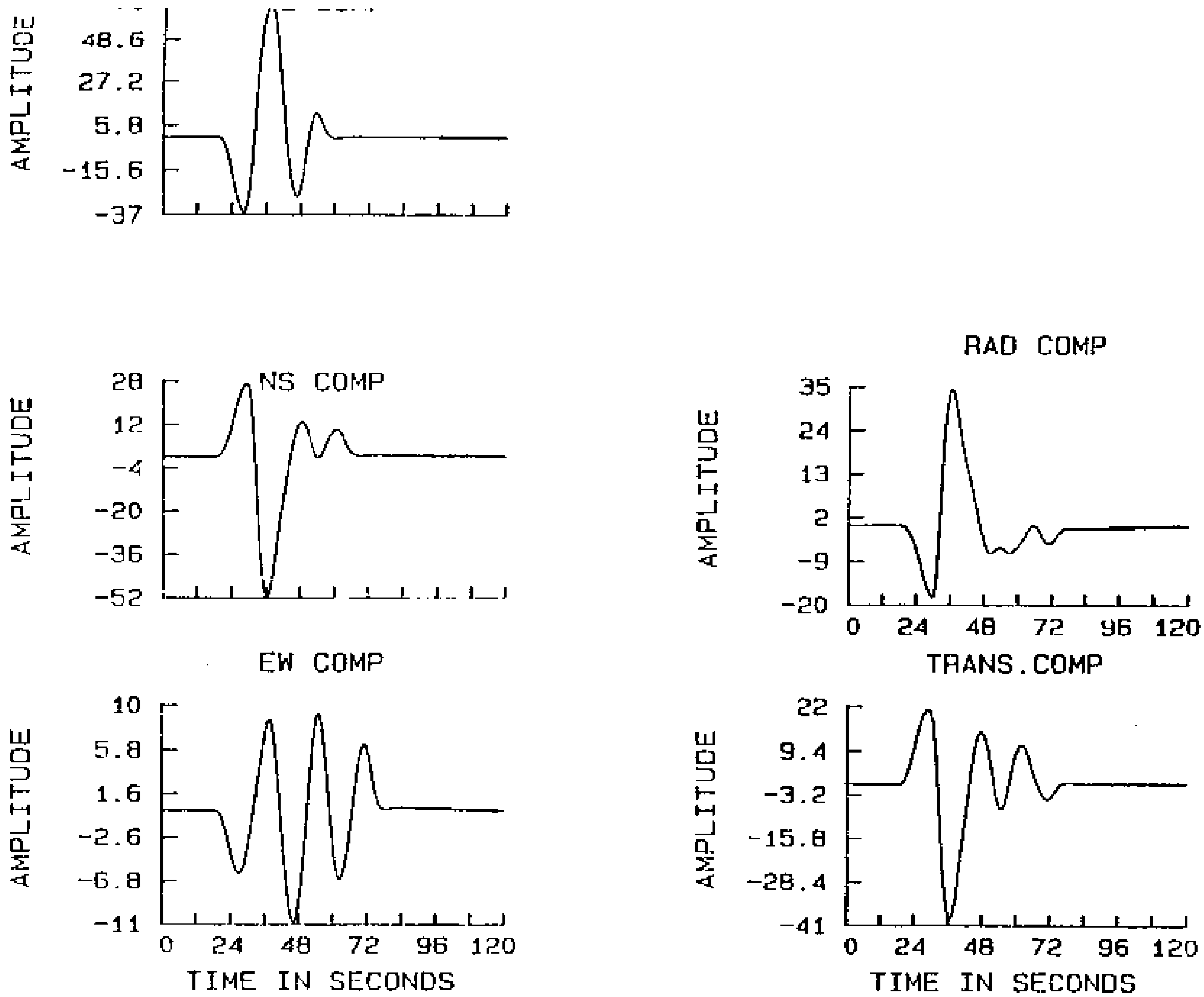

Figure 3.4. Replot of the digitized Riyadh long period seismograms of the earthquake of December 7, 1988.

CHAPTER 4.

DATA ANALYSES AND RESULTS

4.1. INPUT CRUSTAL MODEL

The generation of the theoretical spectra needs an earth model. We started out with the previously determined models. The results from the deep seismic refraction (Prodehl, 1985; Mooney et al, 1985) for central Saudi Arabia show a crustal thickness of about 40 km and an upper mantle velocity of 8.2 km/s. Prodehl (1985) showed a crustal velocity inversion at 10 -12 km depth beneath the Arabian platform and the Moho beneath the Arabian shield is not a first order boundary but rather a transition zone where the velocity increases rapidly from about 7.4 km/s to 8.2 km/s in a few kilometers.

Based on 2-D ray path interpretation of travel time and wave amplitude ratios, Badri (1991) showed that the crust consists of 4 distinct layers approximately 42 km-thick under the Arabian platform which, thins gradually in a southwest direction to about 38 km under the shield. The upper crust consists of 2 layers. The first one has a P wave velocity of about 6.08 km/s and is about 3 km thick and thins to about 1 km in the platform. The second layer has a P wave velocity of about 6.2 km/s and is about 14 km-thick which thins to about 7 km in the platform The intermediate crustal layer has a P wave velocity of about 6.43 km/s and is about 7.5 km thick in the shield and about 16 km-thick in the platform with a velocity about 6.38 km/s. The lower crust has a P wave velocity of 6.85 km/s and 15 km thickness.

A decrease in the upper mantle P_n velocity from 8.2 km/s to 8.15 km/s seems to accompany this crustral thinning. The Moho is sharply defined beneath the shield and gently dips towards the northeast.

Based on the afore-mentioned discussion, we have modified previous crustal models to test our theoretical spectra. It is assumed that there are no lateral variations in the velocity structure. The modified model is given in Table II.

TABLE II

PRELIMINARY MODIFIED CRUSTAL MODEL

THICKNESS KM	P WAVE VELOCITY KM/S	DENSITY GM/CM^3
5.0	4.95	2.10
8.0	5.40	2.30
12.0	6.62	2.50
18.0	7.40	2.90
999.0	8.20	3.08

This initial model indicates that both layer velocities and thicknesses were allowed to vary until a theoretical model was reached which fitted to the observed data. A little changes had to be made in parameters to obtain the best correlation coefficients. However, these variations were constrained by the lithological conditions. We found out that, adding a thin layer with P wave velocity of 5.7 km/s at the top of the model gives a good correlation. The model used afterwards is given in Table III. Below.

TABLE III.

THICKNESS KM	P WAVE VELOCITY KM/S	DENSITY GM/CM^3
2.0	5.7	2.10
10.0	6.1	2.30
8.0	6.35	2.50
12.0	6.80	2.70
12.0	7.45	2.90
999.0	8.20	3.08

4.2. CALCULATION OF THE SPECTRA

4.2.1. OBSERVED SPECTRA USING PITSA

The analyses of the digitized data were done using the PITSA program package.

The three seismogram components for each earthquake were treated simultaneously. The traces were filtered with a band-pass filter whose corner frequencies matched the instrument response curves . This eliminated the effect of signal components outside the pass band of the systems. Then the two horizontal components were rotated along radial and transverse directions. as shown in the sketch below.

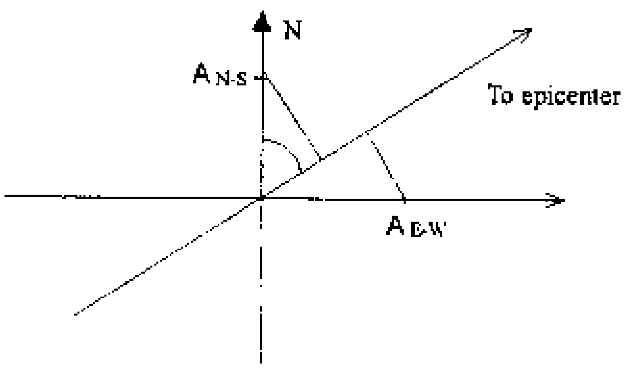

$$R(t) = A_{N-S}\cos(\theta) + A_{E-W}\sin(\theta)$$
$$T(t) = A_{N-S}\sin(\theta) - A_{E-W}\cos(\theta)$$

where θ is the back azimuth from station to the epicenter.

In order to minimize the later arrivals after the P a Hamming window is applied.

The Hamming window is defined as

$$h(t) = \begin{cases} .54 + 0.46\cos\pi(\frac{t}{T}) & 0 \le t < T \\ 0 & |t| \ge T \end{cases}$$

which has the Fourier transform as

$$H(\omega) = 0.54D(\omega) + 0.23[D(\omega + 1/2T) - D(\omega - 1/2T)]$$

where

$$D(\omega) = 2T\left(\frac{\sin \omega T}{\omega T}\right)$$

and ω is the angular frequency

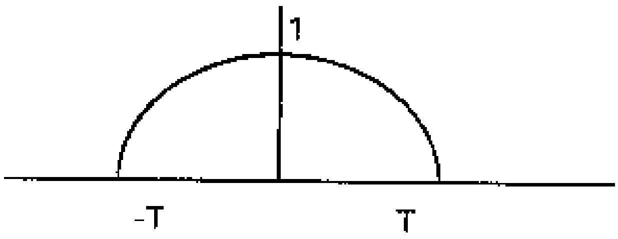

-The spectra for Z and R (radial) are obtained using FFT algorithm of the package.

-The ratio of the spectra of Z and R is obtained using the trace utilities menu of the PITSA.

A flowchart indicating the whole procedure is shown in Figure 4.1.

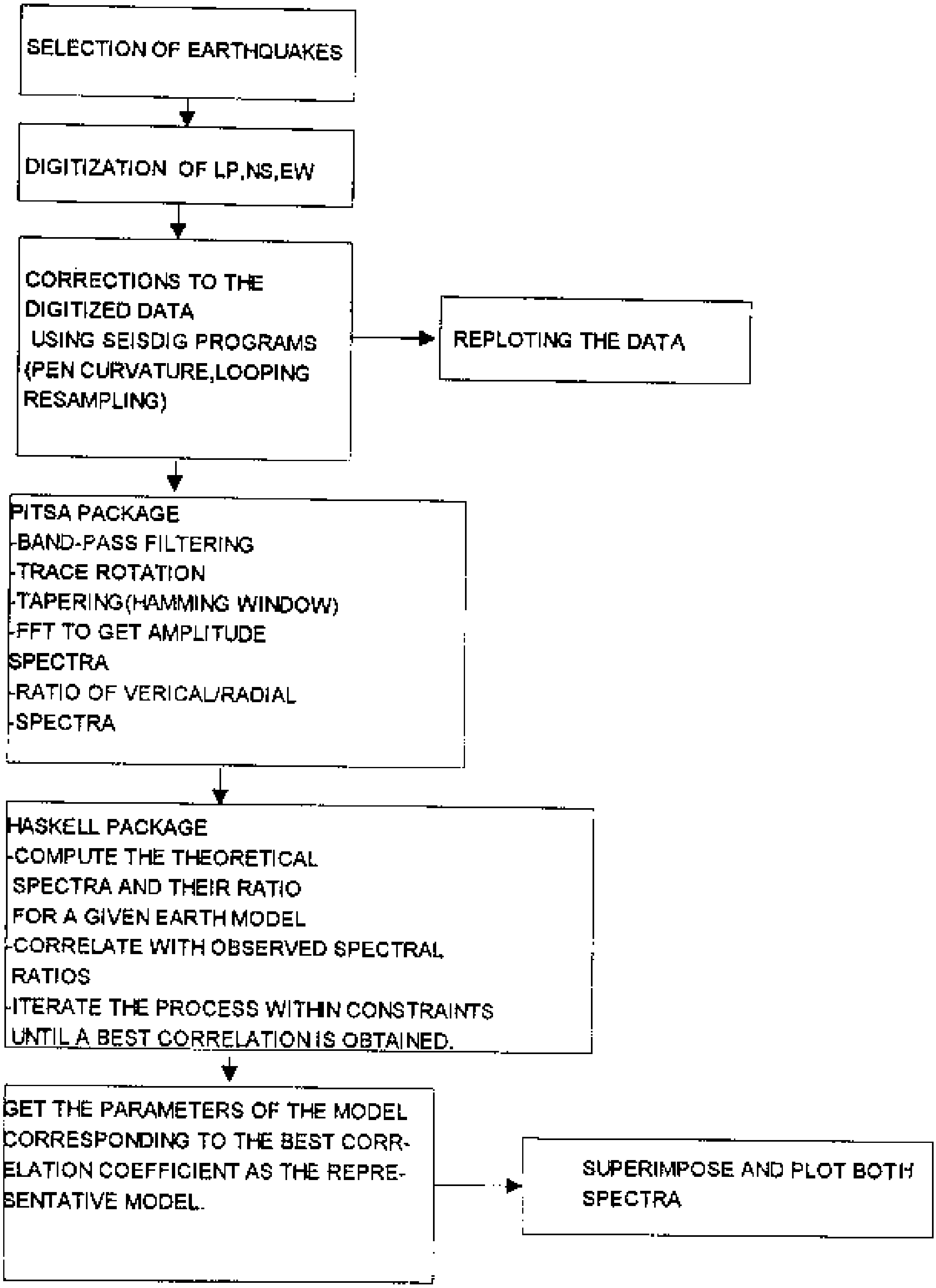

Figure 4.1. Flowchart of the processes

4.2.2. CALCULATIONS OF THE THEORETICAL SPECTRA

In order to generate the theoretical spectra of a given earth model, the Haskell's matrix formalism has been programmed by many investigators i.e., Fernandez (1965), Necioglu (1969), Turkelli (1984). Necioglu (1969) developed the programs to analyze long period S waves in connection to the crustal studies. Turkelli's (1984) programs were written for main frame computers. We adapted them to our PC.

The input to the program is as follows.

the earth model i.e., thickness, P wave velocity and density of each layer (S wave velocities are calculated within the program.

the desired frequency range; beginning frequency, frequency increment and the number of frequencies to be calculated

the angle of emergence, the increment of angle of emergence and number of angles of emergence to be calculated. Generally, the angle of emergence calculated for the Table 1 is the basis. A few degrees below and above are used to calculate the spectra.

Due to the memory, storage and time limitations of the earlier main frame computer the number of layers in the mathematical modeling of the crust and upper mantle were limited to 3. Now the programs can handle as many layers as one wishes. This is an advantage that the actual situation within the earth can better be approximated by having many thin isotopic, homogenous layers. Within each layer the elastic constants are considered to be constant.

4.2.3. CORRELATION OF THEORETICAL AND OBSERVED SPECTRA

The correlation of theoretical and observed spectral ratios are done by using the formulae in Chapter 3.

The effect of different model parameters on the theoretical spectra was tested by first keeping thickness of the first layers and angle of emergence constant and varying the velocities. Then the velocities and angle emergence were kept constant but the thicknesses varied; finally thicknesses and velocities were kept constant and angle of emergence varied. Figures 4.2-4.8 in Appendix IV show these effects.

The observational and the best correlating theoretical spectral ratios for all the events analyzed are presented in Figures 4.10 to 4.50.

4.3. SOURCE OF ERRORS

In the following sections we discuss the sources that affect the results.

4.3.1. THE EFFECT OF THE SOURCE SPECTRUM

This unknown spectrum affects the frequency content of the P wave arriving to the station. However, working with spectral ratios, one can assume that this unknown effect is eliminated because of the similar character of the source spectrum for each component. But this effect may not be eliminated completely.

4.3.2. THE EFFECT OF CRUSTAL LAYERING AT THE SOURCE

Superposition of the inter-reflections in the source crust of the P wave motion may have an influence on the computed P wave spectra. This effect can be minimized by working with the earthquakes whose foci are beneath the crust. In this study we have not observed any obvious reverberations of this kind riding over P phase.

4.3.3. DIGITIZING ERRORS

The variations in the thickness of the trace can introduce errors both in amplitude and time. This effect was minimized by editing the traces after digitization.

There is an unknown distortion introduced into the records during recording and digitization. This distortion can be written as;

$f(t) = g(t) + e(t)$

where $f(t)$ is the digitized record,

$g(t)$ is the true ground motion and,

$e(t)$ is the error introduced during recording and digitizing.

In our study, we assumed that the linear trend of the baseline during the recording is small. We also assumed that the baseline is put parallel to the time axis. But there was an uncertainty in positioning the baseline. Although PITSA has a correction scheme to correct for baseline uncorrected small errors can contribute the spectrum at lower frequencies as follows.

Let $e(t) = A$ where A is an unknown horizontal shift of the baseline and we let $F(\omega)$ and $G(\omega)$ be the Fourier transforms of the $f(t)$ and $g(t)$, respectively. We can write;

$$F(\omega) = \int f(t) \exp(-i\ \omega)t\ dt = \int g(t)\ \exp(-i\ \omega)t\ dt + A \int \exp(-i\ \omega)t$$

$$= G(\omega) + a\ \pi\ \delta\ (\omega) + 2\ A/i\omega$$

Thus $G(\omega) = F(\omega) - 2\ A/i\omega$ since $\delta(\omega) = 0$ for $\omega \neq 0$.

This may be written as

$$G(\omega) = \mathrm{Re}\,[\,F(\omega)] + i\ \mathrm{Im}\,[\,F(\omega)] + 2\ i\ A/\ \omega$$

$$|\,G(\omega)\,| = \sqrt{\ \{\mathrm{Re}\,[\,F(\omega)]\}^2 + \{\,\mathrm{Im}\,[\,F(\omega)] + 2A/\ \omega\}^2}$$

It can be seen from this short explanation that at low frequencies the error due to a small error "A" in placing baseline can be considerably large.

4.3.4. ASSUMPTION OF HORIZONTAL CRUSTAL LAYERING

It is generally assumed that in the earth models the layers are horizontal, homogenous and isotropic. In the actual case dipping layers are present and may influence the crustal transfer functions. Some of the discrepancies between the observational and theoretical curves may be due to this effect.

4.4. SPATIAL DISTRIBUTION OF EVENTS

As previously mentioned, the frequency ranges of 0.06 Hz to 0.2 Hz are consistent with the instrument amplitude response (for long period seismographs) and 0.0166 Hz to 2.0 Hz (for intermediate period seismographs) cover a large number of frequencies that were present in the P-waves of the earthquakes analyzed. It also means that the Nyquist frequency is large enough to cause aliasing.

Forty events with depths from 20 to 250 km were analyzed to deduce the crustal structure under Riyadh station. Since the number of suitable events were limited, we were forced to include events with distances of less than 10^0 (minimum distance 8.6^0) and depths of less than 20 km. (minimum depth 10 km) and above 250 km. There was only one event with a depth of 600 km.

According to epicentral distribution and the geological settings of the study area, the analyzed events could be grouped with respect to their azimuth ranges as follows.

First group from 20^0 to 120^0 (north east and east)

Second group from 130^0 to 220^0 (south and southwest) and

Third group from 230^0 to 360^0 (northwest and north) .

Tables IV, V and VI list the events in each group. Figure 4.9 the polar plot of the events analyzed.

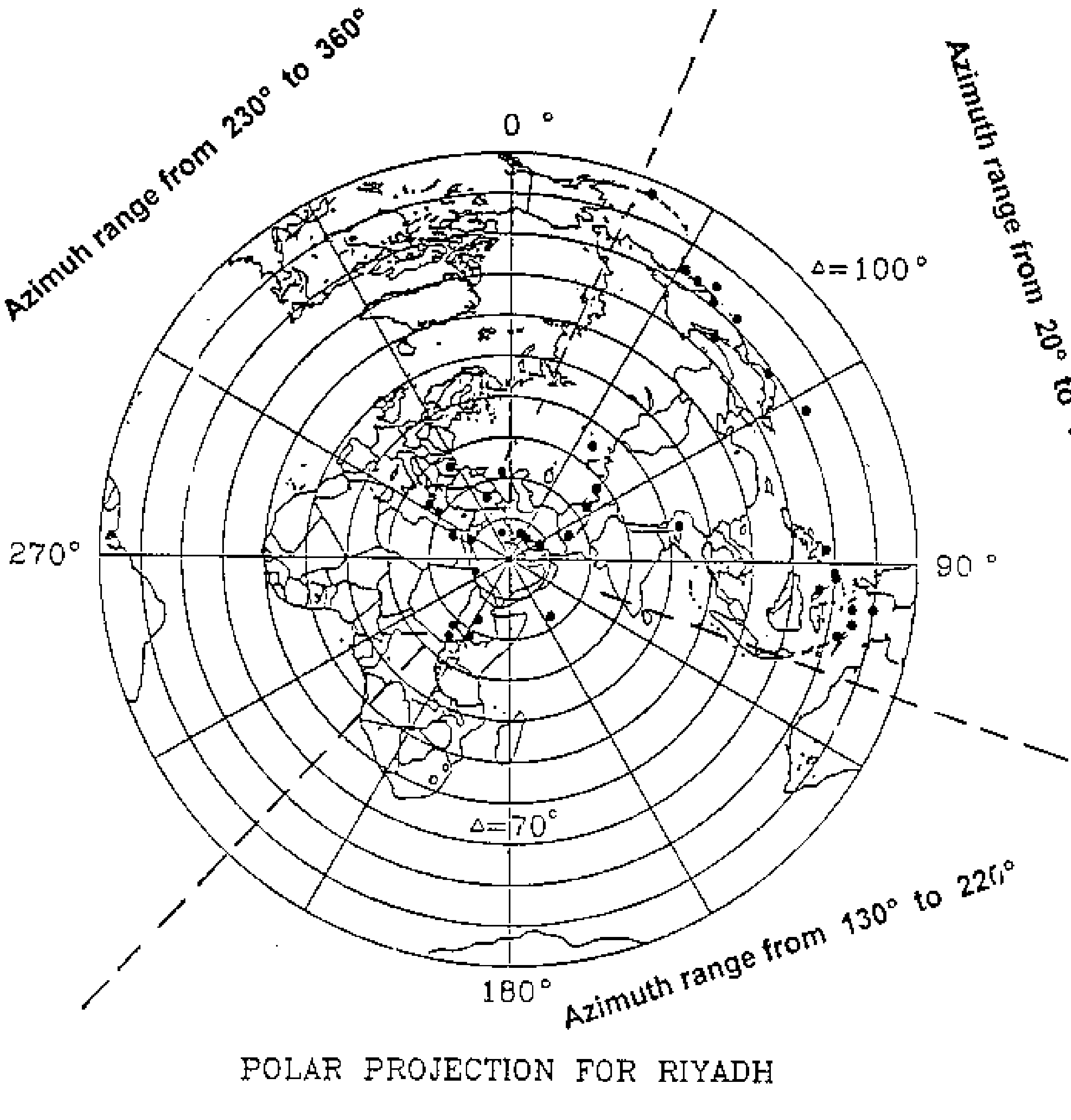

Figure 4.9. Polar projection of the analyzed earthquakes listed in Tables IV, V and VI.

4.4.1. EVENTS FROM AZIMUTHS 20^0 TO 120^0.

There were twenty-five events within the azimuths range between 20^0 and 120^0. The epicentral distances varied in the range 8.6^0 to 84^0 as shown in the Table I. Only 2 events were selected among the high correlation coefficients (above 0.85) and presented in this chapter. The models and spectral plots of these 2 events are shown in Figures 4.10 and 4.11. The rest of the events in this group with less correlation coefficients is presented in Figures 4.16 to 4.38 in Appendix V.

Characteristically, the spectral ratios, both observed and theoretical, in Figures 4.5, 16, 17, 20, 22, 23, 25, 27, 29, 30, 31, 32, 33, 34, 35, 36, 37, 38, 39 show a clear peak very close to 0.1 Hz. (0.09-0.12 Hz.). It is obvious that the ratio peaks shift towards the lower frequencies where the crust becomes thicker. The distant events Figures 4.18, 19, 20, 21, 24, 28, 29, 34, 36 show 2 more peaks at 0.13 and 0.15 Hz. These 2 peaks could be due to the contamination of the diffracted P waves when the epicenter has large distance.

Analyses of the twenty-six events show a range of P velocity of 5.35 to 5.85 km/s for the first 2 km. This velocity range represents an unconsolidated sedimentary material underlain by thicker layer with higher P velocity. The thickness of the second layer ranges from 7 to 11 km with P velocity range from 6.10 to 6.50 km/.s which represents consolidated materials. The third layer shows velocity range from 6.35 to 6.70 km/s with thickness of 5-8 km. The fourth layer shows a velocity range from 6.8 to 6.95 km/s with thickness of 12 to 17 km. The lower crustal P wave velocity shows a range of 7.40 to 7.60 km/s with thickness of 10 to 12 km. All models indicate a transition zone velocity between lower crust and upper mantle at a depth of about 43 to 46 km with P wave velocity of 8.20 km/s.

Generally, one-peak response (Figures 4.10 and 11) indicates a good P wave velocity contrast within the crustal layers(between upper and lower crust) and less contrast between lower and upper mantle (transition zone). The average model derived from this azimuth range is shown in Table IV.

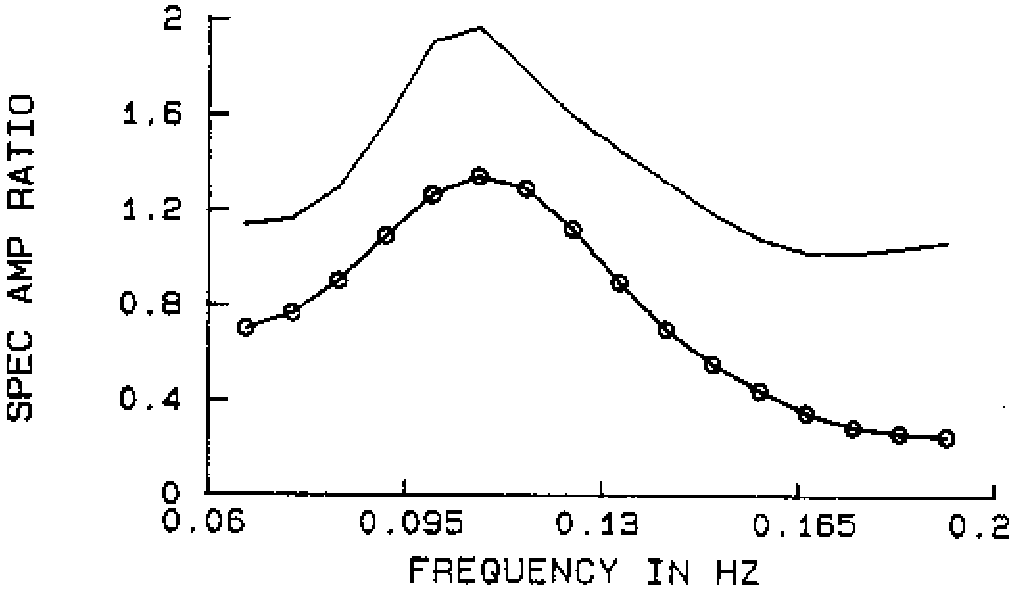

EPI. COORDINATES	28.24 N, 55.37 E
DISTANCE	8.6°
BACK AZIMUTH	64°
DEPTH	18 KM
MAGNITUDE(m_b)	5.4
ANGLE OF EMERGENCE	44°

THICKNESS (KM)	P VELOCITY (KM/S)	DENSITY (GM/CM^3)
2	5.6	2.1
8	6.6	2.3
7	6.7	2.5
17	7.05	2.7
11	7.6	2.90
999.00	8.30	3.08

CORRELATION COEFF= .93

Fig. 4.10 Plots of theoretical and observed spectral ratio for earthquake of Nov.06, 1990 (IRAN) and relevant information together with obtained crustal model. Open circles and solid lines represent observed and theoretical curves, respectively.

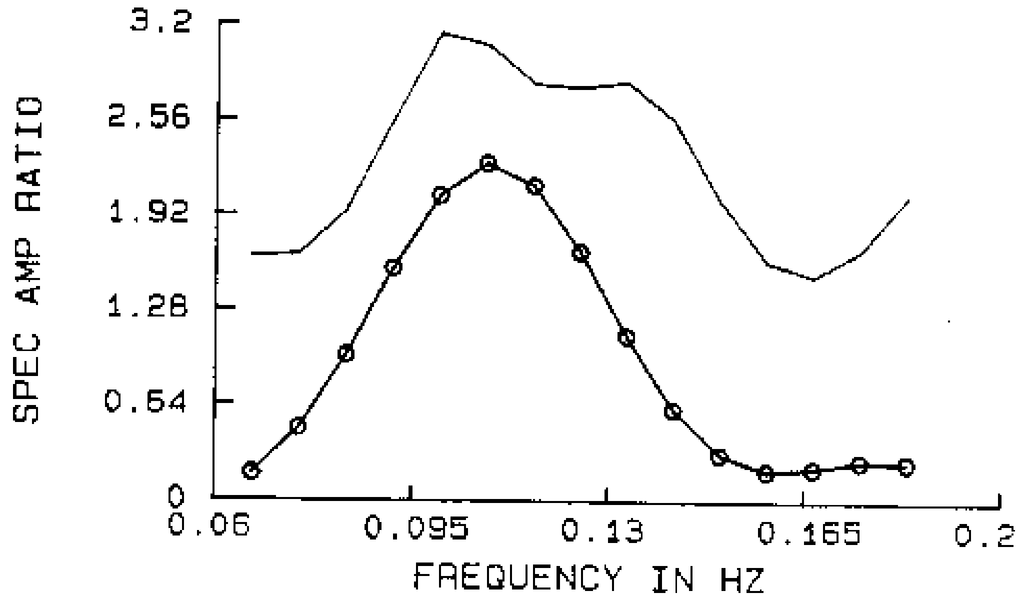

EPI. COORDINATES	36.33° N, 71.12° E
DISTANCE	24.0°
BACK AZIMUTH	55°
DEPTH	213 KM
MAGNITUDE(m_b)	6.4
ANGLE OF EMERGENCE	29.°

THICKNESS (KM)	P VELOCITY (KM/S)	DENSITY (GM/CM^3)
1	5.7	2.1
9	6.5	2.3
8	6.6	2.5
14	6.85	2.7
11	7.55	2.90
999.00	8.2	3.08

CORRELATION COEFF= .90

Fig. 4.11 Pots of theoretical and observed spectral ratio for earthquake of Jul.14, 1991 (AFGHANISTAN) and relevent information together with obtained crustal model. Open circles and solid lines represent observed and theoretical curves, respectively.

TABLE IV

EARTHQUAKES FROM AZIMUTHS 20^0-120^0

LOC	DATE			O.T.			COORD.		DEP	MAG		DIST	B_AZ	T-OFF	EMER
	D	M	Y	H	M	S	LAT	LON	KM	MB	MS	DEG	DEG	DEG	DEG
BONI	8	11	85	18	40	24.8	27.96	140.61	42	5.8	6.1	82.1	62	18	15
MOLU	14	8	86	19	39	13.6	1.79	126.52	33	6.6	7.2	80.1	92	18	15
FOX	5	1	87	12	11	55.7	52.45	-169.38	33	6.1	6.7	97.0	21	16	13
KAMC	19	1	87	6	47	4.3	54.74	163.28	42	5.4	5.2	84.1	31	17	14
HONS	6	2	87	12	23	4.8	36.99	141.79	36	5.9	6.1	79.4	54	19	15
HONS	7	4	87	0	40	43.4	37.36	141.80	29	6.4	6.6	79.3	53	19	15
CHIN	30	4	87	5	17	3.7	39.76	74.57	8	5.7	5.6	27.9	50	33	27
BURM	18	5	87	01	53	05.1	25.27	94.20	50	5.7	5.9	43.0	78	29	24
KAZA	17	7	87	01	17	07.0	49.80	78.11	10	5.8	0.0	35.0	36	28	17
PAKI	10	8	87	10	52	19.9	29.87	63.84	165	5.6	.0	16.1	67	51	40
KAMC	6	10	87	20	11	35.1	52.96	159.97	34	6.1	6.3	83.5	33	18	14
IRAN	30	3	88	2	12	42.8	30.89	50.19	33	5.4	5.7	6.9	26	58	45
AFGH	26	9	88	7	17	.2	36.29	71.37	107	5.6	.	24.2	55	35	29
KURL	9	1	89	13	42	36.4	49.99	153.48	14	6.0	6.4	83.0	41	18	15
MOLU	10	2	89	11	15	24.6	2.31	126.76	44	6.2	6.8	80.1	92	18	15
KURL	11	4	89	3	56	36.9	49.49	159.15	16	6.3	6.6	85.0	37	17	14
XING	17	4	90	1	59	33.4	39.44	74.90	33	6.0	6.2	28.0	51	33	27
SAKH	12	5	90	4	50	8.0	49.04	141.85	600	6.5		75.0	42	20	16
IRAN	6	11	90	18	45	52.2	28.25	55.46	11	6.2	6.7	8.7	64	57	44
KUSH	31	1	91	23	3	33.6	35.99	70.42	142	6.4	.0	23.4	55	36	29
MINA	20	6	91	5	18	52.5	1.20	122.79	31	6.2	7.0	76.9	94	20	16
TIMO	04	7	91	11	43	10.4	-8.10	124.68	29	6.2	7.0	82.6	102	18	15
AFGH	14	7	91	9	9	11.9	36.33	71.12	213	6.4	.0	24.0	55	35	29
KURL	22	12	91	8	43	13.4	45.53	151.02	25	6.3	7.4	82.1	43	18	15
MIND	17	5	92	9	49	19.1	7.24	126.64	33	6.2	7.1	78.0	87	19	16
KUSH	09	8	93	12	42	48.1	36.38	70.86	215	6.2	.0	23.8	55	25	29

4.4.2 EVENTS FROM AZIMUTHS 130^0 -220^0

Only five events in the azimuth range were recorded suitable for this study. The epicentral distances were taken between 13^0 and 24^0. Only 2 events were considered to obtain crustal model with correlation coefficient between observed and theoretical above 0.75 and they are shown in Figures 4.12 and 4.13 and the rest of the plots are shown in Figures 4.39 to 4.42. in Appendix IV. All the plots in Figures 4.40 to 4.43 have one peak at around 0.1 Hz.(0.1-0.13 Hz). Due to the small number of large earthquakes from those azimuths we utilized an event recorded by the intermediate period seismographs at Riyadh station as shown in Figures 4.40 and 4.41. Figure 4.41 represents a wider frequency range to include the higher frequencies up to 0.4 Hz. This figure shows another clear peak at 0.31 Hz. Generally the 5 plots show one peak response and it is shifted towards higher frequencies. This may indicate a thinner crust under the range of azimuths of 130^0 to 220^0. The crustal layers show no clear changes in thickness and P velocity. The total thickness of the crust ranges from 39 to 41 km. The conclusive model for this azimuthal range is shown in Table V.

TABLE V.

EARTHQUAKES FROM AZIMUTHS 130^0-220^0

LOC	DATE			O.T.			COOR		DEP	MAG.		DIST	B_AZ	T-OFF	EMER
	D	M	Y	H	M	S	LAT	LON	KM	MB	MS	DEG	DEG	DEG	DEG
ARAB	14	12	85	18	13	31.5	14.71	58.00	10	5.5	.0	15.0	130.	39	42
ETHI	25	10	87	16	46	13.3	5.41	36.75	12	5.6	6.2	21.4	207	39	31
SUDA	20	5	90	2	22	.6	5.12	32.15	15	6.7	7.1	23.9	217	36	29
SUDA	9	7	90	15	11	20.3	5.39	31.65	13	5.9	6.4	24.0	219	36	29
ETHI	5	3	92	8	55	5.6	11.51	42.81	7	5.5	6.2	13.6	196	53	42

4.4.3 EVENTS FROM AZIMUTHS 230^0 TO 360^0

Nine earthquakes were analyzed within the azimuthal range 230 to 360 degrees. The spectral ratio curves of the representative models are shown in Figures 4.14 and 15 while the rest of the events are shown in Figures 4.44 -50. The resultant models show one peak at 0.1 Hz

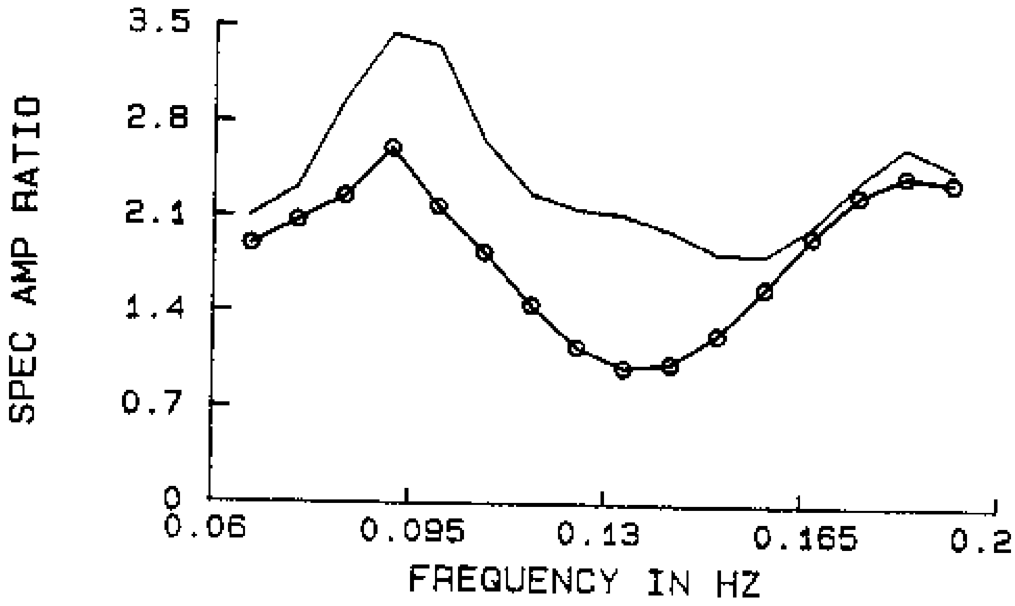

EPI. COORDINATES	14.71 N, 58.00 E
DISTANCE	$15.^0$
BACK AZIMUTH	130^0
DEPTH	10 KM
MAGNITUDE(m_b)	5.5
ANGLE OF EMERGENCE	41.5^0

THICKNESS (KM)	P VELOCITY (KM/S)	DENSITY (GM/CM^3)
2	5.5	2.1
10	6.0	2.3
6	6.45	2.5
13.00	6.95	2.7
11	7.55	2.90
999.00	8.2	3.08

CORRELATION COEFF= .78

Fig. 4.12 Plots of theoretical and observed spectral ratio for earthquake of Dec.14, 1985 (ARABIAN SEA) and relevant information together with obtained crustal model. Open circles and solid lines represent observed and theoretical curves, respectively.

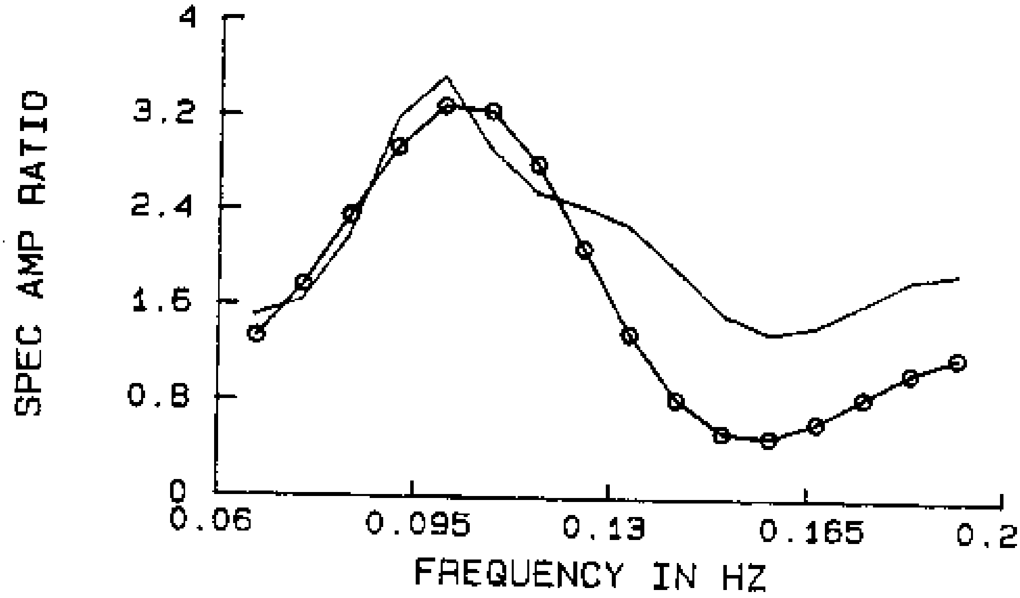

EPI. COORDINATES	05.41° N, 36.75° E
DISTANCE	21.4°
BACK AZIMUTH	207°
DEPTH	12 KM
MAGNITUDE(m_b)	5.6
ANGLE OF EMERGENCE	31°

THICKNESS (KM)	P VELOCITY (KM/S)	DENSITY (GM/CM^3)
2	5.65	2.1
11	6.3	2.3
5	6.7	2.5
16	6.85	2.7
11	7.45	2.90
999.00	8.20	3.08

CORRELATION COEFF= .91

Fig. 4.13 Plots of theoretical and observed spectral ratio for earthquake of Oct.25, 1987 (ETHIOPIA) and relevant information together with obtained crustal model. Open circles and solid lines represent observed and theoretical curves, respectively.

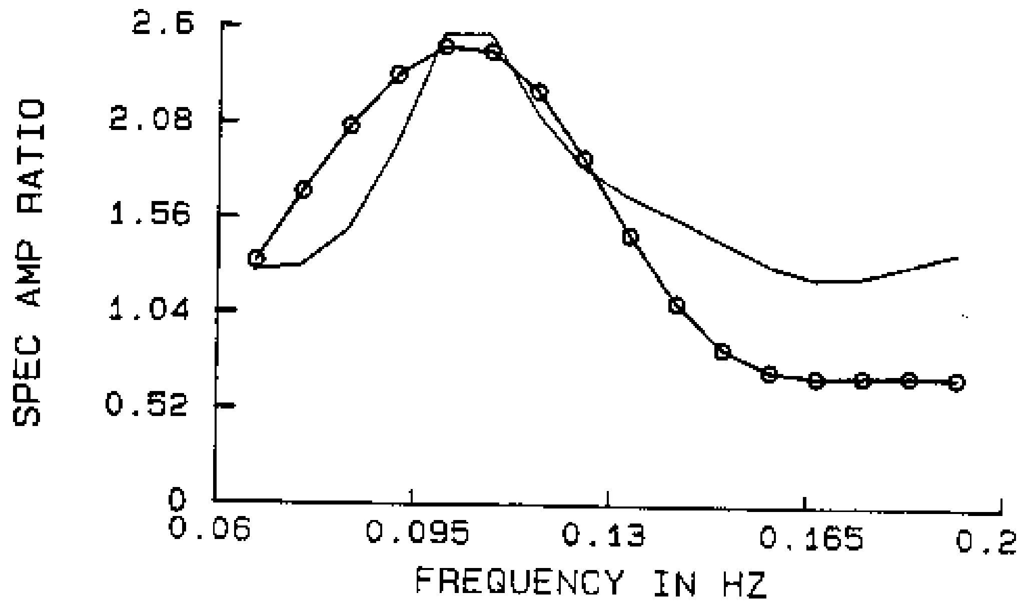

EPI. COORDINATES	39.71° N 39.60° E
DISTANCE	16.1°
BACK AZIMUTH	340°
DEPTH	27 KM
MAGNITUDE(m_b)	6.2
ANGLE OF EMERGENCE	40°

THICKNESS (KM)	P VELOCITY (KM/S)	DENSITY (GM/CM^3)
2	5.6	2.1
10	6.2	2.3
6	6.7	2.5
15	6.9	2.7
10	7.45	2.90
999.00	8.2	3.08

CORRELATION COEFF= .87

Fig. 4.14 Plots of theoretical and observed spectral ratio for earthquake of Mar.13, 1992 (TURKEY) and relevant information together with obtained crustal model. Open circles and solid lines represent observed and theoretical curves, respectively.

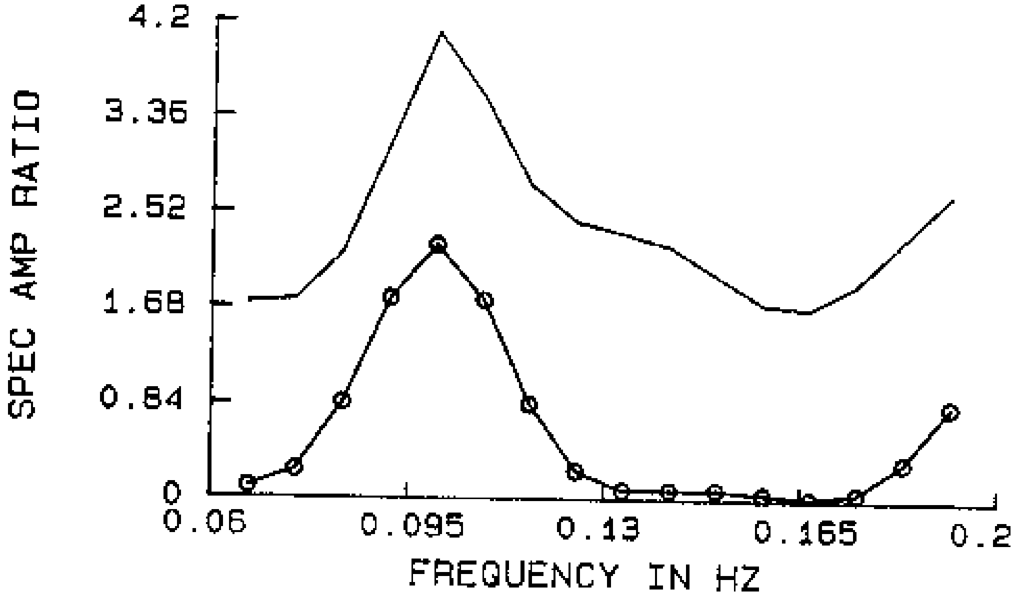

EPI. COORDINATES	45.81 N, 26.67 E
DISTANCE	26.5^0
BACK AZIMUTH	327^0
DEPTH	89 KM
MAGNITUDE(m_b)	6.7
ANGLE OF EMERGENCE	28^0

THICKNESS (KM)	P VELOCITY (KM/S)	DENSITY (GM/CM^3)
2	5.53	2.1
9	6.1	2.3
7	6.75	2.5
11	6.8	2.7
10	7.35	2.90
999.00	8.2	3.08

CORRELATION COEFF= .90

Fig. 4.15 Plots of theoretical and observed spectral ratio for earthquake of May30, 1990 (ROMANIA) and relevant information together with obtained crustal model. Open circles and solid lines represent observed and theoretical curves, respectively.

(0.95 to 0.11 Hz). The representative model was obtained using those events with the highest correlation coefficient and it is presented in Table VI. It indicates a thicker crust of 41 km with a clear contrast between P wave velocity of the layers.

TABLE VI.

EARTHQUAKES FROM AZIMUTHS 230^0 - 360^0

LOC	DATE			O.T.			COORD		DEP	MAG		DIST	B_AZ	T-OFF	EME
	D	M	Y	H	M	S	LAT	LON	KM	MB	MS	DEG	DEG	DEG	DEG
IRAQ	25	07	88	07	58	42.2	42.20	35.94	99	4.9	5.2	11.2	357	55	43
ARME	7	12	88	7	41	24.2	40.99	44.19	5	6.2	6.8	16.3	353	51	40
ROMA	30	5	90	10	40	6:1	45.84	26.67	89	6.7	.0	26.5	327	34	28
TURK	13	3	92	17	18	39.9	39.71	39.60	27	6.2	6.8	16.1	340	51	40
CRET	3	5	92	8	35	36.8	34.97	26.69	29	4.7	.0	20.0	305	29	33
EGYP	12	10	92	13	9	55.5	29.78	31.14	22	5.9	5.3	14.6	293	53	41
MEDI	21	11	92	5	7	21.7	35.92	22.49	65	5.9	.0	23.6	303	36	29
REDS	13	3	93	17	12	26.2	19.63	38.80	10	5.7	5.4	8.8	236	57	44
AQAB	3	8	93	12	43	5.3	28.73	34.55	10.	5.9	5.8	11.5	293	55	43

CHAPTER 5

DISCUSSIONS AND INTERPRETATION

5.1. GENERAL

The crustal and upper mantle velocity structure of the central Arabian Platform has been derived using the analysis of long period P-wave spectral amplitude ratios. The ratio of the vertical to the horizontal component is utilized to obtain crustal transfer function.

Forty well-defined earthquakes recorded at RYD long-period station were selected for the analysis based on the following criteria : focal depths range between 10 and 300 km , body-wave magnitudes greater than 5.0 and the epicentral distances range from 9 to 89 degrees. After selecting the earthquakes which meet certain criteria P wave portions of all 3 components on the analog records were digitized. Spectral analysis calculations were based on comparing the observed spectral ratios with those computed from theoretical P-wave motion obtained using the "Thomson- Haskell " matrix formulation for horizontally layered crustal models.

Generally, the resultant model is not unique. However, putting some constrains from other disciplines increases the accuracy of the results. The sensitivity of the transfer functions to the changes of model parameters indicates that the peak at the lowest frequency is directly related to the total thickness of the crust. Thicker crust shifts the position of the peak to lower frequencies and the higher the velocity contrast the higher the amplitudes and vice versa. This method is easy to apply and requires only seismograms of a single station. It is not required to know the magnitude, source mechanism and arrival time of earthquakes.

The derived crustal model indicates a change in crustal thickness in three different azimuthal groups : 1) from 20° to 120° (NE to SE) 2) from 130° to 220° (SE to SW) and 3) from 230° to

360° (SW to N) . The selection of the most suitable model was based on the identification of theoretical model which exhibits the highest cross correlation coefficient with the observed transfer function ratio. The model parameters were perturbed within the constrains imposed by tectonics, geology and the results of other geophysical studies. The model suggested that the crust consists of five distinct layers. The upper crustal layer has a P-wave velocity of 5.60 km/sec and it is about 2 km thick. The second layer has a velocity of about 6.20 km/sec and 10.0 km thick . The third layer shows a velocity of 6.50 km/sec and 7 km thick. The fourth layer shows a P velocity of 6.80 km/s and thickness of 18 km. The lower layer has a velocity of about 7.50 km/sec and 11 km thick. The Mohorovicic discontinuity beneath the Arabian Platform varies from 44 km depth in the NE and to 41 km depth in the NW and SW with 8.2 km/sec mantle velocity.

5.2. REPRESENTATIVE CRUSTAL MODELS

It can be concluded from section 2.3 that the derived crustal model indicates a change in crustal thickness in three different azimuthal groups : 1) from 20° to 120° (NE to SE) 2) from 130° to 220° (SE to SW) and 3) from 230° to 360° (SW to N) . The model parameters were perturbed within the constrains imposed by tectonics, geology and the results of other geophysical studies. The selection of the most suitable model was based on the identification of theoretical model which exhibits the highest cross correlation coefficient with the observed transfer function ratio. According to the above criteria, this study suggested three different models as follows :

a. Model for N-NE-E and SE of Riyadh

TABLE VII. DEDUCED CRUSTAL MODEL FOR N-NE-E-SE OF RIYADH

THICKNESS KM	P WAVE VELOCITY KM/S	DENSITY GM/CM^3
2.0	5.60	2.10
10.0	6.24	2.30
6.0	6.60	2.50
15.0	6.80	2.70
11.0	7.53	2.90
999.0	8.30	3.08

b. Model for S - SW of Riyadh

TABLE VIII. DEDUCED CRUSTAL MODEL FOR S-SW OF RIYADH

THICKNESS KM	P WAVE VELOCITY KM/S	DENSITY GM/CM^3
1.0	5.60	2.10
10.0	6.20	2.30
6.0	6.50	2.50
12.0	6.80	2.70
11.0	7.50	2.90
999.0	8.20	3.08

c. Model for SW-W and NW

TABLE IX. DEDUCED CRUSTAL MODEL FOR SW-W TO NW-N OF RIYADH

THICKNESS KM	P WAVE VELOCITY KM/S	DENSITY GM/CM^3
1.0	5.60	2.10
10.0	6.20	2.30
7.0	6.50	2.50
13.0	6.80	2.70
10.0	7.45	2.90
999.0	8.30	3.08

The overall average crustal model obtained from this study is given in Table VII

We note that there is agradational crust-mantle boundary. In general, the crust beneath the Riyadh area appears to have a clear division at the middle and lower crust at about 20 km-depth.

TABLE X. DEDUCED CRUSTAL MODEL FOR RIYADH

THICKNESS KM	P WAVE VELOCITY KM/S	DENSITY GM/CM^3	
2.0	5.60	2.10	UPPER CRUST
10.0	6.20	2.30	"
7.0	6.50	2.50	"
14.0	6.80	2.70	MIDDLE CRUST
11.0	7.50	2.90	LOWER CRUST
999.0	8.20	3.08	UPPER MANTLE

5.2. GEOTECTONIC IMPLICATIONS

The refined results for the seismic velocity structure for the Arabian Platform suggested that the crust consists of four distinct layers. The first crustal layer has a P-wave velocity of about 5.60 km/sec and is about 2.0 km thick. The second layer has a velocity of about 6.20 km/sec and 10.0 km thick . The third layer shows a velocity of 6.50 km/sec and 12 km thick. The fourth layer has a P wave velocity of 6.80 km/s and 14 km thickness. The lower crustal layer has a velocity of about 7.50 km/sec and 11.0 km thick. The Mohorovicic discontinuity beneath the Arabian Platform varies from 44 km depth in the NE and SE with 8.2 km/sec mantle velocity to 40 km depth in the NW and SW with 8.1 km/sec mantle velocity. The observed low heat flow supports high lower crustal velocities (Gettings and Showail, 1982).

Comparison of these seismically-defined features with surface geology and other geophysical data yields good correlation and a consistent model of the crust. From the above and comparing with previous crustal models (Mooney et al., 1985 ; Prodehl , 1985 ; Badri, 1991 ; Mokhtar et al., 1992) , we distinguish a crust of three layers for the Arabian Platform. The upper crust of 19 km thickness with a velocity of 6.1 km/sec. which is composed predominantly a very thin layer of unconsolidated sediments in the upper parts and consolidated two thick layers in the lower parts. The middle crust which is the thickest layer with velocity of 6.80 km/s. The lower crust has average velocity of 7.50 km/sec and thickness of 11 km. Meissner (1986) indicated that P-wave velocities in the range 7.1-7.8 km/sec are typical of dense gabbros, eclogite , high grade granulites or mixture of crust-mantle. The upper crustal velocities generally increase across this boundary to the NE-SE indicating either a change in the composition of basement rocks or a northwestward dip of the shield. Moony et al.(1985) mapped the basement surface beneath the sediments of the platform and indicated that the surface is faulted in a horst and graben pattern. Offsets due to faulting are of the order of 1000 m and maximum sediment thickness obtained was about 1.75 km.

Considering the three different azimuthal groups mentioned earlier, distant earthquakes from the first group include 26 earthquakes from Iran, Pakistan, Afghanistan, China, Indonesia, Japan and Philippine Islands. It indicates that the thickness of the upper middle and lower crust reaches about 19, 14 and 11 km, respectively which are the highest compare with the other two groups with average velocities of 6.10, 6.80 and 7.50 km/sec, respectively.

This result is slightly different from those obtained by Mokhtar et al. (1993). They indicated that the P-wave velocity of the uppermost layers along the path from southern Iran to RYD station reaches to 5.27 km/sec at 3 km depth and 5.9 km/sec at 17 km depth. They indicated that the average thickness of each of the upper and lower crust of the platform is about 20 km . The upper mantle velocity ranges between 7.4 and 7.49 km/sec.

The second azimuthal group involves five earthquakes trom the Arabian Sea, Ethiopia and Sudan. The average crustal thickness to the Moho is 40 km. This indicates that the crustal thickness in the platform in this range seems to have lower thicknesses than the first group by 4 km and by 1 km than the third group. The third azimuthal group includes nine earthquakes from Armenia, Romania, Turkey, Egypt, Mediterranean, Crete, Iraq, Red Sea and gulf of Aqaba. Very well fitting is shown between the observed and theoretical spectra. The thickness of the upper middle and lower crust is 18 ,13 and 10 km respectively.

5.3. COMPARISON OF THE RESULTS WITH PREVIOUS STUDIES

Two deduced crustal models show crustal thicknesses of 42 km with a clear velocity change between upper , intermediate and lower crustal layers. The upper crust consists of 3 layers, including a superficial thin layer at the top. The average velocity of the upper crust is 6.1 km/s with a total thickness of 18 km. The velocity of 6.8 km/s represents the intermediate crust with at otal;thickness of 14 km. The lower crust appears t bew thinner than the other crustal layer (10 km) with velocity of 7.5 km/s.

On the other hand Badri (1991) suggested that the upper lower (intermediate) crust increases in thickness from 7.5 km under the shield to 16 km beneath the platform. This would make the lower crust 31 km beneath the platform region. The boundary between the upper and lower crust occurs at a depth of 10 km and the Moho occurs at about 43 km.

The model resulting from the inversion of the surface wave dispersion data from southern Red Sea to Riyadh path (Mokhtar et al. 1992) shows that the shear wave velocity near the surface is 3.47 km/s and the velocity increases at a depth of 4 km from 3.5 km/s to 3.85 km/s at 13 km depth. The lower part of the upper crust seems to have shear wave velocity of 3.87 km/s at 23 km depth.

CHAPTER 6.

CONCLUSIONS AND RECOMMENDATIONS

6.1. CONCLUSIONS

The objective of this study was to determine the crustal and upper mantle structure beneath the Arabian platform from the spectral analysis of long period P- wave amplitude ratios.

In order to achieve our objectives, suitable earthquakes which were recorded at Riyadh long-period station during the period from 1986 to 1994 have been utilized for the analysis based on the following criteria : focal depths range between 10 and 300 km , body-wave magnitudes greater than 5.0 and the epicentral distances range from 9 to 89 degrees. Spectral analysis calculations were based on comparing the observed spectral ratios with those computed from theoretical P-wave motion obtained using the " Thomson- Haskell " matrix formulation for horizontally layered crustal models.

The derived crustal model indicates a change in crustal thickness in three different azimuthal sectors : 1) from 20 to 120 degrees (NE to SE) , 2) from 125 to 220 degrees (SE to SW) and 3) from 225 to 360 degrees (SW to N). The selection of the most suitable model was based on the identification of theoretical model which exhibits the highest cross correlation coefficient with the observed transfer function ratio.

The model suggested that the crust consists of five distinct layers. The upper crustal layer has a P-wave velocity of about 5.6 km/sec and is about 2.0 km thick. The second layer has a velocity of about 6.2 km/sec and 10 km thick . The third layer shows a velocity of 6.5 km/sec and 7 km thick. The fourth layer has a velocity of about 6.8 Km/sec and 14 km thick.

The lower crustal layer has a velocity of about 7.5 km/sec and 11 km thick. The Mohorovicic discontinuity beneath the Arabian Platform varies from 44 km depth in the NE and SE to 41 km depth in the NW and SW with 8.2 km/sec upper mantle velocity.

6.2.RECOMMENDATIONS FOR FURTHER INVESTIGATIONS

The present work represent the first detailed study of the central Arabia using earthquake data for crustal structure studies. The geology of this region was given more attention. Applying Thomson-Haskell matrix formulation in our study has been found to be a good , economic, and reliable technique for crustal structure determination on the basis of single-station seismic data through system identification techniques. The accuracy of this method is based primarily on the quality and frequency band of seismic data and number of the parameter pertaining to the layered crustal model . The derived model is not unique due to the theoretical assumption in this method and also due to the complexity of the crustal structure of the earth. This method can be used effectivelv in combination with seismic refraction or gravity surveying.

In order to fully understand the detail geophysical and seismological picture of central Arabia, this study recommends an extensive research covering the following points :

1. An expensive but potentially insightful line of research is to carry out a detailed seismic deep refraction and gravity profiles between Riyadh and the Arabian Gulf in the east to obtain a precise bulk composition of crustal layers and improve velocity model.

2. Investigation of the crustal structure beneath Dhahran station from the spectral analysis of long period P-wave data based on the Thomson- Haskell matrix formulation. This will be integrated with our results for correlating and comparing crustal thickness variations.

3. Upgrading of the analog to digital recordings at Riyadh and Dhahran stations is strongly recommended for getting better quality signals, time consuming and make it possible to include short period data in the analysis.

4. Installation of strong motion accelerographs to estimate the attenuation characteristics in the region and to evaluate the seismic hazard assessment.

The aforementioned recommendations would not significantly change our basic conclusions in this study but would help create parallel tracks of investigation.

CHAPTER 7.

REFERENCES

Badri, M., 1989. Qp and velocity crustal structure of central Saudi Arabia, KACST Project Final rep. 09-006 , 135 pp.

Badri, M.,1991. "Crustal structure of central Saudi Arabia, from seismic refraction profiling", *Tectonophysics* ,185 , 357 - 374 .

Barazangi, M.,1981 . "Evaluation of seismic risk along the western part of the Arabian plate discussion and recommendation", *Bull. Fac. Earth. Sci.*, 4 , King Abdulaziz Univ., 77 - 87 .

Ben-Menahem, A., A. Nur, and Vared, M., 1976. "Tectonics, seismicity and structure of the Afro-Eurasian junction- The breaking of an incoherent plate", *Phys.Earth. Planet. Inter.*, 12 , 1-50 .

Bonjer, K.P., K. Fuchs and J. Wohlenber, 1970. "Crustal structure of the East African Rise System from spectral response ratios of long-period body waves", *Z. Geophys*, Vol 36, pp. 287-297.

Dewey, J.F., W.C. Pitman, W. B. F. Ryan, and Bonnian, J., 1973." Plate tectonics and the evolution the Alpine system", *Bull. Geol. Soc. Amer.*, 84 , 3137 - 3180 .

Ellis, R.M. and P.W. Basham, 1968. "Crustal Characteristics form Short- Period P-Waves",*Bull. Seis. Soc. Am.*, Vol. 58, pp.1681-1700

Fernandez, L. M.,S.J. 1965. The determination of crustal thickness from the spectrum of P waves. Scientific Report No.13. St. Louis University.

Fernandez, L. M. and J. Carrega, 1968, " The thickness of the Crustal United States and La Paz, Bolivya, from the spectrum of longitudinal seismic waves" *Bull. Seis. Soc. Am.*., Vol. 58, No. 2, pp.711- 741.

Gettings, M.E and A. Showail, 1982. Heat flow measurements at shot points along the 1978 Saudi Arabian Deep Refraction Line,1, Results of measurements. Open File Report. USGS-OF-02-39 , 98 pp, Saudi Arabian Deputy Ministry for Min. Resources, Jeddah, Saudi Arabia.

Girdler, R. W., 1969 . The Red Sea : A geophysical background. In : E. T. Degens and D. A. Ross (Editors), Hot brines and recent heavy metal deposits in the Red Sea. Springer , New York , pp. 8- 58.

Girdler, R. and Styles, P., 1974 . "Two stages Red Sea floor spreading", *Nature* , 247 , 7-11

Girdler, R. and Styles ,P.,1978. " Sea-floor spreading in the western Gulf of Aden", *Nature*, 271 , 15 - 617 .

Greenwood, W. R., R. E. Anderson, R. J. Fleck, and Roberts, R. J., 1980. "Precambrian geologic history and plate tectonic evolution of the Arabian Shield ", *Saudi Arabian Dir. Gen. Miner. Resour. Bull.*, Vol. 24 , 35 pp.

Hall ,S.B.A., J. Andreasen, and Girdler, R. W., 1976 . "Total-intensity magnetic anomaly map of the Red Sea and adjacent coastal areas : A Description and primary interpretation". *Saudi Arabian Proj. Rep.* 206 , 36 p.

Hasegewa, H. S., 1971. " Crustal transfer ratios of short and long period body waves recorded at Yellowknife", *Bull. Seis. Soc. Am.* , Vol. 61, pp 1303-1320.

Haskell,N.A. ,1953, " The dispersion of surface waves on multilayered media", *Bull. Seis. Soc. Am.* , Vol. 43, pp. 17-34.

Herrmann, R. B., 1978. Computer programs in earthquake seismology Vol.1 :General programs, Department of Earth and Atmospheric Sciences, St. Louis University.

IASPEI Software Library Volume 2. 1990. Toolbox for plotting and displaying seismic and other data. Edited by W.H.K. Lee, Published by IASPEI in collaboration with Seismological Society of America

IASPEI Software Library Volume 5. 1992. Programmable Interactive Toolbox for Seismological Analysis PITSA)by Frank Scherbaum and James Johnson Published by IASPEI in collaboration with United Nations Educational, Scientific and Cultural Organization and Seismological Society of America

Knopoff, L., and Fouda, A. A., 1975. Upper mantle structure under the Arabian Peninsula . *Tectonophysics* , 26 , 121 - 134 .

Kurita, T.(1972 a) ." Regional variations in the structure of the crust in the cenral United States from P wave spectra" ,*J. Phys. Earth,* Vol 20.

Kurita, T. (1972 b). "Upper mnatle structure in the central United States from P and S wave spectra", *J. Phys. Earth*, Vol 20.

Kurita, T. (1972 c). "Upper mantle structure in teh western United States", *EOS*, Am. Geophys. Union, Vol 53, pp 1045.

Leblanc,G., 1967, "Truncated crustal transfer functions and fine crustal structure determination", *Bull. Seis. Soc. Am.* Vol 57, No.4 pp. 719- 733

Le Pichon, X. and Francheteau, 1978 . "A plate tectonic analysis of the Red Sea-Gulf of Aden Area" *Tectonophysics* , 46 , 369 - 406 .

Meissner, R., 1986, . The continental Crust. Academic press, Orlando, Florida, 426 p.

Mokhtar, T. A., R. B. Herrman, and Russell, D. R. ., 1988. " Seismic velocity and Q model for the shallow structure of the Arabian Shield from short-period Rayleigh waves", *Geophysics*, 53, 1379 - 1387.

Mokhtar , T. A., M. Maamoun, and Al-Amri , A.M., 1992. Seismic structure of the Arabian Peninsula from surface waves. KACST project final rep. 10-48 259 pp.

Mooney, W.D., M.E. Gettings, H.R. Blank and J. Healy, 1985. Saudi Arabian seismic deep refraction profile, a travel time interpretation for crustal and upper mantle structure, *Tectonophysics* 111, 173-246

Necioglu, A. 1969. Study of S- Wave Pectral Properties, M.S. Thesis, St. Louis University, Missouri, U.S.

Necioglu, A., B. Maddison and N. Turkelli, (1981). " A study of crustal and upper mantle structure of northwestern Turkey", *Geophysical Research Letters* Am. Geophy. Union, Vol. 8, No. 1

Niazi, M., 1968 . "Crustal thickness in Saudi Arabian Peninsula ", *Geophy. J. R. Ast. Soc.*, 15 , 545 - 547.

Phinney, R. A., 1964, " Structure of the Earth's Crust form Spectral Behavior of Long-Period Body Waves" , *J. Geophy. Res.*, Vol. 69, No.14, pp. 2997-3017

Powers, R. W., L. F. Ramirez, L. F., C.D. Redmond and Elberg, E. 1966. Geology of the Arabian Peninsula - Sedimentary geology of Saudi Arabia. U.S. Geological Survey prof. pap., 560-D , 147 pp .

Prodehl , C., 1985. "Interpretation of a seismic refraction survey across the Arabian Shield in western Saudi Arabia " , *Tectonophysics* , 111, 247 - 282 .

Stocklin, J., 1968 . "Structural history and tectonics of Iran : a review" , *Bull. Amer. Ass. Petr. Geol.* .52 , 1229 - 1258 .

Takin, M., 1972. "Iranian geology and continental drift in the Middle East" , *Nature* , 235 , 147 - 150 .

Thomson, W. T., 1950, " Transmission of elastic waves through a stratified medium " , *J.Appl. Physics,* Vol. 21 p 89.

Turkelli, N. 1984. Seismic Investigation of the Crustal Structure in Central Anatolia, Ph.D. Thesis, Middle East Technical University, Ankara, Turkey.

APPENDIX I.

RIYADH STATION INSTRUMENT RESPONSE CURVES

Figures 1.5 to 1.10

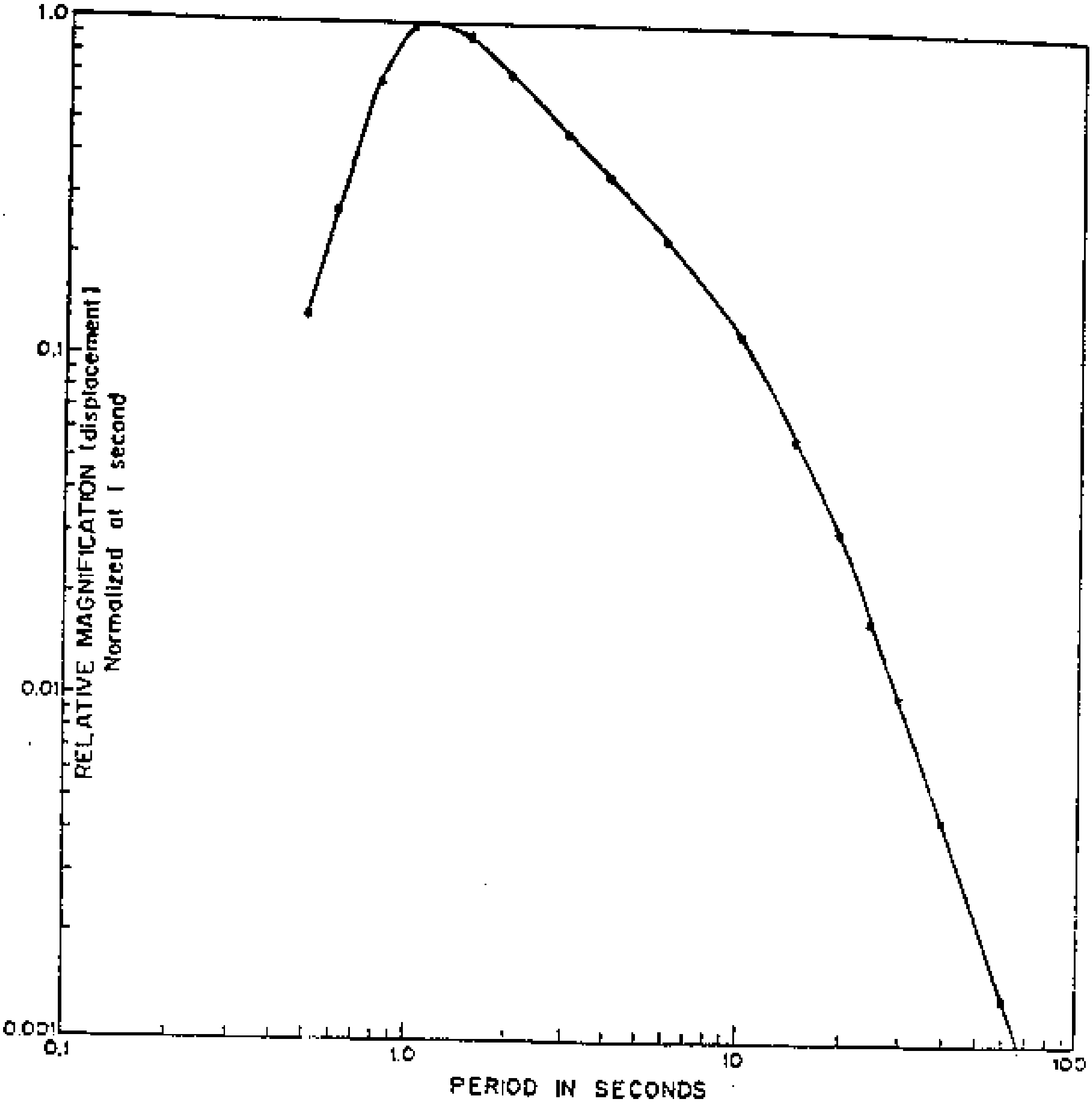

Figure 1.5. Amplitude response curve for LP vertical wide band seismograph at RYD

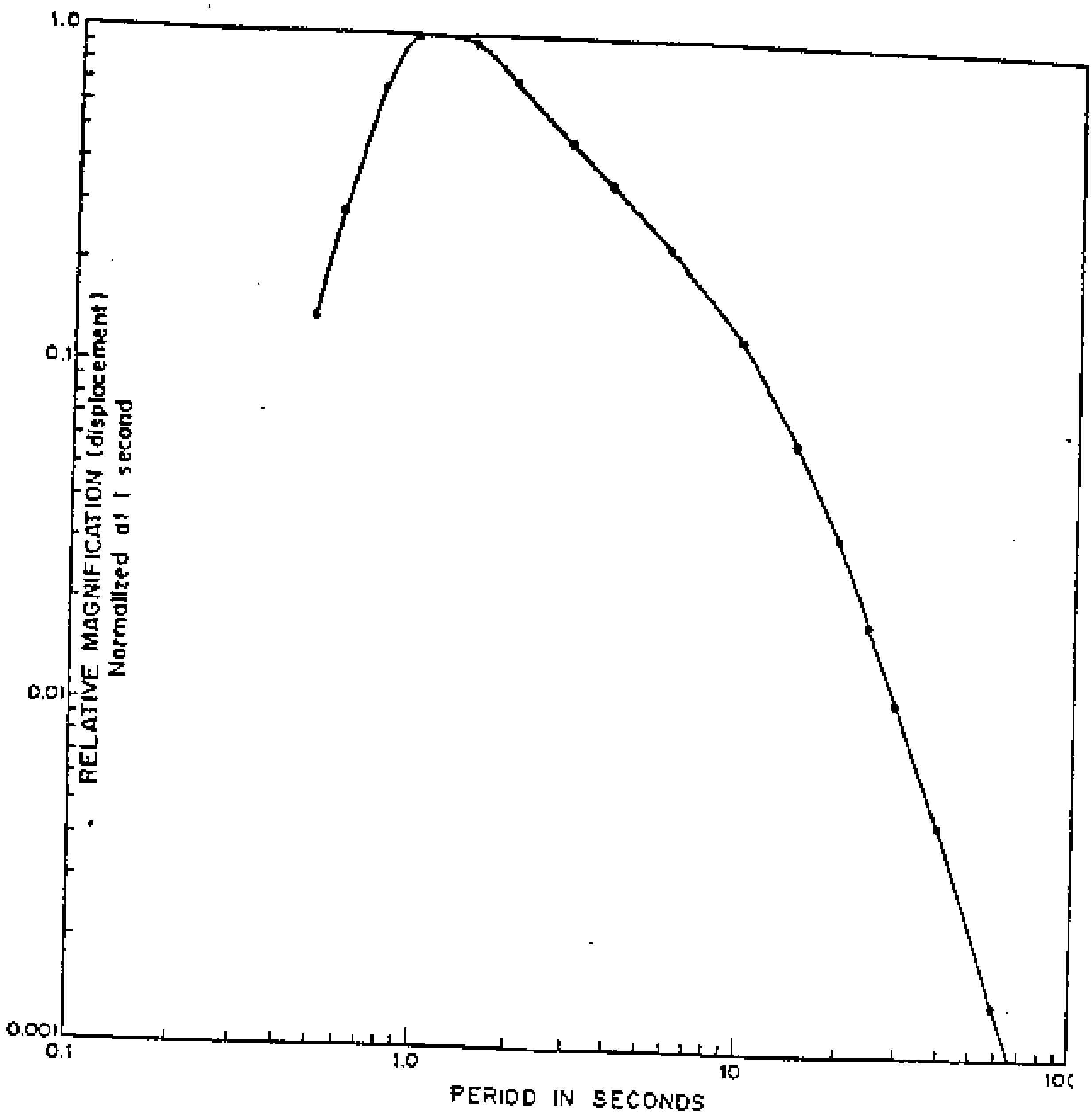

Figure 1.6. Amplitude response curve for LP E-W wide band seismograph at RYD

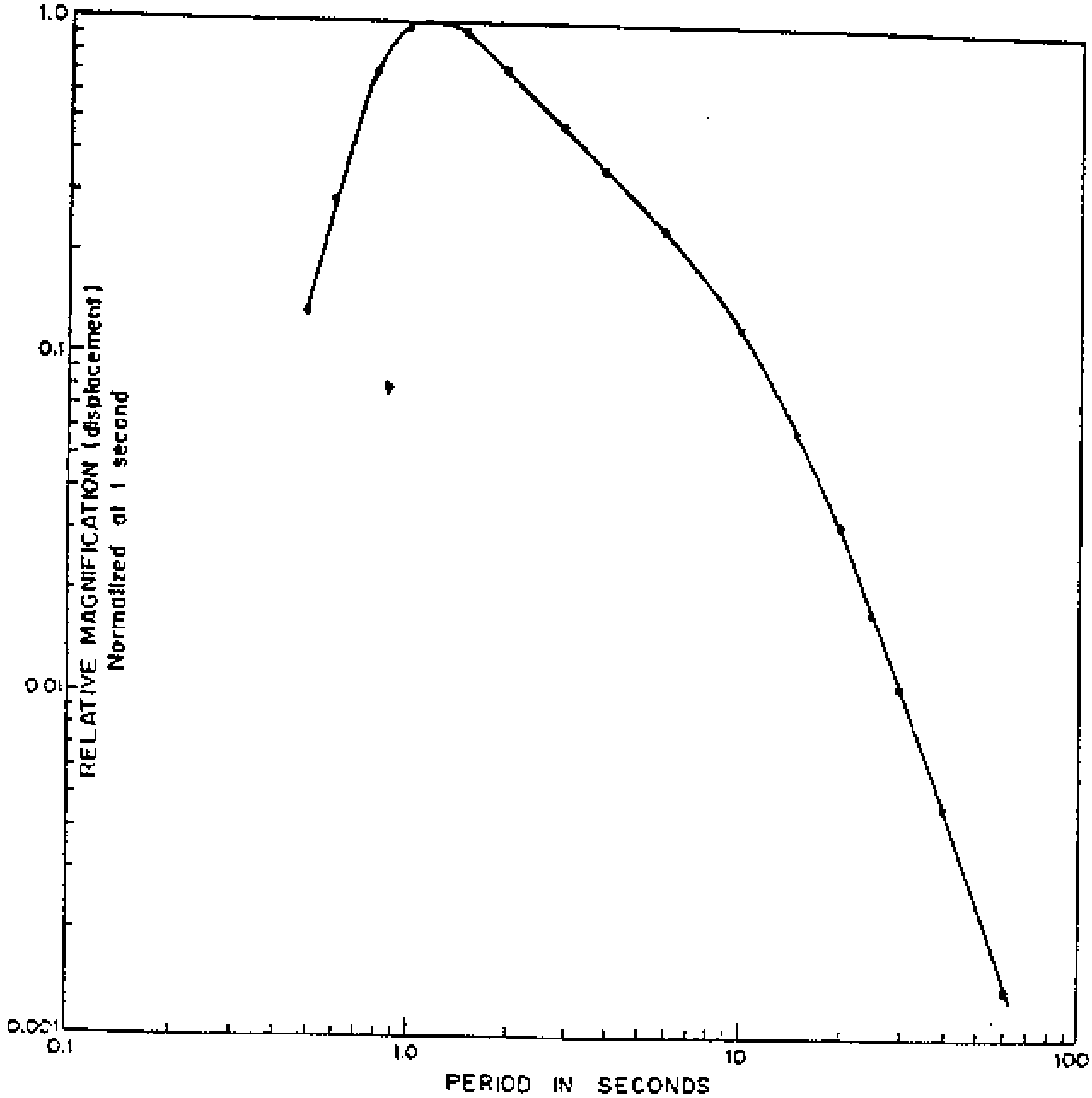

Figure 1.7. Amplitude response curve for LP N-S wide band seismograph at RYD

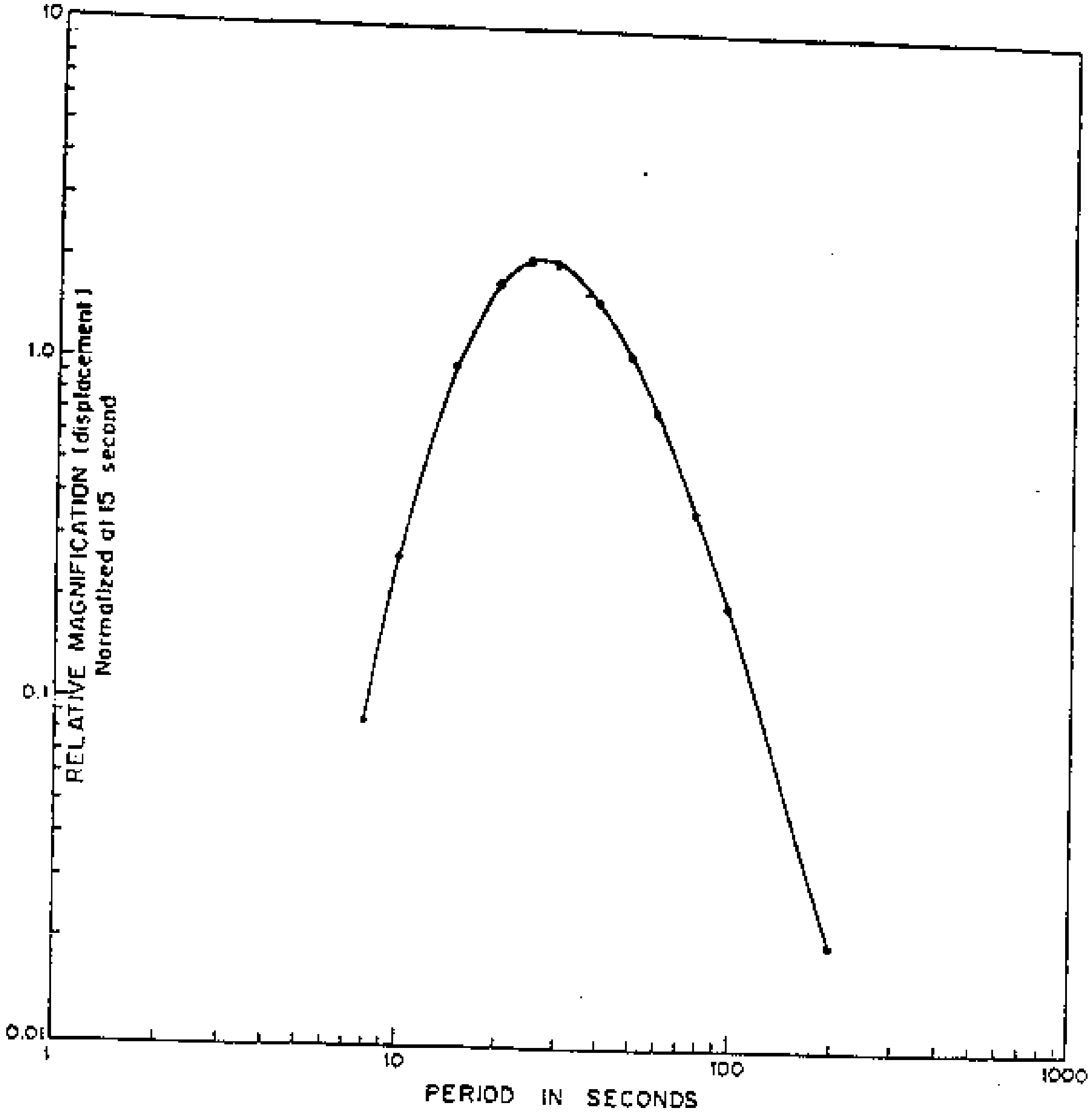

Figure 1.8. Amplitude response curve for LP vertical narrow band seismograph at RYD

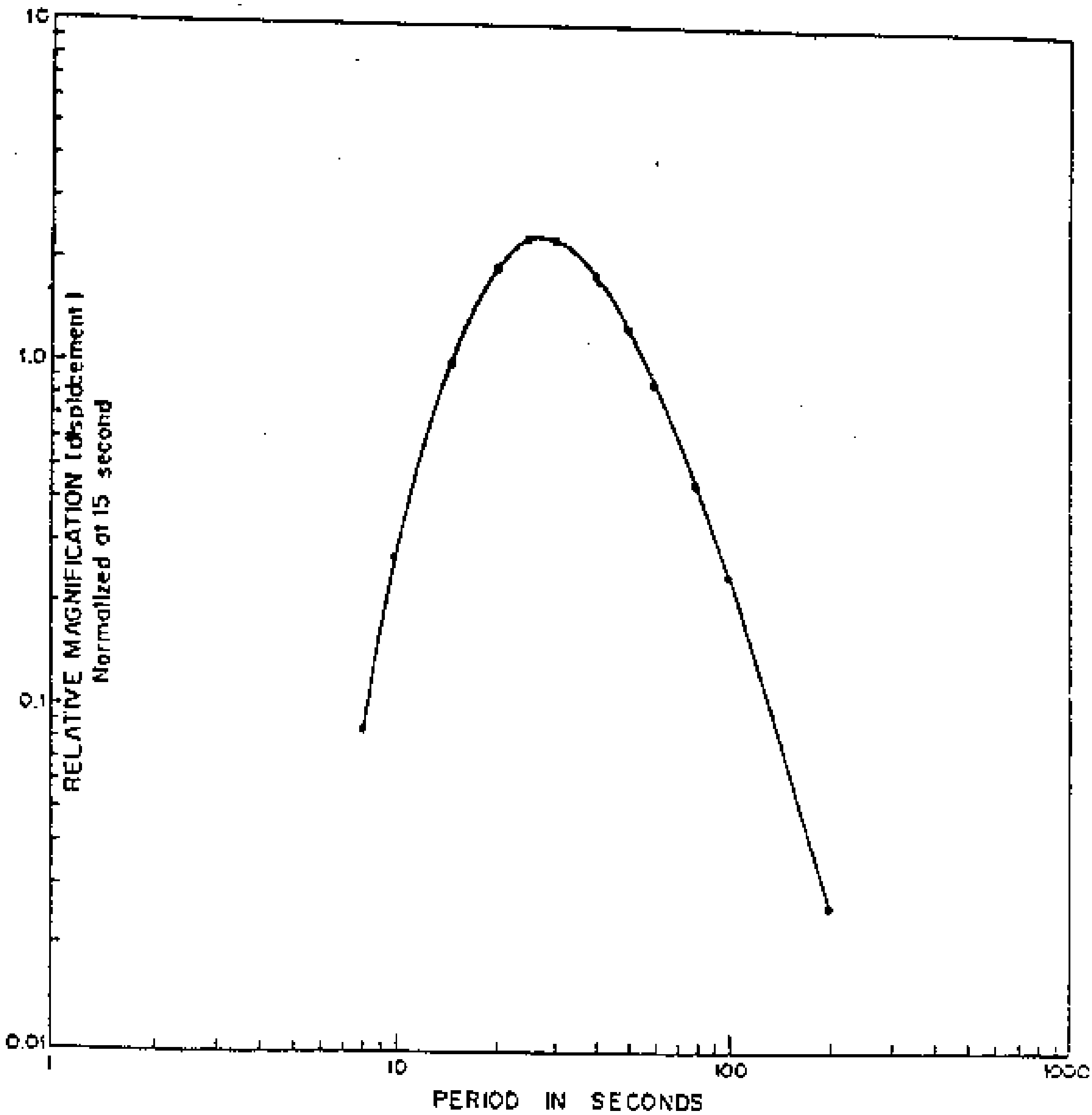

Figure 1.9. Amplitude response curve for LP E-W narrow band seismograph at RYD

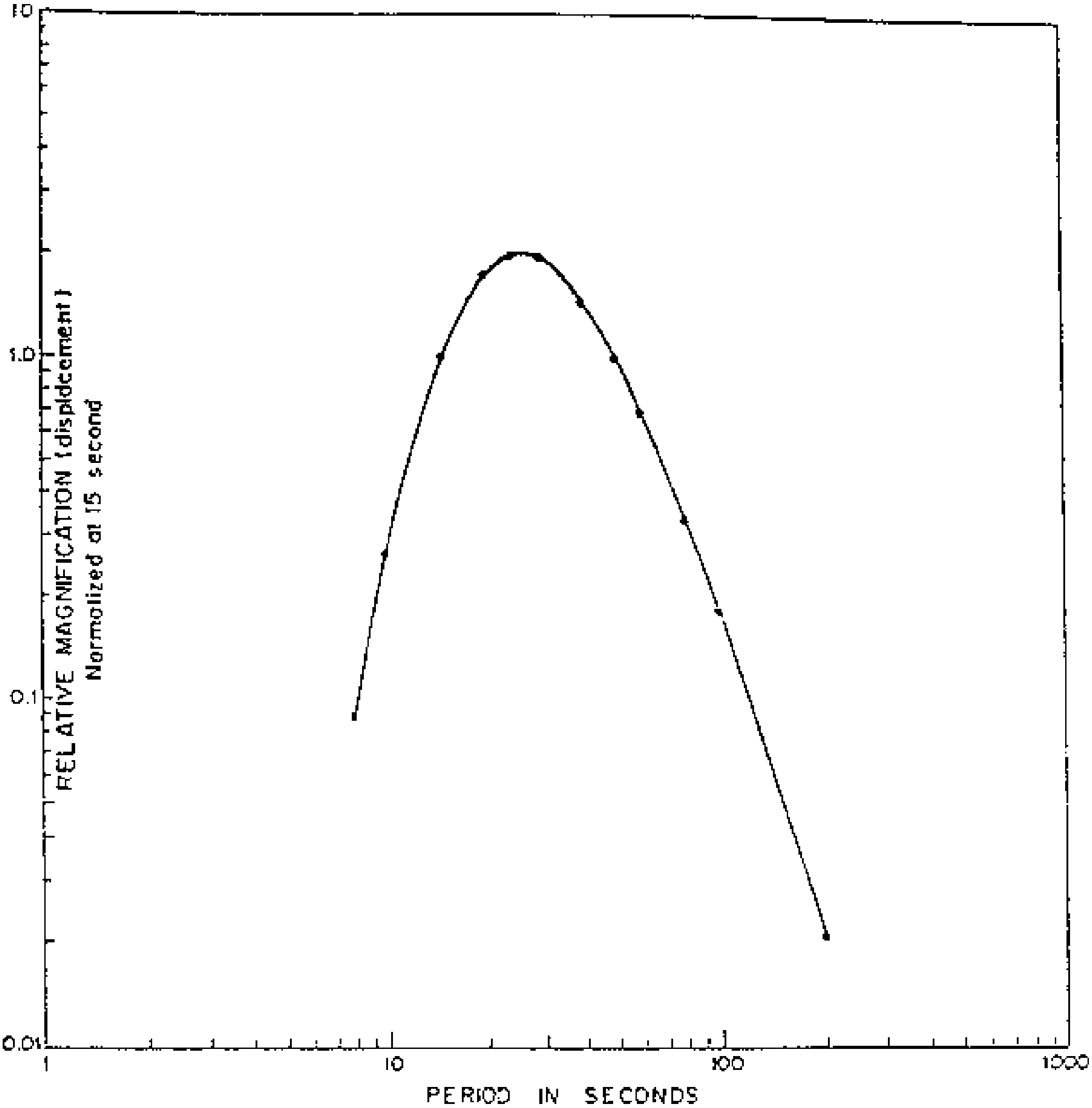

Figure 1.10 Amplitude response curve for LP N-S narrow band seismograph at RYD

APPENDIX II.

LIST OF THE EARTHQUAKES ANALYZED

TABLE I

LIST OF THE EARTHQUAKES ANALYZED

	LOC	DATE			O.T			COOR	DEP	DEP	MAGN		DIST	B_AZ	T-OFF	EMER
		D	M	Y	H	M	S	LAT	LON	KM	MB	MS	DEG	DEG	DEG	DEG
1.	BONI	8	11	85	18	40	24.8	27.96	140.61	42	5.8	6.1	82.1	62	18	15
2.	ARAB	14	12	85	18	13	31.5	14.71	58.00	10	5.5	0.0	15.0	130	39	42
3.	IRAN	12	7	86	7	54	26.8	29.96	51.58	10	5.7	5.6	6.8	39	58	45
4	MOLU	14	8	86	19	39	13.6	1.79	126.52	33	6.6	7.2	80.1	92	18	15
5.	FOX	5	1	87	12	11	55.7	52.45	-169.4	33	6.1	6.7	97.0	21	16	13
6.	KAMC	19	1	87	6	47	4.3	54.74	163.28	42	5.4	5.2	84.1	31	17	14
7.	HONS	6	2	87	12	23	4.8	36.99	141.79	36	5.9	6.1	79.4	54	19	15
8.	HONS	7	4	87	0	40	43.4	37.36	141.80	29	6.4	6.6	79.3	53	19	15
9.	CHIN	30	4	87	5	17	3.7	39.76	74.57	8	5.7	5.6	27.9	50	33	27
10.	KUSH	5	5	87	15	40	47.5	36.48	70.67	202	5.8	.0	23.7	54	36	29
11	BURM	18	5	87	01	53	05.1	25.27	94.20	50	5.7	5.9	43.0	78	29	24
12	KAZA	17	7	87	1	17	7.0	49.80	78.11	0	5.8	.0	35.0	36	28	17
13.	PAKI	10	8	87	10	52	19.9	29.87	63.84	165	5.6	.0	16.1	67	51	40
14	KAMC	6	10	87	20	11	35.1	52.96	159.97	34	6.1	6.3	83.5	33	18	14
15.	ETHI	25	10	87	16	46	13.3	5.41	36.75	12	5.6	6.2	21.4	207	39	31
16	IRAN	30	3	88	2	12	42.8	30.89	50.19	33	5.4	5.7	6.9	26	58	45
17	BAND	30	5	88	21	11	11.3	-7.50	128.32	86	6.5	.0	85.6	100	17	14
18	IRAQ	25	7	88	7	58	42.2	42.20	35.94.	99	4.9.	5.2	11.2	357	55	43
19	AFGH	26	9	88	7	17	.2	36.29	71.37	107	5.6	.	24.2	55	35	29
20.	ARME	7	12	88	7	41	24.2	40.99	44.19	5	6.2	6.8	16.3	353	51	40
11	KURL	9	1	89	13	42	36.4	49.99	153.48	14	6.0	6.4	83.0	41	18	15
22	MOLU	10	2	89	11	15	24.6	2.31	126.76	44	6.2	6.8	80.1	92	18	15
23.	KURL	11	4	89	3	56	36.9	49.49	159.15	16	6.3	6.6	85.0	37	17	14
24	BAND	7	7	89	19	41	18.8	-4.82	128.97	34	5.5	4.8	85.1	97	17	14
25.	XING	17	4	90	1	59	33.4	39.44	74.90	33	6.0	6.2	28.0	51	33	27
26	SAKH	12	5	90	4	50	8.0	49.04	141.85	600	6.5		75.0	42	20	16
27.	SUDA	20	5	90	2	22	1.6	5.12	32.15	15	6.7	7.1	23.9	217	36	29
28.	ROMA	30	5	90	10	40	6.1	45.84	26.67	89	6.7	.0	26.5	327	34	28
29.	SUDA	9	7	90	15	11	20.3	5.39	31.65	13	5.9	6.4	24.0	219	36	29
30.	IRAN	6	11	90	18	45	52.2	28.25	55.46	11	6.2	6.7	8.7	64	57	44
31.	KUSH	31	1	91	23	3	33.6	35.99	70.42	142	6.4	.0	23.4	55	36	29
32.	MINA	20	6	91	5	18	52.5	1.20	122.79	31	6.2	7.0	76.9	94	20	16
33.	ETHI	5	3	92	8	55	5.6	11.51	42.81	7	5.5	6.2	13.6	196	53	42
34.	TURK	13	3	92	17	18	39.9	39.71	39.60	27	6.2	6.8	16.1	340	51	40
35.	CRET	3	5	92	8	35	36.8	34.97	26.69	29	4.7	.0	20.	305	29	33
36.	EGYP	12	10	92	13	9	55.5	29.78	31.14	22	5.9	5.3	14.6	293	53	41
37.	MIND	17	5	92	9	49	19.1	7.24	126.64	33	6.2	7.1	78.0	87	19	16
38.	MEDI	21	11	92	5	7	21.7	35.92	22.49	65	5.9	.0	23.6	303	36	29
39.	REDS	13	3	93	17	12	26.2	19.63	38.80	10	5.7	5.4	8.8	236	57	44
40.	AQAB	3	6	93	12	43	5.3	28.73	34.55	10	5.9	5.8	11.5	293	55	43

APPENDIX III.

PLOTS OF THE DIGITIZED SEISMOGRAMS

EARTHQUAKE OF NOV.8, 1985

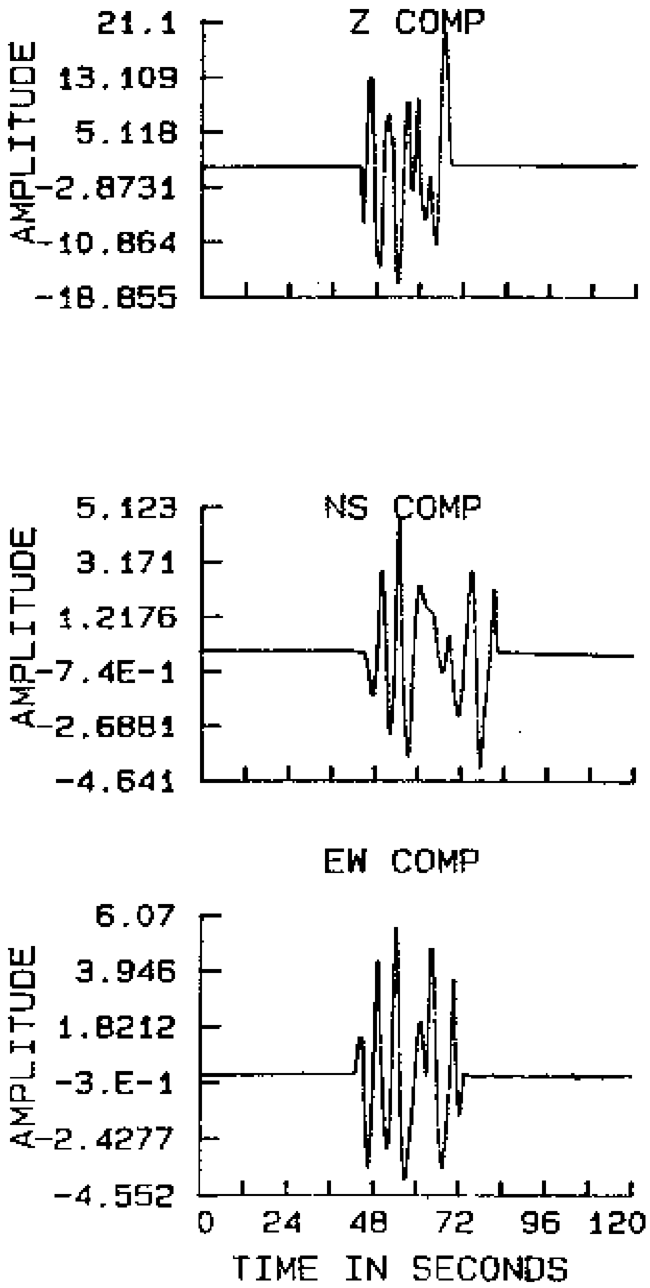

EPI.DIST : 82.1 deg.DEPTH : 42 Km.
BACK AZ. : 62 deg.
ANGLE OF EMER: 15 deg.
EPI. COORD : 27.96N.140.61 E.
MAGNITUDE mb : 5.8

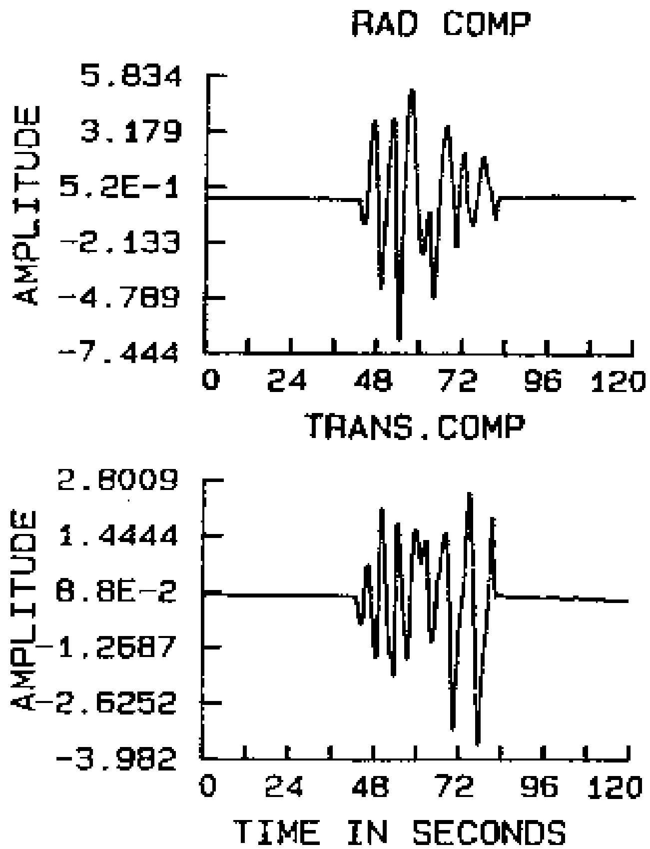

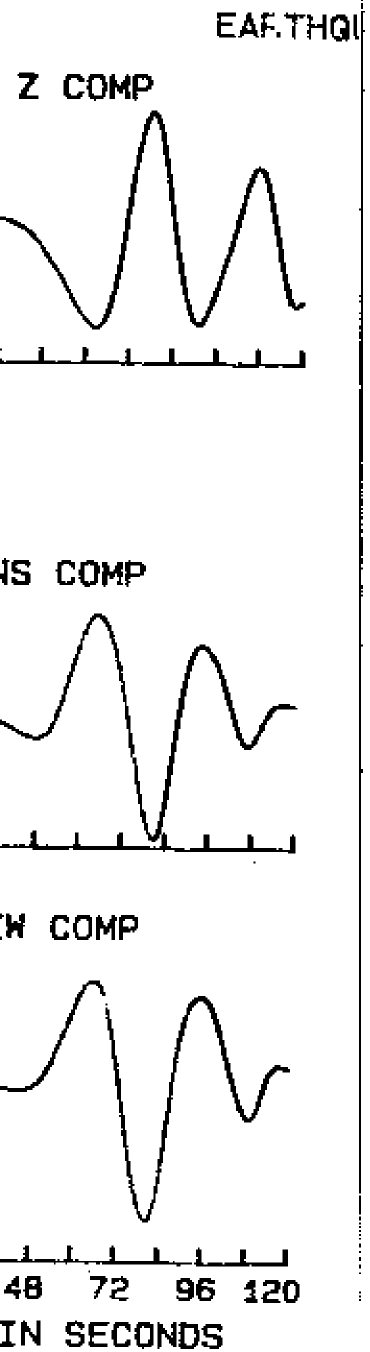

EARTHQUAKE OF JUL. 12, 1986

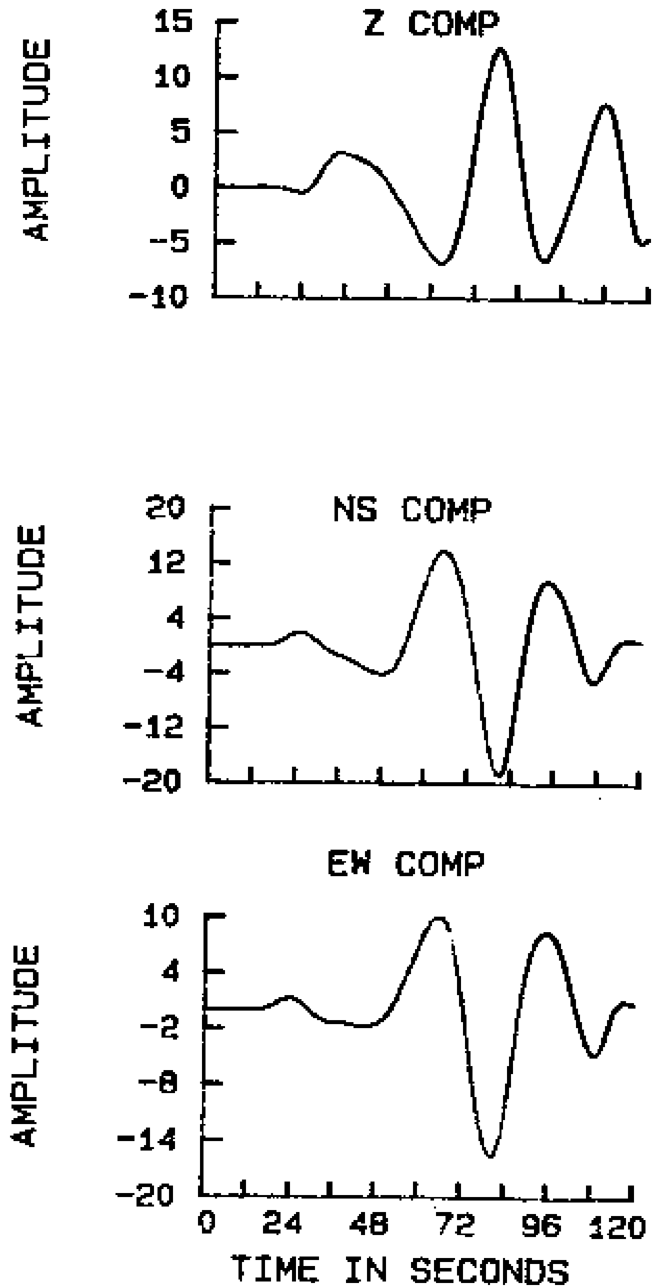

EPI.DIST : 6.8 deg. DEPTH : 10 Km.
BACK AZ. : 39 deg.
ANGLE OF EMER: 45 deg.
EPI. COORD : 29.96N. 51.58 E.
MAGNITUDE mb : 5.6

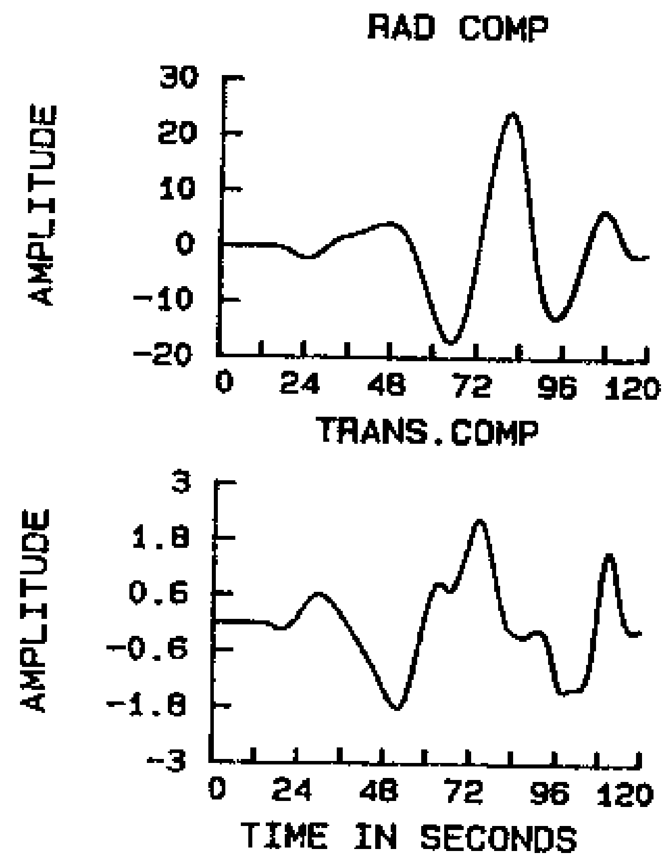

EARTHQUAKE OF AUG.14, 1986

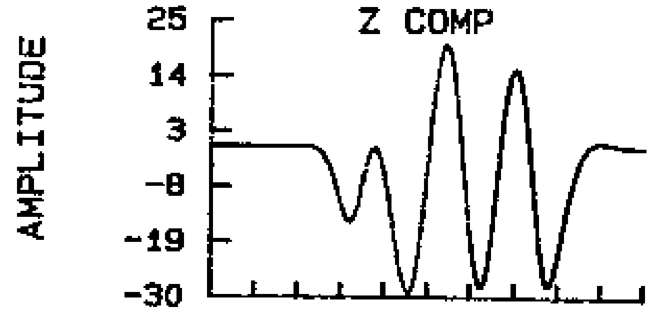

EPI.DIST : 80.1 deg.DEPTH : 33 Km.
BACK AZ. : 92 deg.
ANGLE OF EMER: 15 deg.
EPI. COORD : 1.79N.126.52 E.
MAGNITUDE mb : 6.6

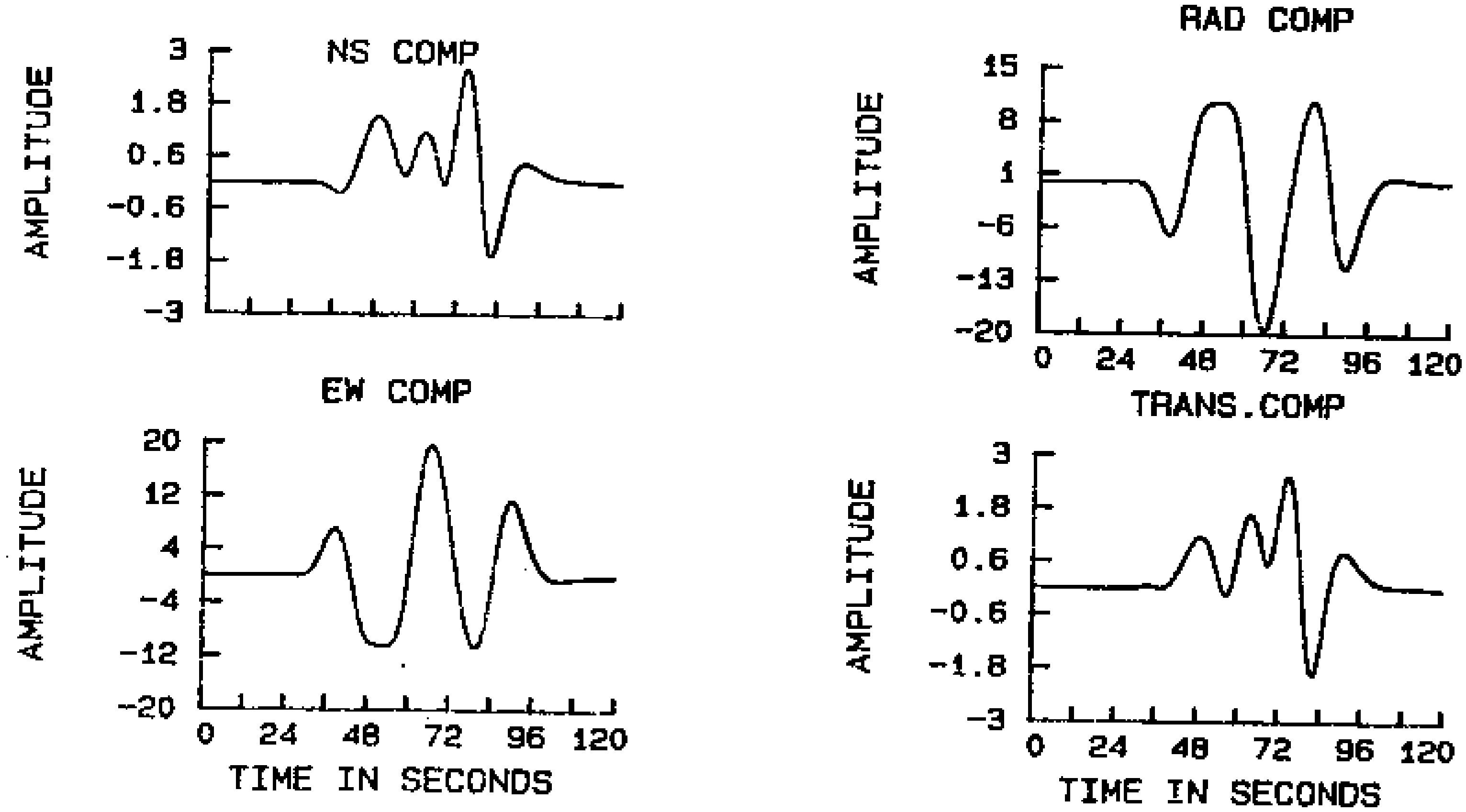

EARTHQUAKE OF APR.30, 1987

EPI.DIST : 27.9 deg.DEPTH : 8 Km.
BACK AZ. : 50 deg.
ANGLE OF EMER: 27 deg.
EPI. COORD : 39.76 N. 74.57 E.
MAGNITUDE mb : 5.7

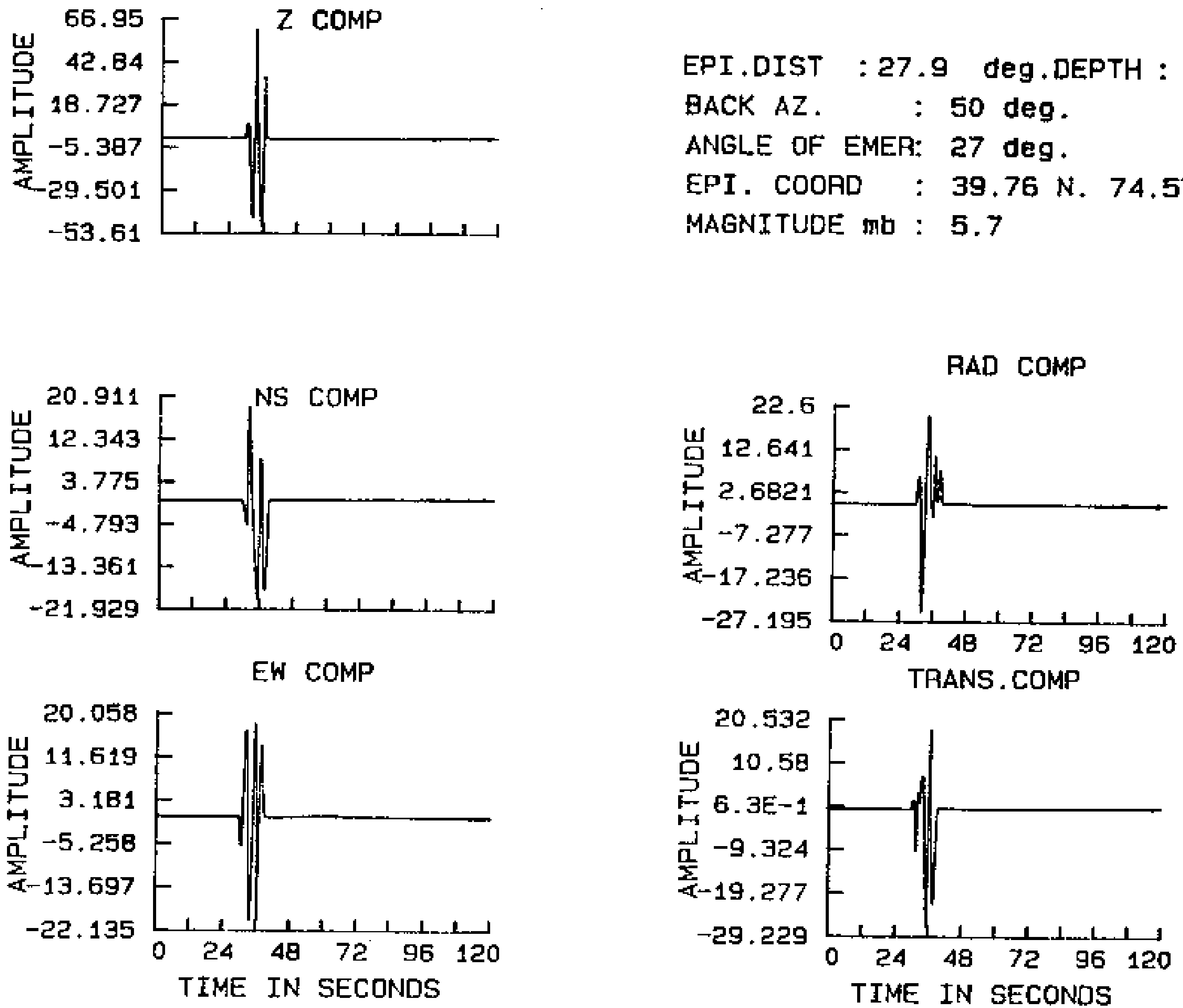

EARTHQUAKE OF MAY 5, 1987

EPI.DIST : 23.7 deg.DEPTH : 202 Km.
BACK AZ. : 54 deg.
ANGLE OF EMER: 29 deg.
EPI. COORD : 36.48 N. 70.67 E.
MAGNITUDE mb : 5.8

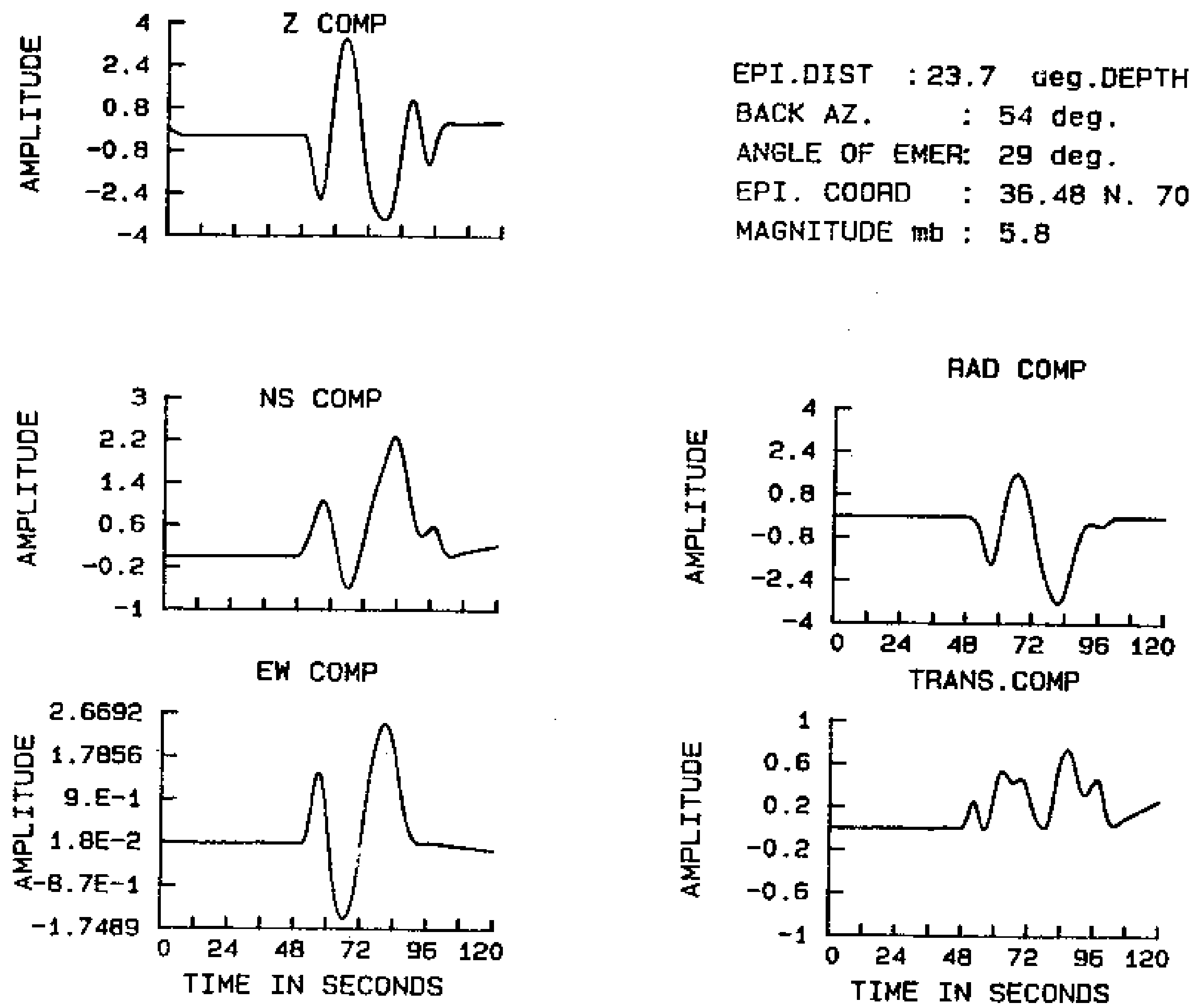

EARTHQUAKE OF MAY 18, 1987

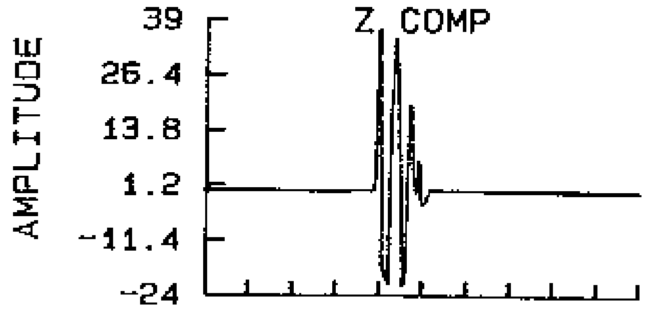

EPI.DIST : 43 deg.DEPTH : 50 Km.
BACK AZ. : 78 deg.
ANGLE OF EMER: 24 deg.
EPI. COORD : 25.27 N. 94.20 E.
MAGNITUDE mb : 5.7

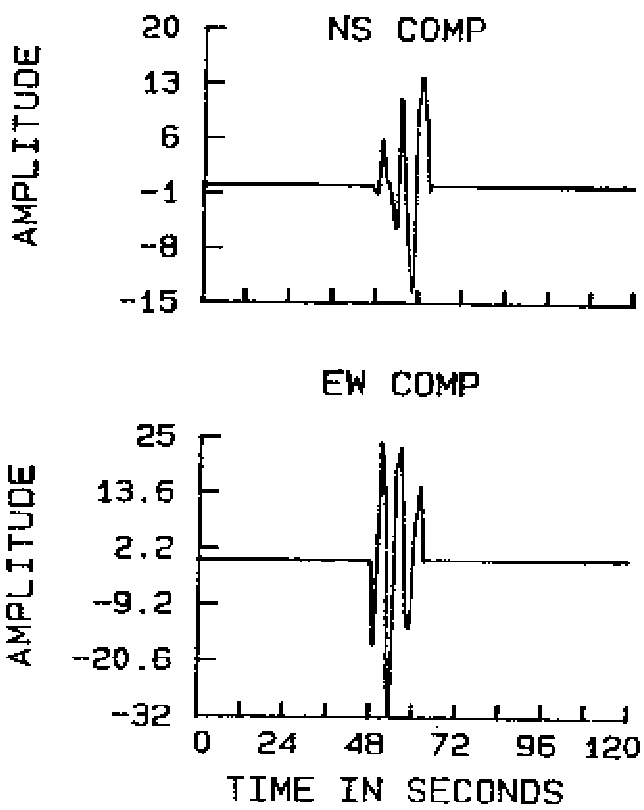

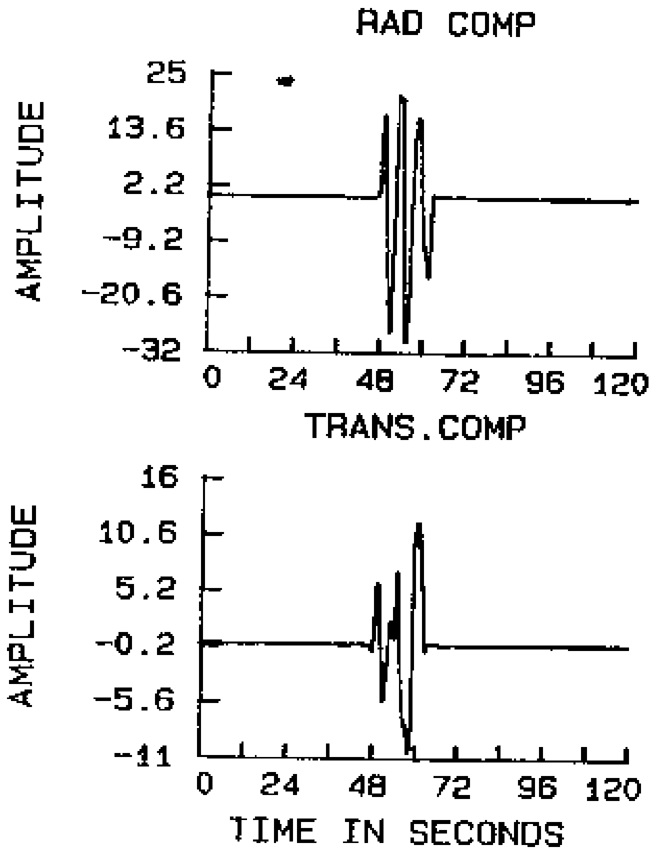

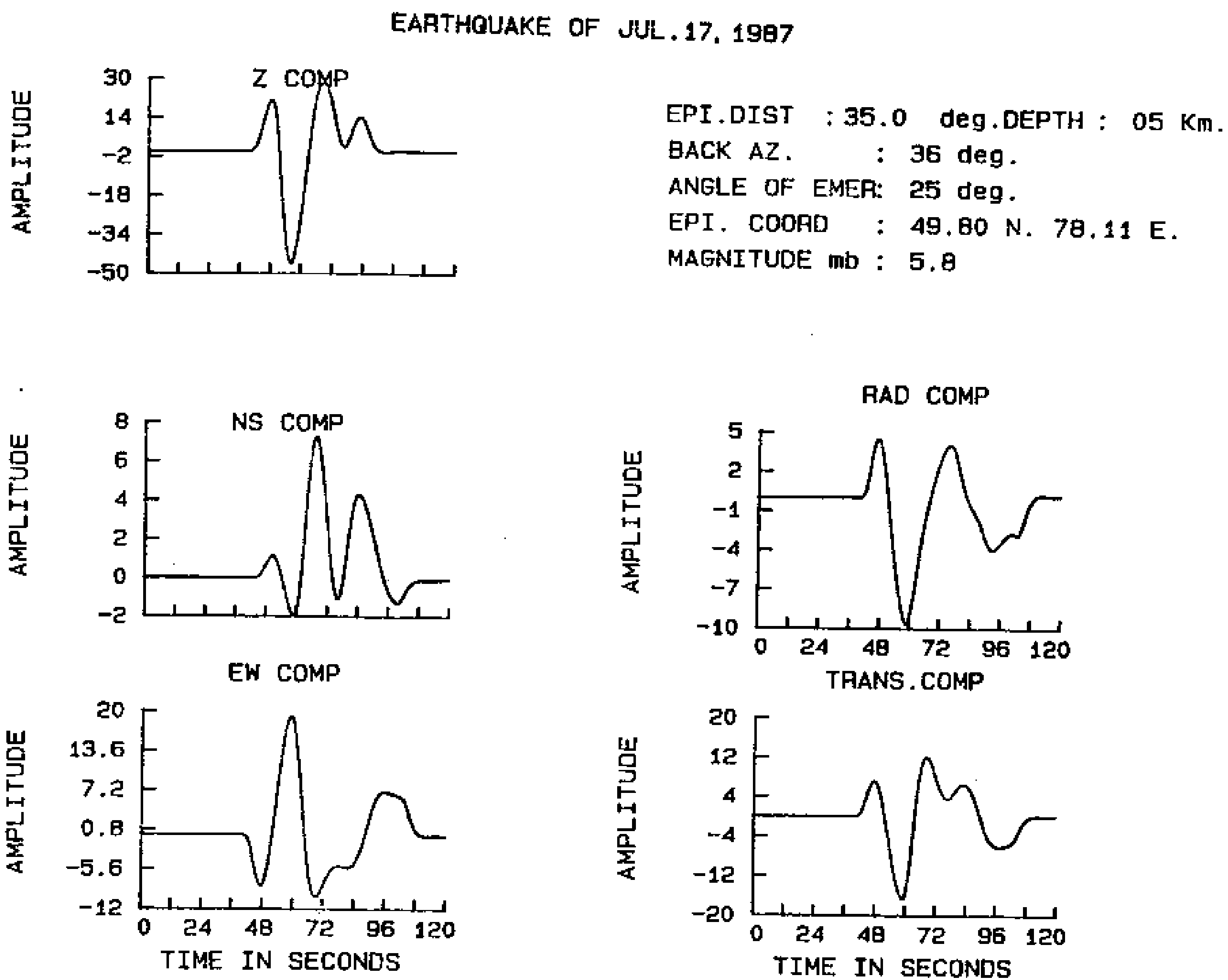
EARTHQUAKE OF JUL.17.1987
EPI.DIST : 35.0 deg.DEPTH : 05 Km.
BACK AZ. : 36 deg.
ANGLE OF EMER: 25 deg.
EPI. COORD : 49.80 N. 78.11 E.
MAGNITUDE mb : 5.8
Z COMP
NS COMP
EW COMP
RAD COMP
TRANS.COMP
AMPLITUDE
30
14
-2
-18
-34
-50
8
6
4
2
0
-2
20
13.6
7.2
0.8
-5.6
-12
5
2
-1
-4
-7
-10
20
12
4
-4
-12
-20
0 24 48 72 96 120
TIME IN SECONDS

EARTHQUAKE OF AUG.10, 1987

EPI.DIST : 16.1 deg.DEPTH : 165 Km.
BACK AZ. : 67 deg.
ANGLE OF EMER: 40 deg.
EPI. COORD : 29.87 N. 63.84 E.
MAGNITUDE mb : 5.6

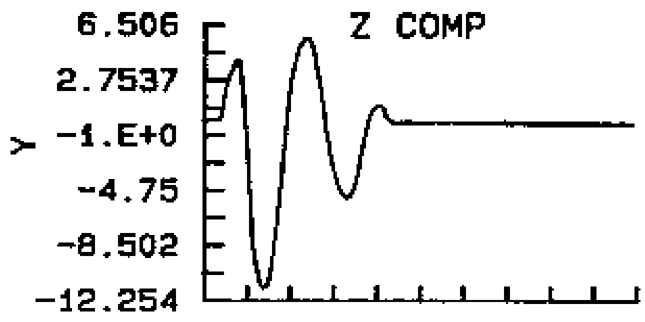

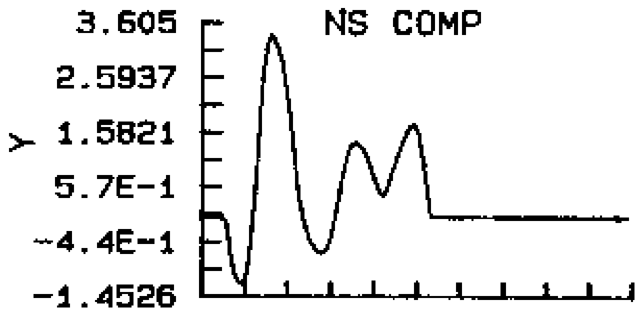

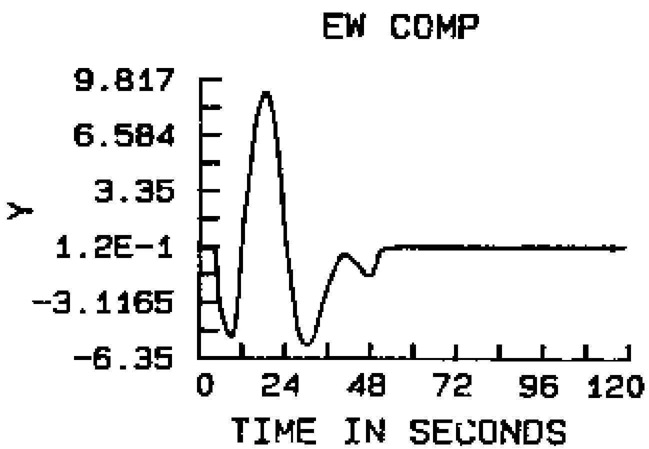

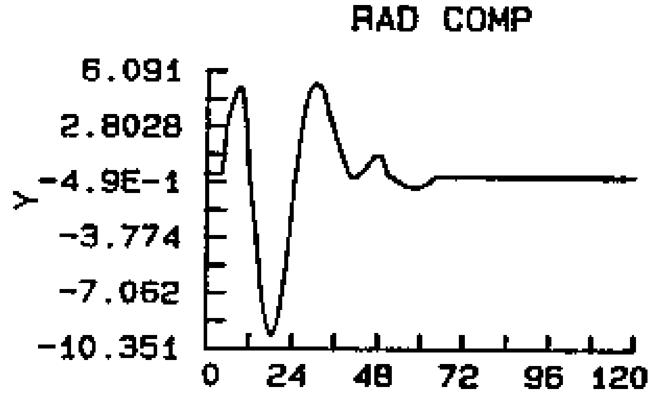

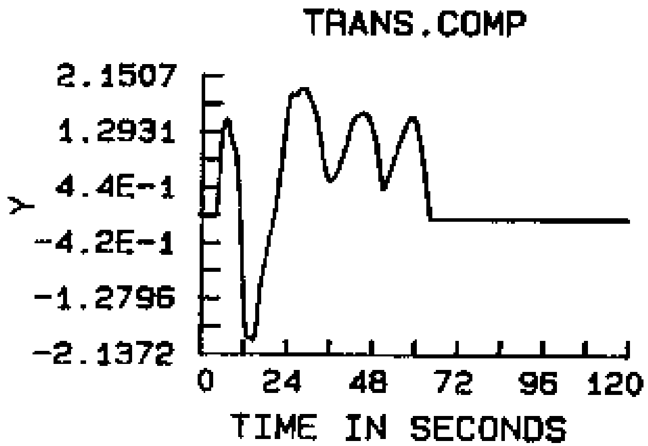

EARTHQUAKE OF OCT.6. 1987

EPI.DIST : 83.5 deg.DEPTH : 34 Km.
BACK AZ. : 33 deg.
ANGLE OF EMER: 14 deg.
EPI. COORD : 52.96 N.159.97 E.
MAGNITUDE mb : 6.1

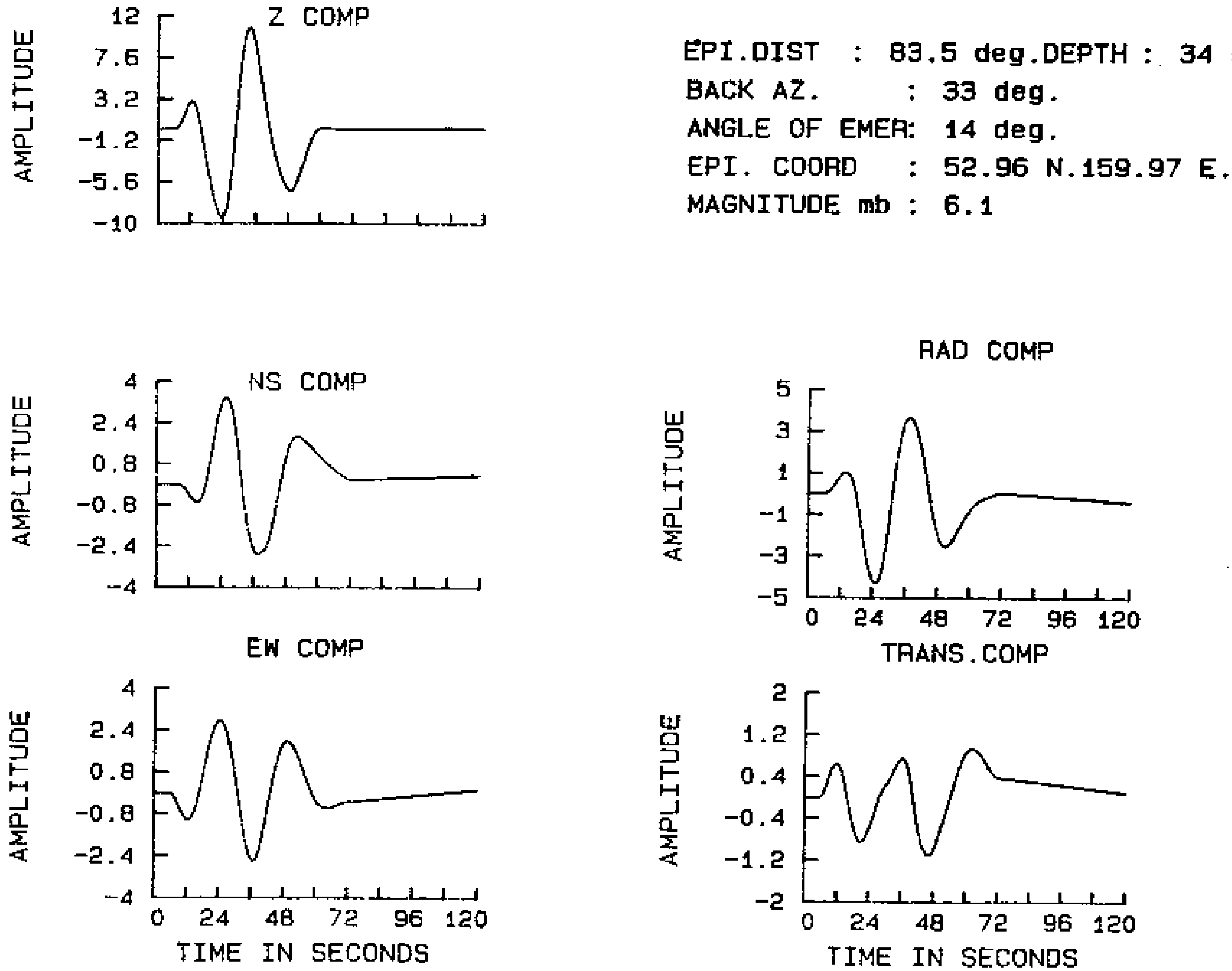

EARTHQUAKE OF OCT.25, 1987

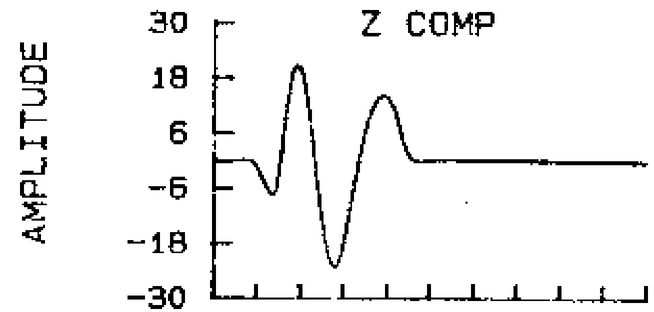

EPI.DIST : 21.4 deg.DEPTH : 12 Km.
BACK AZ. :207 deg.
ANGLE OF EMER: 31 deg.
EPI. COORD : 05.41 N. 36.75 E.
MAGNITUDE mb : 5.6

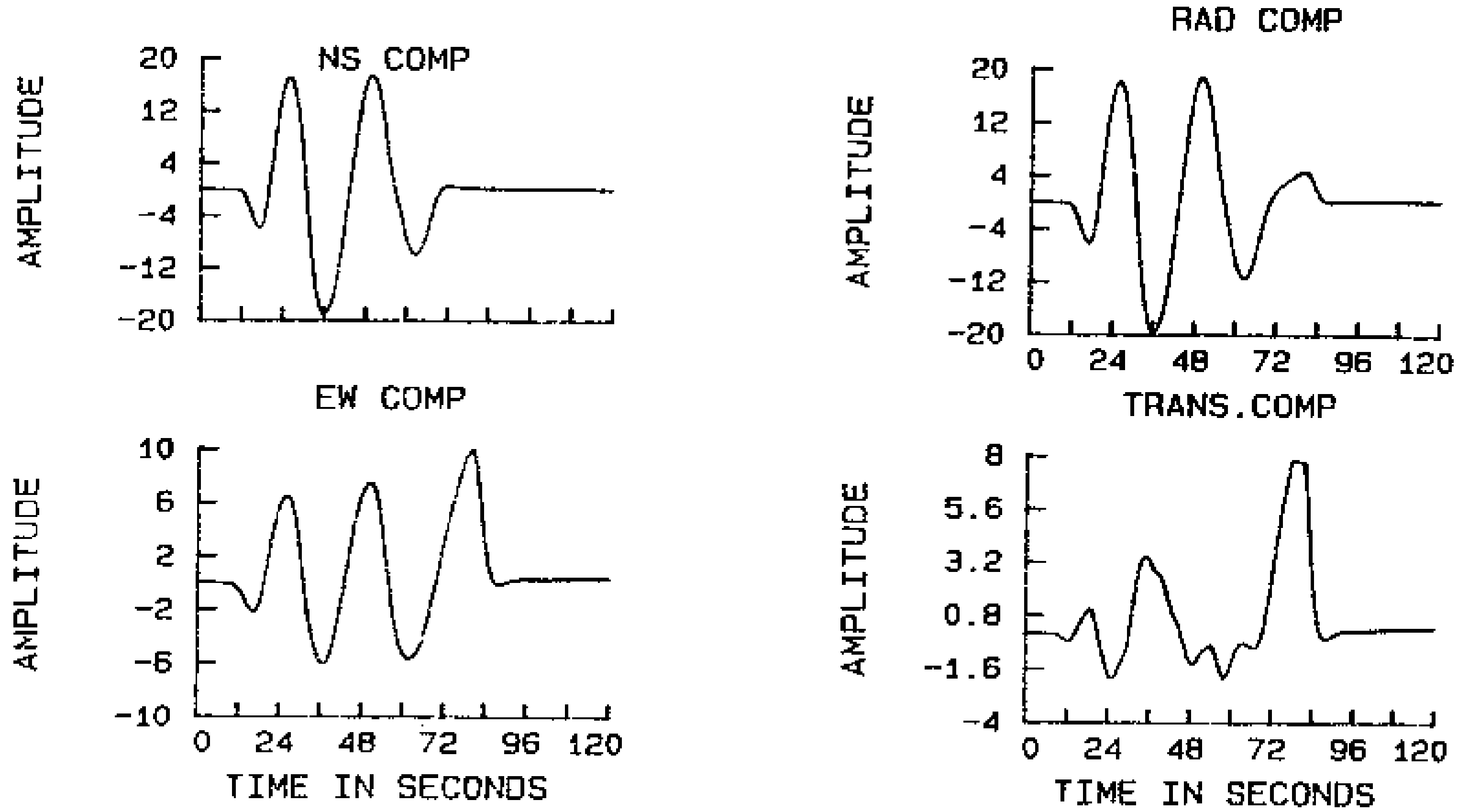

EARTHQUAKE OF MAY 30, 1988

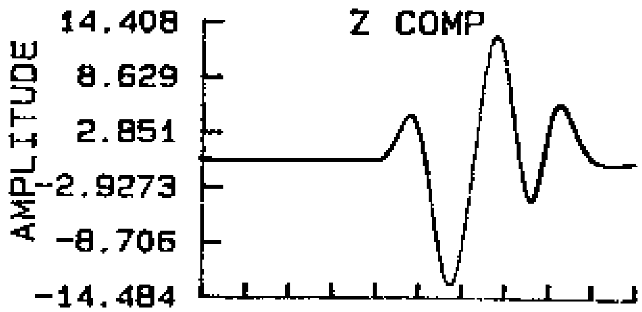

EPI.DIST : 85.6 deg.DEPTH : 86 Km.
BACK AZ. : 100 deg.
ANGLE OF EMER: 14 deg.
EPI. COORD : 07.51 S.128.32 E.
MAGNITUDE mb : 6.5

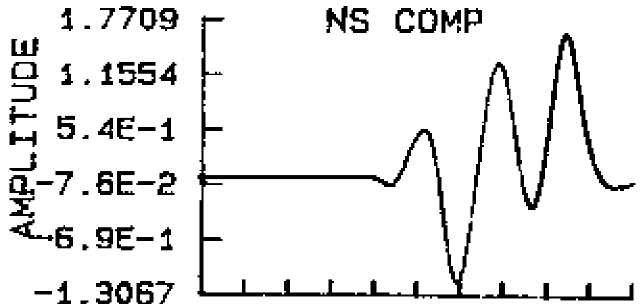

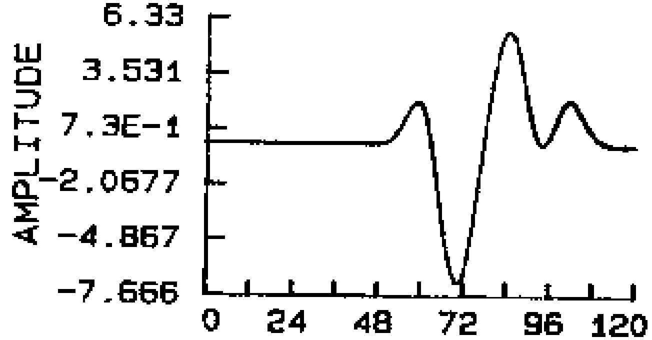

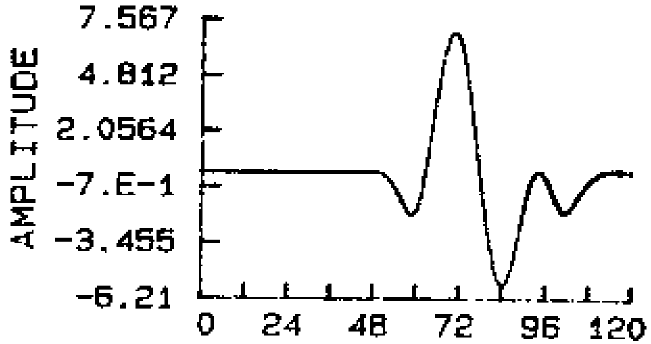

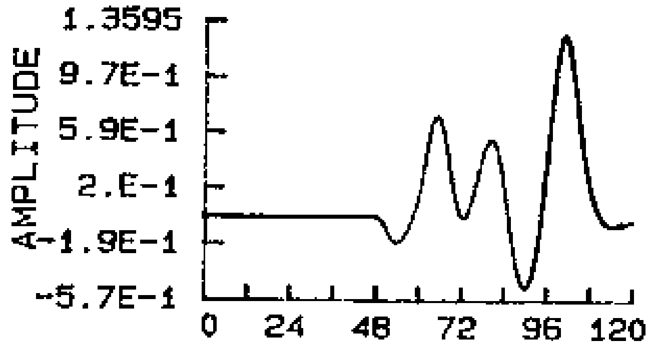

EARTHQUAKE OF JUL.25, 1988

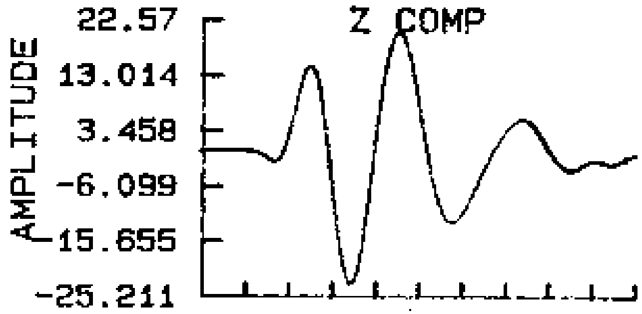

EPI.DIST : 11.2 deg.DEPTH : 77 Km.
BACK AZ. : 357 deg.
ANGLE OF EMER: 43 deg.
EPI. COORD : 42.20 N. 35.94 E.
MAGNITUDE mb : 4.9

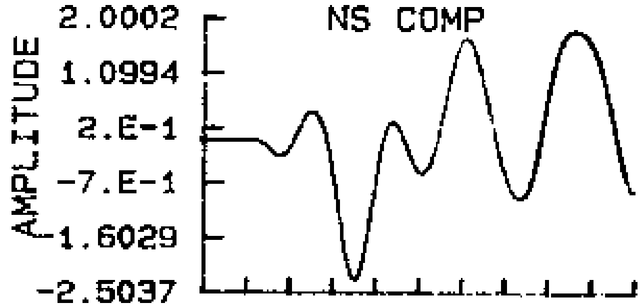

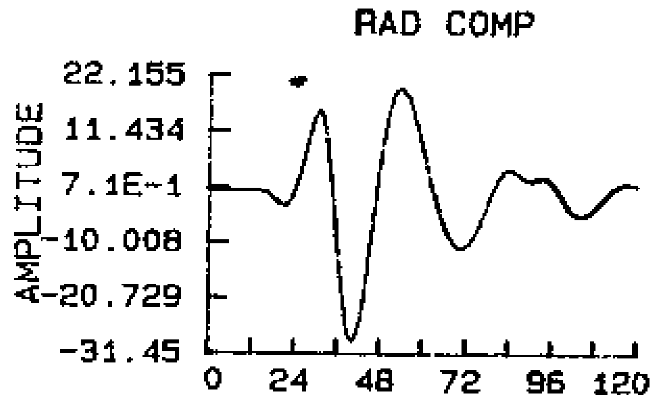

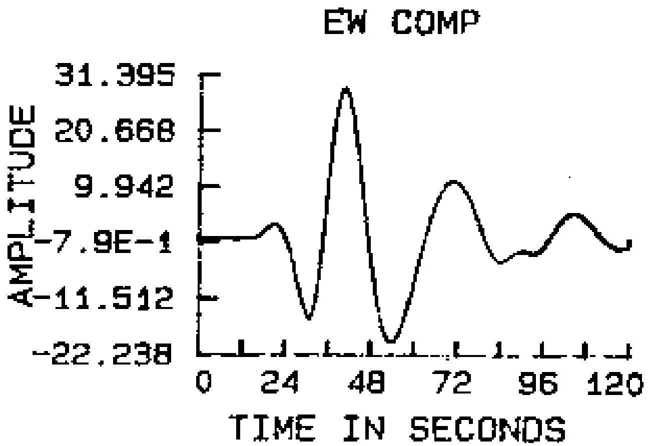

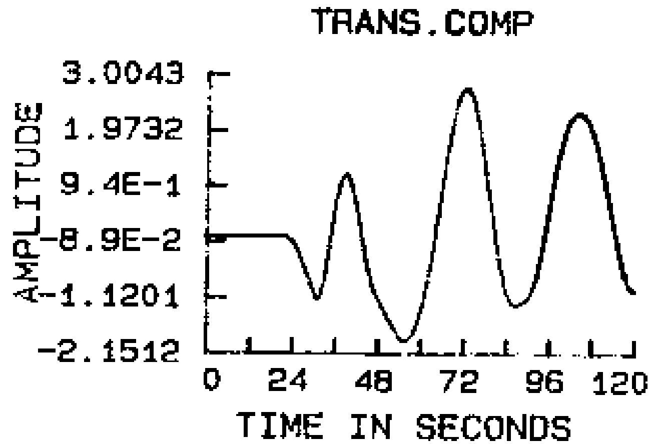

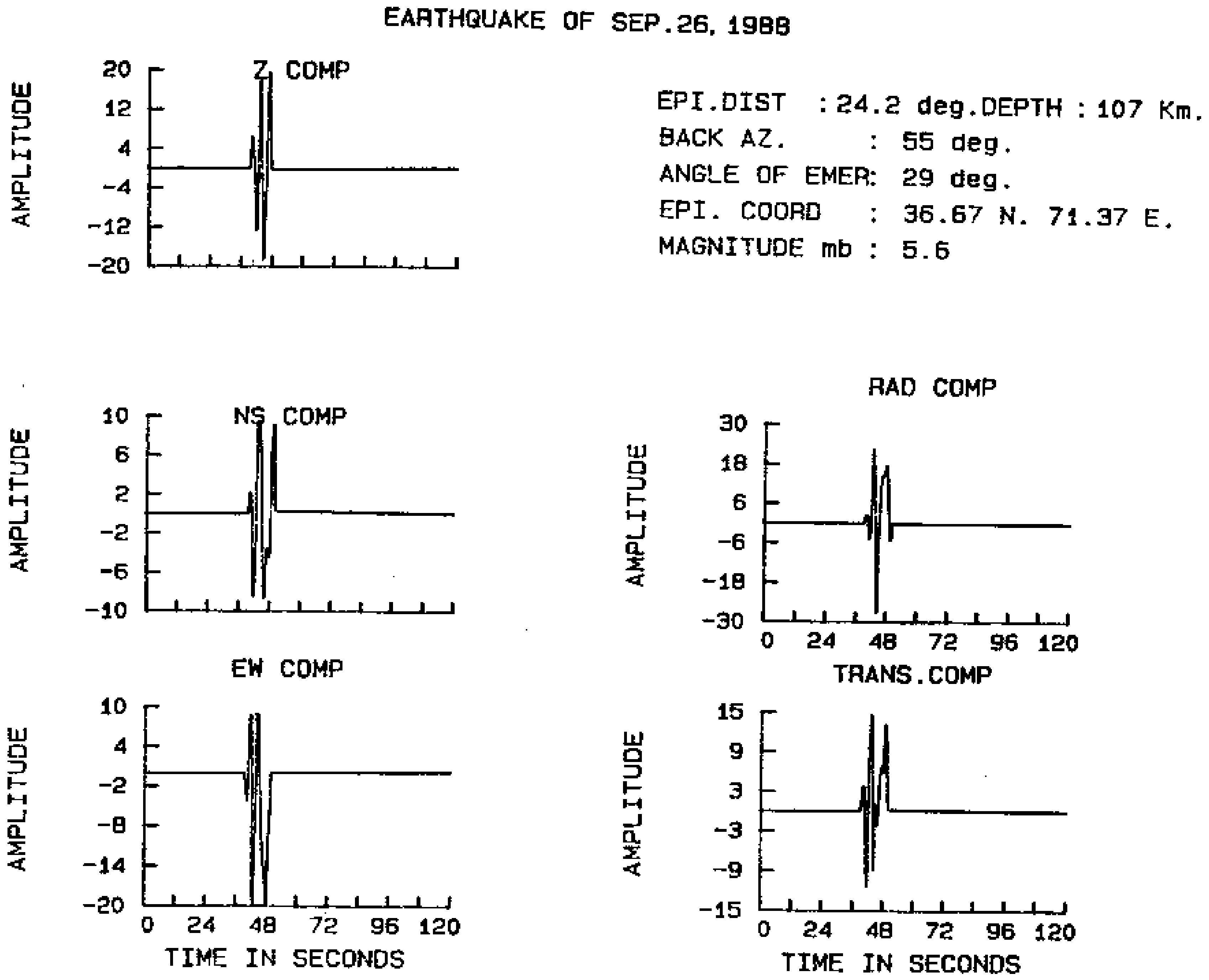
EARTHQUAKE OF SEP.26, 1988
EPI.DIST : 24.2 deg.DEPTH : 107 Km.
BACK AZ. : 55 deg.
ANGLE OF EMER: 29 deg.
EPI. COORD : 36.67 N. 71.37 E.
MAGNITUDE mb : 5.6
Z COMP
NS COMP
EW COMP
RAD COMP
TRANS.COMP
AMPLITUDE
20 12 4 -4 -12 -20
10 6 2 -2 -6 -10
10 4 -2 -8 -14 -20
30 18 6 -6 -18 -30
15 9 3 -3 -9 -15
0 24 48 72 96 120
TIME IN SECONDS

EARTHQUAKE OF JAN.9, 1989

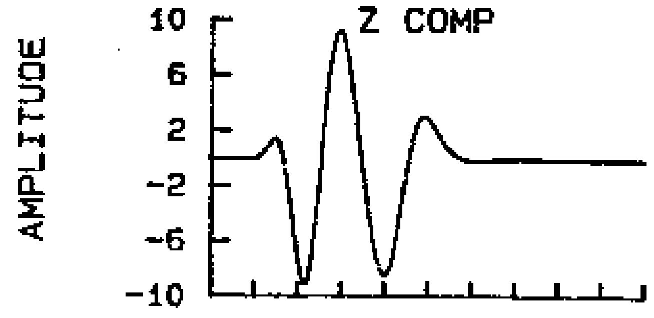

EPI.DIST : 83.0 deg.DEPTH : 14 Km.
BACK AZ. : 41 deg.
ANGLE OF EMER: 14 deg.
EPI. COORD : 46.99 N.153.48 E.
MAGNITUDE mb : 6.0

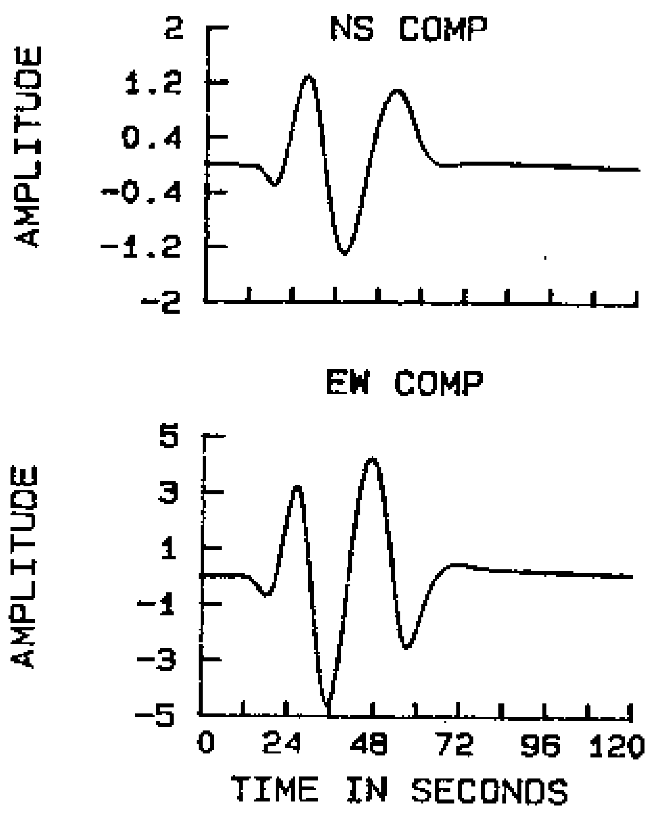

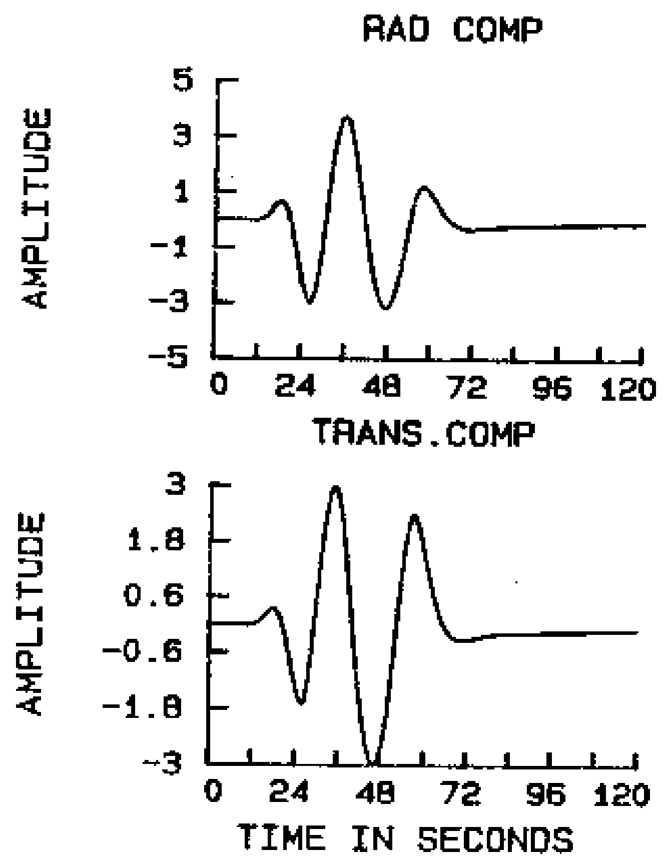

EARTHQUAKE OF FEB.10, 1989

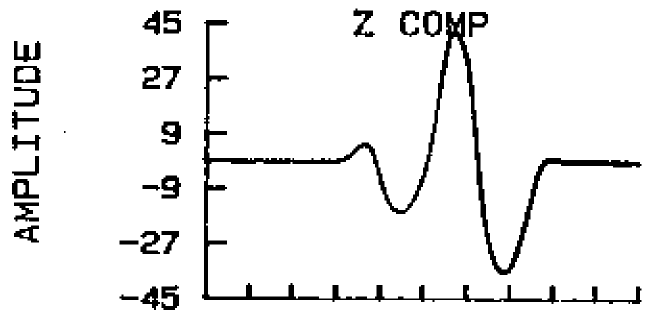

EPI.DIST : 80.1 deg.DEPTH : 44 Km.
BACK AZ. : 92 deg.
ANGLE OF EMER: 15 deg.
EPI. COORD : 2.31 N.126.76 E.
MAGNITUDE mb : 6.2

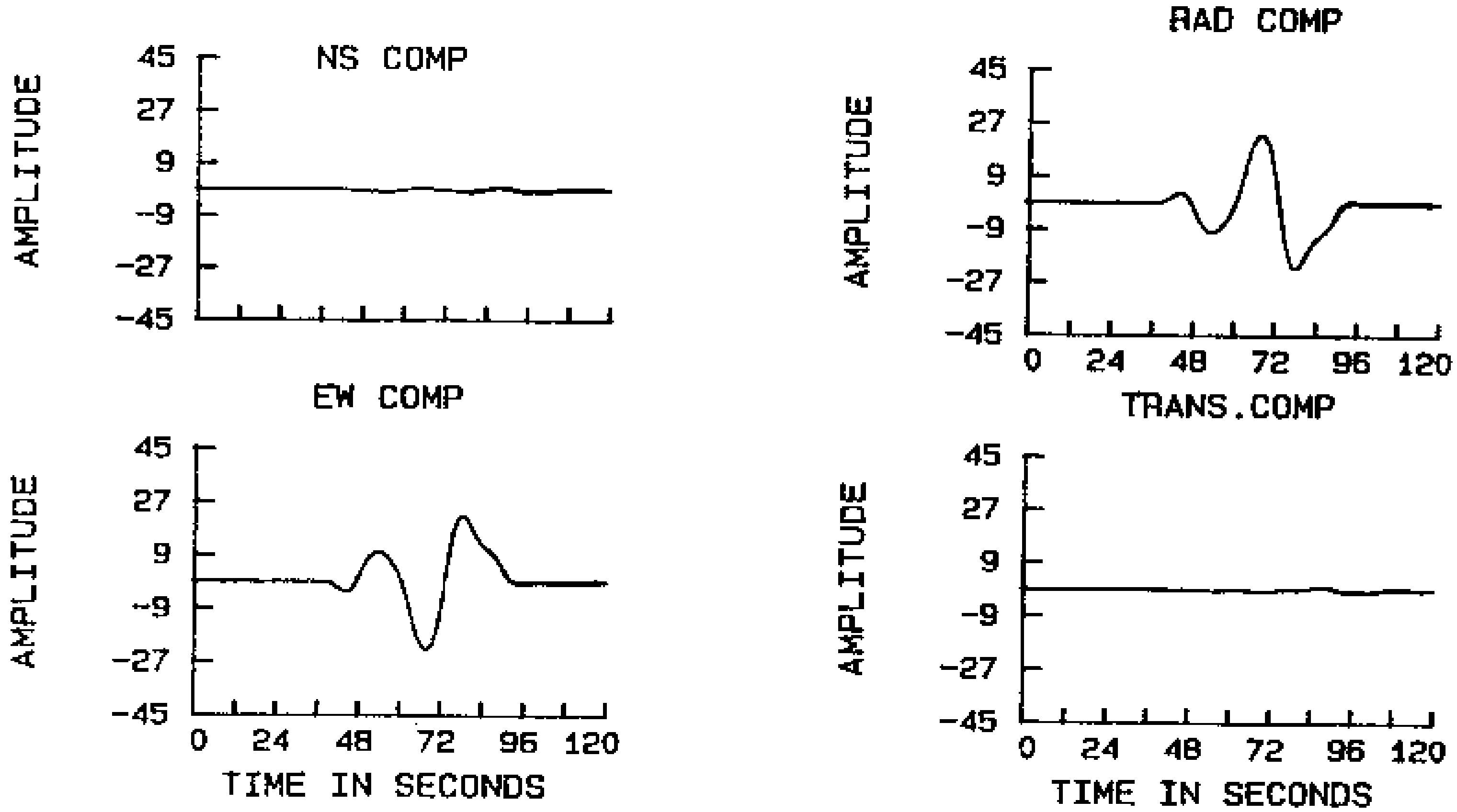

EARTHQUAKE OF APR.11,1989

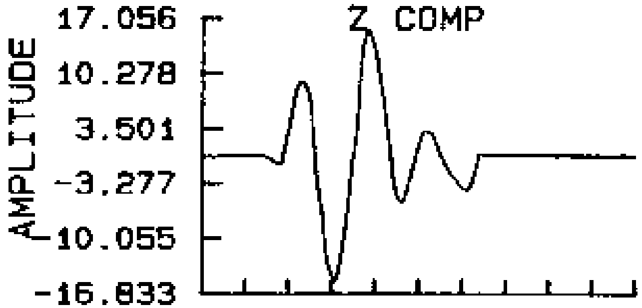

EPI.DIST : 85.0 deg.DEPTH : 16 Km.
BACK AZ. : 37 deg.
ANGLE OF EMER: 14 deg.
EPI. COORD : 49.49 N.159.15 E.
MAGNITUDE mb : 6.3

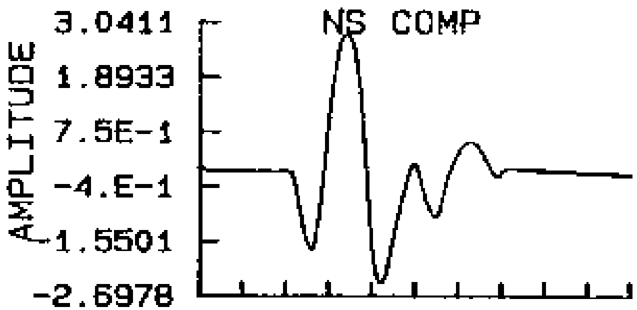

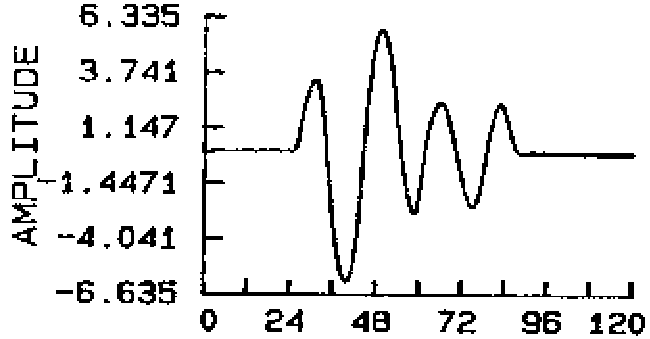

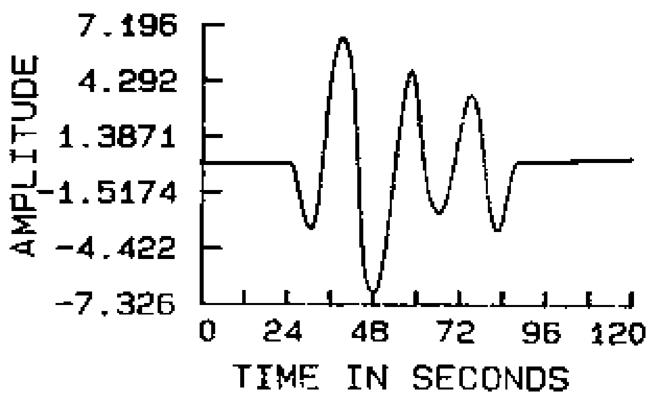

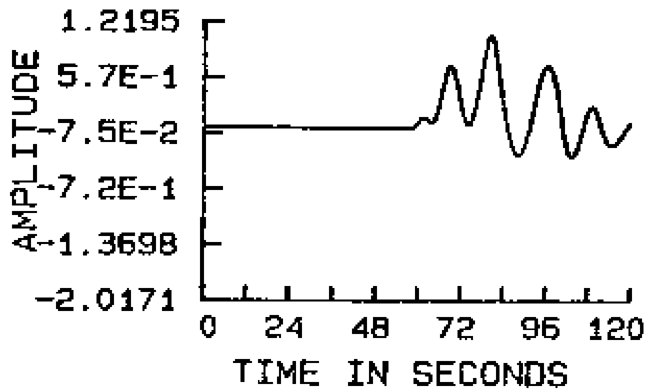

EARTHQUAKE OF JUL.7, 1989

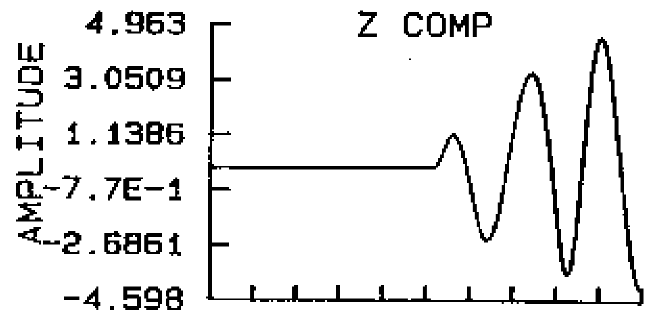

EPI.DIST : 86.1 deg.DEPTH : 34 Km.
BACK AZ. : 97 deg.
ANGLE OF EMER: 14 deg.
EPI. COORD : 4.82 S.128.97 E.
MAGNITUDE mb : 5.5

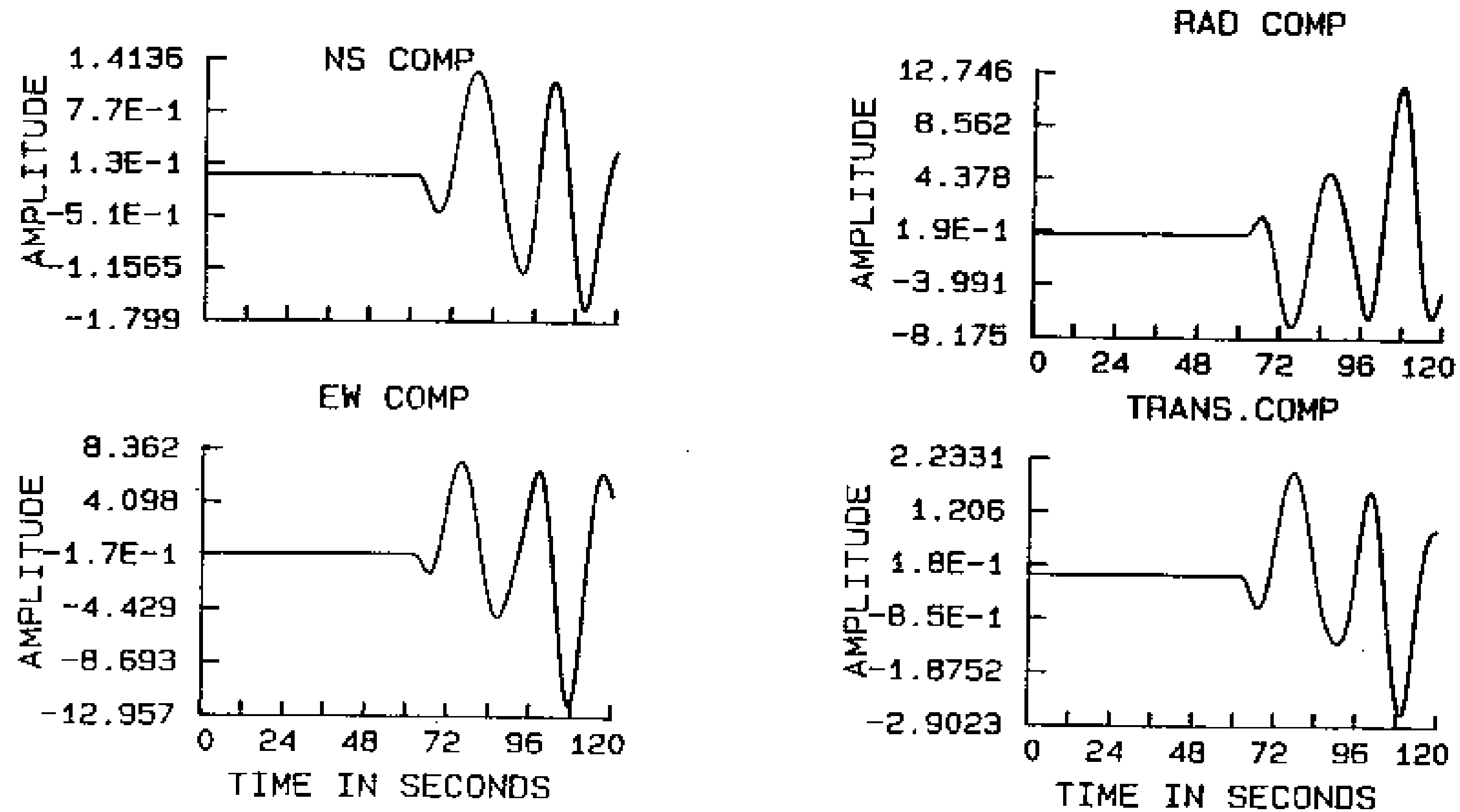

EARTHQUAKE OF APR.17,1990

EPI.DIST : 28.0 deg.DEPTH : 33 Km.
BACK AZ. : 51 deg.
ANGLE OF EMER: 27 deg.
EPI. COORD : 39.44 N. 74.90 E.
MAGNITUDE mb : 6.0

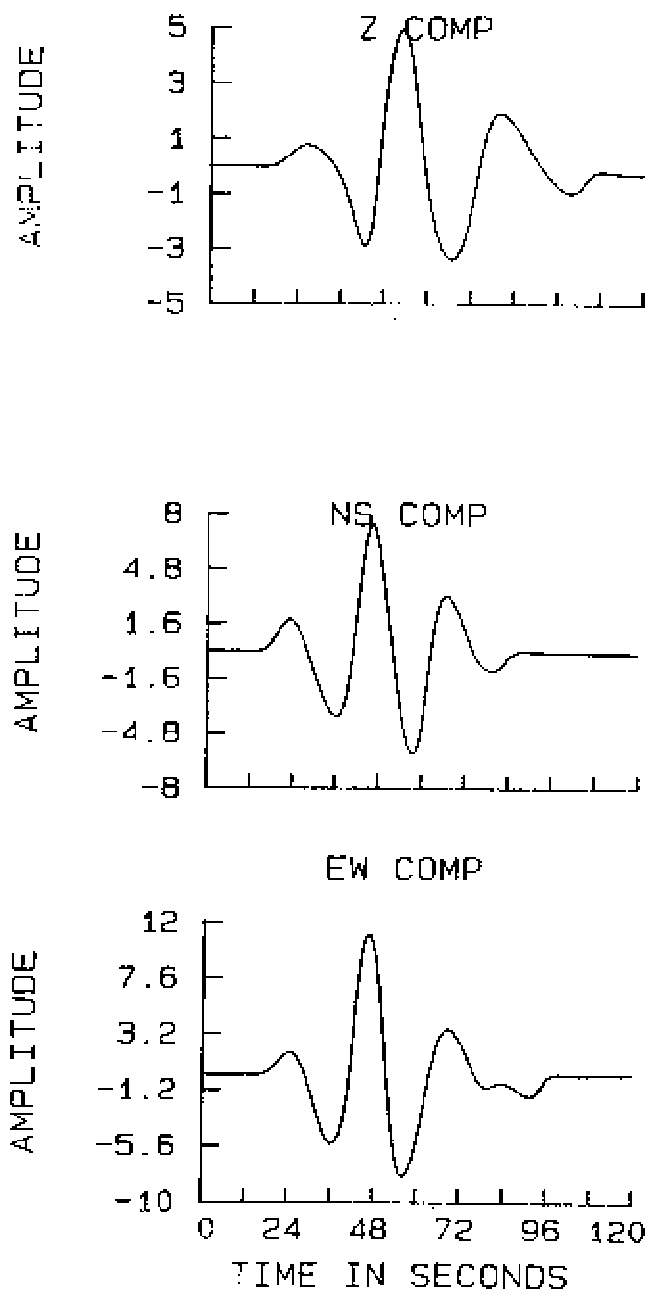

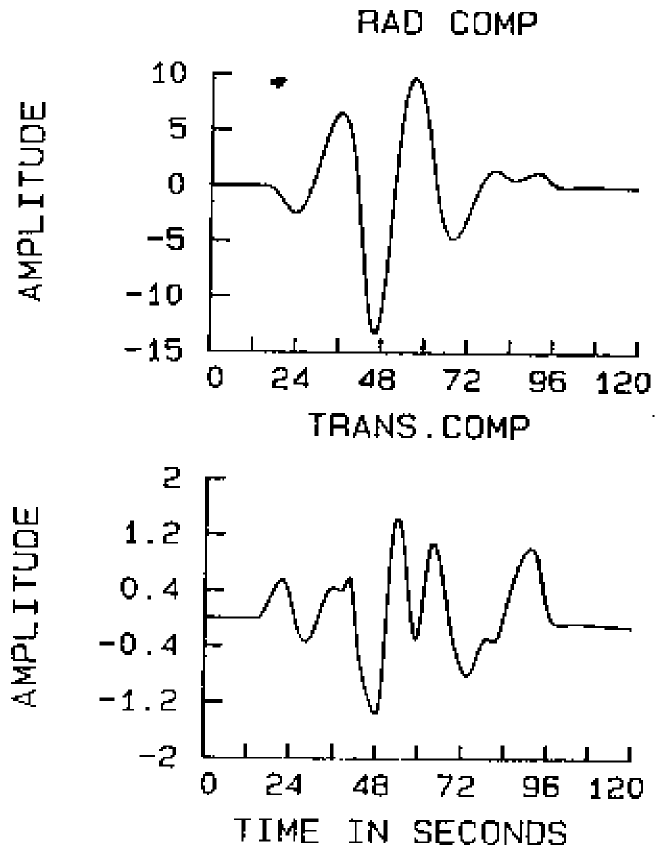

EARTHQUAKE OF FEB.10, 1989

EPI.DIST : 80.1 deg.DEPTH : 44 Km.
BACK AZ. : 92 deg.
ANGLE OF EMER: 15 deg.
EPI. COORD : 2.31 N. 126.76 E.
MAGNITUDE mb : 6.2

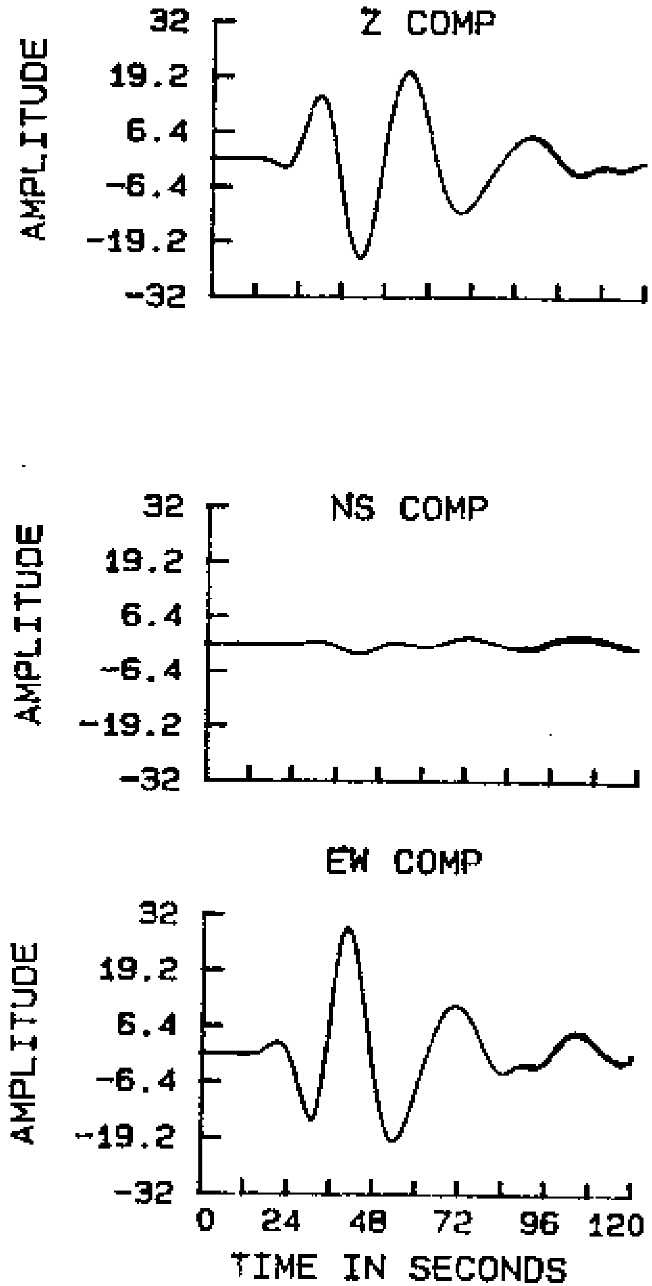

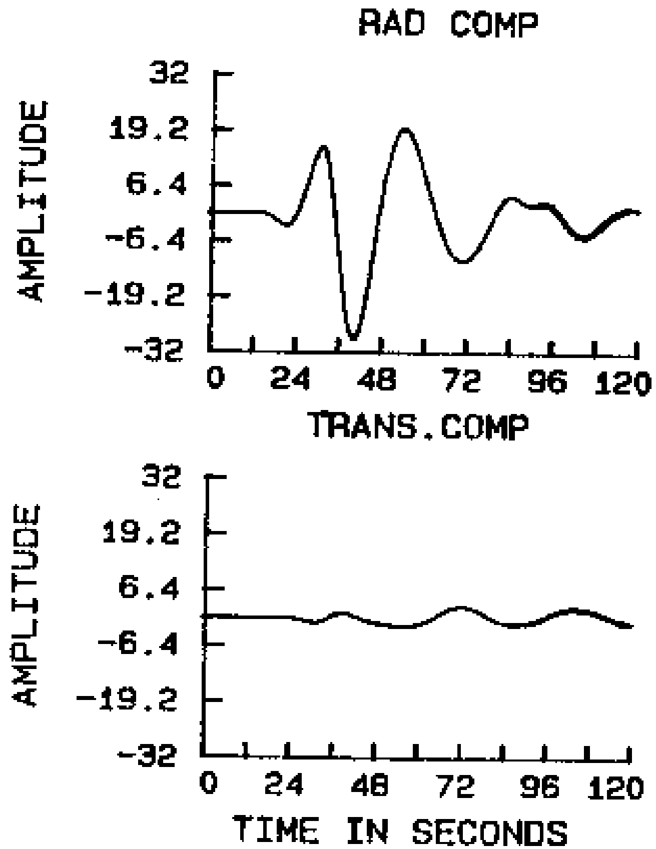

EARTHQUAKE OF MAY 12, 1990

EPI.DIST : 75.0 deg.DEPTH : 600 Km.
BACK AZ. : 42 deg.
ANGLE OF EMER: 16 deg.
EPI. COORD : 49.04 N.141.85 E.
MAGNITUDE mb : 6.5

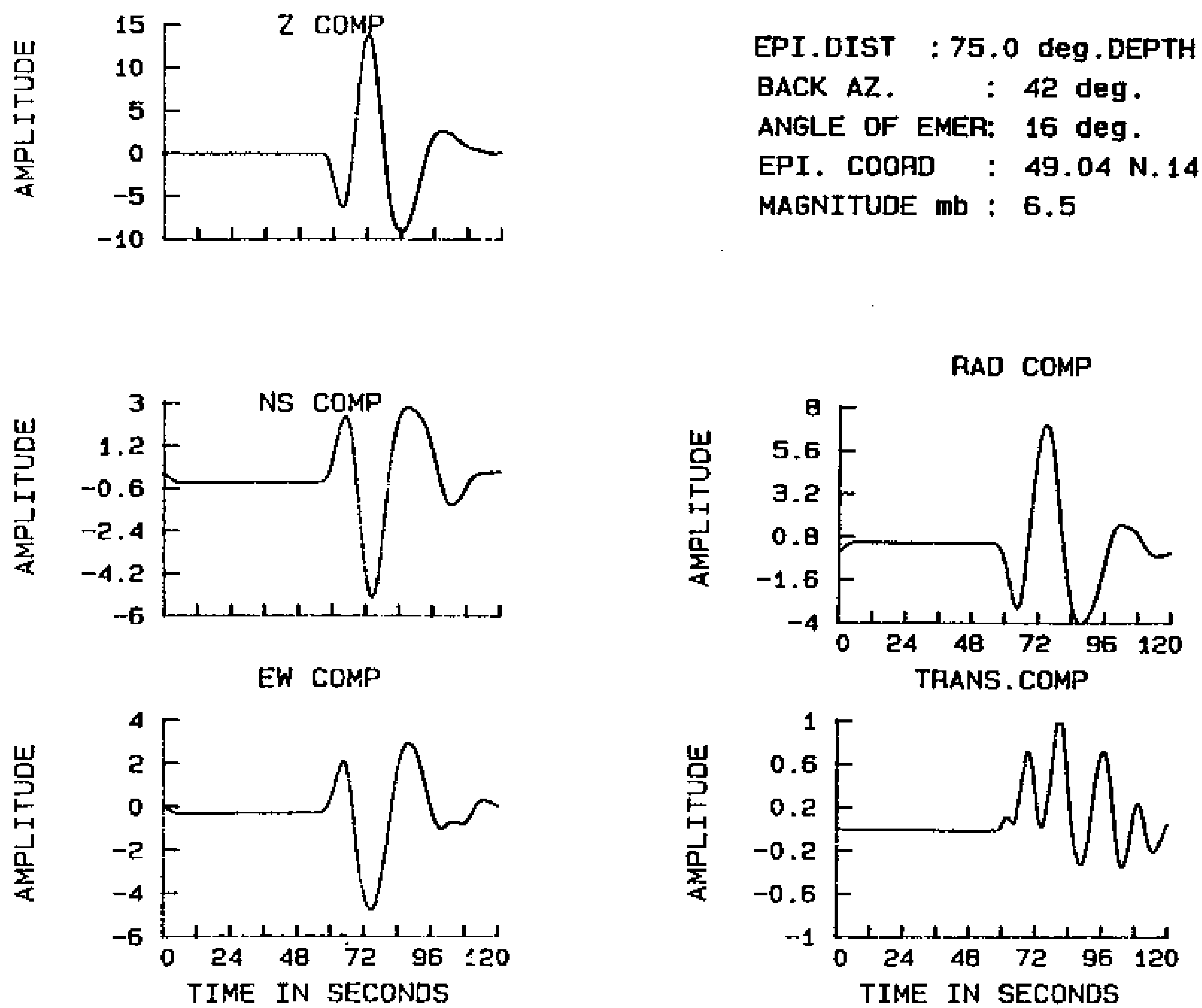

EARTHQUAKE OF NOV.6, 1990

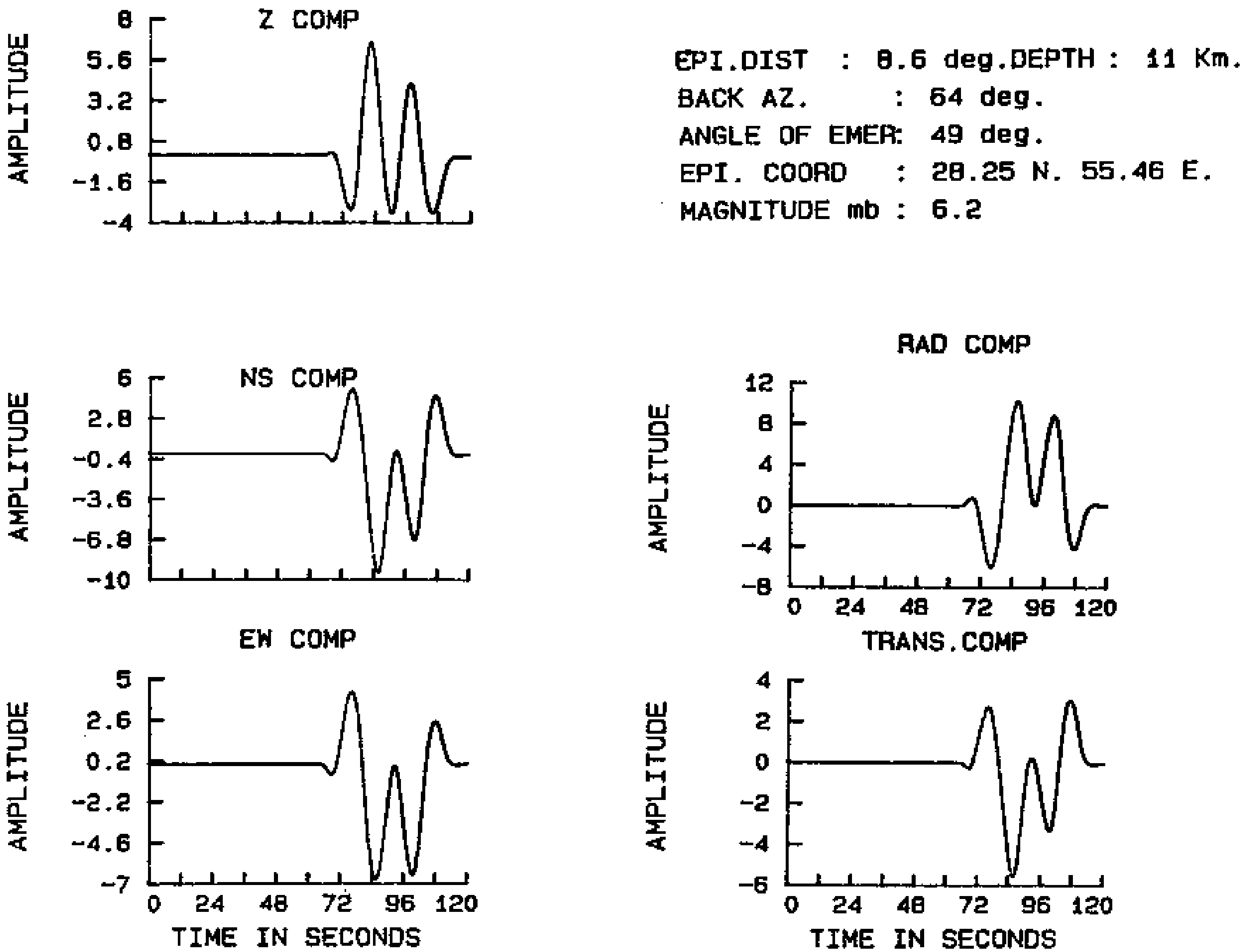

EARTHQUAKE OF JUN.20, 1991

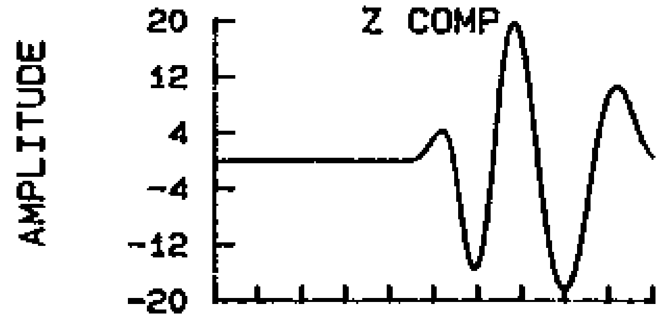

EPI.DIST : 76.9 deg. DEPTH : 31 Km.
BACK AZ. : 94 deg.
ANGLE OF EMER: 16 deg.
EPI. COORD : 1.20 N.122.79 E.
MAGNITUDE mb : 6.2

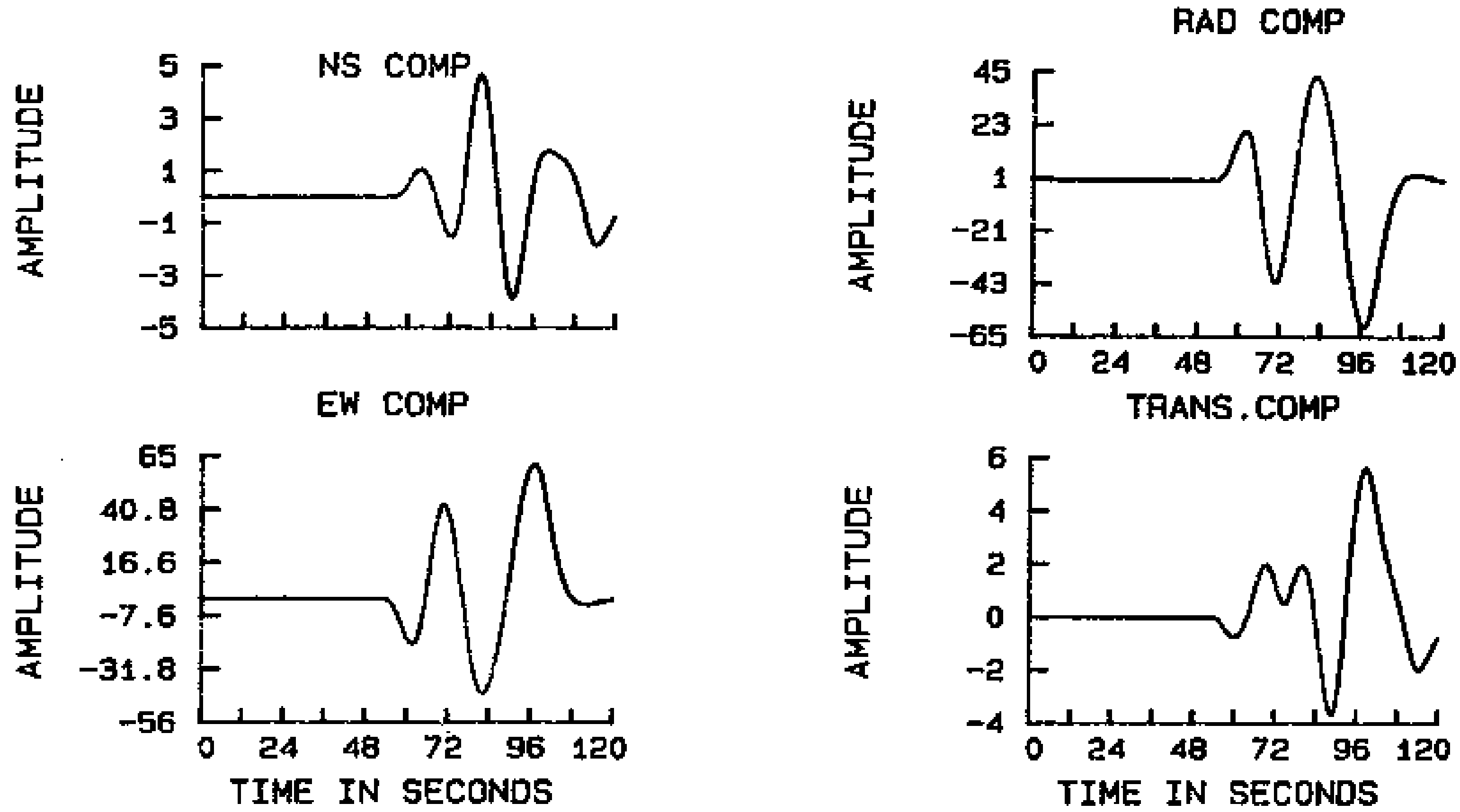

EARTHQUAKE OF MAY 17, 1992

EPI.DIST : 78.0 deg.DEPTH : 33 Km.
BACK AZ. : 87 deg.
ANGLE OF EMER: 16 deg.
EPI. COORD : 07.24 N.126.64 E.
MAGNITUDE mb : 6.2

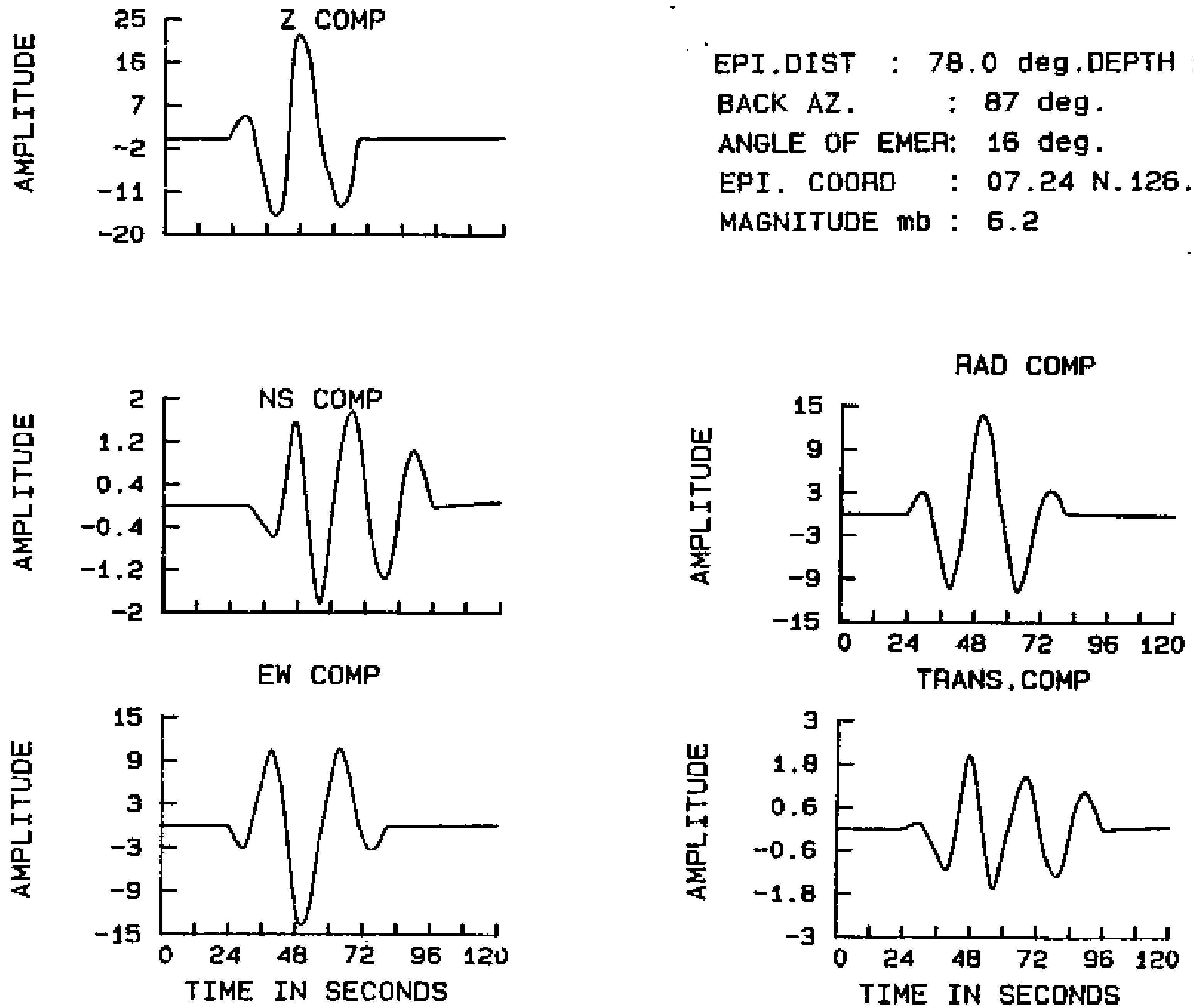

EARTHQUAKE OF NOV.21.1992

EPI.DIST : 23.6 deg.DEPTH : 65 Km.
BACK AZ. : 303 deg.
ANGLE OF EMER: 29 deg.
EPI. COORD : 35.92 N. 22.49 E.
MAGNITUDE mb : 5.9

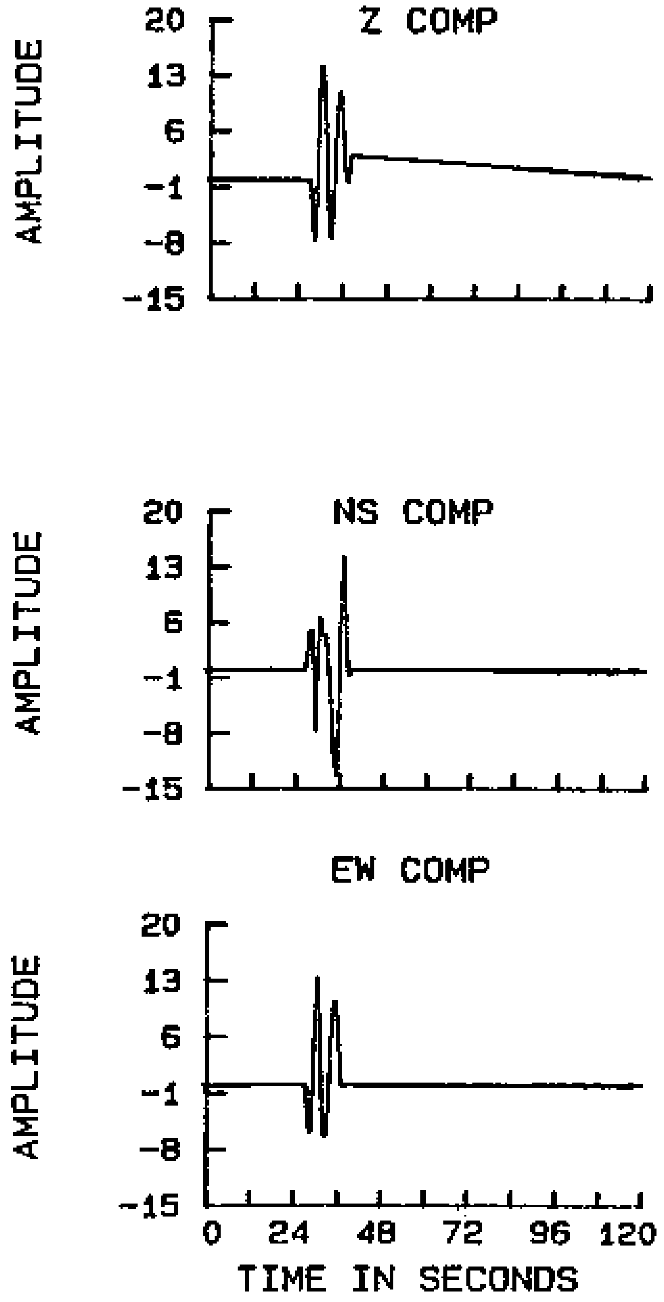

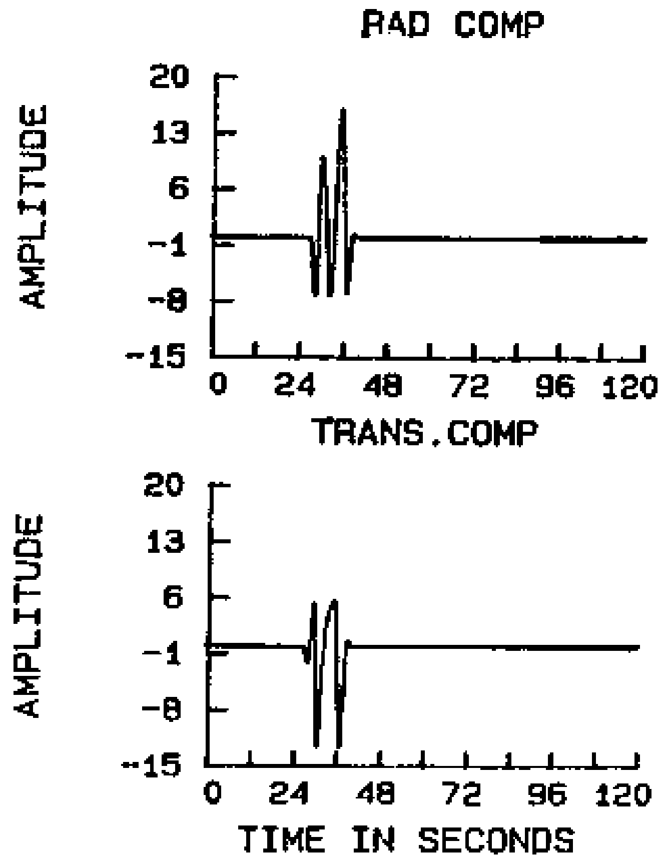

EARTHQUAKE OF MAR.13, 1993

EPI.DIST : 8.8 deg.DEPTH : 10 Km.
BACK AZ. : 237 deg.
ANGLE OF EMER: 44 deg.
EPI. COORD : 19.63 N. 38.80 E.
MAGNITUDE mb : 5.7

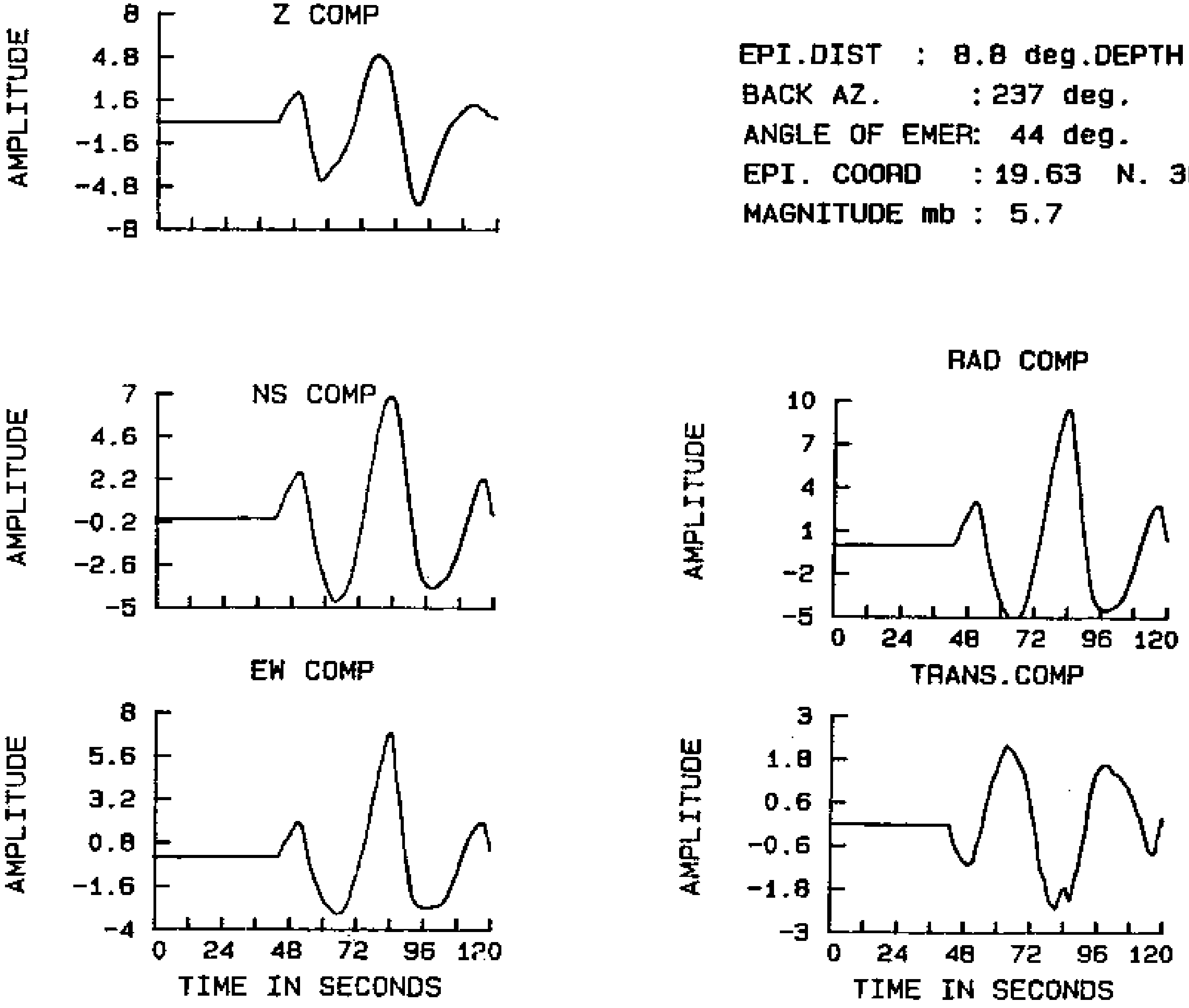

EARTHQUAKE OF AUG.9, 1993

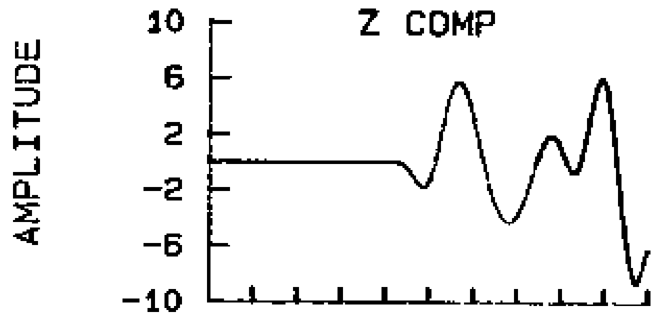

EPI.DIST : 23.8 deg.DEPTH : 215 Km.
BACK AZ. : 55 deg.
ANGLE OF EMER: 29 deg.
EPI. COORD : 36.38 N. 70.87 E.
MAGNITUDE mb : 6.2

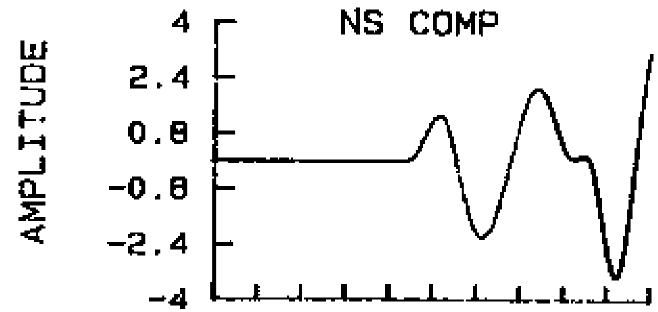

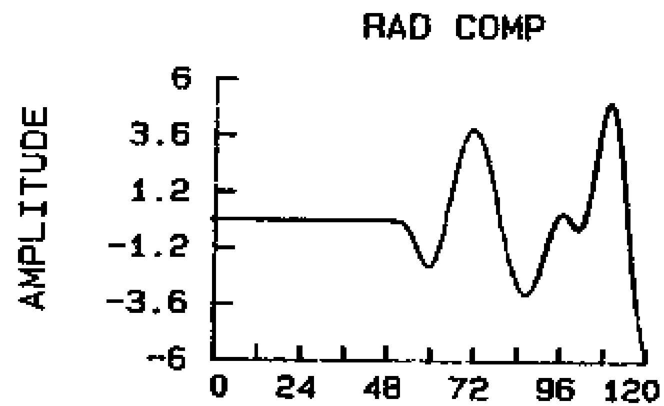

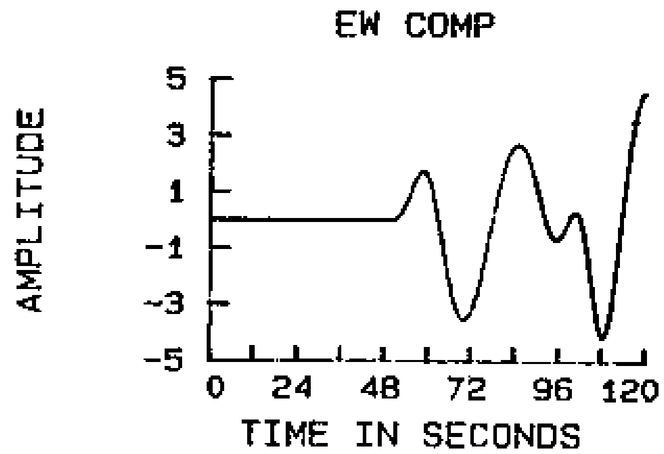

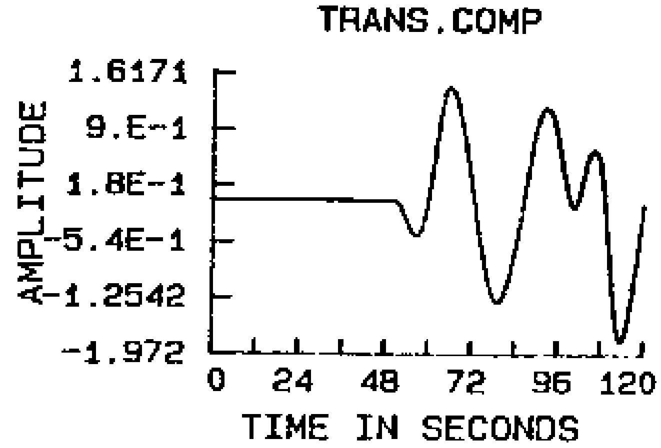

APPENDIX IV.

THE EFFECT OF THE MODEL PARAMETERS ON

THE SHAPE OF THE SPECTRA

Figures 4.2-4.8

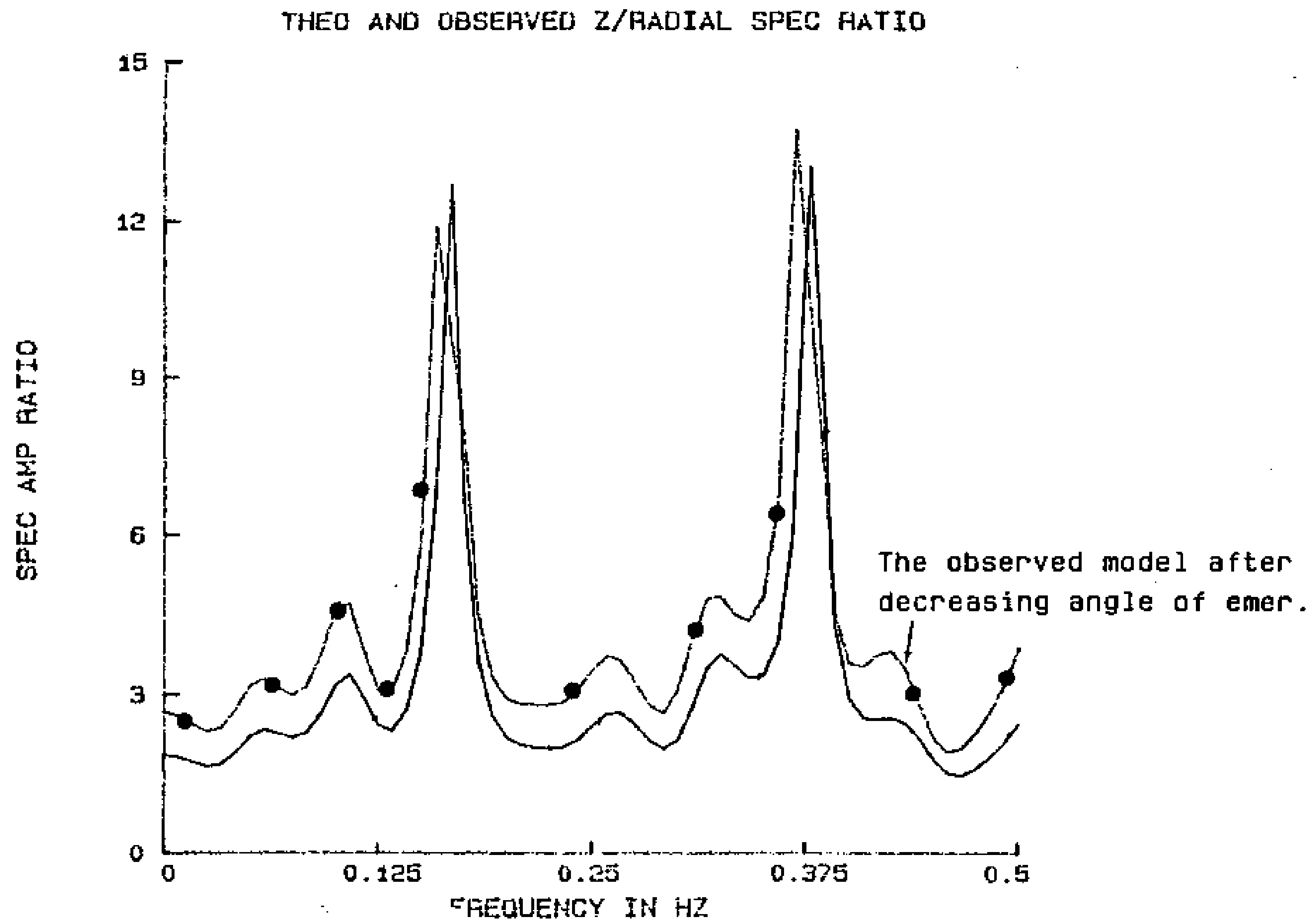
THEO AND OBSERVED Z/RADIAL SPEC RATIO
15
12
9
6
3
0
SPEC AMP RATIO
0
0.125
0.25
0.375
0.5
FREQUENCY IN HZ
The observed model after
decreasing angle of emer.

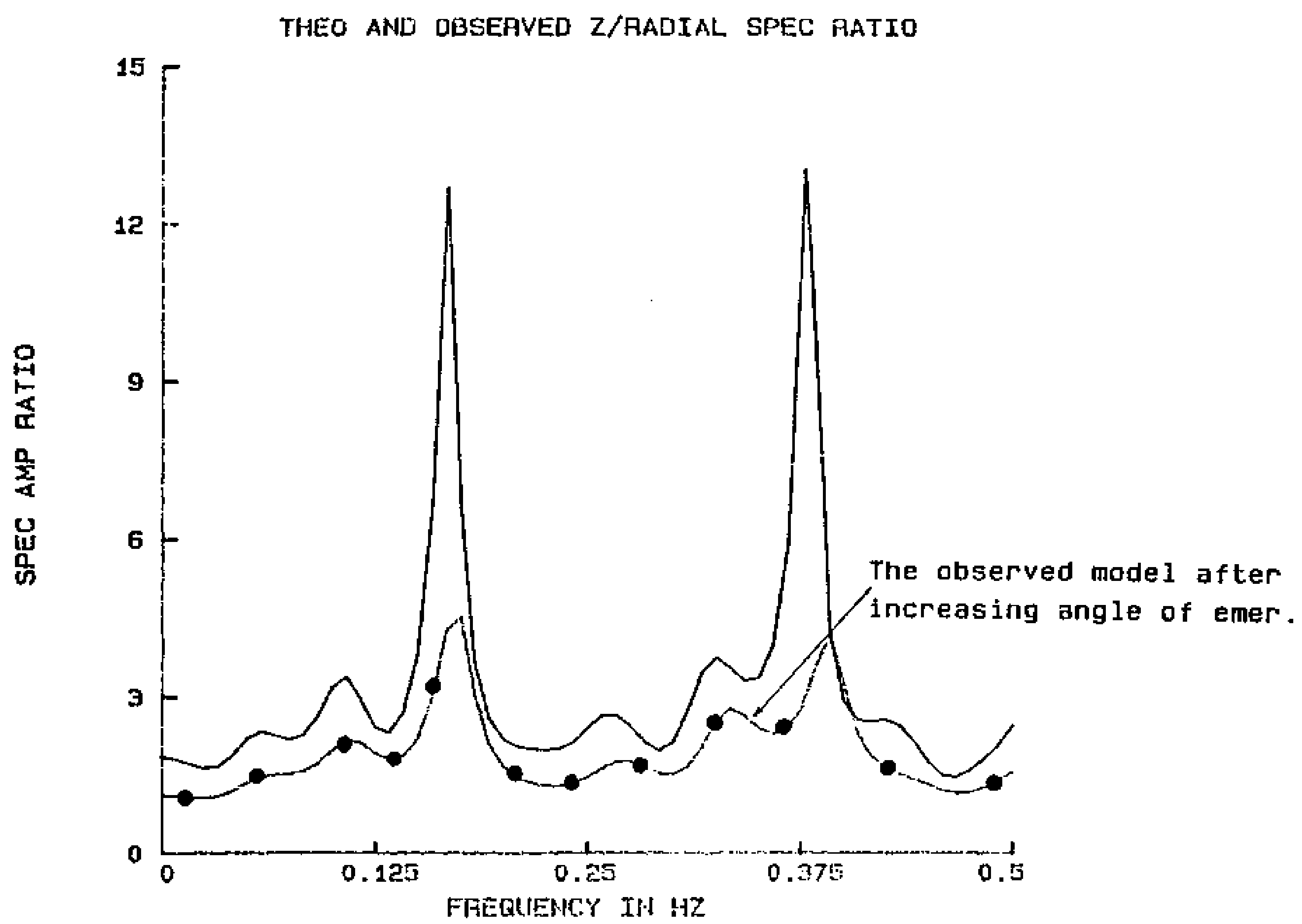
THEO AND OBSERVED Z/RADIAL SPEC RATIO
SPEC AMP RATIO
15
12
9
6
3
0
0
0.125
0.25
0.375
0.5
FREQUENCY IN HZ
The observed model after
increasing angle of emer.

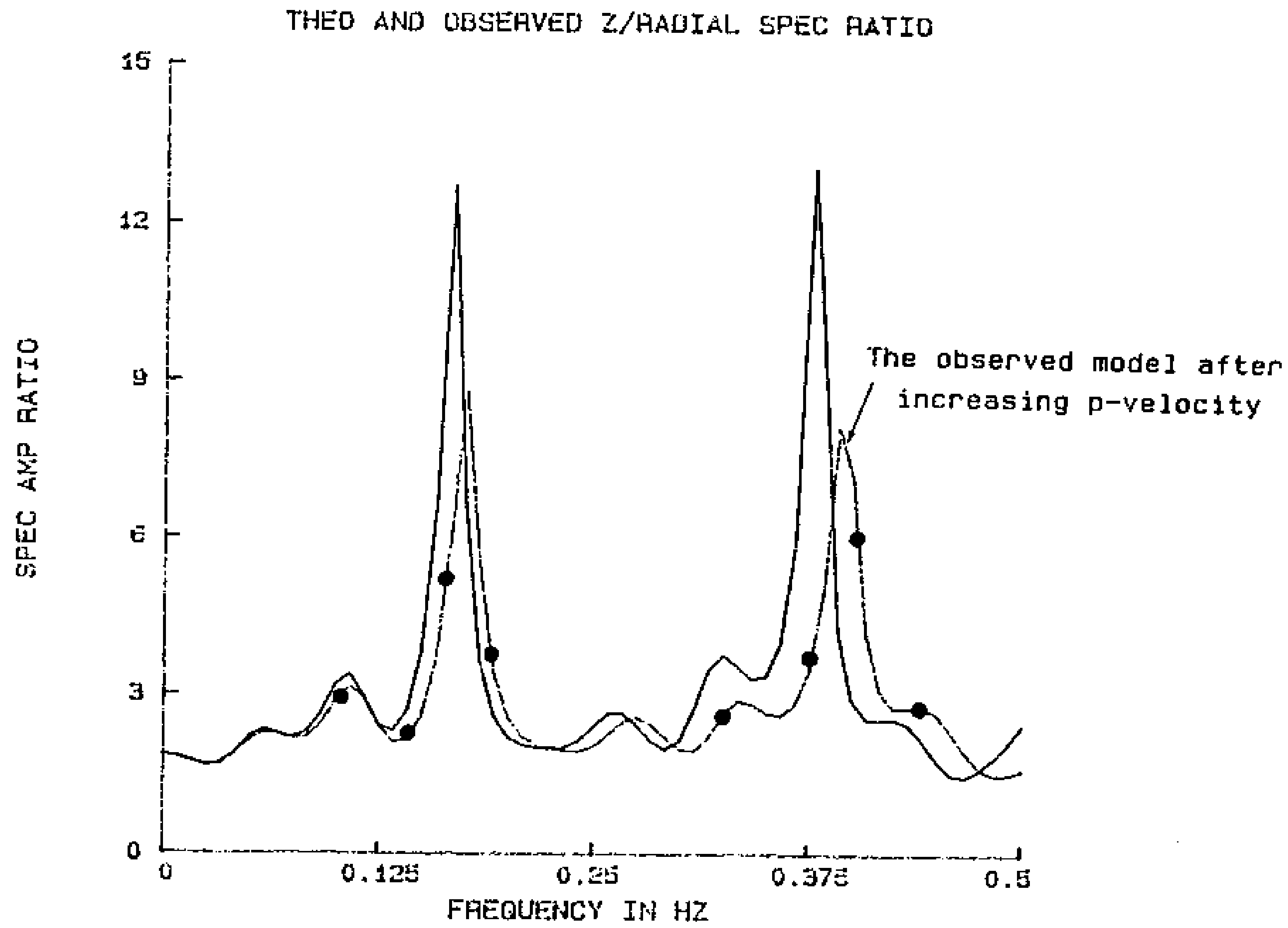
THEO AND OBSERVED Z/RADIAL SPEC RATIO
SPEC AMP RATIO
15
12
9
6
3
0
0
0.125
0.25
0.375
0.5
FREQUENCY IN HZ
The observed model after
increasing p-velocity

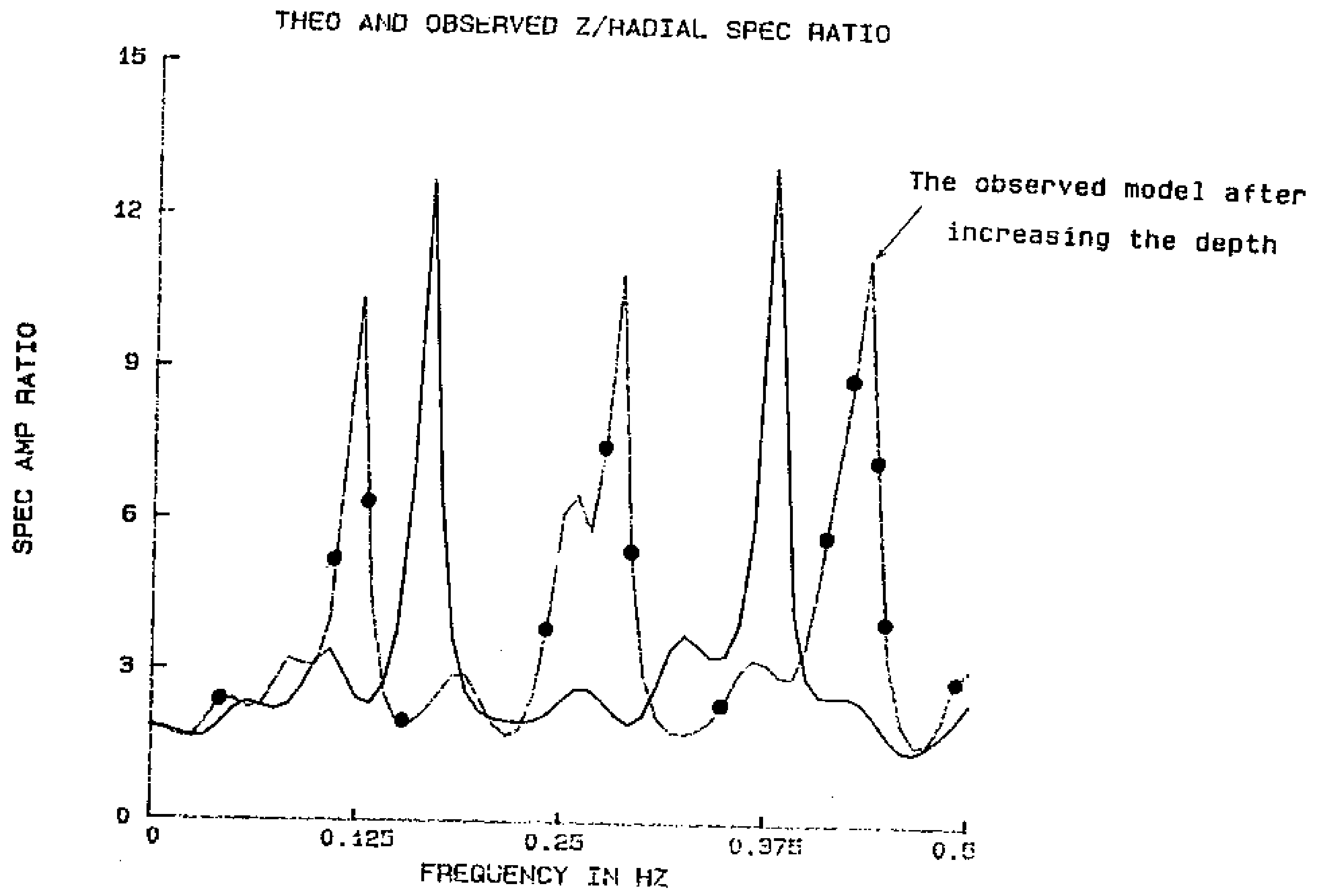

THEO AND OBSERVED Z/RADIAL SPEC RATIO
SPEC AMP RATIO
15
12
9
6
3
0
0
0.125
0.25
0.375
0.5
FREQUENCY IN HZ
The observed model after
increasing the depth

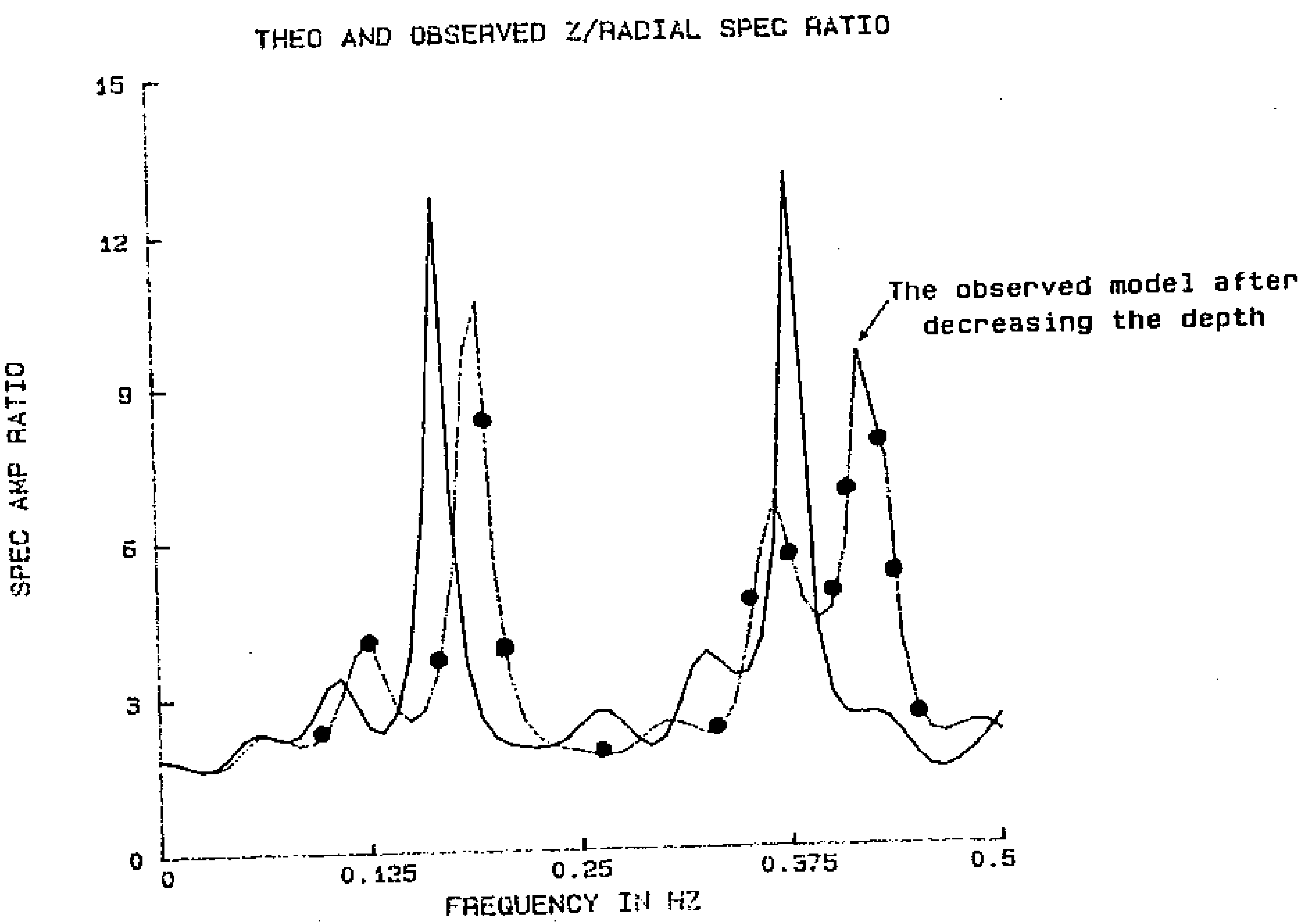
THEO AND OBSERVED Z/RADIAL SPEC RATIO
SPEC AMP RATIO
15
12
9
6
3
0
0
0.125
0.25
0.375
0.5
FREQUENCY IN HZ
The observed model after
decreasing the depth

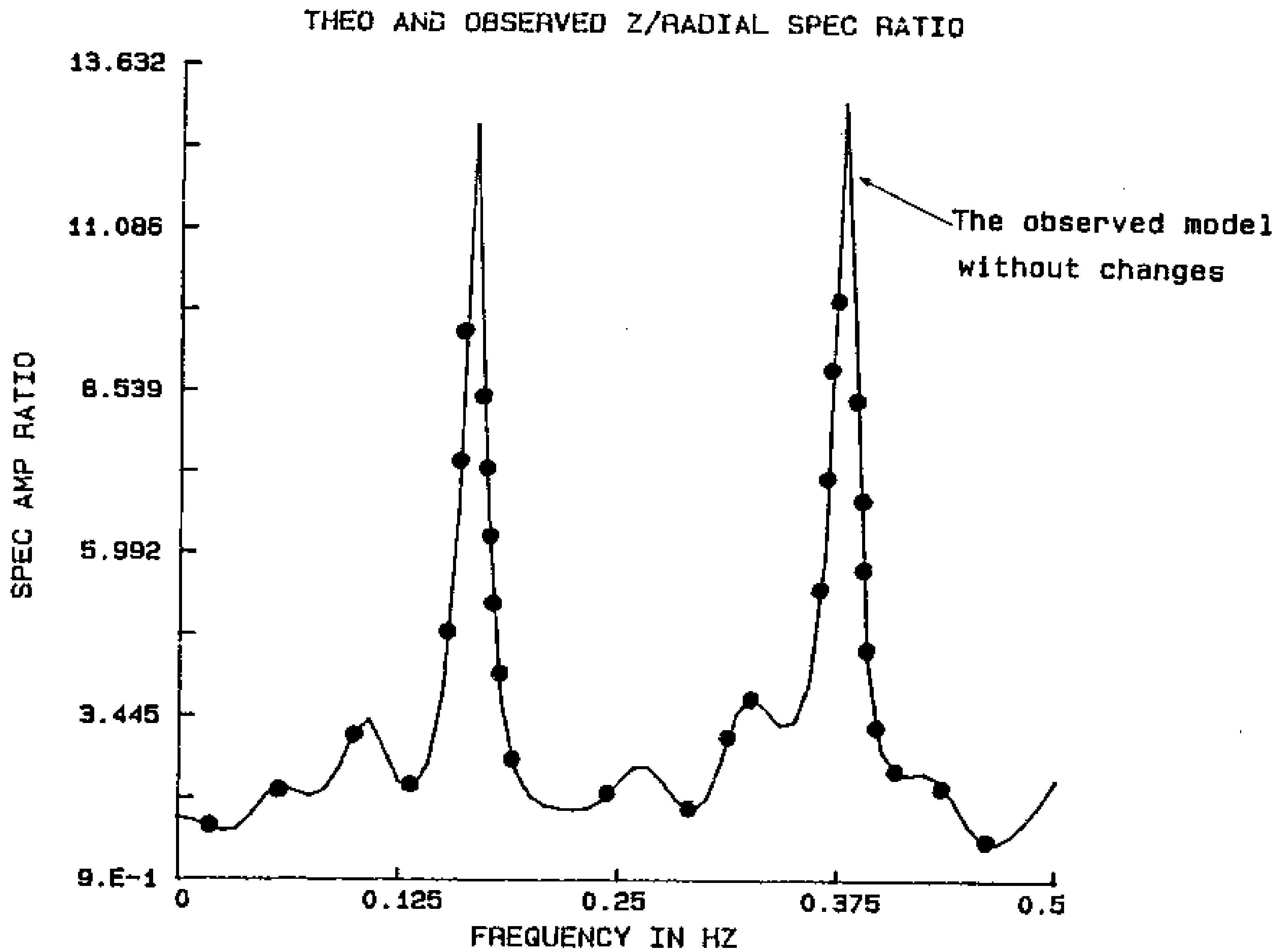

THEO AND OBSERVED Z/RADIAL SPEC RATIO
SPEC AMP RATIO
13.632
11.086
8.539
5.992
3.445
9.E-1
0
0.125
0.25
0.375
0.5
FREQUENCY IN HZ
The observed model
without changes

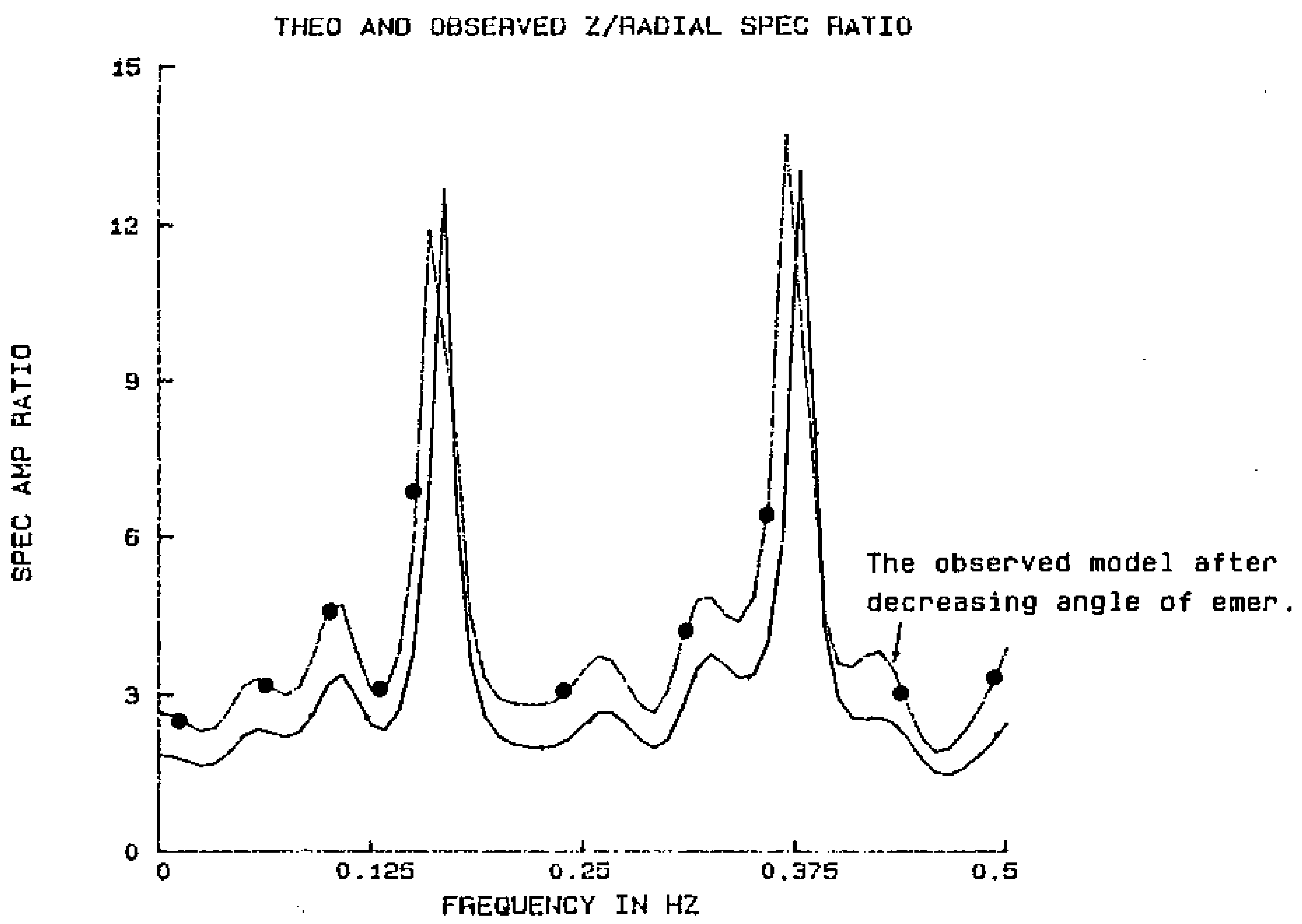
THEO AND OBSERVED Z/RADIAL SPEC RATIO
SPEC AMP RATIO
0
3
6
9
12
15
0
0.125
0.25
0.375
0.5
FREQUENCY IN HZ
The observed model after
decreasing angle of emer.

APPENDIX V.

RESULTANT CRUSTAL MODELS TOGETHER

WITH THE THEORETICAL AND OBSERVED SPECTRA

Figures 4.16 to 4.50

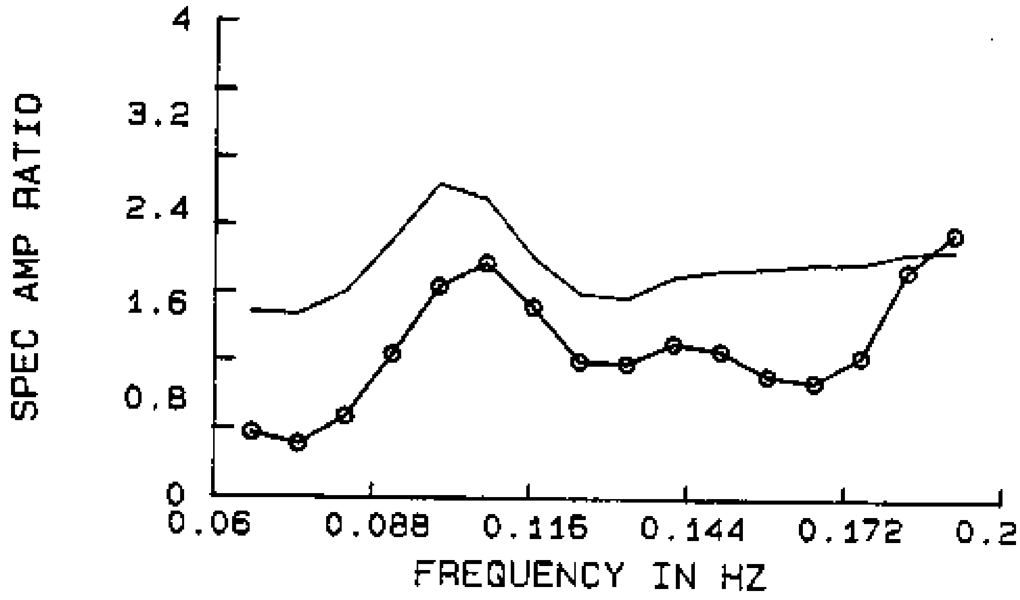

EPI.COORDINATES	35.99°N 70.42°E
DISTANCE	23.4°
BACK AZIMUTH	55°
DEPTH	142KM
MAGNITUDE(m_b)	6.4
ANGLE OF EMERGENCE	29°

THICKNESS (KM)	P VELOCITY (KM/S)	DENSITY (GM/CM^3)
1	5.7	2.1
9	6.1	2.3
9	6.55	2.5
12	6.8	2.7
11	7.55	2.90
999.00	8.30	3.08

CORRELATION COEFF= 0.96

Fig 4.16 Plots of theoretical and observed spectral ratio for earthquake of Jan.31, 1991 (KUSH) and relevant information together with observed crustal model. Open circles and solid lines represent observed and theoretical curves, respectively.

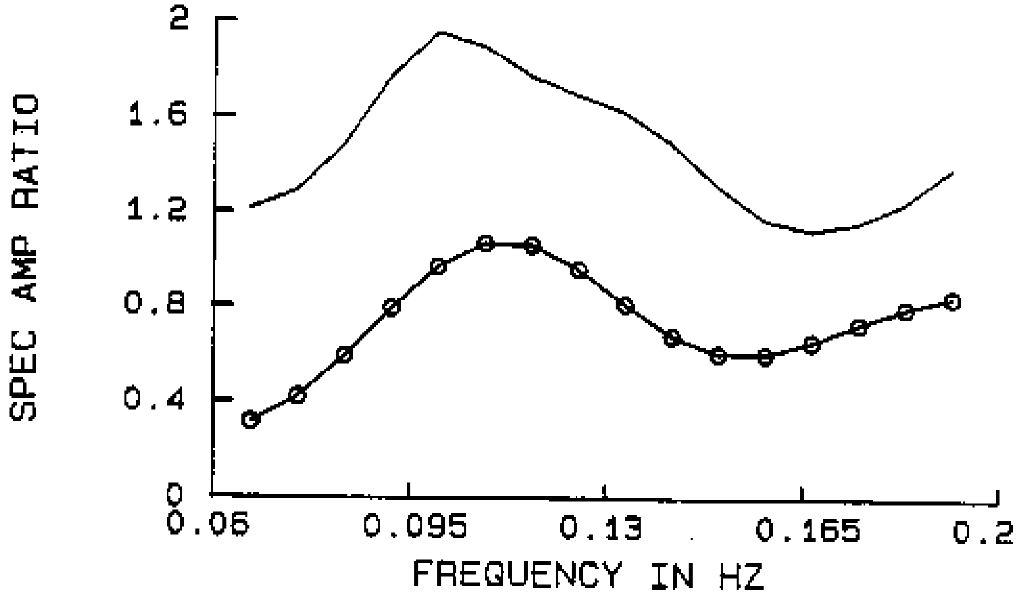

EPI. COORDINATES	30.89 N, 50.19 E
DISTANCE	6.9^0
BACK AZIMUTH	26^0
DEPTH	33 KM
MAGNITUDE(m_b)	5.4
ANGLE OF EMERGENCE	45^0

THICKNESS (KM)	P VELOCITY (KM/S)	DENSITY (GM/CM^3)
1	5.5	2.1
9	6.1	2.3
8	6.55	2.5
14	6.8	2.7
14	7.80	2.90
999.00	8.2	3.08

CORRELATION COEFF= .88

Fig. 4.17 Plots of theoretical and observed spectral ratio for earthquake of Mar.30, 1988 (IRAN) and relevant information together with obtained crustal model. Open circles and solid lines represent observed and theoretical curves, respectively.

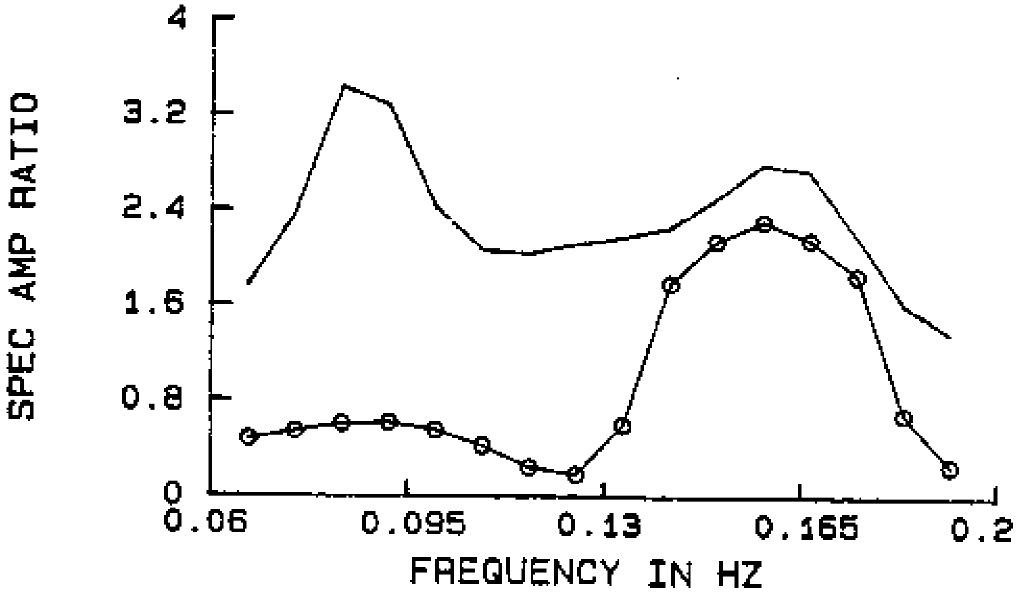

EPI. COORDINATES	29.87° N 63.84° E
DISTANCE	16.1°
BACK AZIMUTH	67°
DEPTH	165 KM
MAGNITUDE(m_b)	5.6
ANGLE OF EMERGENCE	40°

THICKNESS (KM)	P VELOCITY (KM/S)	DENSITY (GM/CM^3)
2	5.5	2.1
11	6.0	2.3
9	6.35	2.5
15	6.9	2.7
11	7.45	2.90
999.00	8.2	3.08

CORRELATION COEFF= .52

Fig.4.18 Plots of theoretical and observed spectral ratio for earthquake of Aug.10, 1987 (PAKISTAN) and relevant information together with obtained crustal model. Open circles and solid lines represent observed and theoretical curves, respectively.

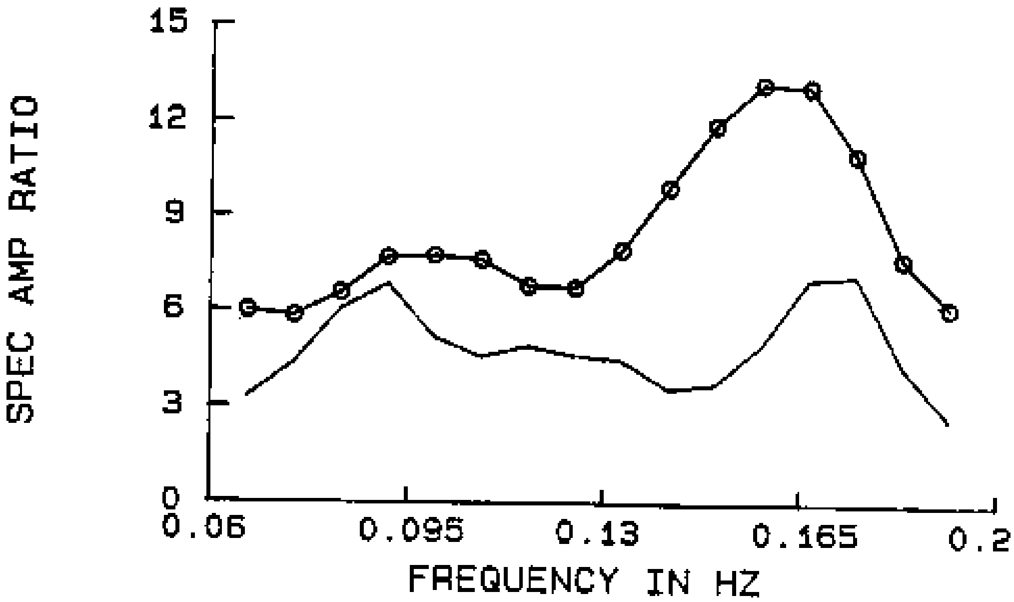

EPI. COORDINATES	54.74 N, 163.28 E
DISTANCE	84.1°
BACK AZIMUTH	31°
DEPTH	42 KM
MAGNITUDE(m_b)	5.4
ANGLE OF EMERGENCE	14.°

THICKNESS (KM)	P VELOCITY (KM/S)	DENSITY (GM/CM³)
2	5.7	2.1
11	6.1	2.3
8.00	6.45	2.5
13	6.75	2.7
12	7.4	2.90
999.00	8.20	3.08

CORRELATION COEFF= .62

Fig. 4.19 Plots of theoretical and observed spectral ratio for earthquake of Jan.19, 1987 (KAMCHATKA) and relevant information together with obtained crustal model. Open circles and solid lines represent observed and theoretical curves, respectively.

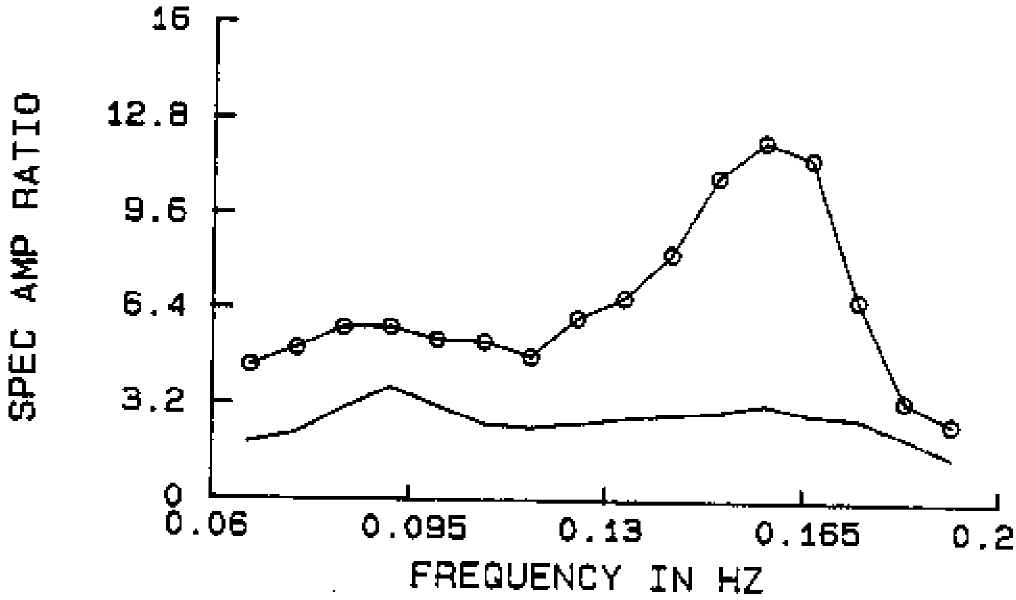

EPI. COORDINATES	37.36°N,141.80°E
DISTANCE	79.3°
BACK AZIMUTH	53°
DEPTH	33 KM
MAGNITUDE(m_b)	6.4
ANGLE OF EMERGENCE	15°

THICKNESS (KM)	P VELOCITY (KM/S)	DENSITY (GM/CM^3)
2.00	5.7	2.0
11.0	6.10	2.15
9.0	6.45	2.30
12.0	6.75	2.50
11.0	7.45	2.90
999.00	8.20	3.08

CORRELATION COEFF= .56

Fig.4.20 Plots of theoretical and observed spectral ratio for earthquake of April07, 1987 (JAPAN) and relevant information together with obtained crustal model. Open circles and solid lines represent observed and theoretical curves, respectively.

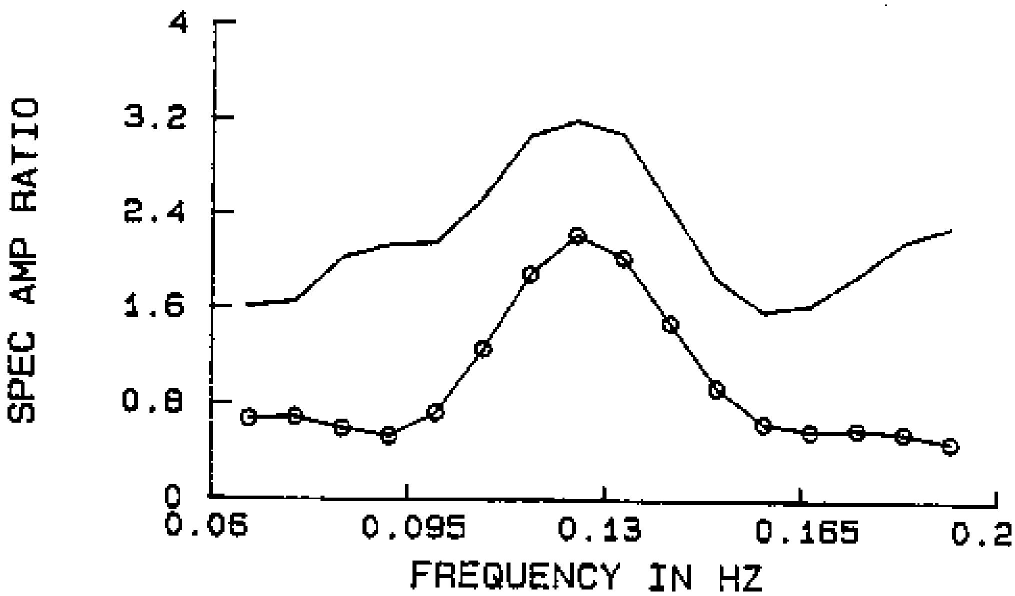

EPI. COORDINATES	39.44°N 74.90°E
DISTANCE	28.00°
BACK AZIMUTH	51°
DEPTH	33 KM
MAGNITUDE(m_b)	6.0
ANGLE OF EMERGENCE	27°

THICKNESS (KM)	P VELOCITY (KM/S)	DENSITY (GM/CM^3)
1	5.65	
9	6.4	4.60
6	6.7	2.30
17	6.85	2.50
12	7.55	2.90
999.00	8.20	3.08

CORRELATION COEFF= .45

Fig.4.21. Plots of theoretical and observed spectral ratio for earthquake of April17,1990 (CHINA) and relevant information together with obtained crustal model.Open circles and solid lines represent observed and theoretical curves, respectively.

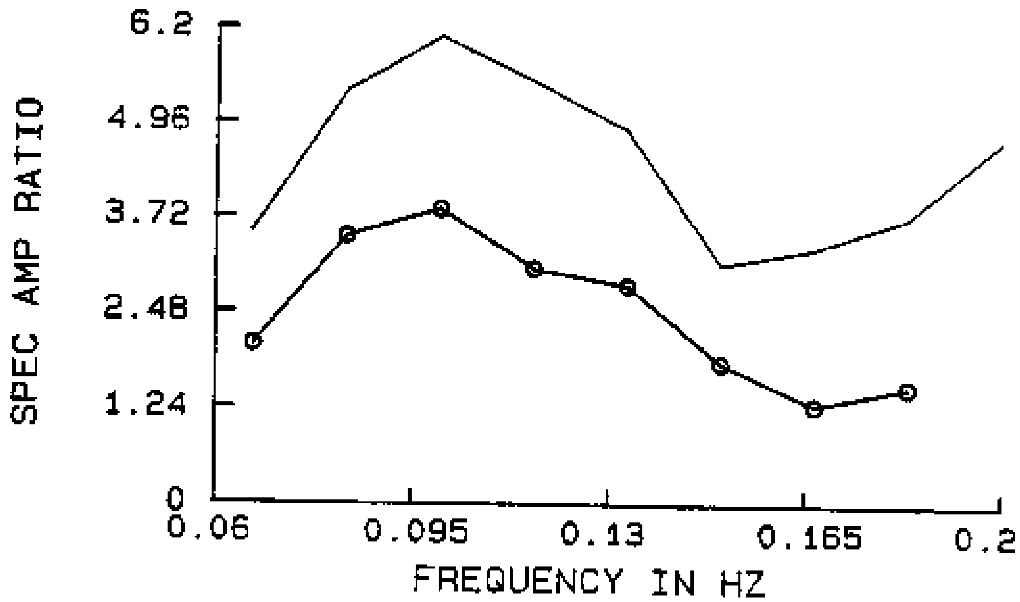

EPI. COORDINATES	07.19° N 126.76° E
DISTANCE	78.1°
BACK AZIMUTH	87°
DEPTH	33 KM
MAGNITUDE(m_b)	6.4
ANGLE OF EMERGENCE	16°

THICKNESS (KM)	P VELOCITY (KM/S)	DENSITY (GM/CM^3)
2	5.7	2.1
8	6.3	2.3
9	6.7	2.5
14	6.85	2.7
12	7.45	2.90
999.00	8.30	3.08

CORRELATION COEFF= .37

Fig. 4.22 Plots of theoretical and observed spectral ratio for earthquake of May17, 1992 (MIND) and relevant information together with obtained crustal model. Open circles and solid lines represent observed and theoretical curves, respectively.

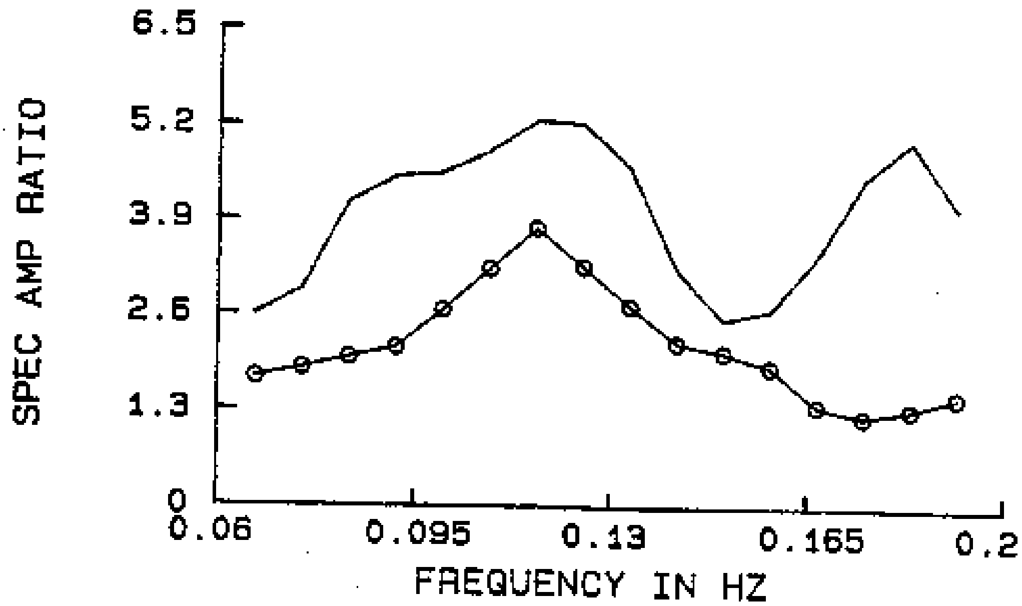

EPI. COORDINATES	01.79°N,126.52°E
DISTANCE	80.1°
BACK AZIMUTH	92°
DEPTH	33 KM
MAGNITUDE(m_b)	6.6
ANGLE OF EMERGENCE	15°

THICKNESS (KM)	P VELOCITY (KM/S)	DENSITY (GM/CM^3)
2	5.65	2.1
10	6.4	2.3
6	6.7	2.5
17	6.8	2.7
12	7.55	2.90
999.00	8.20	3.08

CORRELATION COEFF= .26

Fig.4.23 Plots of theoretical and observed spectral ratio for earthquake of Aug14, 1986 (MOLUCA) and relevent information together with obtained crustal model. Open circles and solid lines represent observed and theoretical curves, respectively.

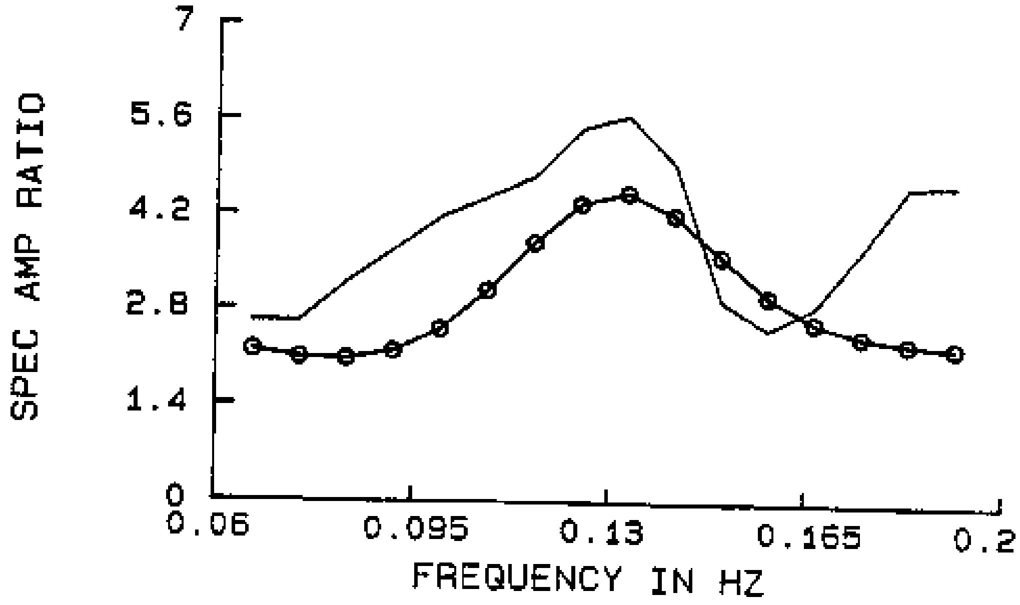

EPI. COORDINATES	27.96° N 140.61° E
DISTANCE	82.1°
BACK AZIMUTH	62°
DEPTH	42 KM
MAGNITUDE(m_b)	5.82
ANGLE OF EMERGENCE	15°

THICKNESS (KM)	P VELOCITY (KM/S)	DENSITY (GM/CM^3)
2	5.8	2.1
11	6.0	2.3
9	6.65	2.5
15	6.8	2.7
11	7.55	2.90
999.00	8.30	3.08

CORRELATION COEFF= .41

Fig. 4.24 Plots of theoretical and observed spectral ratio for earthquake of Nov.08, 1985 (BONI) and relevant information together with obtained crustal model. Open circles and solid lines represent observed and theoretical curves, respectively.

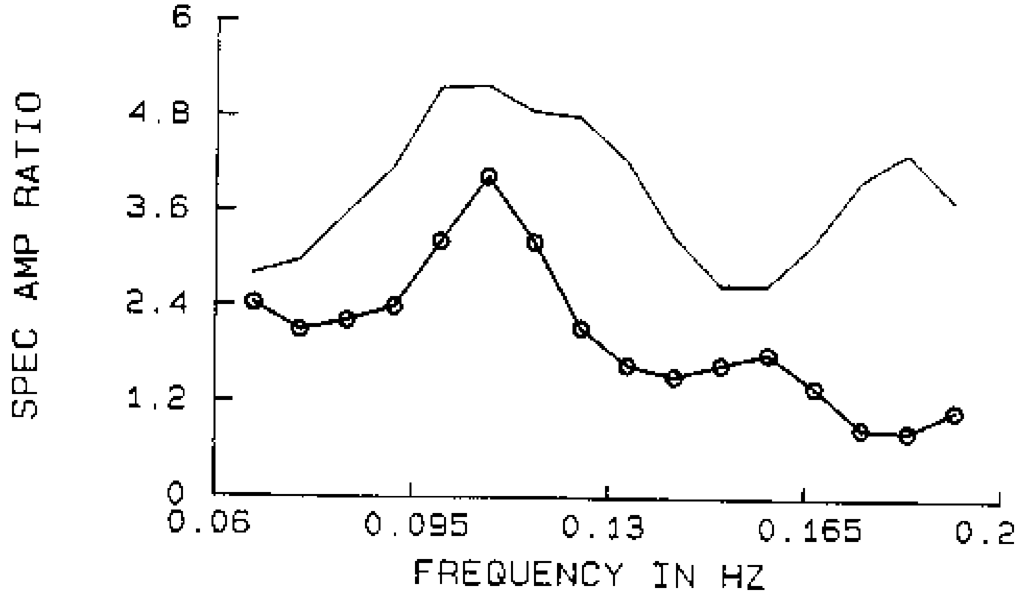

EPI. COORDINATES	36.99° N 141.79° E
DISTANCE	79.4°
BACK AZIMUTH	54°
DEPTH	36 KM
MAGNITUDE(m_b)	5.9
ANGLE OF EMERGENCE	15°

THICKNESS (KM)	P VELOCITY (KM/S)	DENSITY (GM/CM^3)
2	5.7	2.1
8	6.2	2.3
6	6.55	2.5
17	6.95	2.7
11	7.45	2.90
999.00	8.30	3.08

CORRELATION COEFF= .33

Fig. 4.25 Plots of theoretical and observed spectral ratio for earthquake of Feb.06, 1987 (HONS) and relevant information together with obtained crustal model. Open circles and solid lines represent observed and theoretical curves, respectively.

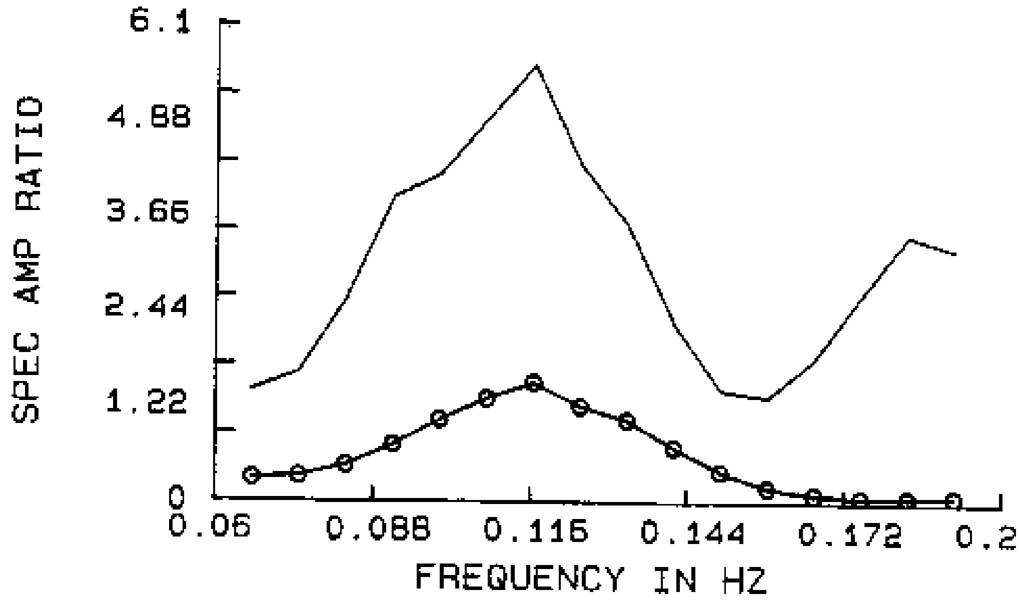

EPI. COORDINATES	01.2° N 122.79° E
DISTANCE	76.9°
BACK AZIMUTH	94°
DEPTH	31 KM
MAGNITUDE(m_b)	6.2
ANGLE OF EMERGENCE	16°

THICKNESS (KM)	P VELOCITY (KM/S)	DENSITY (GM/CM^3)
2	5.65	2.1
8	6.5	2.3
7	6.8	2.5
17	6.95	2.7
12	7.55	2.90
999.00	8.30	3.08

CORRELATION COEFF= .62

Fig 4.26Plots of theoretical and observed spectral ratio for earthquake of Jun.20, 1991 (MINA) and relevant information together with obtained crustal model. Open circles and solid lines represent observed and theoretical curves, respectively.

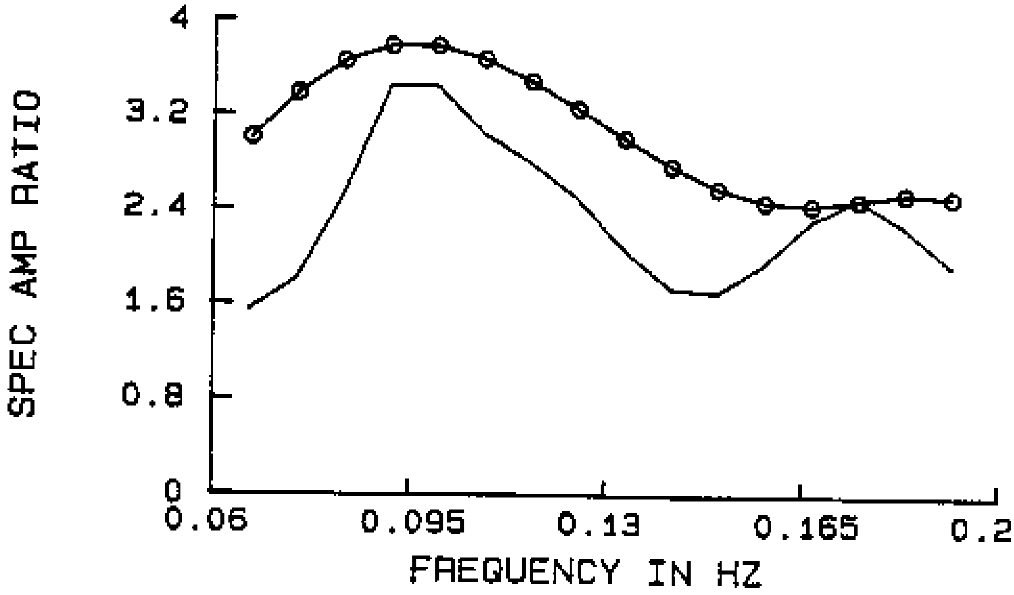

EPI. COORDINATES	36.29°N, 71.37°E
DISTANCE	24.2°
BACK AZIMUTH	55°
DEPTH	107KM
MAGNITUDE(m_b)	5.6
ANGLE OF EMERGENCE	29°

THICKNESS (KM)	P VELOCITY (KM/S)	DENSITY (GM/CM^3)
1	5.7	2.1
11	6.2	2.3
7	6.70	2.30
17	6.80	2.50
12	7.65	2.90
999.00	8.2	3.08

CORRELATION COEFF= 0.62

Fig. 4.27 Plots of theoretical and observed spectral ratio for earthquake of Sept.26, 1988 (AFGH) and relevant information together with obtained crustal model. Open circles and solid lines represent observed and theoretical curves, respectively.

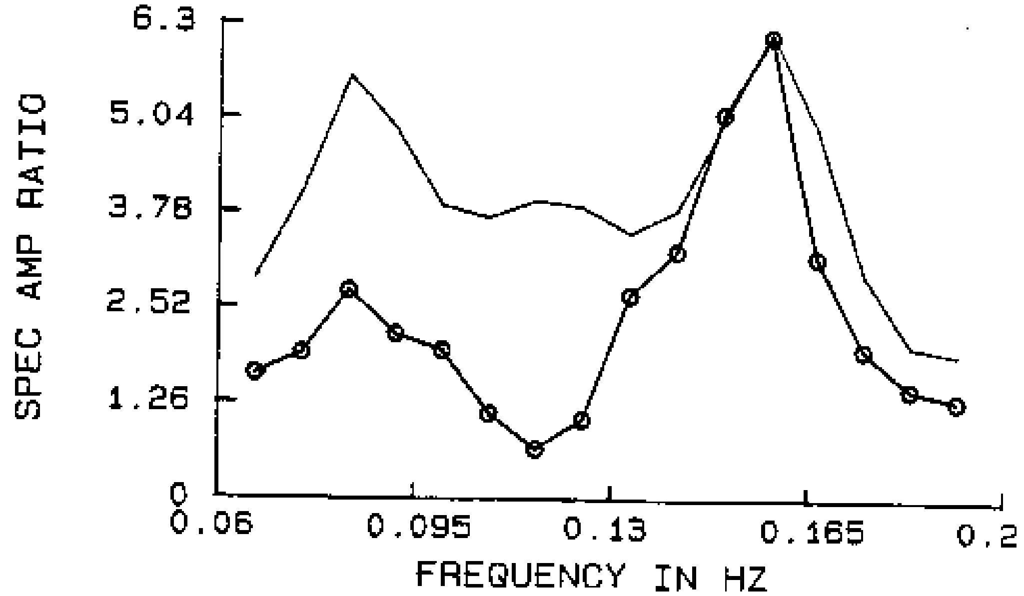

EPI. COORDINATES	48.80°N,78.11°E
DISTANCE	35°
BACK AZIMUTH	36°
DEPTH	0 KM
MAGNITUDE(m_b)	5.8
ANGLE OF EMERGENCE	17°

THICKNESS (KM)	P VELOCITY (KM/S)	DENSITY (GM/CM^3)
1	5.4	2.1
12	6.2	2.3
10	6.55	2.5
14	6.8	2.7
12	7.4	2.90
999.00	8.2	3.08

CORRELATION COEFF= 0.46

Fig. 4.28 Plots of theoretical and observed spectral ratio for earthquake of July17, 1987 (KAZAKHSTAN) and relevant information together with obtained crustal model. Open circles and solid lines represent observed and theoretical curves, respectively.

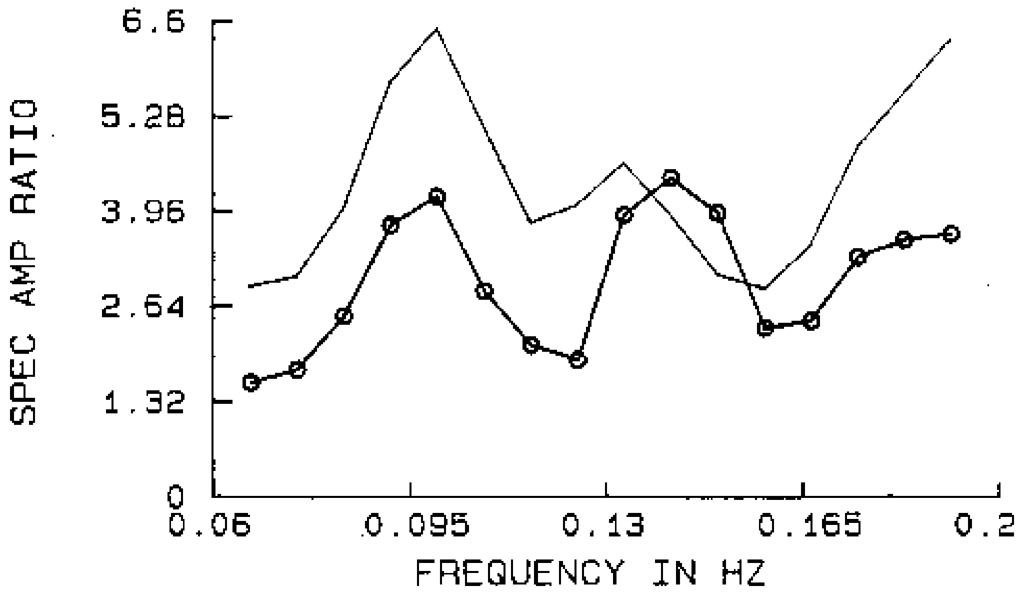

EPI. COORDINATES	49.99° N 153.48° E
DISTANCE	83°
BACK AZIMUTH	41°
DEPTH	14 KM
MAGNITUDE(m_b)	6.0
ANGLE OF EMERGENCE	15°

THICKNESS (KM)	P VELOCITY (KM/S)	DENSITY (GM/CM^3)
2	5.6	2.1
10	6.3	2.3
7	6.55	2.5
13.00	6.7	2.7
11	7.55	2.9
999.00	8.2	3.08

CORRELATION COEFF= .51

Fig. 4.29 Plots of theoretical and observed spectral ratio for earthquake of Jan.09, 1989 (KURIL) and relevant information together with obtained crustal model. Open circles and solid lines represent observed and theoretical curves, respectively.

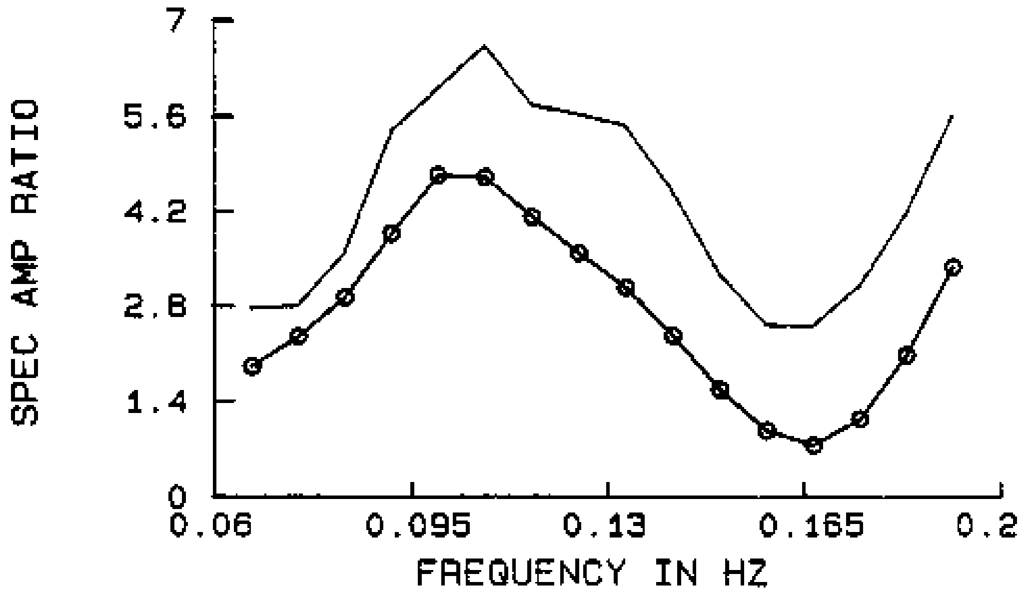

. COORDINATES	52.96° N, 159.97° E
DISTANCE	83.5.°
BACK AZIMUTH	33°
DEPTH	34 KM
MAGNITUDE(m_b)	6.3
ANGLE OF EMERGENCE	14°

THICKNESS (KM)	P VELOCITY (KM/S)	DENSITY (GM/CM^3)
1.00	4.80	2.10
6.00	6.20	2.30
15.00	7.50	2.50
23.00	7.80	2.90
999.00	8.30	3.08

CORRELATION COEFF= .78

Fig. 4.30 Plots of theoretical and observed spectral ratio for earthquake of Oct.06, 1987 (KAMCHATKA) and relevant information together with obtained crustal model. Open circles and solid lines represent observed and theoretical curves, respectively.

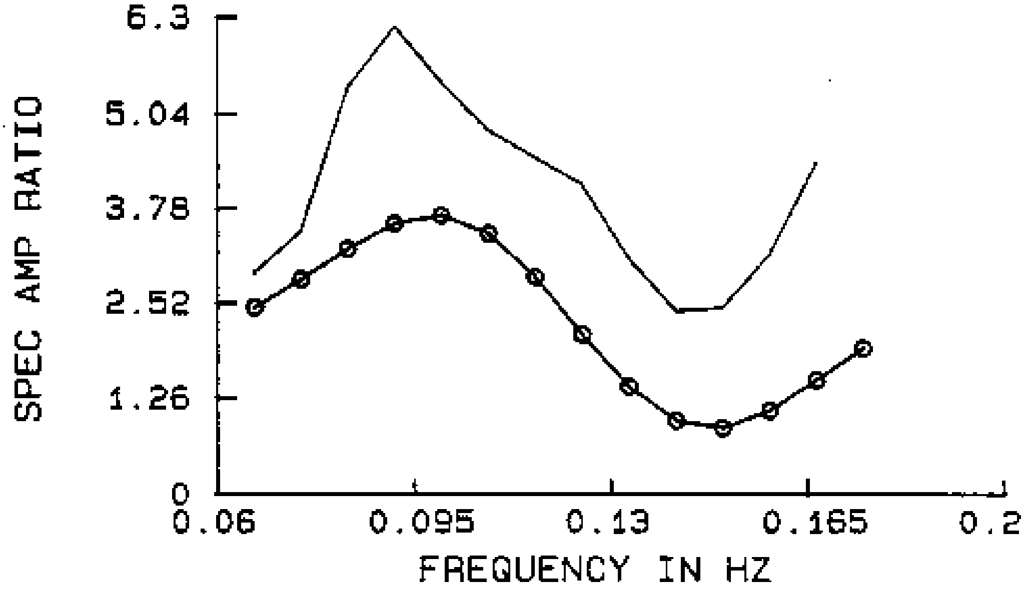

EPI. COORDINATES	49.04 N 141.85 E
DISTANCE	75.0°
BACK AZIMUTH	42.°
DEPTH	600 KM
MAGNITUDE(m_b)	6.5
ANGLE OF EMERGENCE	16^0

THICKNESS (KM)	P VELOCITY (KM/S)	DENSITY (GM/CM^3)
2	5.5	2.1
10	6.4	2.3
7	6.6	2.5
17	6.95	2.7
12	7.6	2.90
999.00	8.2	3.08

CORRELATION COEFF= .74

Fig. 4.31 Plots of theoretical and observed spectral ratio for earthquake of May12, 1990 (SAKH) and relevant information together with obtained crustal model. Open circles and solid lines represent observed and theoretical curves, respectively.

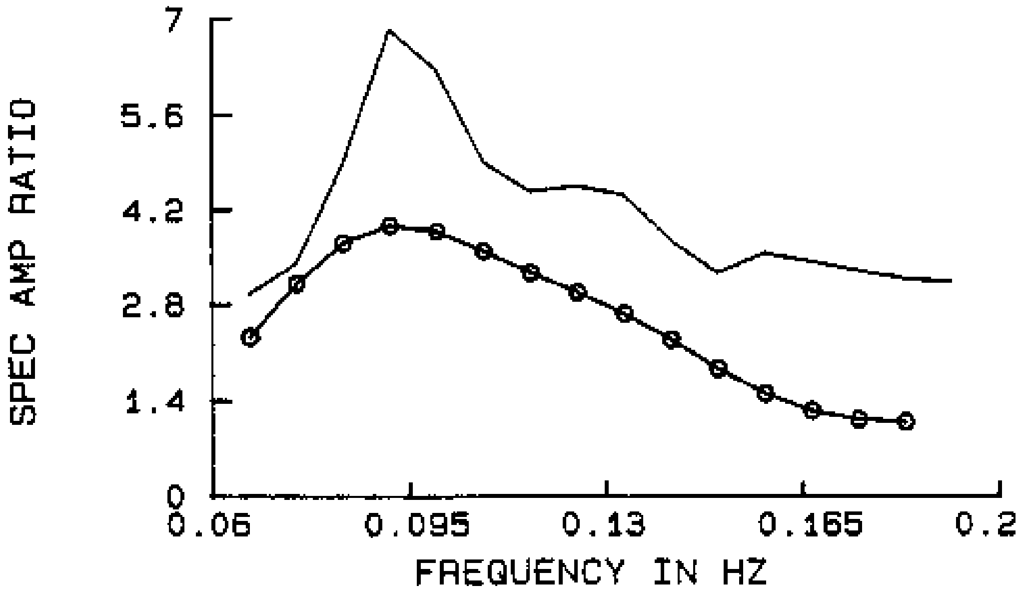

EPI. COORDINATES	45.53 N, 151.02 E
DISTANCE	82.1.^{0}
BACK AZIMUTH	43^0
DEPTH	25 KM
MAGNITUDE(m_b)	6.3
ANGLE OF EMERGENCE	15.^{0}

THICKNESS (KM)	P VELOCITY (KM/S)	DENSITY (GM/CM^3)
2	5.8	
11	6.20	2.10
8.00	6.55	2.30
13	6.8	2.50
11	7.55	2.90
999.00	8.30	3.08

CORRELATION COEFF= .66

Fig. 4.32 Plots of theoretical and observed spectral ratio for earthquake of Dec.22, 1991 (KURIL ISL) and relevant information together with obtained crustal model. Open circles and solid lines represent observed and theoretical curves, respectively.

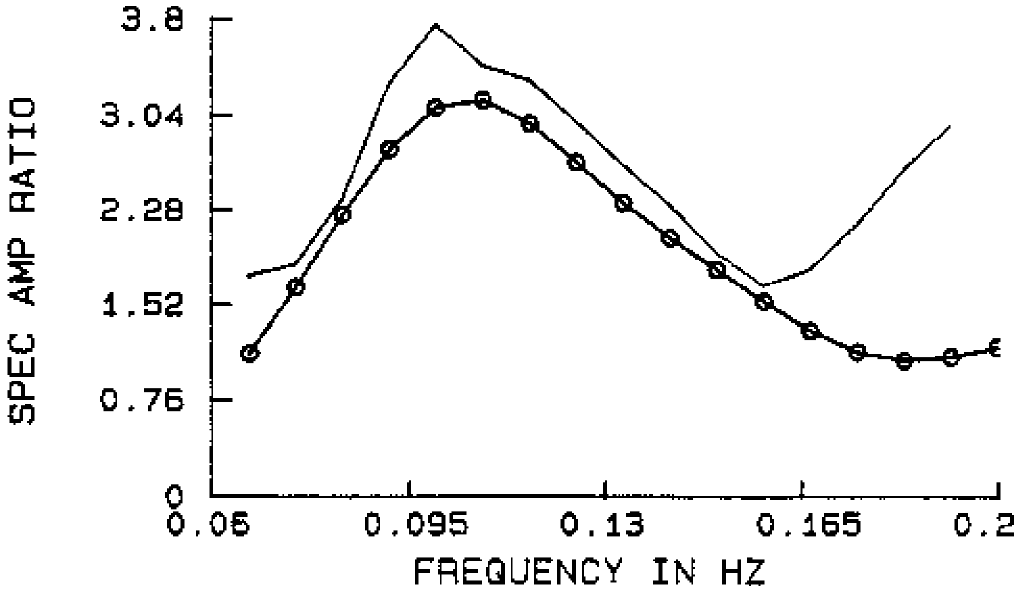

EPI. COORDINATES	25.27° N, 94.20° E
DISTANCE	43°
BACK AZIMUTH	78°
DEPTH	50 KM
MAGNITUDE(m_b)	5.7
ANGLE OF EMERGENCE	24°

THICKNESS (KM)	P VELOCITY (KM/S)	DENSITY (GM/CM^3)
2	5.35	2.1
7	6.2	2.3
7	6.65	2.5
17	6.95	2.7
12	7.5	2.90
999.00	8.2	3.08

CORRELATION COEFF= .79

Fig. 4.33 Plots of theoretical and observed spectral ratio for earthquake of May18, 1987 (BURMA) and relevant information together with obtained crustal model. Open circles and solid lines represent observed and theoretical curves, respectively.

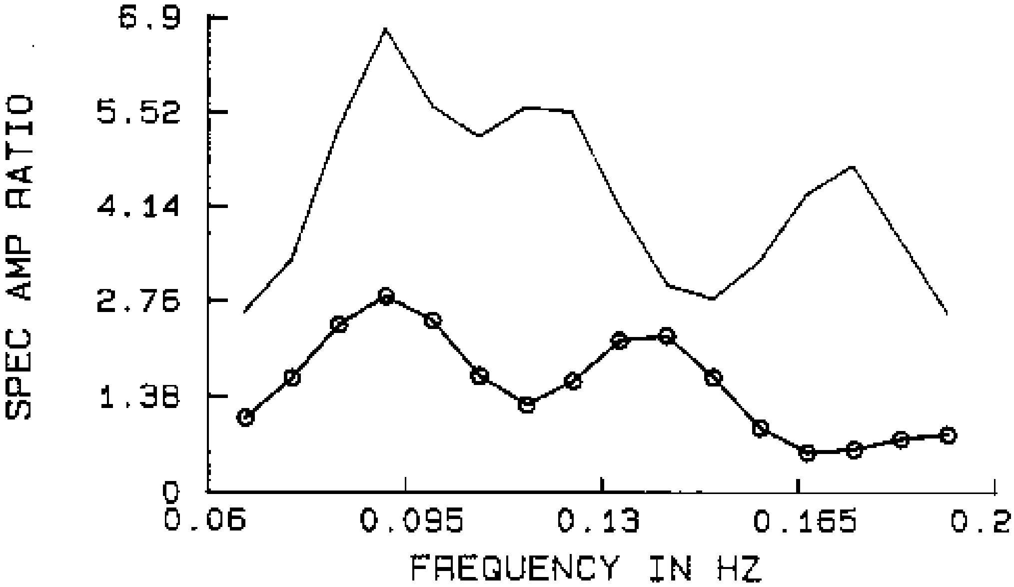

EPI. COORDINATES	8.1°S, 124.68°E
DISTANCE	82.6°
BACK AZIMUTH	102°
DEPTH	29KM
MAGNITUDE(m_b)	6.2
ANGLE OF EMERGENCE	15°

THICKNESS (KM)	P VELOCITY (KM/S)	DENSITY (GM/CM^3)
2	5.6	2.1
11	6.1	2.3
9	6.7	2.5
12	6.95	2.7
10	7.45	2.90
999.00	8.2	3.08

CORRELATION COEFF= .43

Fig. 4.34 Plots of theoretical and observed spectral ratio for earthquake of jul.04, 1991 (TIMO) and relevant information together with obtained crustal model. Open circles and solid lines represent observed and theoretical curves, respectively.

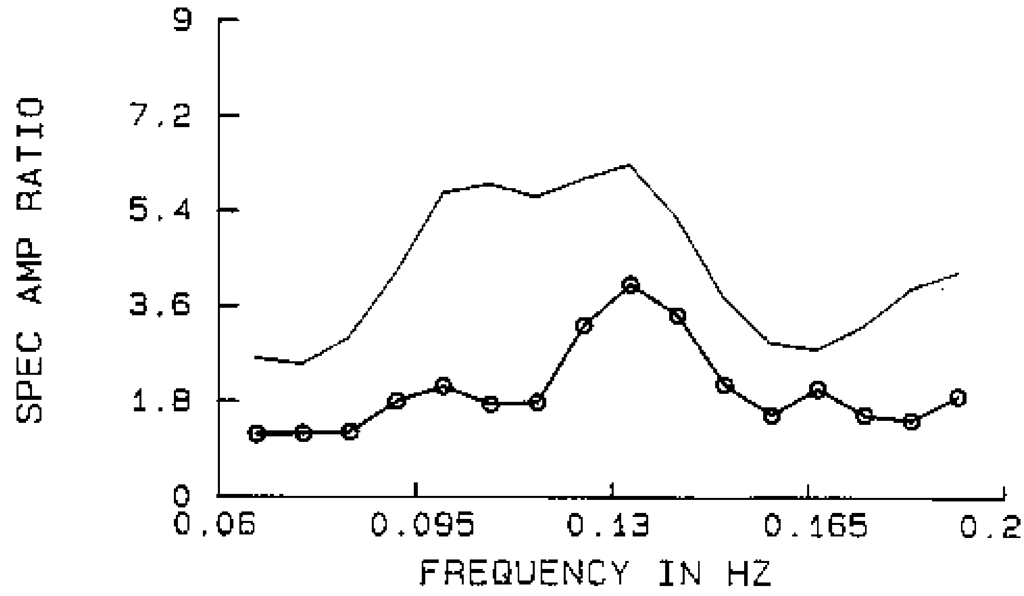

EPI. COORDINATES	2.31° N, 126.76° E
DISTANCE	80.1.^{0}
BACK AZIMUTH	92^0
DEPTH	44 KM
MAGNITUDE(m_b)	6.2
ANGLE OF EMERGENCE	15.^{0}

THICKNESS (KM)	P VELOCITY (KM/S)	DENSITY (GM/CM^3)
1	5.5	2.1
10	6.4	2.3
5	6.85	2.5
17	6.95	2.7
11	7.60	2.90
999.00	8.2	3.08

CORRELATION COEFF= .50

Fig. 4.35 Plots of theoretical and observed spectral ratio for earthquake of Feb.10, 1989 (MOLUCA) and relevant information together with obtained crustal model. Open circles and solid lines represent observed and theoretical curves, respectively.

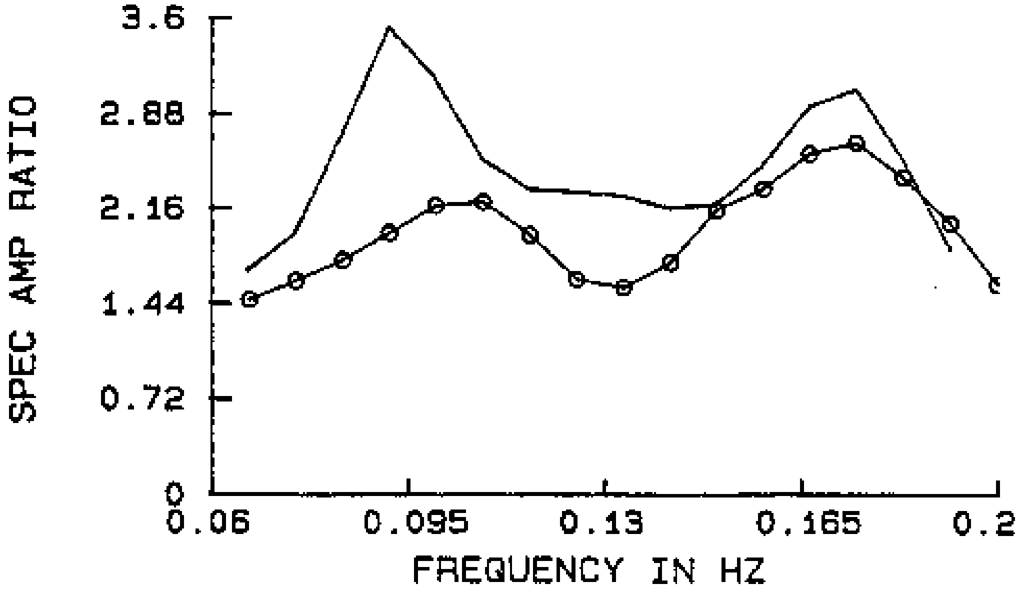

EPI. COORDINATES	36.38°N, 70.86°E
DISTANCE	23.8°
BACK AZIMUTH	55°
DEPTH	215 KM
MAGNITUDE(m_b)	6.2
ANGLE OF EMERGENCE	29°

THICKNESS (KM)	P VELOCITY (KM/S)	DENSITY (GM/CM^3)
1.0	5.55	2.1
11.0	6.1	2.3
9.0	6.55	2.5
14.0	6.75	2.7
11.0	7.4	2.90
999.00	8.30	3.08

CORRELATION COEFF= .70

Fig. 4.36 Plots of theoretical and observed spectral ratio for earthquake of Aug09,1993 (KUSH) and relevant information together with obtained crustal model. Open circles and solid lines represent observed and theoretical curves, respectively.

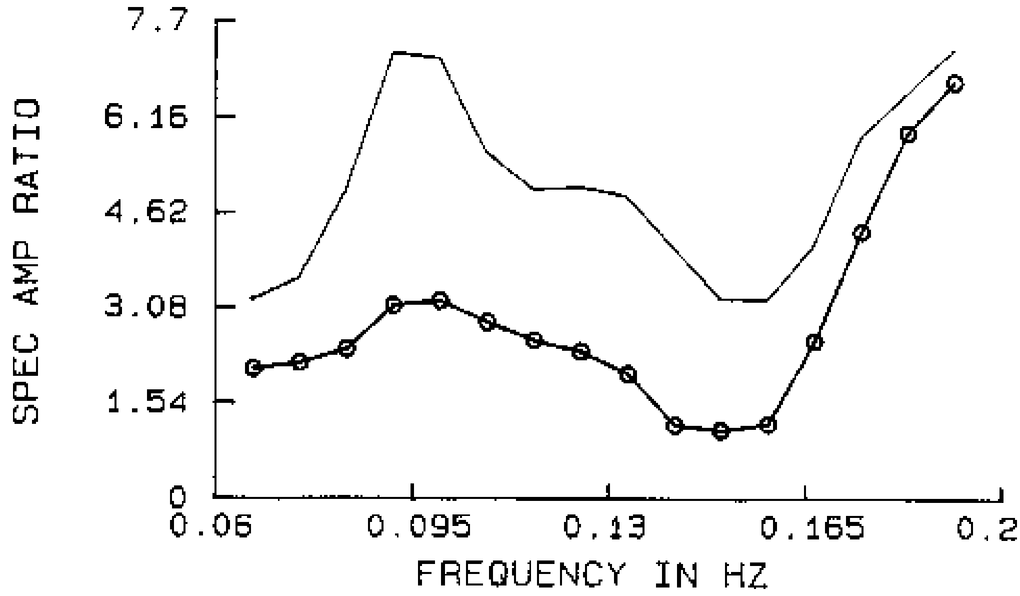

EPI. COORDINATES	52.45 N, 169.38 W
DISTANCE	97.0°
BACK AZIMUTH	21°
DEPTH	33 KM
MAGNITUDE(m_b)	6.1
ANGLE OF EMERGENCE	13.°

THICKNESS (KM)	P VELOCITY (KM/S)	DENSITY (GM/CM^3)
1	5.6	2.1
11	6.4	2.3
7	6.60	2.5
14	6.85	2.7
11	7.5	2.90
999.00	8.20	3.08

CORRELATION COEFF= .34

Fig. 4.37 Plots of theoretical and observed spectral ratio for earthquake of Jan.05, 1987 (FOX.ISL.) and relevant information together with obtained crustal model. Open circles and solid lines represent observed and theoretical curves, respectively.

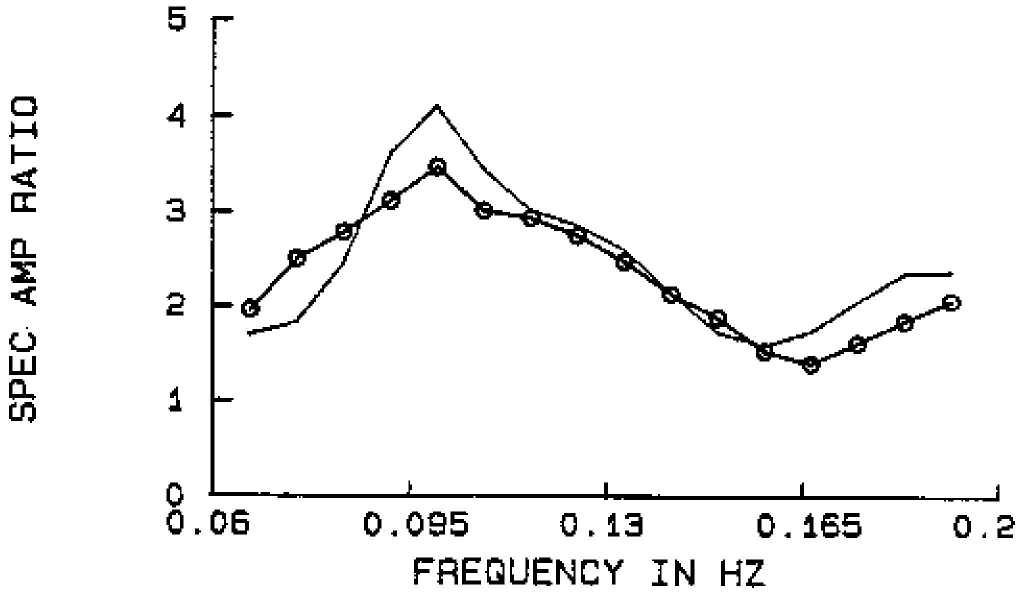

EPI. COORDINATES	39.76°N 74.57°E
DISTANCE	27.9°
BACK AZIMUTH	50°
DEPTH	8 KM
MAGNITUDE(m_b)	5.7
ANGLE OF EMERGENCE	27°

THICKNESS (KM)	P VELOCITY (KM/S)	DENSITY (GM/CM^3)
2	5.7	2.10
11	6.4	2.30
5	6.7	2.50
10	6.85	2.7
10	7.55	2.9
999.00	8.2	3.08

CORRELATION COEFF= .26

Fig.4.38 Plots of theoretical and observed spectral ratio for earthquake of April30, 1987 (CHINA) and relevant information together with obtained crustal model. Open circles and solid lines represent observed and theoretical curves, respectively.

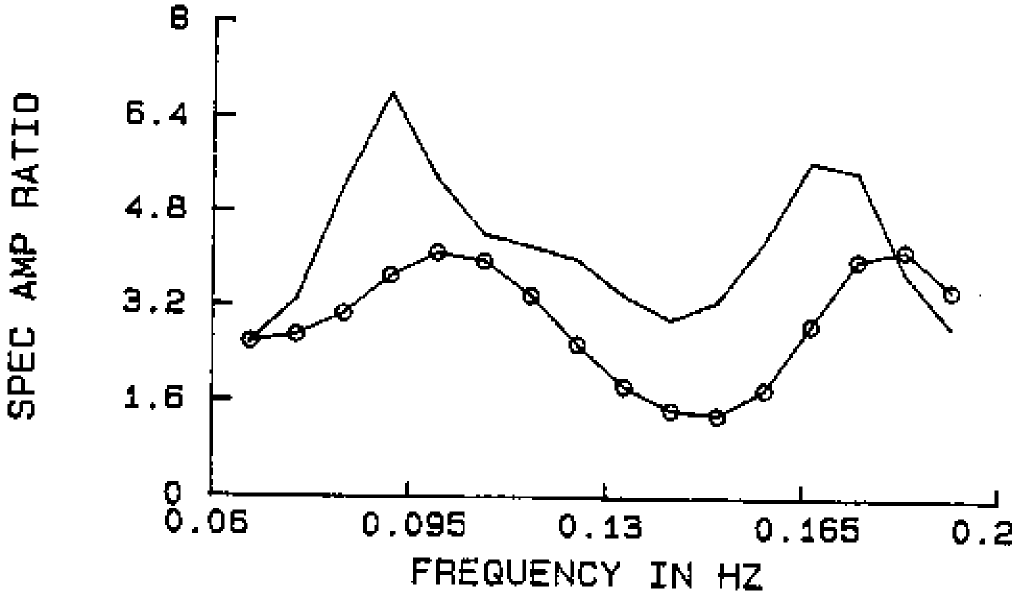

EPI. COORDINATES	49.49°N, 159.15°E
STANCE	85.0°
BACK AZIMUTH	37°
DEPTH	16 KM
MAGNITUDE(m_b)	6.3
ANGLE OF EMERGENCE	16°

THICKNESS (KM)	P VELOCITY (KM/S)	DENSITY (GM/CM^3)
2.0	5.8	2.1
10.0	6.2	2.3
8.0	6.65	2.5
16.0	6.8	2.7
11.0	7.55	2.90
999.00	8.20	3.08

CORRELATION COEFF= 0.66

Fig. 4.39 Plots of theoretical and observed spectral ratio for earthquake of April 11, 1989 and relevant information with obtained crustal model. Open circles and solid lines indicate observed and theoretical curves, respectively.

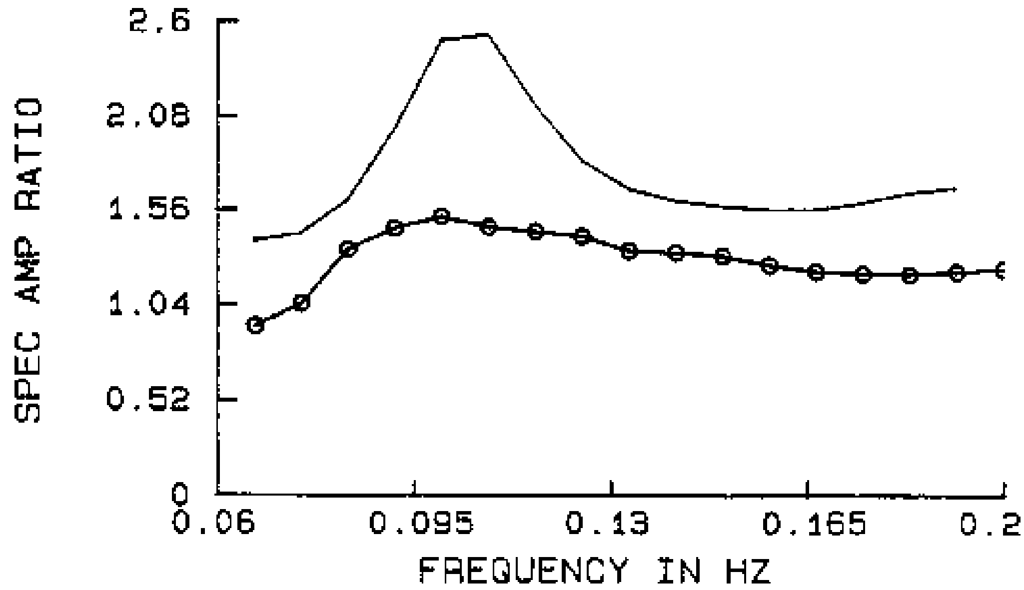

EPI. COORDINATES	11.51° N, 42.81° E
DISTANCE	13.6°
BACK AZIMUTH	196°
DEPTH	07 KM
MAGNITUDE(m_b)	5.5
ANGLE OF EMERGENCE	42°

THICKNESS (KM)	P VELOCITY (KM/S)	DENSITY (GM/CM^3)
1.00	5.85	2.10
11	6.0	2.3
7	6.35	2.5
12	6.75	2.7
10	7.45	2.90
999.00	8.2	3.08

CORRELATION COEFF= .52

Fig. 4.40 Plots of theoretical and observed spectral ratio for earthquake of Mar.05, 1992 (ETHIOPIA) and relevant information together with obtained crustal model. Open circles and solid lines represent observed and theoretical curves, respectively.

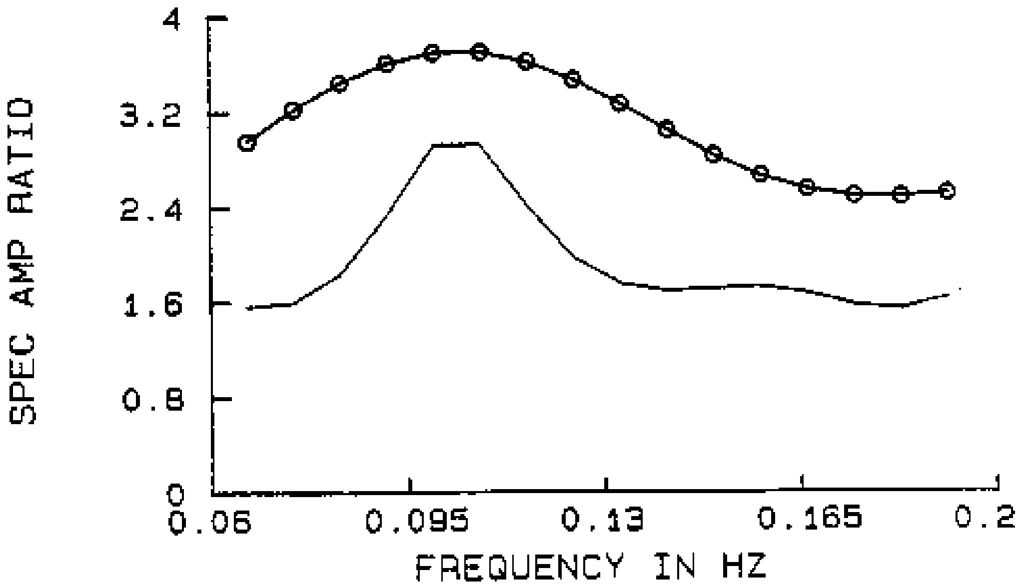

EPI. COORDINATES	05.39° N 31.65° E
DISTANCE	24.1°
BACK AZIMUTH	219°
DEPTH	13 KM
MAGNITUDE(m_b)	5.9
ANGLE OF EMERGENCE	29°

THICKNESS (KM)	P VELOCITY (KM/S)	DENSITY (GM/CM^3)
2	5.5	2.1
9	6.3	2.3
7	6.45	2.5
11	6.9	2.7
10	7.55	2.90
999.00	8.2	3.08

CORRELATION COEFF= .74

Fig. 4.41 .Plots of theoretical and observed spectral ratio for earthquake of Jul.09, 1990 (SUDAN), and relevant information together with obtained crustal model. Open circles and solid lines represent observed and theoretical curves, respectively.

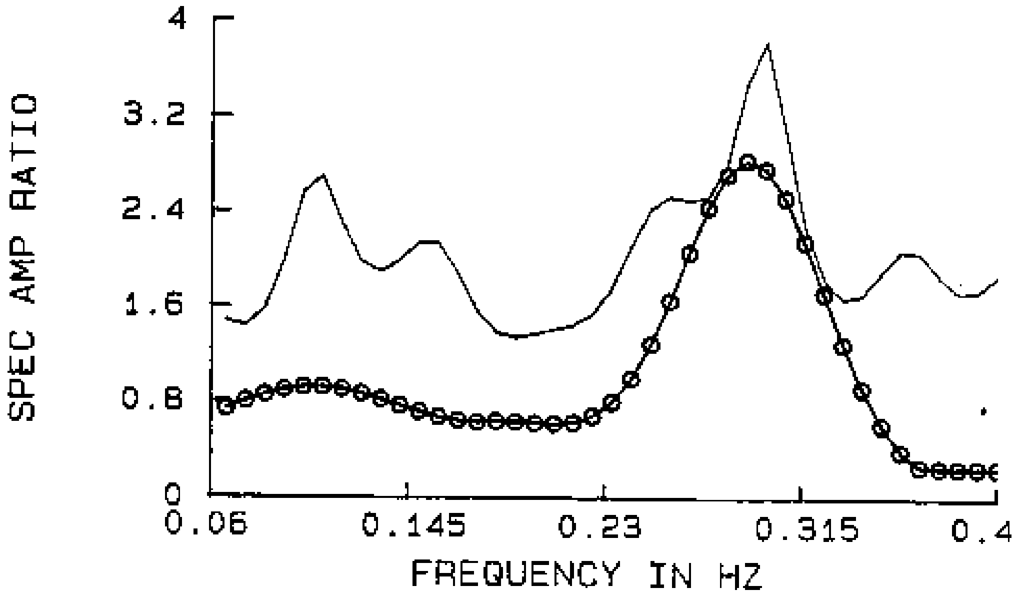

EPI. COORDINATES	05.39° N 31.65° E
DISTANCE	24.1°
BACK AZIMUTH	219
DEPTH	13 KM
MAGNITUDE(m_b)	5.9
ANGLE OF EMERGENCE	29°

THICKNESS (KM)	P VELOCITY (KM/S)	DENSITY (GM/CM^3)
2	5.5	2.1
9	6.1	2.3
7	6.7	2.5
11	6.8	2.7
10	7.35	2.90
999.00	8.2	3.08

CORRELATION COEFF= .70

Fig 4.42 Plots of theoretical and observed spectral ratio for earthquake of Jul.09, 1990 (SUDAN) and relevant information together with obtained crustal model. Open circles and solid lines represented observed and theoretical curves, respectively.

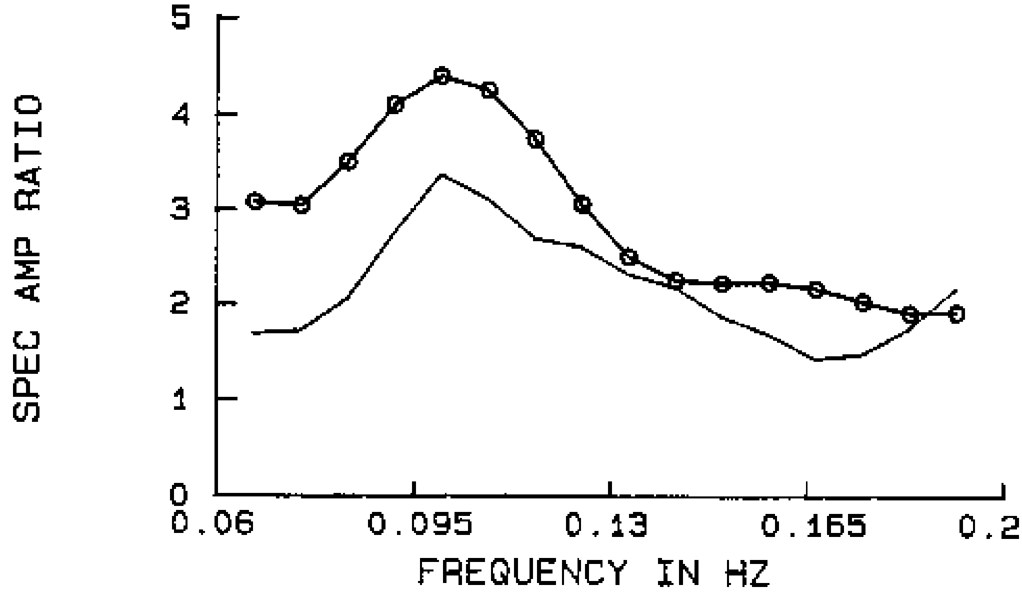

EPI. COORDINATES	5.39° N, 31.65° E
DISTANCE	23.9°
BACK AZIMUTH	219°
DEPTH	13 KM
MAGNITUDE(m_b)	5.9
ANGLE OF EMERGENCE	29°

THICKNESS (KM)	P VELOCITY (KM/S)	DENSITY (GM/CM^3)
1	5.5	2.1
10	6.35	2.3
6	6.4	2.5
13	6.8	2.7
12	7.45	2.90
999.00	8.2	3.08

CORRELATION COEFF= .45

Fig. 4.43 Plots of theoretical and observed spectral ratio for earthquake of May20, 1990 (SUDAN) and relevant information together with obtained crustal model. Open circles and solid lines represent observed and theoretical curves, respectively.

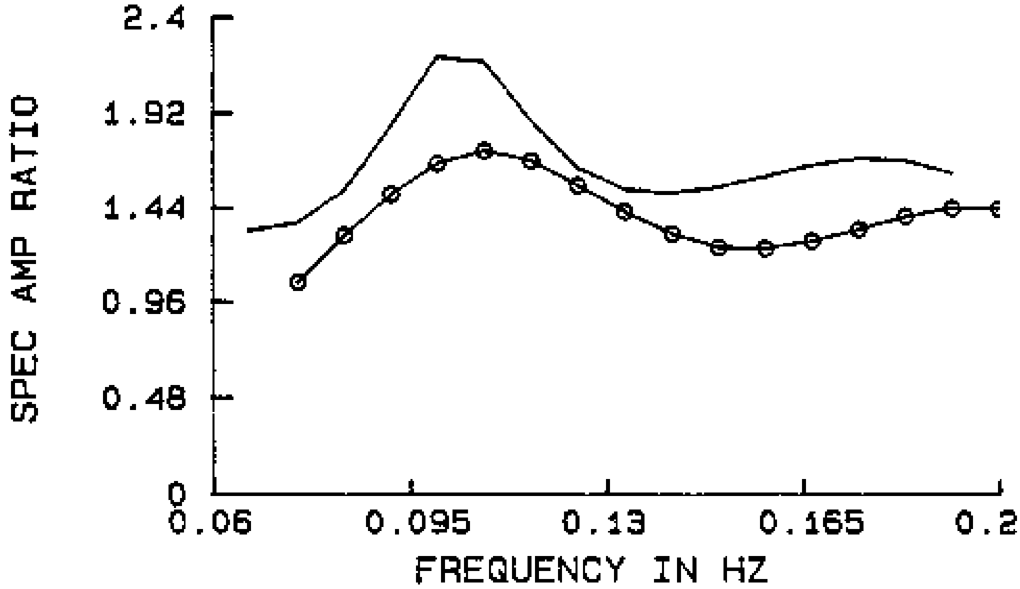

EPI. COORDINATES	28.73° N 34.55° E
DISTANCE	11.5°
BACK AZIMUTH	293°
DEPTH	10 KM
MAGNITUDE(m_b)	5.9
ANGLE OF EMERGENCE	43^0

THICKNESS (KM)	P VELOCITY (KM/S)	DENSITY (GM/CM^3)
2.0	5.6	2.1
9.0	6.0	2.3
9.0	6.5	2.5
12.0	6.8	2.7
10.0	7.45	2.90
999.00	8.30	3.08

CORRELATION COEFF= .95

Fig. 4.44 Plots of theoretical and observed spectral ratio for earthquake of Aug03,1993 (AQABA) and relevant information together with obtained crustal model. Open circles and solid lines represent observed and theoretical curves, respectively.

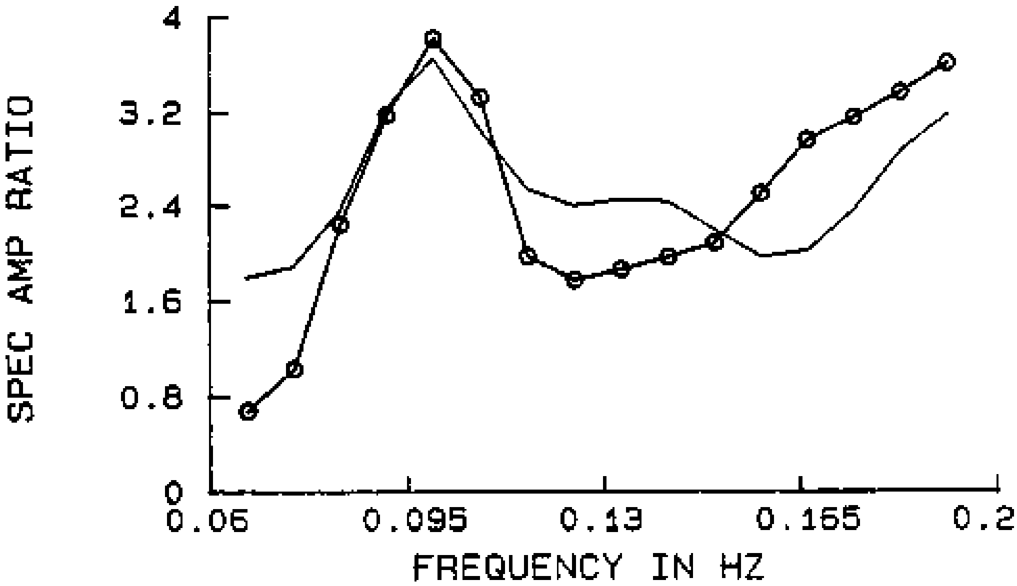

EPI. COORDINATES	35.92° N 22.49° E
DISTANCE	23.6°
BACK AZIMUTH	303°
DEPTH	65 KM
MAGNITUDE(m_b)	5.9
ANGLE OF EMERGENCE	29°

THICKNESS (KM)	P VELOCITY (KM/S)	DENSITY (GM/CM^3)
1	5.5	2.1
11	6.1	2.3
7	6.3	2.5
12.00	6.75	2.7
10	7.45	2.90
999.00	8.2	3.08

CORRELATION COEFF= .60

Fig. 4.45 Plots of theoretical and observed spectral ratio for earthquake of Nov.21, 1992 (MEDITERRANEAN SEA) and relevant information together with obtained crustal model. Open circles and solid lines represent observed and theoretical curves, respectively.

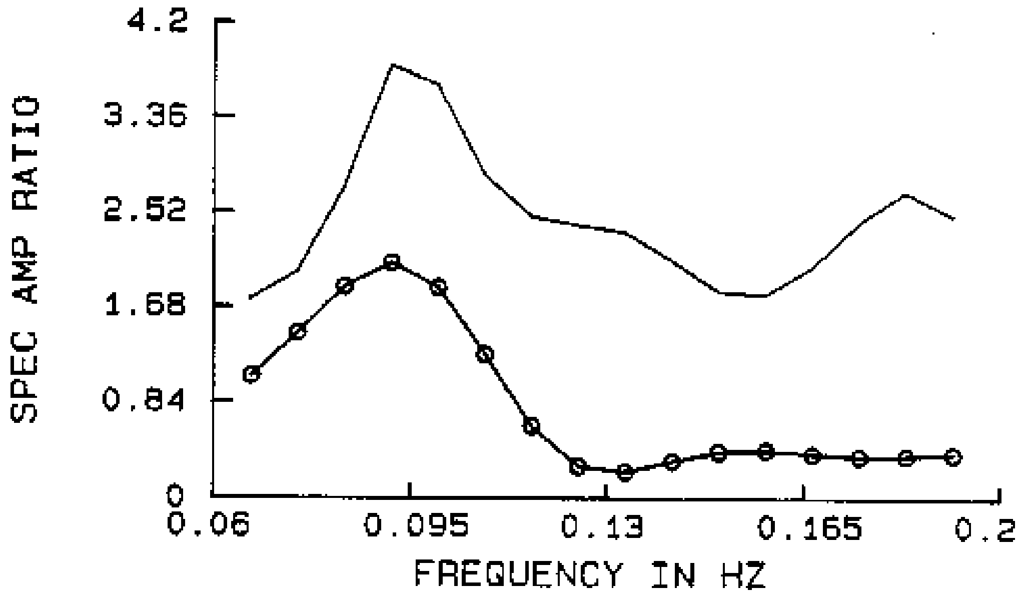

EPI. COORDINATES	34.97° N 26.69° E
DISTANCE	20.°
BACK AZIMUTH	305°
DEPTH	29 KM
MAGNITUDE(m_b)	4.7
ANGLE OF EMERGENCE	33°

THICKNESS (KM)	P VELOCITY (KM/S)	DENSITY (GM/CM^3)
1	5.55	2.1
13	6.1	2.3
6	6.5	2.5
13.00	6.75	2.7
11	7.45	2.90
999.00	8.2	3.08

CORRELATION COEFF= .75

Fig. 4.46 Plots of theoretical and observed spectral ratio for earthquake of May03, 1992 (CRETE) and relevant information together with obtained crustal model. Open circles and solid lines represent observed and theoretical curves, respectively.

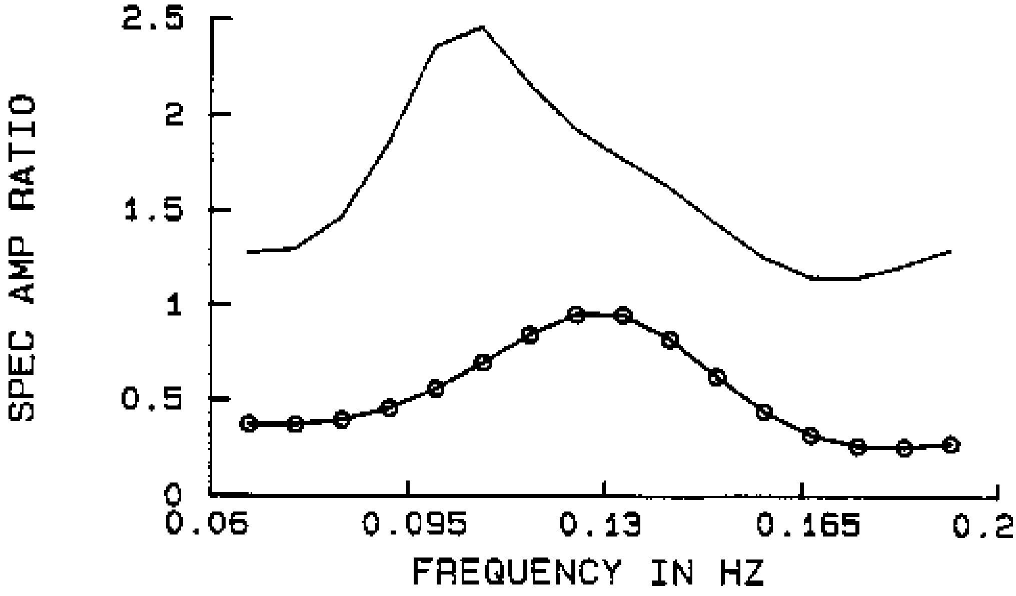

EPI. COORDINATES	29.78° N, 31.14° E
DISTANCE	14.6.°
BACK AZIMUTH	293°
DEPTH	22 KM
MAGNITUDE(m_b)	5.9
ANGLE OF EMERGENCE	41°

THICKNESS (KM)	P VELOCITY (KM/S)	DENSITY (GM/CM^3)
1	5.55	2.1
10	6.3	2.3
6	6.5	2.5
15	6.75	2.7
11	7.5	2.90
999.00	8.2	3.08

CORRELATION COEFF= .86

Fig. 4.47 Plots of theoretical and observed spectral ratio for earthquake of Oct.12, 1992 (EGYPT) and relevant information together with obtained crustal model. Open circles and solid lines represent observed and theoretical curves, respectively.

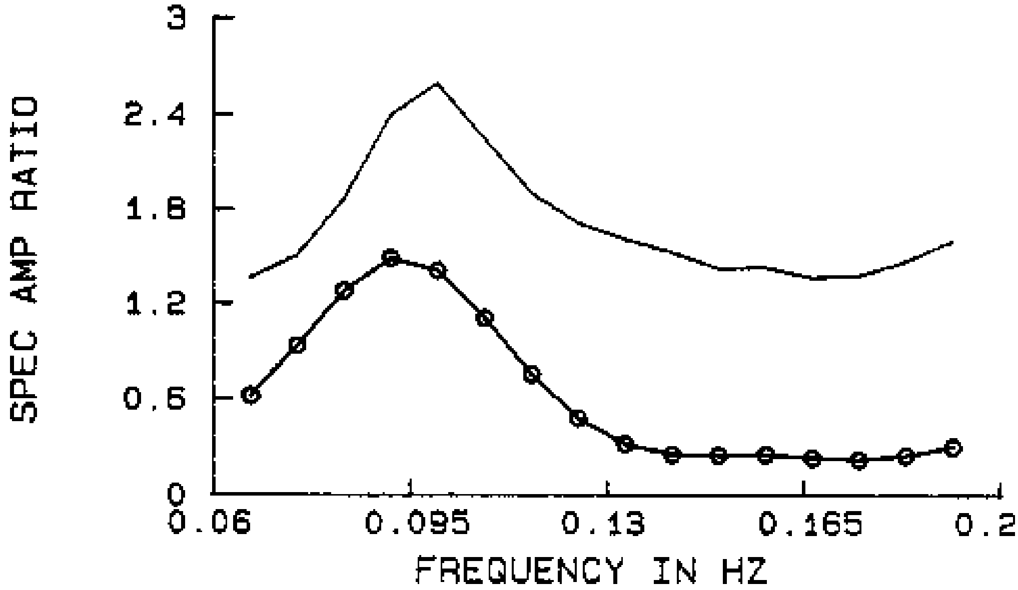

EPI. COORDINATES	40.99 N, 44.19 E
DISTANCE	16.3^0
BACK AZIMUTH	353^0
DEPTH	22 KM
MAGNITUDE(m_b)	6.2
ANGLE OF EMERGENCE	40^0

THICKNESS (KM)	P VELOCITY (KM/S)	DENSITY (GM/CM^3)
2	5.6	2.1
9	6.2	2.3
17	6.4	2.5
13	6.8	2.7
10	7.60	2.90
999.00	8.2	3.08

CORRELATION COEFF= .65

Fig. 4.48 Plots of theoretical and observed spectral ratio for earthquake of Dec.07, 1988 (ARMENIA) and relevant information together with obtained crustal model. Open circles and solid lines represent observed and theoretical curves, respectively.

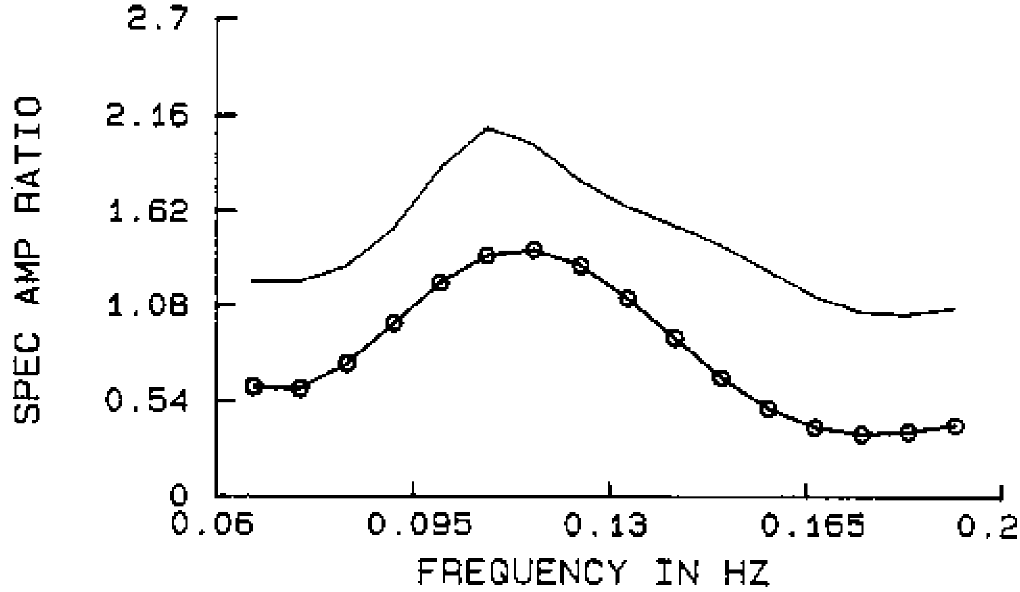

EPI. COORDINATES	35.94 N, 45.94 E
DISTANCE	11.2°
BACK AZIMUTH	357°
DEPTH	77 KM
MAGNITUDE(m_b)	4.9
ANGLE OF EMERGENCE	43.°

THICKNESS (KM)	P VELOCITY (KM/S)	DENSITY (GM/CM^3)
1	5.65	2.1
10	6.5	2.3
6	6.7	2.5
14	6.85	2.5
11	7.5	2.90
999.00	8.20	3.08

CORRELATION COEFF= .57

Fig. 4.49 Plots of theoretical and observed spectral ratio for earthquake of July25, 1988 (IRAQ) and relevent information togethger with obtained crustal model. Open circles and solid lines represent observed and theoretical curves, respectively.

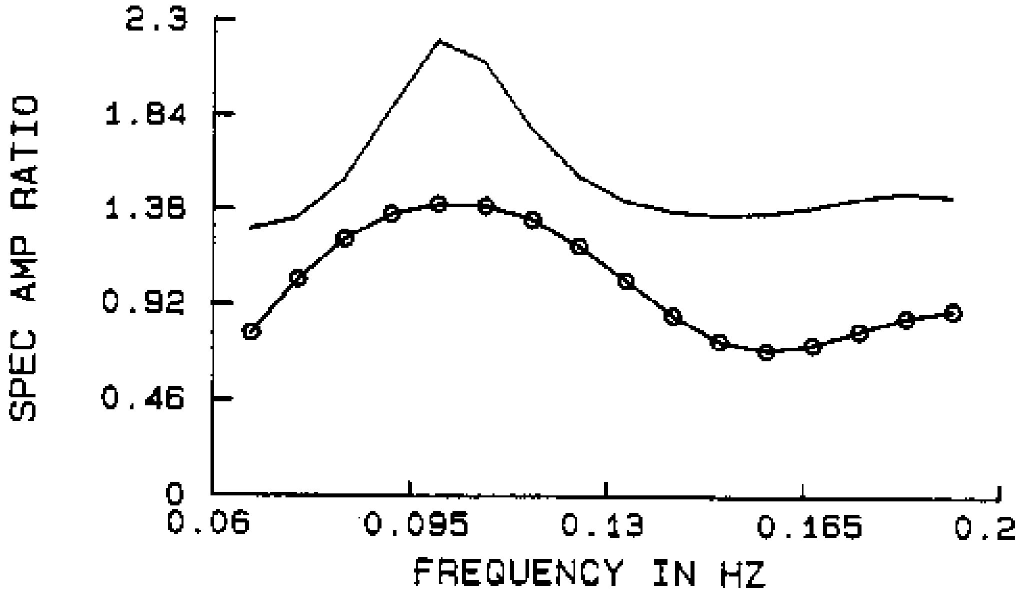

EPI. COORDINATES	19.63°N, 38.80°E
DISTANCE	8.8°
BACK AZIMUTH	236°
DEPTH	10 KM
MAGNITUDE(m_b)	5.7
ANGLE OF EMERGENCE	44°

THICKNESS (KM)	P VELOCITY (KM/S)	DENSITY (GM/CM^3)
2	5.6	
10	6.2	2.10
8	6.5	2.30
13	6.9	2.50
10	7.45	2.90
999.00	8.20	3.08

CORRELATION COEFF= .89

Fig. 4.50 Plots of theoretical and observed spectral ratio for earthquake of Mar.13, 1993(RED SEA) and relevant information together with obtained crustal model. Open circles and solid lines represent observed and theoretical curves, respectively.

APPENDIX VI.

LIST OF COMPUTER PROGRAMS

LIST OF COMPUTER PROGRAMS

```
C       PROGRAM TO CALCULATE THEORETICAL SPECTRA FOR HORIZONTALLY
C       LAYERED CRUSTAL MODEL AND CORRELATE IT WITH THE OBSERVED
C       SPECTRA. TO FIND THE MAXIMUM CORRELATION THE LAYER PARAMETERS
C       ARE SYSTEMATICALLY CHANGED. AFTER FINDING THE MAXIMUM
C       THE RELATED PARAMETERS ARE USED ONE MORE TO CALCULATE THE
C       CRUSTAL
C       RESPONSE. THE OBSERVED AND CALCULATED SPECTRA ARE PLOTTED ON
C       THE SCREEN AND PRINTER.
        REAL XIN1 , FREQI , ANGIP
        COMMON D(10), A(10), B(10), RHO(10), FREQI(260), PAUOWI(260),
        CXIN1(260)
        CHARACTER*12 FINPUT1,FINPUT2
        COMMON  PWDTPI(260), PUDTPI(260),WDTP,UDTP,AUOW, ANGIP
        CHARACTER*12 FILE3, FILE4 ,FILE5, FILE6, FILE7
C       DEFINITION OF VARIABLES
C           NOL      = NUMBER OF LAYERS
C           CNTRL    =
C           AGIP1    = INITIAL ANGLE OF INCIDENCE
C           DANGI    = INCREMENT OF ANGLE OF INCIDENCE
C           NOANG    = NUMBER OF ANGLES
C           FMIN     = MINIMUM FREQUENCY
C           FINC     = FREQUENCY INCREMENT
C           NOF      = NUMBER OF FREQUENCUES
C           D        = THICKNESS  OF LAYER
C           A        = P WAVE VELOCITY
C           RHO      = DENSITY
C
C       INPUT FILE1 CONTAINS;
C       1. NUMBER CF LAYERS,CR
C       2. EARTH MODEL
C       3. INITIAL ANGLE OF INCIDENCE, INCREMENT OF ANGLE OF INCIDENCE
C          AND NUMBER OF ANGLES
C       4. MINIMUM FREQUENCY, INCREMENT OF FREQUENCY AND NUMBER OF
C          FREQUENCUES
        WRITE(5,200)
 200    FORMAT ( ' ENTER THE NAME OF THE INPUT FILE1 ')
        READ(5,210) FINPUT1
 210    FORMAT(A12)
C       READ FILE2 FOR OBSERVED DIGITIZED DATA
        WRITE(5,240)
 240    FORMAT ( ' ENTER THE NAME OF THE INPUT FILE2 SPECTRA ')
        READ(5,210)FINPUT2
        WRITE(5,241)
 241    FORMAT( ' ENTER THE NAME OF THE INPUT FILE3 PARAMETERS' )
        READ(5,210) FILE4
        WRITE(5,231)
 231    FORMAT ( ' WRITE THE NAME OF THE OUTFPUT FILE ')
        READ(5,251) FILE3
```

```
 251   FORMAT(A12)
C      WRITE(5,261)
C261   FORMAT( ' WRITE THE OUTPUT FILE NAME FOR VERTICAL  SPECTRUM ')
C      READ(5,251) FILE5
C      WRITE(5,264)
WRITE(5,265)
 265   FORMAT( ' WRITE THE NAME OF THE OUTPUT FILE FOR RATIO SPECTUM
       ')
       READ(5,251) FILE7
       OPEN(UNIT=1,FILE=FINPUT1,STATUS='OLD')
       OPEN(UNIT=2,FILE=FINPUT2,STATUS='OLD')
       OPEN(UNIT=4,FILE=FILE4,STATUS='OLD')
       OPEN(UNIT=3,FILE=FILE3,STATUS='NEW')
       OPEN(UNIT=7,FILE=FILE7,STATUS='NEW')
C      OPEN(UNIT=8,FILE=FILE6,STATUS='NEW')
C      OPEN(UNIT=9,FILE=FILE7,STATUS='NEW')
C*******************************************
       READ(1,1) NOL,CR
 3     FORMAT(3F10.4)
       DO 2 I=1,NOL
       READ(1,3) D(I),A(I),RHO(I)
       WRITE(3,3) D(I),A(I),RHO(I)
 2     CONTINUE
 1     FORMAT(I3,F5.3)
       READ(1,4) AGIP1,DANGI,NOANG
 4     FORMAT(2F11.9,I3)
       WRITE(3,4) AGIP1,DANGI,NOANG
       READ(1,*) FMIN,FINC,NOF
       WRITE(3,4) FMIN,FINC,NOF
C
       DO 7 N=1,260
       READ(2,*,END=71)  FREQI(N),XIN1(N)
       WRITE(3,*) FREQI(N),XIN1(N)
  7    CONTINUE
 71    NPTS=N-1
C      THE NUMBER OF FREQUENCY POINTS I.E., IS GOING TO BE TAKEN FROM
C      THE OBSERVED SPECTRUM. NPTS
       NOF = NPTS
       READ(4,53) KA,KB,KC,KD,KE,KF,KG
  53   FORMAT(7I5)
C
       WRITE(3,53) KA,KB,KC,KD,KE,KF,KG
       RA = RHO(1)
C
       RB1 = D(1)
       RB2 = D(2)
       RB3 = D(3)
       RB4 = D(4)
C
       RC1 = A(1)
       RC2 = A(2)
       RC3 = A(3)
       RC4 = A(4)
C
       AMAX = 0.
       AA1 = 0.
```

```
      AA2 = 0.
      AA3 = 0.
      AA4 = 0.
C
      DD1 = 0.
      DD2 = 0.
      DD3 = 0.
      DD4 = 0.
C
C
C
      DO 41 JA = 1,KA
C        THICKNESS VARIATION
      DO 42  JB =1,KB

C     FIRST AND SECOND LAYERS COMBINATION. WHILE SECOND LAYER
C     THICKNESS
C     IS INCREASED ONE KM., FIRST LAYER THICKNESS IS BEING DECREASED
C     ONE KM.
C     TOTAL CRUSTAL THICKENESS IS KEPT AS CONSTANT IN THIS LOOP.
C
      DO 43 JC=1,KC
C
C     FOURTH LAYER AND THIRD LAYER COMBINATION. WHILE FOURTH LAYER
C     THICKNESS IS INCREASED ONE KM., THIRD LAYER THICKNESS IS BEING
C     DECREASED ONE KM.
C     TOTAL CRUSTAL THICKNESS IS KEPT AS CONSTANT IN THIS LOOP.
C
C
C     VELOCITY VARIATION
      DO  44 JD=1,KD
C     FIRST LAYER VELOCITY INCREMENT BY 0.2 KM/SEC
C
      DO 47 JE=1,KE
C     SECOND LAYER VELOCITY INCREMENT BY 0.2 KM/SEC
C
      DO 48 JF =1,KF
C
C     THIRD LAYER VELOCITY INCREMENT BY 0.2 KM/SEC
C
      DO 49 JG =1,KG
C     FOURTH LAYER VELOCITY INCREMENT BY 0.2 KM/SEC
C
      CALL TF (NOL,AGIP1,DANGI,NOANG,FMIN,FINC,NOF)
      CALL CR1(R,T,NPTS)
C     WRITE(5,666)RB4,D(1),D(2),D(3),D(4)
C666  FORMAT(1X,'TOTAL =',F5.2,2X,'D(1)=',F5.2,2X,'D(2)=',F5.2,2X,
C    C'D(3)=',F5.2,2X,'D(4)=',F5.2)

C
      IF (AMAX.GE.R) GO TO 887
      AMAX =R
      AA1 = A(1)
      AA2 = A(2)
      AA3 = A(3)
      AA4 = A(4)
```

```
      DD1 = D(1)
      DD2 = D(2)
      DD3 = D(3)
      DD4 = D(4)
C
C 887  IF (R.GT.0.01) WRITE (3,6)JA,JB,JC,JD,JE,JF,R,T,D(1),D(2),D(3),
C    *A(1),A(2),A(3)
 887  CONTINUE
 6    FORMAT(7I3,10(F7.2,1X))
      A(4) = A(4) +0.2
 49   CONTINUE
      A(4) =RC4
      A(3) =A(3)+0.2
 48   CONTINUE
      A(4)=RC4
      A(3)= RC3
      A(2)=A(2)+0.2
 47   CONTINUE
      A(4) = RC4
      A(3) = RC3
      A(2) =RC2
      A(1) =A(1)+0.2
 44   CONTINUE
      A(1) = RC1
      A(2) = RC2
      A(3) = RC3
      A(4) = RC4
C
      D(4) = D(4)+1.
      D(3) = D(3)-1.
 43   CONTINUE
 888  A(1) = RC1
      A(2) = RC2
      A(3) = RC3
      A(4) = RC4
      D(4) = RB4
      D(3) = RB3
      D(2) = D(2)+1.
      D(1) = D(1)-1.
  42  CONTINUE
      RB4 = RB4 + 1.
C
      D(1) = RB1
      D(2) = RB2
      D(3) = RB3
      D(4) = RB4
      A(1) = RC1
      A(2) = RC2
      A(3) = RC3
      A(4) = RC4
C
 41   CONTINUE
 16   FORMAT (6(I2,2X),2X,2(F5.2,2X),5X,6(F5.2,2X))
      WRITE (3,6) JA,JB,JC,JD,JE,JF,JG,R,T,D(1),D(2),D(3),D(4),
     *A(1),A(2),A(3),A(4)
      WRITE (3,892) AMAX
```

```
 892  FORMAT (1H ,'CORRELATION COEFF=' F6.2)
      WRITE (3,10) D(NOL-1),A(NOL-1), B(NOL-1), RHO(NOL-1),ANGIP
      WRITE (3,10) D(NOL),A(NOL),B(NOL),RHO(NOL),AGIP1
  10  FORMAT (F10.4,10X,4F10.4)
      A(1)= AA1
      A(2) = AA2
      A(3) = AA3
      A(4) = AA4
C
      D(1) = DD1
      D(2) = DD2
      D(3) = DD3
      D(4) = DD4
C
      WRITE(3,9993)
C
      CALL TF (NOL,AGIP1,DANGI,NOANG,FMIN,FINC,NOF)
      CALL CR1(R,T,NPTS)
      WRITE (3,1111) AMAX,AA1,DD1,AA2,DD2,AA3,DD3,AA4,DD4
 1111 FORMAT(///,'MAX=',F4.2,2X,'VP1=',F5.3,2X,'H1=',F5.2,
     12X,'VP2=',F5.3,2X,'H2=',F5.2,2X,'VP3=',F5.3,2X,'H3=',F5.2,
     2'VP4=',F5.3,2X,'H4=',F5.2,//)

8    FORMAT(2A6)
C
 9993 FORMAT(////)
      WRITE(3,9993)
      DO 9992 I=1,NOL
      WRITE(3,3) D(I),A(I),RHO(I)
 9992 CONTINUE
      DO 784 JQ=1,NOF
      WRITE(7,789) FREQI(JQ),PAUOWI(JQ)
 784  CONTINUE
      WRITE(3,4565) R
 789  FORMAT( F11.9,2X,F12.9)
 4565 FORMAT(1H , 'CORRELATION COEFF=    ' ,F4.2 )
      WRITE(3,111)A(1),D(1),RHO(1),AGIP1
      WRITE(3,113)A(2),D(2),RHO(2),AGIP1
 111  FORMAT(/,3X,'CR=',F10.4,1X,'VP1=',F10.4,1X,'H1=',F10.4,
     *1X,'RHO1=',F10.4,1X,'ANG.OF INC.=',F10.4)
 113  FORMAT(//,1X,'CR=',F10.4,1X,'VP2=',F10.4,1X,'H2=',F10.4,
     *1X,'RHO2=',F10.4,2X,'ANG.OF INC.=',F10.4)
      CLOSE(UNIT=1)
      CLOSE(UNIT=2)
      CLOSE(UNIT=3)
      CLOSE(UNIT=4)
      CLOSE(UNIT=7)
      CLOSE(UNIT=8)
      CLOSE(UNIT=9)
      STOP
      END
C
      SUBROUTINE TF(NOL,AGIP1,DANGI,NOANG,FMIN,FINC,NOF)
C     THIS PROGRAM IS DESIGNED TO CALCULATE THE TRANSFER FUNCTIONS
C     OF THE VERTICAL AND HORIZONTAL COMPONENTS OF LONGITUDINAL
C     SEISMIC WAVES IN A LEVERED MEDIUM, AND THE FIRST PARTIAL
```

```
C     DERIVATIVE OF THESE TRANSFER FUNCTIONS WITH RESPECT TO THE
C     THICKNESS ,THE ELAS PARAMETERS AND THE DENSITIES OF ANY OF THE
C     LAYERS OF THE SYSTEM. BESIDES THIS PROGRAM CALCULATES THE
      RANSFER C     FUNCTION FOR THE APPARENT ANGLE OF EMERGENCE, THIS
      IS, THE RATIO
C     OF THE VERTICAL TO THE HORIZONTAL COMPONENT AND ITS FIRST
C     PARITIAL DERIVATIVES.
C
       DIMENSION FL(10),DGAM(10),DGAM1(10),DRA(10),
      1DH(9),ELTAD(9),PA11(9),PA12(9),PA13(9),PA14(9),
      2PA21(9),PA22(9),PA23(9),PA24(9),PA31(9),PA32(9),PA33(9),
      3PA34(9),PA42(9),PA43(9),PA44(9),PEA11(9),PEA12(9),PEA21(9),
      4PEA22(9),PEA31(9),PEA32(9),PA41(9),PEA41(9),PEA42(9)
       DIMENSION DPDPR(9),DPDQL(9),DPDQR(9),DPDGL(9),DRB(9),DPDGR(9),
      1DDRAL(9),DDRAR(9),DDRBR(9),DPDPL(9),DDRBL(9)
       DIMENSION GAFI(260),PPHWPI(260),PPHUPI(260),PPHUWI(260)
       DIMENSION PUDTPI(260),PWDTPI(260)
       COMMON (10),A(10),B(10),RHO(10),FREQI(260),PAUOWI(260),XIN1(260)
       COMMON FINPUT1,FILE3, ANGIP
C
       COMMON  PWDTPI, PUDTPI,WDTP,UDTP,AUOW
       SIGN(VAR)=ABS(VAR)/VAR
C      READ IN THE NUMBER OF LAYERS PLUS ONE OF THE SYSTEM
C      READ IN LAYER CONSTANTS,D(I)=THICKNESS OF THE I LAYER,
C      FL(I)=PARAMETER LAMDA OF THE I TH LAYER,RHO(I)=DENSITY OF THEI
C      READ IN CHANGES IN THE LAYER    PARAMETERS. IF THE  PARTIAL
C      DERIVATIVE IS DESIRED   WITH  RESPECT  TO THE  PARAMETER, MAKE
C      ELTAD(I)=1.
C
C
 2     DO 3 I=1,NOL
       B(I)=A(I)/1.73205
 3     FL(I)=RHO(I)*A(I)*A(I)/3.
       N=NOL
C      DO 100 I=1,NOL-1
C      READ (1,101) ELTAD(I)
C      WRITE(3,101) ELTAD(I)
C100   CONTINUE
C      READ AGIP1=INITIAL ANGLE OF INCIDENCE,DANGI=INCREMENT OF THE
C      ANGLE NOANG=NUMBER OF ANGLES TO BE CALCULATED
 7001 ANGIP=AGIP1-DANGI
C      IF(ANGIP.EQ.AGIP1) GO TO 1021
 101   FORMAT (3F10.4)
       DO 310 IA=1,NOANG
       FREQ=FMIN-FINC
 5004 ANGIP=ANGIP+DANGI
       C=A(NOL)/SIN(ANGIP/57.295780)
       SININ=A(NOL)*SIN(ANGIP/57.29578)/A(1)
       SINE=(1.-2.*(SININ**2)/3.)
       COSE=SQRT(1.-SINE**2)
       TANE=SINE/COSE
       EM=ATAN(TANE)*57.29578
       AIM=90.-EM
C      COMPUTE REUSABLE VARIABLES FOR THE LAYERS
       DO 1346 M=1,NOL
       DH(M)=RHO(M)*C*C
```

```
      COVA=C/A(M)
      COVB=C/B(M)
      DRA(M)=SQRT(ABS(COVA**2-1.))
      DRB(M)=SQRT(ABS(COVB**2-1.))
      COVP=1./DRA(M)
      COVS=1./DRB(M)
      DPDGL(M)=2./DH(M)
      DPDGR(M)=-2.*FL(M)/(DH(M)*RHO(M))
      DDRAL(M)=-DH(M)*COVP/(6.*FL(M)*FL(M))
      DDRAR(M)=C*C*COVP/(6.*FL(M))
      DDRBL(M)=-DH(M)*COVS/(2.*FL(M)*FL(M))
      DDRBR(M)=C*C*COVS/(2.*FL(M))
      DPDPL(M)=-DH(M)*D(M)*COVP/(6.*FL(M)*FL(M))
      DPDPR(M)=D(M)*C*C*COVP/(6.*FL(M))
      DPDQL(M)=-DH(M)*D(M)*COVS/(2.*FL(M)*FL(M))
      DPDQR(M)=D(M)*C*C*COVS/(2.*FL(M))
      DGAM(M)=2.*FL(M)/DH(M)
 1346 DGAM1(M)=DGAM(M)-1.
      DO 310 IFR=1,NOF
      FREQ=FREQ+FINC
      GAF=FREQ*D(1)/A(1)
      WVNO=6.2831853*FREQ/C
      A11=1
      A12=0
      A21=0
      A22=1
      A31=0
      A32=0
      A41=0
      A42=0
      ND=0
C     COMPUTE THE ELEMENTS OF A MATRIX FOR REMAINING LAYERS
      N1=NOL-1
      DO 1345 M=1,N1
      GAM=DGAM(M)
      GAMM1=DGAM1(M)
      RA=DRA(M)
      RB=DRB(M)
      H=DH(M)
      P=WVNO*D(M)*RA
      Q=WVNO*D(M)*RB
      SINP=SIN(P)
      W=SINP/RA
      X=RA*SINP
      COSP=COS(P)
      SINQ=SIN(Q)
      Y=SINQ/RB
      Z=RB*SINQ
      COSQ=COS(Q)
      RHOM=RHO(M)
      ZZ=RB*COSQ
      XX=RA*COSP
      YY=COSQ/RA
      WW=COSP/RA
      YYY=COSQ/RB
      DM=D(M)
```

```
      NDM=0
      B11=GAM*COSP-GAMM1*COSQ
      B12=GAMM1*W+GAM*Z
      B13=-(COSP-COSQ)/H
      B14=(W+Z)/H
      B21=GAM*X+GAMM1*Y
      B22=-GAMM1*COSP+GAM*COSQ
      B23=-(X+Y)/H
      B24=B13
      B31=H*GAM*GAMM1*(COSP-COSQ)
      B32=H*(GAMM1*GAMM1*W+GAM*GAM*Z)
      B33=B22
      B34=B12
      B41=-H*(GAM*GAM*X+GAMM1*GAMM1*Y)
      B42=B31
      B43=B21
      B44=B11
      ELTAD(M) =0.
C     IF(ELTAD(M)) 10,11,10
C       CALCULATE THE   PARTIAL DERIVATIVES OF THE MATRIX ELEMENTS
C       WITH RESPECT TO THE THICKNESS OF THE CORRESPONDENT LAYER
 10   ND = ND+1
      PA11(ND) = WVNO*(-GAM*X+GAMM1*Z)
      PA12(ND) = WVNO*(GAMM1*COSP+GAM*RB**2*COSQ)
      PA13(ND) = (X-Z)*WVNO/H
      PA14(ND) = WVNO*(COSP+RB**2*COSQ)/H
      PA21(ND) = -WVNO*(GAM*RA**2*COSP+GAMM1*COSQ)
      PA22(ND) = WVNO*(GAMM1*X-GAM*Z)
      PA23(ND) = WVNO*(RA**2*COSP+COSQ)/H
      PA24(ND) = PA13(ND)
      PA31(ND) = -H*GAMM1*GAM*WVNO*(X-Z)
      PA32(ND) = H*(GAMM1**2*WVNO*COSP+GAM**2*RB**2*COSQ*WVNO)
      PA33(ND) = PA22(ND)
      PA34(ND) = PA12(ND)
      PA41(ND) = H*(GAM**2*RA**2*WVNO*COSP+GAMM1**2*WVNO*COSQ)
      PA42(ND) = PA31(ND)
      PA43(ND) = PA21(ND)
      PA44(ND) = PA11(ND)
 11   CONTINUE

C     MULTIPLY MATRICES
      EA11=B11*A11+B12*A21+B13*A31+B14*A41
      EA12=B11*A12+B12*A22+B13*A32+B14*A42
      EA21=B21*A11+B22*A21+B23*A31+B24*A41
      EA22=B21*A12+B22*A22+B23*A32+B24*A42
      EA31=B31*A11+B32*A21+B33*A31+B34*A41
      EA32=B31*A12+B32*A22+B33*A32+B34*A42
      EA41=B41*A11+B42*A21+B43*A31+B44*A41
      EA42=B41*A12+B42*A22+B43*A32+B44*A42
      NF=ND-NDM
      NF1=NF+1
      IF(NDM)54,55,54
 54   DO 30 I=NF1,ND
      PEA11(I)=PA11(I)*A11+PA12(I)*A21+PA13(I)*A31+PA14(I)*A41
      PEA12(I)=PA11(I)*A12+PA12(I)*A22+PA13(I)*A32+PA14(I)*A42
      PEA21(I)=PA21(I)*A11+PA22(I)*A21+PA23(I)*A31+PA24(I)*A41
```

```
      PEA22(I)=PA21(I)*A12+PA22(I)*A22+PA23(I)*A32+PA24(I)*A42
      PEA31(I)=PA31(I)*A11+PA32(I)*A21+PA33(I)*A31+PA34(I)*A41
      PEA32(I)=PA31(I)*A12+PA32(I)*A22+PA33(I)*A32+PA34(I)*A42
      PEA41(I)=PA41(I)*A11+PA42(I)*A21+PA43(I)*A31+PA44(I)*A41
 30   PEA42(I)=PA41(I)*A12+PA42(I)*A22+PA43(I)*A32+PA44(I)*A42
55    CONTINUE
      A11=EA11
      A12=EA12
      A21=EA21
      A22=EA22
      A31=EA31
      A32=EA32
      A41=EA41
      A42=EA42
      IF(NF)50,1344,50
50    DO 31 I=1,NF
      PEA11(I)=B11*PA11(I)+B12*PA21(I)+B13*PA31(I)+B14*PA41(I)
      PEA12(I)=B11*PA12(I)+B12*PA22(I)+B13*PA32(I)+B14*PA42(I)
      PEA21(I)=B21*PA11(I)+B22*PA21(I)+B23*PA31(I)+B24*PA41(I)
      PEA22(I)=B21*PA12(I)+B22*PA22(I)+B23*PA32(I)+B24*PA42(I)
      PEA31(I)=B31*PA11(I)+B32*PA21(I)+B33*PA31(I)+B34*PA41(I)
      PEA32(I)=B31*PA12(I)+B32*PA22(I)+B33*PA32(I)+B34*PA42(I)
      PEA41(I)=B41*PA11(I)+B42*PA21(I)+B43*PA31(I)+B44*PA41(I)
31    PEA42(I)=B41*PA12(I)+B42*PA22(I)+B43*PA32(I)+B44*PA42(I)
1344  CONTINUE
      IF(ND)60,1345,60
60    DO 38 I=1,ND
      PA11(I)=PEA11(I)
      PA12(I)=PEA12(I)
      PA21(I)=PEA21(I)
      PA22(I)=PEA22(I)
      PA31(I)=PEA31(I)
      PA32(I)=PEA32(I)
      PA41(I)=PEA41(I)
 38   PA42(I)=PEA42(I)
 1345 CONTINUE
 1349 A21=-A21
      A41=-A41
      GAM=DGAM(N)
      GAMM1=DGAM1(N)
      RA=DRA(N)
      RB=DRB(N)
      H=DH(N)
C     COMPUTE THE ELEMENTS FOR THE E INVERSE OF THE LAST LAYER
      B11=-GAM*COVA**2
      B13=1./(RHO(N)*A(N)*A(N))
      B22=GAMM1*COVA**2/RA
      B24=B13/RA
      B44=1./(H*GAM)
      B33=-B44/RB
      B31=-B33*GAMM1*H
      B42=1.
      EA11=B11*A11+B13*A31
      EA12=B11*A12+B13*A32
      EA21=B22*A21+B24*A41
      EA22=B22*A22+B24*A42
```

```
      EA31=B31*A11+B33*A31
      EA32=B31*A12+B33*A32
      EA41=B42*A21+B44*A41
      EA42=B42*A22+B44*A42
      DR=EA21*EA32-EA11*EA42-EA12*EA41+EA22*EA31
      DI=EA11*EA32+EA21*EA42-EA12*EA31-EA22*EA41
      DENSQ=DR*DR+DI*DI
      UPNR=EA32*DI-EA42*DR
      UPNI=EA32*DR+EA42*DI
      UDTP=((2./DENSQ)*SQRT(UPNR*UPNR+UPNI*UPNI))*COVA
      PHUPD=ATAN(-UPNI/UPNR)-(1.-SIGN(UPNR))*SIGN(UPNI)*1.57079
      WPNI=EA41*DR+EA31*DI
      WPNR=-EA31*DR+EA41*DI
      WDTP=((2./DENSQ)*SQRT(WPNR*WPNR+WPNI*WPNI))*COVA
      AUOW=WDTP/UDTP
      PHWPD=ATAN(-WPNI/WPNR)-(1.-SIGN(WPNR))*SIGN(WPNI)*1.57079
      PHUOW=PHWPD-PHUPD
      ABPH=ABS(PHUOW)-3.14159
      IF(ABPH) 610,610,611
611   IF(PHUOW) 612,610,613
612   PHUOW=PHUOW+6.2832
      GO TO 610
 613  PHUOW=PHUOW-6.2832
 610  CONTINUE
C     WRITE(7,303) FREQ,WDTP,PHWPD,UDTP,PHUPD,AUOW,PHUOW
303  FORMAT( 7(F9.4,2X))
      FREQI(IFR)=FREQ
      GAFI(IFR)=GAF
      PWDTPI(IFR)=WDTP
      PPHWPI(IFR)=PHWPD
      PUDTPI(IFR)=UDTP
      PPHUPI(IFR)=PHUPD
      PAUOWI(IFR)=AUOW
      PPHUWI(IFR)=PHUOW
C     FOR INVERSE MATRIX OF LAST LAYER
      IF(ND)99,310,99
 99   DO 32 I=1,ND
      PA21(I)=-PA21(I)
      PA41(I)=-PA41(I)
      PEA11(I)=B11*PA11(I)+B13*PA31(I)
      PEA12(I)=B11*PA12(I)+B13*PA32(I)
      PEA21(I)=B22*PA21(I)+B24*PA41(I)
      PEA22(I)=B22*PA22(I)+B24*PA42(I)
      PEA31(I)=B31*PA11(I)+B33*PA31(I)
      PEA32(I)=B31*PA12(I)+B33*PA32(I)
      PEA41(I)=B42*PA21(I)+B44*PA41(I)
      PEA42(I)=B42*PA22(I)+B44*PA42(I)
      PDR=PEA21(I)*PEA32(I)-PEA11(I)*PEA42(I)-PEA12(I)*PEA41(I)+
     * PEA22(I) *PEA31(I)
      PDI=PEA11(I)*PEA32(I)+PEA21(I)*PEA42(I)-PEA12(I)*PEA31(I)-
     1 PEA22(I) *PEA41(I)
      PUR=DR*PEA42(I)+DI*PEA32(I)-EA42*PDR-EA32*PDI
      PUI=DI*PEA42(I)-DR*PEA32(I)-EA42*PDI*EA32*PDR
      PWR=-DR*PEA31(I)-DI*PEA41(I)+EA41*PDI+EA31*PDR
      PWI=DR*PEA41(I)-DI*PEA31(I)-EA41*PDR+EA31*PDI
      D2R=DR*DR-DI*DI
```

```
      D2I=2.*DR*DI
      PUPNR=PUR*D2R+PUI*D2I
      PUPNI=PUI*D2R-PUR*D2I
      PDENSQ=D2R*D2R+D2I*D2I
      PUDTP=(2./PDENSQ)*COVA*SQRT(PUPNR*PUPNR+PUPNI*PUPNI)
      PPHUPD=ATAN(-PUPNI/PUPNR)-(1.-SIGN(PUPNR))*SIGN(PUPNI)*1.57079
      PWPNR=PWR*D2R+PWI*D2I
      PWPNI=-PWR*D2I+PWI*D2R
      PWDTP=(2./PDENSQ)*COVA*SQRT(PWPNR*PWPNR+PWPNI*PWPNI)
      PPHWPD=ATAN(-PWPNI/PWPNR)-(1.-SIGN(PWPNR))*SIGN(PWPNI)*1.57079
      PRR=-EA42*PEA31(I)+EA32*PEA41(I)+PEA42(I)*EA31-EA41*PEA32(I)
      PRI=EA32*PEA31(I)+EA42*PEA41(I)-EA41*PEA42(I)-EA31*PEA32(I)
      P2R=EA42**2-EA32**2
      P2I=2.*EA42*EA32
      PRPNR=PRR*P2R-PRI*P2I
      PRPNI=PRR*P2I+PRI*P2R
      PRDESQ=P2R*P2R+P2I*P2I
      PMUOQ=(1./PRDESQ)*SQRT(PRPNR*PRPNR+PRPNI*PRPNI)
      PPHUOW=ATAN(-PRPNI/PRPNR)-(1.-SIGN(PRPNR))*SIGN(PRPNI)*1.57079
32    CONTINUE
310   CONTINUE
 1021 RETURN
      END
C
C     SUBROUTINE CROSSCORRELATION
      SUBROUTINE CR1(R,T,NPTS)
      COMMON (10),A(10),B(10),RHO(10),FREQI(260),PAUOWI(260),XIN1(260)
      COMMON  PWDTPI, PUDTPI,WDTP,UDTP,AUOW
      NIN1=NPTS
      NIN2=NPTS
      IB1=1
      IE1=NPTS
      IB2=1
      IE2=NPTS
      LEN1=NPTS
      SX=0.0
      SY=0.0
      SXY=0.0
      SXX=0.0
      SYY=0.0
      DO 101  J=1,LEN1
      J1=IB1+J-1
      J2=IB2+J-1
      SX=SX+XIN1(J1)
      SY=SY+PAUOWI(J2)
      SXY=SXY+XIN1(J1)*PAUOWI(J2)
      SXX=SXX+XIN1(J1)**2
      SYY=SYY+PAUOWI(J2)**2
 101  CONTINUE
      AN=LEN1
      R=(AN*SXY-SX*SY)/SQRT((AN*SXX-SX*SX)*(AN*SYY-SY*SY))
      T=R*SQRT((AN-2.0)/(1.0-R*R))
C     WRITE(3,2001) I,IB1,IE1,IB2,IE2,LEN1,R,T
 2001 FORMAT(1X,6I8,2F14.6)
      RETURN
      END
```